DEVELOPMENT OF NOVEL CONTROLLED RELEASE FORMULATIONS OF ANTI-TNF FOR RHEUMATOID ARTHRITIS AND MODELING OF RELEASE BEHAVIORS

A THESIS SUBMITTED TO
THE GRADUATE SCHOOL OF NATURAL AND APPLIED SCIENCES
OF
MIDDLE EAST TECHNICAL UNIVERSITY

BY

ÖZGE ERDEMLİ

IN PARTIAL FULFILLMENT OF THE REQUIREMENTS
FOR
THE DEGREE OF DOCTOR OF PHILOSOPHY
IN
ENGINEERING SCIENCES

AUGUST 2013

Approval of the thesis:

DEVELOPMENT OF NOVEL CONTROLLED RELEASE FORMULATIONS OF ANTI-TNF FOR RHEUMATOID ARTHRITIS AND MODELING OF RELEASE BEHAVIORS

submitted by **ÖZGE ERDEMLİ** in partial fulfillment of the requirements for the degree of **Doctor of Philosophy in Engineering Sciences Department, Middle East Technical University** by,

Prof. Dr. Canan Özgen _____
Dean, Graduate School of **Natural and Applied Sciences**

Prof. Dr. Murat Dicleli _____
Head of Department, **Engineering Sciences**

Assoc. Prof. Dr. Ayşen Tezcaner _____
Supervisor, **Engineering Sciences Dept., METU**

Assoc. Prof. Dr. Dilek Keskin _____
Co-Supervisor, **Engineering Sciences Dept., METU**

Examining Committee Members:

Prof. Dr. Menemşe Gümüşderelioğlu _____
Chemical Engineering Dept., Hacettepe University

Assoc. Prof. Dr. Ayşen Tezcaner _____
Engineering Sciences Dept., METU

Assist. Prof. Dr. Senih Gürses _____
Engineering Sciences Dept., METU

Assoc. Prof. Dr. Erkan Demirkaya _____
Pediatric Rheumatology Dept., GATA

Assoc. Prof. Dr. Hüseyin Özkan _____
Orthopaedics and Traumatology Dept., GATA

Date: _____

I hereby declare that all information in this document has been obtained and presented in accordance with academic rules and ethical conduct. I also declare that, as required by these rules and conduct, I have fully cited and referenced all material and results that are not original to this work.

Name, Last name: Özge Erdemli

Signature   :

ABSTRACT

DEVELOPMENT OF NOVEL CONTROLLED RELEASE FORMULATIONS OF ANTI-TNF FOR RHEUMATOID ARTHRITIS AND MODELING OF RELEASE BEHAVIORS

Erdemli, Özge

Ph. D., Department of Engineering Sciences

Supervisor   : Assoc. Prof. Dr. Ayşen Tezcaner

Co-Supervisor: Assoc. Prof. Dr. Dilek Keskin

July 2013, pages 160

Anti-TNFα drugs are widely used in treatment of rheumatoid arthritis. However, long term use of these drugs involves systemic effects. New era in medication involves controlled delivery systems that will provide local sustained release of drug. This study aims to develop a novel intra-articularly injectable etanercept (ETN) loaded poly(ε-caprolactone) (PCL) or methoxypoly(ethyleneglycol)-poly(ε-caprolactone)-methoxypoly(ethyleneglycol) (MPEG-PCL-MPEG) microspheres (patent pending) for the treatment of chronic inflammatory arthritides (CIA).

MPEG-PCL-MPEG was synthesized by ring-opening polymerization. Immunoglobulin G (IgG) was used as a model protein for optimization of microsphere preparation. MPEG-PCL-MPEG microspheres had higher encapsulation efficiency than PCL ones for both IgG and ETN. Presence of MPEG was found to have protective effect on loaded and released protein. Microspheres had mean particle sizes around 5 μm. Total amounts of biologically active protein released from MPEG-PCL-MPEG microspheres were significantly higher than from PCL microspheres. ETN release mechanism obeyed to anomalous transport in PBS and in cell culture medium whereas it followed Fickian diffusion in synovial fluid.

Sustained ETN release from microspheres resulted with a significant decrease in pro-inflammatory cytokines and matrix metalloproteinase levels, while conserving viability of fibroblast-like synovial cells (FLS) compared to free drug. There was no significant variation in the gene expressions among groups.

This study showed that presence of MPEG improved the properties of PCL microspheres as delivery system by providing higher ETN stability, release and encapsulation efficiency, besides improving the degradation properties and increasing hydrophilicity, and thus biocompatibility. MPEG-PCL-MPEG and PCL microspheres are promising systems for an effective local treatment approach in CIA.

ÖZ

ROMATOİD ARTİRİT TEDAVİSİNE YÖNELİK ANTİ-TNF İÇİN YENİLİKÇİ KONTROLLÜ SALIM FORMÜLASYONLARININ GELİŞTİRİLMESİ VE SALIM DAVRANIŞLARININ MODELLENMESİ

Erdemli, Özge
Doktora, Mühendislik Bilimleri Bölümü
Tez Yöneticisi   : Doç. Dr. Ayşen Tezcaner
Ortak Tez Yöneticisi   : Doç. Dr. Dilek Keskin

Anti-TNF ilaçlar romatoid artrit tedavisinde sıklıkla kullanılmaktadır. Fakat, bu ilaçların uzun süreli kullanımı sistemik etkilere neden olmaktadır. Yeni dönem ilaç tedavisi, bölgesel uzun süreli ilaç salımı sağlayan kontrollü salım sistemlerini içermektedir. Bu çalışmada, kronik iltihaplı artiritin lokal tedavisinde kullanılmak üzere eklem içi enjeksiyon ile uygulanabilen yeni (patent bekleyen) etanercept (ETN) yüklü polikaprolakton (PCL) veya metoksipoli(etil glikol)- polikaprolakton-metoksipoli(etil glikol) (MPEG-PCL-MPEG) mikrokürelerin geliştirilmesi amaçlanmıştır.

MPEG-PCL-MPEG üç bloklu kopolimeri, halka açılması polimerleşmesi ile sentezlenmiştir. Mikrokürelerin hazırlanma metodunun optimizasyonu için immunoglobulin G (IgG) model protein olarak kullanılmıştır. MPEG-PCL-MPEG mikroküreler, PCL mikrokürelerden daha yüksek IgG ve ETN yükleme verimliliğine sahiptir. Mikrokürelerin yapısında bulunan MPEG'ün yüklenen ve salınan protein üzerinde koruyucu bir etkiye sahip olduğu görülmüştür. Mikrokürelerin ortalama parçacık boyutları 5 µm civarındadır. MPEG-PCL-MPEG mikrokürelerden ortama salınan biyolojik olarak aktif toplam protein miktarları, PCL mikjrokürelerden ortama salınan miktarlardan belirgin olarak yüksektir. PBS ve hücre kültür ortamında, salım mekanizması anormal tip difüzyon modeline uyarken sinoviyal sıvıda Fickian difüzyon modeline uymaktadır.

Mikrokürelerden sürekli ETN salımı, pro-enflamatuar sitokinlerin ve matriks metalloproteinazların düzeylerinde belirgin bir düşüşe neden olurken bir yandan da fibroblast benzeri sinoviyal hücrelerin (FLS) canlılığını yüksek dozdaki serbest ilaç

uygulamasına göre daha iyi korumuştur. Gruplar arasında gen ekspresyonlarında belirgin bir değişim olmamıştır.

Bu çalışmada, yüksek ETN kararlılığı, salım miktarı ve yükleme verimliliği sağlayan ve bunun yanında bozunum özelliklerini geliştirerek yapının hidrofilikliğini ve dolayısıyla biyouyumluluğunu artıran MPEG'in yapıda bulunmasının taşıma sistemi olarak PCL mikrokürelerin özelliklerini geliştirdiği gösterilmiştir. MPEG-PCL-MPEG ve PCL mikroküreler, kronik iltihaplı artritde etkili bir lokal tedavi yaklaşımı olarak umut verici sistemlerdir.

Anahtar Kelimeler: Romatoid Artrit, Eklem içi Uygulama, Anti-TNF İlaç, Mikroküre, Amfifilik Üçbloklu Kopolimer

To the memory of my father
and
To my family

ACKNOWLEDGMENTS

post graduate study. The happy memory of my father still provides a persistent inspiration in my life.

TABLE OF CONTENTS

LIST OF TABLES

LIST OF FIGURES

FIGURES

LIST OF ABBREVIATIONS

AS	Ankylosing Spondylitis
BCA	Bicinchoninic Acid
bFGF	Basic Fibroblast Growth Factor
BSA	Bovine Serum Albumin
CE	Confirmite Europeenne
CIA	Chronic Inflammatory Arthritides
CRP	C-Reactive Protein
DMARD	Disease Modifying Anti-Rheumatic Drug
DMEM	Dulbecco's Modified Eagle Medium
DMSO	Dimethyl Sulfoxide
DNA	Deoxyribonucleic Acid
DSC	Differential Scanning Calorimetry
ε-CL	ε-caprolactone
EDTA	Ethylenediaminetetraacetic Acid
ELISA	Enzyme-Linked Immunosorbent Assay
ETN	Etanercept
ESR	Erythrocyte Sedimentation Rate
FBS	Fetal bovine serum
FDA	Food and Drug Administration
FLS	Fibroblast-Like Synovial Cells
FT-IR	Fourier Transform Infrared
GM-CSF	Granulocyte/Macrophage Colony Stimulating Factor
GPC	Gel Permeation Chromatography
HLA-DR4	Human Leukocyte Antigen-DR4
HMDI	Hexamethylene Diisocyanate
HPLC	High-Performance Liquid Chromatography
IFNγ	Interferon γ
IGF-I	Insulin Like Growth Factor
IgG	Immunoglobulin G
IL	Interleukin
IPDI	Isophorone Diisocyanate
JIA	Juvenile Idiopathic Arthritis
Ltβ	Lymphotoxin β
MCP-1	Macrophage Inflammatory Protein 1
MMP	Matrix Metalloproteinase
$\mathbf{M_n}$	Number Average Molecular Weight
MPEG	Methoxy Poly(ethylene glycol)

MTT	[3-(4, 5-dimetiltiazol-2-yl)-2, 5-difeniltetrazolyum bromide]
MTX	Methotrexate
M_w	Weight Average Molecular Weight
NMR	Nuclear Magnetic Resonance
NSAID	Non-Steroidal Anti-Inflammatory Drug
OA	Osteoarthritis
OD	Optical Density
PBS	Phosphate Buffered Saline
PCL	Poly(ε-caprolactone)
PDGF	Platelet-Derived Growth Factor
PEG	Poly(ethylene glycol)
PEO	Poly(ethylene oxide)
PGA	Poly (glycolic acid)
PHEMA	Poly(2-hydroxyethyl methacrylate)
PLA	Poly (lactic acid)
PLF-68	Pluronic F-68
PLLA	Poly (L-lactic acid)
PLGA	Poly(lactic-co-glycolide)
PMMA	Poly(methyl methacrylate)
PsA	Psoriatic Arthritis
PU	Poly(urethane)
PVA	Poly(vinyl alcohol)
PVDF	Polyvinylidene Difluoride
RA	Rheumatoid Arthritis
RANKL	Receptor Activator of Nuclear Factor β
RF	Rheumatoid Factor
rtPCR	Real-Time Polymerase Chain Reaction
S.D.	Standard Deviation
SDS	Sodium Dodecyl Sulfate
S.E.	Standard Error
SEM	Scanning Electron Microscopy
S.E.M.	Standard Error of the Mean
T_d	Decomposition Temperature
T_g	Glass Transition Temperature
TGA	Thermogravimetric Analysis
TGF-β	Transforming Growth Factor β
Th	T helper
THF	Tetrahydrofuran
T_m	Melting Temperature
TNFα	Tumor Necrosis Factor α
Treg	T regulatory
TRIS	Tris (Hydroxymethyl) Aminomethane

VEGF   Vascular Endothelial Growth Factor

CHAPTER 1

INTRODUCTION

1.1. Anatomy and Physiology of Joints

The skeletal system provides support for the body, mechanical protection for internal organs and acts together with skeletal muscles to make body movement possible. It consists of both fused and individual bones and joints. Joints are the regions of connections between two bones and they enable movement. Joints can be classified according to their degree of movement such as diarthrosis (movable joints), amphiarthrosis (partially movable joints), and synarthrosis (immovable joints) and according to the nature of the connecting tissues such as fibrous, cartilaginous and synovial joints. Most of the joints in the body are diarthrosis and all diathrodial joints are synovial joints. Permitting limited movement and transferring forces from one bone to other are the major functions of synovial joints. Examples of synovial joints include the small joints of the hand, elbow, knee, shoulder, and hip.

The basic structure of a typical synovial joint is shown in Figure 1.1. Synovial joints are composed of several musculo-skeletal tissues such as bone, synovium, articular cartilage, synovial fluid and tensile tissues such as ligament and tendon attached at entheses. In synovial joint, articulating bones are covered by a layer of a hyaline cartilage which absorbs shock and reduces friction during movement. The main anatomic property that distinguishes a synovial joint from other joint types is the presence of a joint capsule (synovial cavity) surrounding the joint and the existence of synovial fluid in this joint capsule. The surfaces of synovial joint cavity are lined by a soft tissue called synovium or synovial membrane. Synovium consists of two layers: subintima (outer layer) and intima (inner layer). Subintima consists of a variety of connective tissues cells, fat cells, and blood and lymphatic vessels while intima consists of an extremely thin sheet of synovial intimal cells (synoviocytes). Synovial intimal cells are composed of two morphologically different types of cells: macrophages (type A cells) and fibroblast-like synovial cells (FLS; also known as synovial fibroblasts or type B cells) [1, 2]. Type A cells are non-fixed cells with an antigen-presenting ability and they are important for removal of cell debris and wastes in the joint cavity. Type B cells produce specialized matrix components such as collagens, hyaluronan and fibronectin [3].

Synovium secretes a small amount of thick fluid, synovial fluid (synovia), into the joint cavity. Two main functions of synovial fluid are to support the mechanical function of joints by cushioning and lubricating of the articulating surfaces, and to play role in the nourishment of articular cartilage by acting as a transport medium for nutrition. Synovial fluid is a dialysate of plasma and contains all of the proteins found in plasma except various high–molecular weight proteins such as fibrinogen, beta 2 macroglobulin, and alpha 2 macroglobulin [4]. This dialysate of plasma and a mucopolysaccharide (hyaluronate) synthesized by the synovium are combined to produce synovial fluid. Additionally, glucose, uric acid, a variety of cells such as lymphocytes, monocytes and neutrophils and many enzymes like alkaline phosphatase, acid phosphatase, lactic dehydrogenase have also been found in the normal synovial fluid [4, 5]. The sodium salt of hyaluronic acid (*ca* 3 mg/ml) and blood plasma proteins such as albumin (*ca* 11 mg/ml) and globulins (*ca* 7 mg/ml) are the most abundant macromolecules in normal synovial fluid [6]. Hyaluronic acid (hyaluronan) is constructed from the repeated disaccharide units of N-acetyl glucosamine and D-glucuronic acid and it has an average molecular weight in the range of 4 to 5 x10^6 Da in healthy adults [7] and it is responsible for the viscosity of synovial fluid [8]. Hyaluronic acid with a high concentration in synovial fluid is essential for healthy joint function because hyaluronic acid provides exceptional viscoelasticity and lubricating properties, especially during high shear conditions. However, hyaluronic acid alone can not provide boundary lubrication, which is the ability of synovial fluid to reduce friction between opposed and pressurized cartilaginous surfaces independent of viscosity. Lubricin is another abundant component of synovial fluid and it is responsible for the boundary lubrication of articular cartilage [9, 10]. Lubricin is a mucinous glycoprotein with globular amino- and carboxyl-terminal domains and a central region that is extensively modified by O-linked oligosaccharide side chains. In a previous study, they showed that lubricin dissipates strain energy within synovial fluid besides lubricating joint surfaces [11].
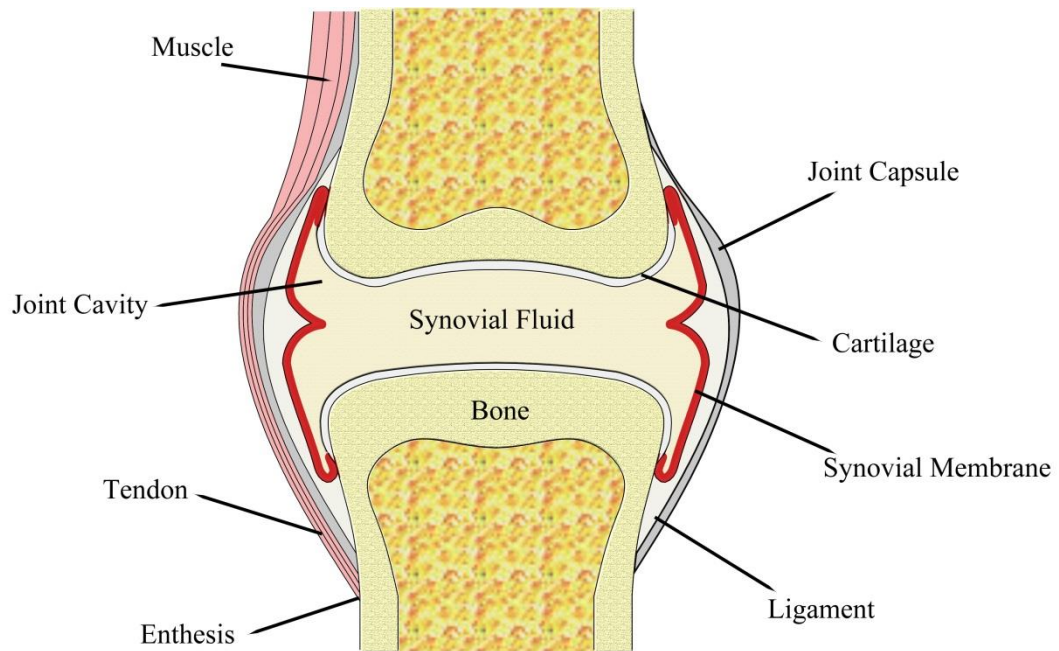
Figure 1.1. The structure of a typical synovial joint

1.2. Joint Disorders

Joint disorders may occur as a result of a trauma (the damage experienced in sports activities and daily life, i.e. falling down, collisions and accidents, etc.), age-related, degenerative or inflammatory diseases. Rheumatic diseases are used to describe a range of diseases that involve inflammation and loss of function of joints or surrounding connective tissue and they can be classified into three general groups: the arthritides, the connective tissue diseases, and the vasculitides.

Arthritides involve more than 100 different diseases and they can be divided into two major groups; degenerative or inflammatory arthritis. Degenerative arthritis, also known as osteoarthritis (OA), is defined generally as a non-inflammatory condition of articular cartilage resulting from natural aging, genetic predisposition, or abnormal biomechanical forces that cause an alteration of metabolic process and destruction of articular cartilage [12]. Inflammatory arthritis is characterized by inflammation of synovial tissues, often leading to destruction of cartilage and bone tissues. Most common inflammatory arthritides in adults are rheumatoid arthritis (RA), psoriatic arthritis (PsA) and ankylosing spondylitis (AS).

Inflammatory arthritis is generally classified into seropositive, seronegative, infectious, and crystal induced groups. Seropositive and seronegative arthritides classification is based on the presence or absence of rheumatoid factor (RF), an immunoglobulin which reacts with gamma globulin, in the blood samples of the patients. RA is a seropositive arthritis whereas AS and PsA are seronegative arthritides. RA, a systemic autoimmune disease, is the most common chronic inflammatory arthritis and is characterized by pain, swelling, stiffness, and inflammation of synovial membrane (synovitis) which often results in joint destruction and disability [13-16]. AS cause chronic inflammatory back pain and stiffness in the spine (vertebral joints), hip and sacrum and sacroiliac joints [17]. PsA is an inflammatory arthritis associated with psoriasis in which scaly red and white patches develop on skin [18].

Juvenile idiopathic arthritis (JIA) is a term used to describe the most common rheumatic disease of childhood [19] and begins before the age of 16 years and persists for at least 6 weeks [20]. Subtypes of JIA are oligoarticular JIA (50%–60%), polyarticular JIA (30–35%), systemic-onset JIA (10–20%), juvenile PsA (2–15%) and enthesitis-related arthritis (1–7%) [20]. Five or fewer joints are affected in oligoarticular JIA during the first 6 months, whereas five or more joints are affected in polyarticular JIA within the first 6 months. Systemic JIA is the most severe type of this disease. Juvenile PsA is an asymmetric arthritis that often affects the knees, ankles and the small joints of the hands and feet. Enthesitis-related arthritis subtype includes patients with juvenile AS and arthritis associated with inflammatory bowel disease.

1.3. Rheumatoid Arthritis

Rheumatoid arthritis (RA) is a systemic disease characterized by pain, cellular hyperplasia (swelling), stiffness, presence of serum autoantibodies including antibodies directed against the Fc portion of immunoglobulins (rheumatoid factor) and against citrullinated peptides (anti-citrullinated peptide antibodies) [21] and inflammation of synovial membrane which can results in progressive joint destruction, disability, and premature mortality. Approximately 0.8% (range: 0.3 − 2.1%) of adult population worldwide is affected by RA and women are affected two to three times as often as men [22]. Although the cause of RA is not yet fully known, a specific group of human leukocyte antigen-DR4 (HLA-DR4) alleles, a phosphatase involved in antigen receptor signaling in lymphocytes (PTPN22), a molecule involved in regulating B cell activation (FcRL3), an enzyme involved in conversion of citrulline to arginine in proteins (PADI4) and a molecule involved in regulation of T cell activation (CTLA4) are known to be major genetic risk factors for RA [22]. Other potential risk factors for developing RA include female sex, older age, smoking, climate, urbanization, silicate exposure, or infectious agents [22, 23].

1.3.1. Pathophysiology of Rheumatoid Arthritis

At joint level, remarkable alterations in synovial membrane are observed during RA and these changes vary as disease progresses. In early stages, tissue edema and fibrin deposition are noticeable and can evidence itself clinically with pain and joint swelling [24]. After a short time, the number of macrophages and fibroblast-like synovial cells in intimal lining of the synovium undergoes dramatic increase (hyperplasia) and depth of intimal lining becomes 10-15 cells thick (hypertrophy). Cellular number and content of the subintimal layer of the synovium also undergoes dramatic alterations, with proliferating blood vessels (neovascularization) and infiltration of inflammatory cells such as macrophages, B cells, T cells, mast cells and plasma and dendritic cells [25]. Activated endothelial cells in synovium express adhesion molecules that enable the transit of inflammatory cells into from the bloodstream into synovium [13]. At later stages of RA, hyperplasia supported by neovascularization leads to formation of locally invasive synovial tissue (pannus) at the interface between synovium and articular bone and cartilage [24]. This pannus tissue, histologically different from other regions of the synovial membrane, is responsible for erosions at articular cartilage and subchondral bone and joint space narrowing (Figure 1.2). Pannus tissue consists of both inflammatory, especially macrophages and T cells, resident mesenchymal cells, plasma cells and endothelial dendritic cells. Additional to the pannus formation, there is accumulation of the synovial fluid, which is mainly constituted by neutrophils. Later, pannus tissue can cause thinning of the articular cartilage and erosion of bone. Different cell types and their interactions with each other play important roles at the pathogenesis of RA. Interactions between these cells are mediated by numerous networks of various types of cytokines, chemical messengers secreted by cells (Figure 1.3).

T helper (Th) cells, macrophages, and FLS and their interactions play important roles in in both initiating and maintaining RA [14, 26-28]. B cells, neutrophils, chondrocytes, osteoclasts, and endothelial cells are the other minor cell types participated in RA pathogenesis [29-33]. Mature Th cells, a sub-group of lymphocytes, can differentiate into effector cells (Th1, Th2, and Th17 cells) or regulatory cells (Treg cells).These cells play important roles in the networks of different cell to cell interactions that govern the development and chronicity of rheumatoid synovitis [34]. Additionally, the imbalance of these cells may also be responsible for the development and continuity of RA [35]. Th1 cells appear in the induction of some autoimmune diseases [36] and they produce some cytokines such as interferon γ (IFNγ), interleukin-2 (IL-2), and tumor necrosis factor α (TNFα) which participate in RA development [37]. Especially, IFNγ is an important cytokine that stimulates inflammatory reactions in RA by activating macrophages and improving the activity of natural killer cells [37]. TNFα released by Th1 cells can activate synovial fibroblast-like cells, macrophages and cartilage cells and it can stimulate intercellular adhesion molecule expression in endothelial cells to promote adhesion and

penetration of leukocyte and vascular endothelium, leading to local inflammation [37]. Th2 cells produce some cytokines IL-4, IL-5, IL-9, IL-10, IL-13, and IL-25 [36]. IL-10 released from Th2 cells can inhibit proliferation of Th1 cells [38]. Therefore, imbalance of Th1/Th2 can be partially responsible for the development of RA. More recently identified Th17 cells are shown to participate in the induction of many autoimmune diseases and these cells produce some cytokines such as IL-17a, IL-17f, IL-6,IL-21, IL-22, IL-26 and TNFα [36, 39]. In early stages of RA, Th17 cells induce macrophages, synovial fibroblasts, osteoblasts, and chondrocytes via the production of IL-17a, IL-17f, and IL-21 [40]. Th1 cells participate in the inflammatory process in later stages of RA [40]. Besides, Th17 cells can stimulate the ligand for the receptor activator of nuclear factor β (RANKL) to upregulated expression especially in the later stage of RA, which play important role in the activation of osteoclast and bone absorption [41]. In RA, Th17 cells may recruit B cells to inflammation site [39], which can produce rheumatoid factor, IL-6, IL-10, lymphotoxin-β (Ltβ) and TNFα [29, 42, 43]. B cells can decrease T cell responses via producing IL-10 [29] and they stimulate synovial fibroblasts through the secretion of Ltβ and TNFα [42].

In RA, macrophages and FLS are two leading cell types in formation of pannus tissue that invade and cause erosion in articular cartilage and bone. As described above, T cells promote the activation of macrophages and FLS via cell contact and releasing some cytokines. Activated macrophages produce some cytokines, such as IL-1β, TNFα, IL-6, IL-8, granulocyte/macrophage colony stimulating factor (GM-CSF), macrophage inflammatory protein 1α (MCP-1) [44] and these cytokines stimulate the development of chronic inflammation. Especially, TNFα is a key cytokine in the pathogenesis of RA and it stimulates FLS activation and survival, leukocyte and endothelial cell activation, pain-receptor sensitization and angiogenesis in RA [43]. Furthermore, macrophages promote subchondral bone destruction by differentiation into osteoclasts [27]. FLS play important roles in maintenance of inflammation in the joint microenvironment and they are key mediators of joint destruction [25]. These cells show anchorage-independent growth, loss of contact inhibition and increased proliferation (hyperplasia) during RA [45]. The mechanism of synovial hyperplasia is unclear but some cytokines, such as basic fibroblast growth factor (bFGF), platelet-derived growth factor (PDGF) and transforming growth factor β (TGF-β), can induce FLS proliferation [43]. FLS also produce PDGF, bFGF and TGF-β to trigger further FLS growth [43]. Another important pathologic characteristic of FLS in RA is their improved ability to produce various cytokines, proangiogenic factors and chemokines [46]. FLS is activated by IL-1β, IL-17 and TNFα and these pro-inflammatory cytokines in turn produce TNFα, IL-1β, IL-6, IL-7, IL-15, IL-16, IL-18, vascular endothelial growth factor (VEGF) and GM-CSF [25, 43, 46]. TNFα, IL-7, IL-15, and IL-16 released from FLS promote T-cell and B-cell migration, activation, and survival [47]. Additionally, the production of VEGF, bFGF and IL-18 by FLS stimulates angiogenesis [43]. In early stages of RA, activated FLS show an invasive phenotype and overgrowth on articular cartilage surface. They then destroy cartilage and bone tissue, sequentially. Production of matrix metalloproteinases (MMPs), matrix degrading

6

enzymes, including MMP-1, MMP-13, and MMP-3 released by FLS results in local invasion and degradation of articular cartilage and bone [48, 49]. FLS also secrete RANKL, which promote osteoclasts from their macrophage precursors and induce their bone-resorbing activity [43].
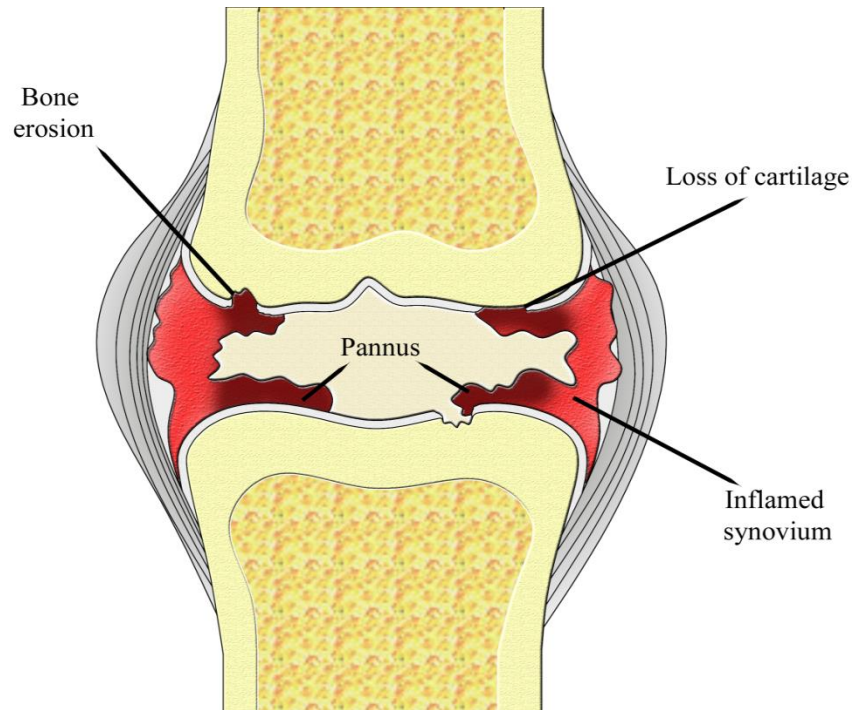
Figure 1.2. The structure of a RA synovial joint

Figure 1.3. The cytokine pathway and cells in RA development

1.3.2. Treatment of Rheumatoid Arthritis

Maximization of joint function, reduction in joint inflammation and pain, and consequently prevention of joint destruction and deformity are the main goals of therapy for RA [15, 22, 50]. In past decades, RA has been treated with the "pyramid approach", in which treatment of patients started with aspirin or other non-steroidal anti-inflammatory drugs (NSAIDs), and continued with changing doses or adding other medications such as disease modifying anti-rheumatic drugs (DMARDs) with progression of symptoms [51]. However, this approach has been replaced with "reverse pyramid" approach, which involve much earlier and consistent use of mono or combination DMARDs compared to "pyramid approach" [51].

Generally, medical management of RA involves a NSAID, and a selective use of glucocorticoids or non-biologic or biologic DMARDs for slowing disease progression [52]. NSAIDs, salicylates or cyclooxygenase-2 inhibitors, show analgesic, antipyretic, and anti-inflammatory effects. NSAIDs have been studied extensively in treatment of RA and shown to primarily decrease joint pain, tenderness and joint stiffness without significantly reducing joint swelling or lowering acute-phase proteins in the blood [53]. However, NSAIDs should not be used alone since they have been insufficient to slow the clinical or radiographic progression [54]. NSAIDs are usually employed as a bridge therapy while waiting for glucocorticoids or DMARDs to become effective. Glucocorticoids, a class of steroid hormones, have been widely used in the treatment of RA because of their anti-inflammatory and immunosuppressive properties [22]. Additionally, they may also postpone the development and progression of bone erosion [22]. Beside the low-dose oral application, intra-articular glucocorticoids application has been also used in the treatment of RA when the systemic application has failed to resolve inflammation. Glucocorticoids can be used for short term and their long-term use is limited by concerns about their toxicity. They can be used as a monotherapy or used in DMARD combination regime. In early times, DMARDs were used only for the most severe cases because of doubts about their toxicity and lack of effectiveness. However, two studies showed that DMARDs can improve functional outcome and slow disease activity more than NSAIDs or corticosteroids alone [55, 56]. DMARDs, a variety of chemically diverse drugs, impede both inflammatory and destructive processes of RA through different routes. DMARDs are divided into two groups: non-biologic DMARDS and biologic DMARDS. Mainly used non-biologic DMARDs are intramuscular or oral gold salts, sulfasalazine, D-penicillamine, hydroxychloroquine, sulphasalazine, and methotrexate (MTX) [22, 57]. In more severe cases, combination of DMARDs appears to be more effective than single agents. DMARDs are also known as "slow-acting anti-rheumatic drugs" and their effectiveness may last from weeks to month. Additionally, their use in clinic is limited by related adverse events, ranging from symptoms of minor intolerance to serious blood and liver toxicity.

After the discovery of the pro-inflammatory role of cytokines, the involvement of different cell types and their surface molecules in the development of RA, new biologic DMARDs have been developed in the last decade [58]. Many of these biologic therapies modify the immune response by blocking the effect of pro-inflammatory cytokines or by acting on various immune cells such as the B lymphocyte or the interaction between the T cell and the antigen presenting cell [57]. Biologic DMARDs mainly inhibit specific component of immune system whereas non-biologic DMARDs modify the immune system as a whole. Therefore, their application is more specific and is less likely to cause adverse events compared to non-biologic DMARDs. Currently, different classes of biologic DMARDs are approved for the treatment of inflammatory arthritis, including TNFα blocking agents, IL-1 receptor antagonist (anakinra), IL-6 receptor blocking monoclonal antibody (tocilizumab), T cell-activation inhibitor (abatacept), anti-CD20 B cell-depleting monoclonal antibody (rituximab), and a fusion protein of recombinant cytotoxic T lymphocyte antigen 4 (CTLA-4) and immunoglobulin G (IgG) 1 [59]. Moreover, many new biologics are now appearing in early-stage clinical development, including IL-17 receptor-blocking monoclonal antibody (brodalumab), anti-IL-17 monoclonal antibodies (secukinumab and ixekizumab), and alternative IL-6 blocking strategies [59].

TNFα plays a central role in the pathogenesis of RA as described in Section 1.3. With the discovery of its role, TNFα became a potential therapeutic target in RA and its blocking agents have been developed and tested in patients with RA. TNFα blockade was the first big success of biologic therapy and researches related with function of many other cytokines in this disease have followed this. Clinical trials with TNFα blocking agents show high efficacy in RA patients who have failed traditional non-biologic DMARDs [15, 57]. Furthermore, the maintenance of joint functionality, the reduction of disease activity and protection from joint damage are the fascinating benefits of TNF-α blocking agents when therapy is initiated in the early stages of RA [60-62]. Although TNFα and IL-1 have many similar biologic effects, IL-1 is involved in cartilage and bone destruction, whereas TNF-α leads to systemic and local inflammation [63]. In addition, it was shown that blocking TNFα significantly reduces the production of other pro-inflammatory cytokines such as IL-1, IL-6, IL-8, and GM-CSF in cultures of synovial cells from patients with RA [13, 64]. Therefore, anti-TNFα drug administration shows more extensive impact against inflammation compared to the therapies against other pro-inflammatory cytokines. Clinically, five anti-TNFα drugs such as the neutralizing anti-TNFα monoclonal antibodies (adalimumab, golimumab, and infliximab), the polyethylene glycol–linked monoclonal antibody fragment (certolizumab pegol), and the soluble TNFα receptor 2-IgG Fc fusion protein (etanercept, ETN) have been widely used in the treatment of RA. These drugs differ in composition, mechanism of action and pharmacokinetics. All of these anti-TNFα drugs inhibit the inflammatory cascade by binding TNFα to avoid triggering the events that lead to pain, inflammation, and cartilage and bone destruction [15]. ETN, adalimumab and certolizumab are approved as monotherapy for RA whereas infliximab and golimumab are only approved in combination with methotrexate [65].

ETN (trade name Enbrel) is the first specific anti-cytokine therapy approved for RA. [66]. It is a dimeric fusion protein consisting of the extracellular ligand-binding portion of the human 75 kDa TNF-α receptor linked to the Fc portion of the human IgG1 (Figure 1.4). It is also approved for treatment of JIA AS, and PsA. Recombinant deoxyribonucleic acid (DNA) technology in Chinese hamster ovary mammalian cell expression system is used to produce ETN. ETN consists 934 amino acids and has an approximate molecular weight of 150 kDa. It can bind specifically to both TNFα and lymphotoxin (also known TNFβ) to block the interaction of TNF with the cell surface TNF receptors, rendering TNF biologically inactive [67]. ETN can bind to two molecules of TNFα due to its dimeric structure and it is 50 to 1000 fold more efficient than monomeric soluble TNF receptor *in vitro* [67]. ETN administration in patients with RA also reduces the production of pro-inflammatory cytokines such as IL-6 and IL-1, some MMPs (MMP-1, MMP-3), VEGF, anti-cyclic citrullinated peptide antibodies, and rheumatoid factor [68]. Long-term effects of ETN are similar to methotrexate, but it induces improvement in RA symptoms much more rapidly, often within two weeks [69]. It was also shown that ETN administration protects joint with an increase in bone formation and a decrease in bone resorption [70].

ETN is given as a subcutaneous injection either 50 mg once weekly or 25 mg twice weekly (3-4 days apart) for RA (0.8 mg/kg to maximum 25 mg twice weekly dose). After a single subcutaneous administration of 25 mg ETN to healthy volunteers, its peak serum concentration is reached after average 51 hours with a maximum concentration of 1.46 μg/ml and its elimination half-life is 68 hours [71]. Therefore, a twice weekly dosing is applied to maintain a steady-state concentration. Systemic application of ETN at frequent intervals can cause patient discomfort by creating pain and possible side effects such as injection-site reactions and infection risk. Injection-site reactions ranging from mild to moderate in severity are observed in approximately one-third of patients after ETN administration [72]. Infections have also been widely observed as adverse events after systemic application of ETN during placebo-controlled trials [68]. TNFα plays an important role in host responses to infection. For this reason, inhibition of TNFα with systemic application of anti-TNFα drug may increase the risk for disseminated bacterial and/or fungal infections [73]. Additionally, TNFα is important in tumor growth control; therefore, systemic application of anti-TNFα drugs may increase the risk of malignancies [74]. Nearly 5% of patients may develop non-neutralizing anti-etanercept antibodies; but there is no evidence that this relates to development of clinical symptoms [68]. Furthermore, systemic application is not suitable for the patient with limited disease such as monoarthritis [75]. Problems related with systemic application of ETN shows that there is a great need for effective and long lasting local treatment.
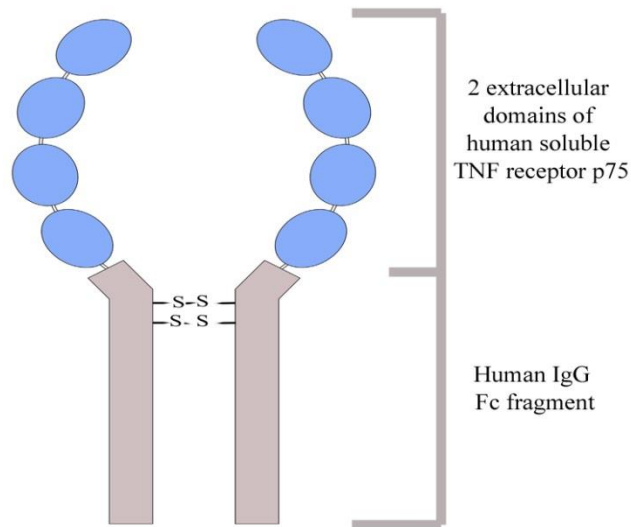
Figure 1.4. Structure of ETN

Intra-articular application can provide the delivery of anti-TNFα drug with high concentrations at the main site of inflammation and minimize the side effects related to systemic administration. Recently, a small number of preliminary clinical studies have tested the efficacy of the existing formulations of anti-TNFα drugs such as ETN, infliximab, and adalimumab for intra-articular use in RA patients [76-82]. However, they were small scale double-blind studies, open-label and case reports conducted with a small number of patients and they have only used the existing formulations. Only systemically administered form of anti-TNFα drugs was applied intra-articularly to the patients in these preliminary clinical studies and intra-articular administration dose was as high as subcutaneous administration dose to increase duration of drug activity. In some of these preliminary clinical trials improvements in the patient's clinical findings (i.e., reduction in joint stiffness and swelling, unconstraint movements, etc.) were observed for a short period [78, 79, 81]. However, in some studies no differences were observed between intra-articularly ETN administered patients and placebo group (buffer injected into joints of patients) [80]. Therefore, these preliminary studies do not give conclusive information about the reliability and effectiveness of this treatment approach. Another important aspect of local therapy is the need for prolonged suppression of inflammation. RA is characterized by chronic inflammation, thus an ongoing anti-inflammatory effect is needed for effective termination of the local disease. However, effects of intra-articular administration of ETN are found short and inadequate. The main reason for the failure of intra-articularly applied drugs may be related to the rapid clearance of drugs from the joint cavity, which is not totally isolated and is in direct equilibrium with the systemic circulation [83]. Moreover, intra-articular route of drug administration can cause serious

side effects such as risk of infection due to numerous injections and local toxicity due to local high dose amounts. Besides the serious side effects and the rapid efflux of drugs from the joint cavity after application, intra-articular administration has also some technical drawbacks related to the cost and time involved in the procedure and patient compliance [50]. For these reasons, drug delivery systems are needed to reduce the adverse effects of high drug dose, to provide sustained suppression of inflammation by longer term drug supply which will eventually improve the potential of intra-articular treatment approach in clinics.

1.4. Controlled Drug Delivery Systems

Controlled drug delivery systems are special be formulations that provide the control on the action of therapeutic substances including traditional drugs, therapeutic peptides, hormones, and etc. in the body. These systems enhance the efficacy and safety of drugs by controlling their rate, time, and place of delivery in the body [84]. The main purpose of application of controlled drug delivery systems is not only to deliver a therapeutic substance in a controlled manner, but also to maintain its level in the body within therapeutic range. Drug delivery systems should be biocompatible as well as being compatible with the drug to be delivered. These systems can modify the biodistribution and pharmacokinetics of the related drug. Moreover, drug delivery systems can eliminate the problems associated with the application of free drug including the environmental or enzymatic degradation, non-specific toxicity, low drug solubility, rapid clearance and inability to cross biological barriers [85]. The average cost and time required to develop a new drug (approximately $500 million and over 10 years) is significantly higher than that for a new drug delivery system (approximately $20–50 million and 3-4 years) [86]. The global market for drug delivery systems was $134.3 billion in 2008 and planned to increase to $196.4 billion in 2014 [87].

Different approaches used for specific cases have been investigated to achieve controlled drug delivery, including localized, targeted, sustained, modulated, feedback controlled and implantable drug delivery approaches [88]. These drug delivery systems can be applied through different routes such as oral, parental (subcutaneous, intra-muscular, intra-venous), transdermal, pulmonary (inhalation), intra-ocular, trans-mucosal and intra-articular. Localized drug delivery simply implies the localization of the therapeutic substance at a particular diseased tissue or organ whereas targeted drug delivery implies more specific delivery of the therapeutic substance to specific cell types. After injection of free drug, its level in the serum follows the profile shown in Figure 1.5, in which the level rises after each drug administration and then decreases until the next administration. However, the level of drug released from a sustained drug delivery system into body remains constant, which is in the therapeutic level between the maximum level (overdose)

13

and the minimum level (under medication dose) for an extended period of time (Figure 1.5). In some cases, it is also desired that the release of therapeutic substance should be immediate. For this purpose, modulatory drug delivery approach is used to provide a pulsatile or ramp release profile. In feedback controlled drug delivery approach, two types of devices have been used: modulated and triggered device. A modulated device can monitor the chemical environment and change release rate of drug continuously in response to a specific marker. In a triggered device, no drug release was observed until the device is stimulated by an external marker. In recent years, sustained release of some drugs has been provided by placing drugs in implantable delivery devices such as micro- and nanodevices [84]. Some of these devices are based on drug diffusion whereas some of them can be triggered by changes in osmotic pressure to release drug.

Especially, polymers have been widely used to design drug delivery carriers and the annual worldwide market for polymeric controlled release system alone is about $60 billion in 2010 [89]. Non-polymer based systems can be also used including liposomes, bioceramics, porous metallic surfaces and pumps [90-93].
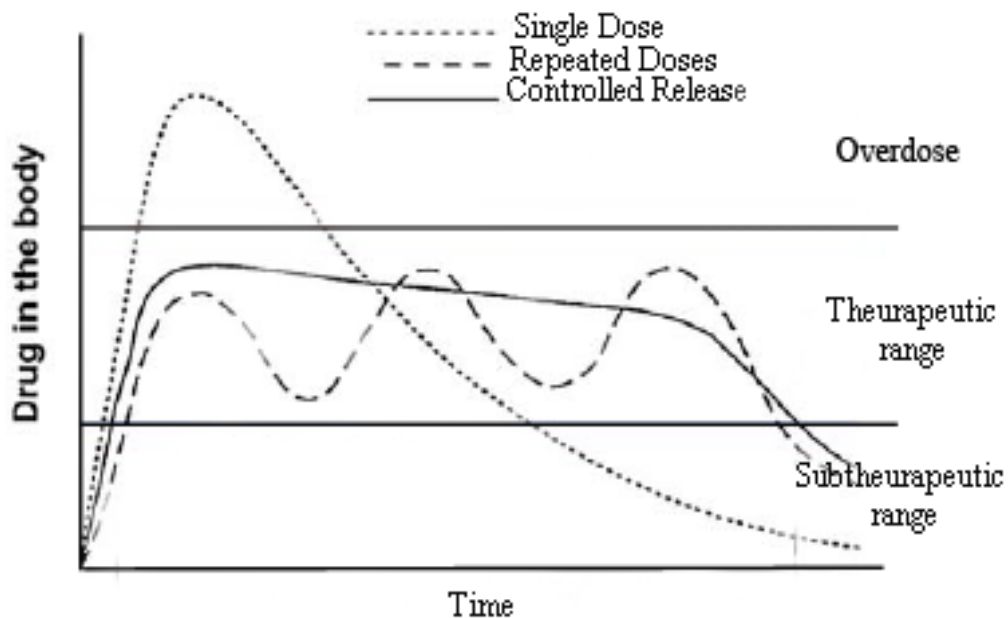
Figure 1.5. Drug levels in the body for different administration methods (modified from [94]

14

1.4.1. Delivery of Therapeutic Proteins

The technological innovations in the field of biotechnology have led to the development of numerous therapeutic proteins and peptides for treatment of various severe chronic diseases such as cancer, diabetes, hepatitis, leukemia, and rheumatoid arthritis [95]. Global biotech drug sales grew twice the rate of traditional small molecule drugs (12.5% vs. 6.4%) with total revenues of $75 billion US in 2007 and biotech drugs accounted for one fifth of all blockbuster drugs in the market as of 2008 [96]. Therapeutic proteins will be developed at an increasing rate because of their roles in cellular functions and the discovery of new proteins due to expanded genomic information. However; in working with therapeutic proteins, there are some challenges arising from their high molecular weight, short half-lives, instability, and immunogenicity. Proteins and peptides are macromolecules that are much bigger than traditional drug molecules and absorbing tissues show low permeability to protein drugs because of their higher molecular sizes [97]. Therapeutic proteins have secondary and tertiary structures, which make them very susceptible to physical and chemical degradation. As a result, protein drugs lose their effectiveness easily after application and require frequent administration to provide the therapeutic level [98]. Moreover, they can denature by heat or by agitation, therefore they must be kept at refrigerated temperatures, along with some stabilizing agents for long-term storage. Thus, these factors limit their therapeutic usefulness in clinical applications.

Several strategies have been used to improve the limitations of clinical use of proteins and peptides, including changing the protein structure (e.g. mutations or covalent attachment of moieties such as poly(ethylene glycol) (PEG) or polysialic acid) and changing formulation of the drug [99]. In the second approach, drug delivery systems such as liposomes, polymeric micro- and nanoparticles, micro- and nanocapsules, diffusion-controlled hydrogels and other hydrophilic systems, microemulsions and multiple emulsions and injectable implants have been widely used to overcome the limitation of protein therapeutics. In the development of protein delivery systems, delivery method (whether invasive or non-invasive), *in vitro* and *in vivo* protein stability, retention of biological activation of protein in formulation (on the shelf as well as post-delivery) and the therapeutic efficient dosage of the protein must be considered. According to these factors, appropriate controlled release formulation parameters such as the material types, methodologies, and excipients to be used and the amount of protein to be loaded should be determined.

In the last three decades, biodegradable microspheres composed of biocompatible polymers have been widely investigated as controlled delivery systems for proteins and peptides due to their versatile administration route and easy production with well-defined physical parameters and desired size range. A successful protein loaded microsphere formulation should have high encapsulation efficiency, loading capacity, and should provide sustained release of the loaded protein with retained bioactivity [100, 101].

Related with the carrier, primary factors determining the encapsulation and release of proteins are the preparation method. Other factors are carrier (mostly polymer) properties such as type, molecular weight, composition, and the size. One of the major requirements of the injectable formulations is injectability; therefore the size of microspheres should be small enough for going through needles.

There are various techniques of formulating protein containing microspheres like double emulsion methods (e.g. water/oil/water, solid/oil/water, water/oil/oil and solid/oil/oil method), spray drying and spray freeze drying, ultrasonic atomization, electrospray, microfluidic, microfabrication, pore-closing and thermoreversible-gel method [100]. The water/oil/water (w/o/w) double emulsion methods have been most widely used among these techniques because of their relatively simple process, suitability in controlling process parameters, and use of inexpensive instruments in these methods [100].

1.4.2. Polymeric Drug Delivery Systems

Polymeric materials mainly chosen for controlled-release purposes show numerous opportunities to enhance the properties of drug delivery systems compared to other types of materials because of their diversity in chemistry, topology, and dimension. Polymeric systems can provide localized and sustained delivery of drugs while protecting them from the physiological environment.

Polymeric drug delivery systems can be divided into three main groups such as polymer-drug conjugate systems, reservoir-based systems, and monolithic matrix systems (Figure 1.6). In polymer-drug conjugate systems, therapeutic substance can be covalently bound to the polymer backbone to improve the mechanism of cellular internalization and cell specificity to achieve optimal release of the drug at the proposed target [102]. Nanoparticles have been widely used for this type of systems due to their high mobility in the small capillaries, allowing efficient uptake and selective drug accumulation at the target site [103]. In reservoir-based systems, drug loaded core is surrounded by a polymer coating and drug release rate is controlled by the molecular weight and composition of polymer, thickness of polymeric membrane, and the properties of the drug, including solubility, particle size, and molecular weight [104]. In the case of monolithic matrix systems, the drug is dispersed or dissolved within the polymeric matrix homogeneously and drug release is controlled by diffusion from polymeric matrix into the surrounding environment and subsequently controlled by both diffusion and polymer degradation for biodegradable polymers. Depending on the desired application, various forms of polymeric drug delivery systems can be chosen to evaluate a successful drug delivery system. Micro- and nanoparticles, micro-and nanocapsules, capsosomes, micelles and dendrimers are mostly used pharmaceutical formulations in which the drug is embedded or encapsulated in the polymer. Additionally, gels and hydrogels are also used as

polymeric drug carriers and they can be used as matrices or capsules. Biodegradable microspheres are the mostly used polymeric drug delivery carriers due to their ability of encapsulating many types of drugs including small molecules, proteins, and nucleic acids and their ease of administration through a syringe needle [105]. They are also generally biocompatible, can provide high bioavailability, and sustained release for long periods. British Broadcasting Corporation's (BBC) analysis showed that the global market for microspheres in 2010 is estimated to be $2 billion and growing at a 5-year compound annual growth rate of 11.6%, reaching global sales of $3.5 billion by 2015 [106].
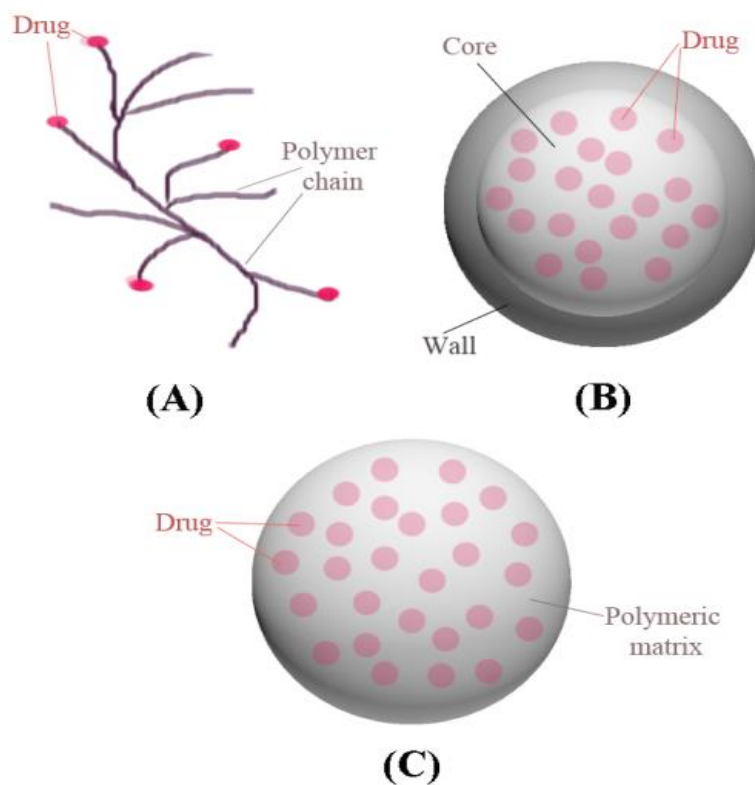
Figure 1.6. Types of polymeric drug delivery systems: **(A)** drug conjugate, **(B)** reservoir-based systems, **(C)** monolithic matrix systems

Selection of polymer matrix for desired application is also an important issue in order to develop a successful drug delivery system. Polymers used in delivery systems of drugs, proteins and cells can be divided into three classes: natural, artificial and synthetic [94]. Some natural polymers are very attractive for preparing drug delivery systems due to their biodegradability and biocompatibility, but some of them present limitations such as

antigenicity and non-uniformity in the properties from batch-to-batch. Proteins (including collagen, albumin, and gelatin) and polysaccharides (including chitosan, alginic acid, and dextran) are the mostly used natural polymers in drug delivery systems. Cellulose derivatives such as hydroxypropylmethylcellulose and ethyl cellulose are biocompatible artificial polymers used in the preparation of drug delivery systems. Depending on the desired application synthetic polymers have been widely used in developing drug delivery systems because of their specific chemical, mechanical, interfacial, and biological properties. Polymer based delivery systems can be tailor made simply by changing the building blocks or the preparation technique. Synthetic polymers used in drug delivery can also be either biodegradable or non-biodegradable. Non-biodegradable synthetic polymers such as poly(methyl methacrylate) (PMMA), poly(2-hydroxyethyl methacrylate) (PHEMA) are stable biological systems and they are mostly used as components of implantable drug delivery systems. However, biodegradable polymers are more attractive for drug delivery applications since no removal or additional manipulation is required after their application. Additionally, a constant release may be obtained by a biodegradable system if polymeric matrix degradation can compensate for the decline of release rate with time. Biodegradable synthetic polymers contain ester, orthoester, amide, urea or urethane groups in their polymer backbone [107]. Aliphatic polyesters, such as poly(ε-caprolactone) (PCL), poly (lactic acid) (PLA), poly (glycolic acid) (PGA), poly(lactic-co-glycolide) (PLGA) and their copolymers are mostly used synthetic polymers in the biomedical devices and drug delivery systems because of their favorable features of biodegradability and biocompatibility.

1.4.2.1. Poly(ε-caprolactone)

Poly(ε-caprolactone) (PCL) has been preferred as a biodegradable carrier for controlled drug release and as a biomaterial in different biomedical applications due to its mechanical properties, biodegradability, biocompatibility and miscibility with a large range of other polymers [108-112]. PCL has also been a major area of interest to develop controlled delivery systems for peptides and proteins [108, 113-115]. It is a highly biocompatible polymer and its non-toxic degradation products are totally eliminated by the body [109]. Additionally, PCL based drug delivery devices had been approved by U.S. Food and Drug Administration (FDA) and Conformité Européenne (CE) [109, 115].

PCL can be synthesized by either ring-opening polymerization of ε-CL (Figure 1.7) using a variety of anionic, cationic and coordination catalysts or via free radical ring-opening polymerization of 2- methylene-1-3-dioxepane [116]. The number average molecular weight (M_n) of PCL can vary from 3,000 to 80,000 g/mol according to the method used and PCL can be graded according to the molecular weight [109]. PCL is a hydrophobic, semi-crystalline polymer and it has a glass transition temperature (T_g) of −60°C and

melting point ranging between 59°C and 64°C, depending on its crystalline nature [109]. Because of its low T_g value, the amorphous phase of PCL shows high molecular mobility at body temperature [117] providing permeability to low molecular weight drugs in delivery systems [118]. Besides showing high permeability to many drugs, it also shows non-toxicity. All of these properties make PCL suitable for drug delivery [108]. Moreover, physical, chemical, and mechanical properties of PCL can be modified by co-polymerization or blending with many other polymers [115].
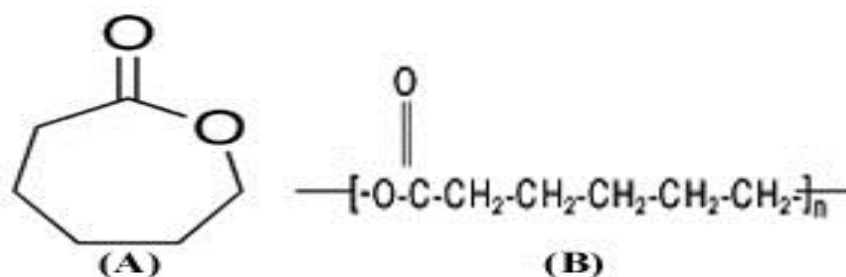
Figure 1.7. Chemical structure of **(A)** ε-CL and **(B)** PCL

The degradation of PCL involves a two-stage degradation phase: random non-enzymatic cleavage, followed by enzymatic fragmentation [115]. The non-enzymatic cleavage, which covers a M_n range of 200,000 to 5000, starts via random hydrolytic chain scission of the ester linkages in amorphous part of PCL in which no weight loss is observed [108]. Water permeability into PCL matrix is the rate limiting step for this non-enzymatic fragmentation. In the second phase of non-enzymatic cleavage, the weight loss from PCL matrix stars after the length of PCL fragments becomes small enough to diffuse out of the polymer bulk to media. However, the weight loss stage can start at much later stage (4–6 months) of PCL degradation [115]. Non-enzymatic cleavage phase is generally accompanied by enzymatic surface erosion characterized by grooves and cracks on the surface. Weight loss has also been related with the increased probability of phagocytosis of smaller fragments produced after hydrolytic chain scission [115].

PCL has a high degree of crystallinity and hydrophobicity, thus it has long degradation time, nearly 2 years *in vivo* [109]. This slow degradation provides the advantage of negligible tendency to generate an acidic environment during degradation compared to PLA and PLGA [109]. Therefore, PCL may be advantageous for sustained release of proteins [119]. Besides not generating an acidic environment during degradation, its high permeability to small drug molecules, its ability to form blends with other polymers and its slow degradation make PCL more suitable for long term drug delivery compared to PLA and PLGA [108]. There are many studies related with drug loaded PCL

microspheres [108, 109, 115]. PCL microspheres can be prepared by oil/water, water/oil/water emulsion solvent extraction/evaporation methods, spray drying technique, solution-enhanced dispersion method and hot melt technique [108]. However, slow *in vivo* degradation kinetics of PCL may also restrict its usage as a versatile matrix material. Ability of PCL to form compatible blends with other polymers can be used to modify its degradation kinetics, which, in turn, can be used to tailor made release profiles [109]. In addition to blending with other polymers, co-polymerization of PCL can also affect the PCL properties such as ionic characteristics, crystallinity, solubility, and degradation pattern resulting in a modified polymer with intended properties for drug delivery [115]. Based on the desired application, PCL properties can be modified by using various natural polymers like starch, hydroxyapatite, chitosan and synthetic polymers namely PEG, poly(urethane) (PU), oxazolines, poly(ethylene oxide) (PEO) and poly (vinyl alcohol) (PVA) [115, 120].

1.4.2.2. Methoxy Poly(ethylene glycol) – Poly(ε-caprolactone) Copolymers

PEG, a hydrophilic, non-immunogenic, non-antigenic polymer, is approved by the U.S. FDA for internal use in biomedical research and applications [121, 122]. PEG is the gold standard for stealth polymers in the field of polymer based drug delivery for prevention of protein adsorption and improvement of biocompatibility of the blood contacting compound [123]. PEG chains introduced to hydrophobic polymers render the so-obtained PEGylated polymers water soluble [124, 125]. In recent years, modification of drugs and drug delivery systems by covalent attachment of one or more PEG chains has been widely used in drug delivery technology [123]. Fabrication of microparticles with PEGylated surfaces can be prepared by addition of PEG and PEG-derivatives during spray-drying or emulsion-based solvent evaporation techniques, copolymerization of PEG with other matrix forming polymers, and formation of microparticles from PEG block or random copolymers [126]. PEG and hydrophobic biodegradable polymer, such as PCL, poly(l-lactic acid), poly(d, l-lactic acid) and PLGA triblock and diblock co-polymers are used to produce PEGylated nanospheres and microspheres for drug delivery [127].

PEG or methoxy poly(ethylene glycol) (MPEG) have been used to form various block copolymers with PCL [120, 128, 129]. The most widely used method to synthesize PEG-PCL diblock and triblock copolymers was ring-opening polymerization from ε-CL and PEG or MPEG with catalyst as shown in Figure 1.8 [120, 130]. Many catalysts such as stannous octoate, stannous chloride, germanium dioxide, tin oxide, and dibutyltin dilaurate have been used in the polymerization [120, 131]. MPEG-PCL-MPEG triblock copolymers can be synthesized from MPEG-PCL diblock copolymers coupled with a coupling agent, such as isophorone diisocyanate (IPDI) and hexamethylene diisocyanate (HMDI) [130].
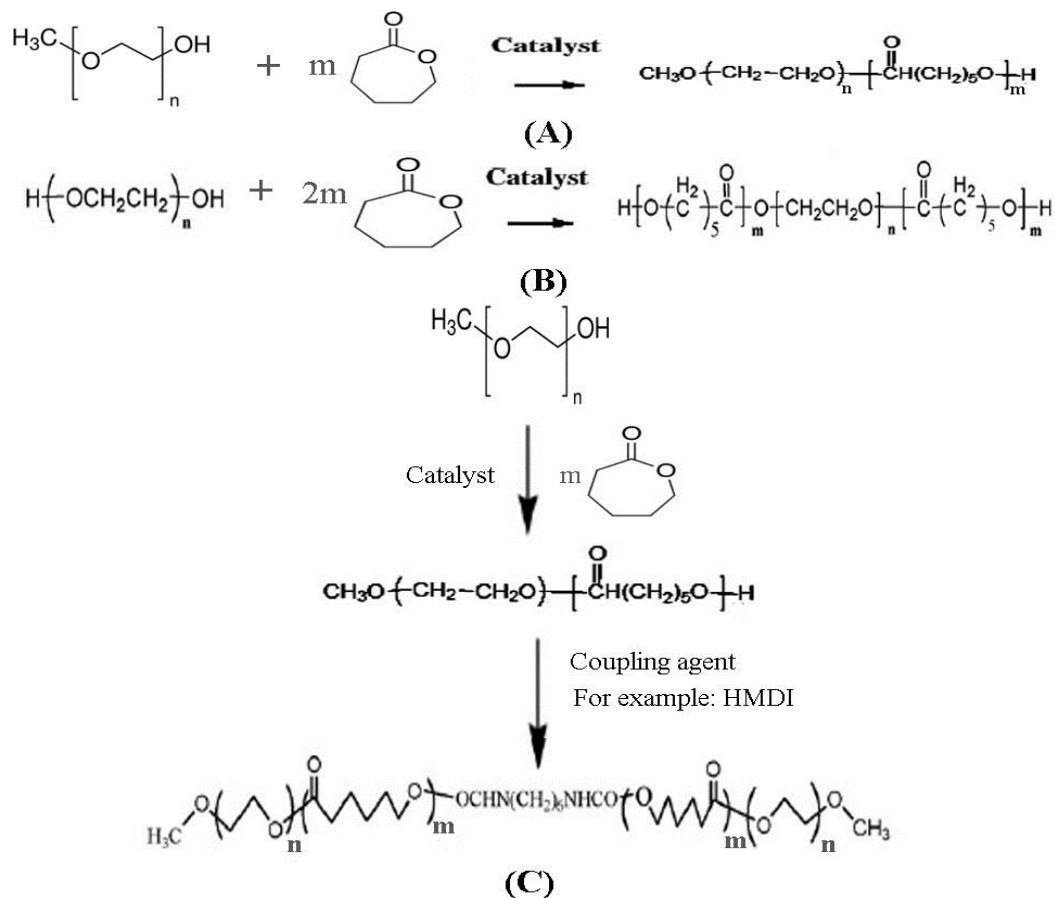
Figure 1. 8. The synthesis of MPEG-PCL **(A)**, PCL-PEG-PCL **(B)** and MPEG-PCL-MPEG **(C)** copolymers

PEG-PCL copolymers are biodegradable and biocompatible polymers that are widely investigated for use in drug delivery systems in various forms such as micelles [132, 133], hydrogels [120, 130, 134, 135], micro- [120, 122, 136] and nanoparticles [120, 137-139]. Micelle, nanoparticle, and microsphere forms of PEG-PCL copolymeric drug delivery systems have mostly been prepared by using MPEG-PCL diblock and triblock copolymers [140-144]. Human serum albumin loaded MPEG-PCL microspheres [122], bovine serum albumin (BSA) loaded PEG-PCL microspheres [145], bFGF loaded PCL-PEG-PCL nanoparticles [137, 138] and insulin loaded PCL-PEG-PCL nanoparticles [146] have been reported as the peptide/protein delivery systems. However, no prior study related with MPEG-PCL-MPEG or PEG-PCL-PEG copolymers in the form of micro/nanoparticle delivery systems for peptides and proteins was found in literature. Only PEG-PCL-PEG hydrogels was used as a delivery system for bFGF in the study of Gong *et al*. [147]. MPEG-PCL-MPEG or PEG-PCL-PEG copolymers are more hydrophilic materials

compared to PEG-PCL, MPEG-PCL, or PCL-PEG-PCL copolymers, which makes them more suitable to incorporate hydrophilic peptide and protein based drugs in aqueous solution.

1.5. Mathematical Modeling of Drug Release from Polymeric Systems

Numerous mathematical models that predict drug release from polymeric systems have been reported in literature [148, 149]. In reservoir systems, drug release is simple to predict and drug delivery takes place after the rate-controlling biodegradable membrane erosion. However, drug release mechanisms from monolithic matrix systems are based on diffusion, swelling, matrix erosion, or combination of these phenomena [150]. For biodegradable polymer matrix, drug release is controlled by its diffusion from polymeric matrix into the surrounding environment and by the hydrolytic cleavage of polymer chains that lead to matrix erosion. As PCL has slow *in vivo* degradation, diffusion is the only possible mechanism by which drugs release from matrix.

If drug release is purely diffusion controlled with constant diffusion coefficients, mathematical modeling of drug release can be simple. For diffusion-controlled microspheres, the release of the drug from the polymeric matrix is obtained by solving Fick's second law of diffusion subject to appropriate boundary conditions. In one dimension/sphere geometry, it is written as [151]

$$\frac{\partial C}{\partial t} = \frac{1}{r^2}\frac{\partial}{\partial r}\left[Dr^2\,\frac{\partial C}{\partial r}\right] \tag{1}$$

where D and C are the diffusion coefficient and drug concentration in the polymer matrix. The boundary conditions are affected by the mass transfer process at the surface and the volume of the surrounding system.

Mathematical modeling of drug delivery systems is very useful in prediction of release kinetics before the release systems are formulated. These models can provide a better understanding of the processes occurring during drug release and they can be used to optimize the existing drug delivery systems. Moreover, mathematical modeling of drug delivery systems involve model fitting on experimental release data and it allows the evaluation of some physical parameters, such as the drug diffusion coefficient. To investigate the kinetics of drug release from controlled release formulation, models can be divided into three groups, including statistical methods (exploratory data analysis method, repeated measures design, multivariate approach), model dependent methods (zero order, first order, Higuchi, Korsmeyer-Peppas model, etc.) and model independent methods (difference factor (f_1), similarity factor (f_2)) [152].

Zero order kinetics involve the superposition of various different mass transport phenomena such as water and drug diffusion, polymer swelling and polymer degradation and the drug release is controlled by all of these mass transport processes. This case can be represented mathematically as:

$$Q_t = k_0 t \qquad (2)$$

where k_0 and Q_t are the rate constant of zero order kinetics and the amount of drug release in time t, respectively.

First order model has been used to describe absorption and/or elimination of some drugs and the release of drug can be expressed by Equation 3.

$$\log C_t = \log C_0 - \frac{k_1 t}{2.303} \qquad (3)$$

where k_1 is the rate constant of first order model. C_0 is the initial amount of drug in the polymer matrix and C_t is the amount of drug remaining in polymer matrix at time t.

Higuchi proposed the first example of a mathematical model to describe drug release from a matrix system [153]. Firstly, this model is valid only for planar systems but it was later modified and extended to consider different geometries and matrix characteristics. This model assumed that initial drug concentration in the matrix is much higher than drug solubility, drug diffusion takes place only in one dimension, drug particles are much smaller than system thickness, matrix swelling and dissolution are negligible, drug diffusivity is constant and perfect sink conditions are always attained in the release environment [152]. Accordingly, simplified model expression can be given by the equation:

$$Q_t = k_H \sqrt{t} \qquad (4)$$

where k_H and Q_t are the rate constant of Higuchi model and the amount of drug release in time t, respectively.

Korsmeyer–Peppas model, a generalized formula derived from the Higuchi equation, implies that the fractional release of drug is exponentially related to release time:

$$\frac{M_t}{M_\infty} = k_P t^n \qquad (5)$$

where k_p is the rate constant of Korsmeyer-Peppas model. M_t and M_∞ are the amount of drug release in time t and ∞, respectively. M_t/M_∞ is the fraction of drug released at time t and n is the diffusion exponent which can be used to characterize both mechanism for

solvent penetration and drug release. Korsmeyer–Peppas model is limited to the first 60% of the cumulative amount of drug release and the release exponent (n) is used to characterize release mechanism and it strongly depends on the geometry of the matrix. For thin films, release mechanism follows pure Fickian diffusion when n is 0.5, and higher values (0.5 < n < 1) shows the anomalous non-Fickian transport. For cylinders, pure Fickian diffusion is generally defined by n=0.45 and the release process in between, 0.45 < n < 1, is characterized as anomalous non-Fickian transport. If n is 0.43 for sphere geometry, it means that release mechanism follows pure Fickian diffusion, and higher values for mass transfer (0.43 < n < 0.85) shows that release follows a non-Fickian model which is denominated as anomalous transport [150]. For the values of n higher than 0.85 or 1, polymer swelling is solely the release rate controlling mechanism and zero order drug release kinetics is observed [150].

1.6. Intra-articular Application of Drug Delivery Systems

Local treatment approach is attractive for delivery of drugs with high concentrations at the main target site of inflammation and for minimizing the side effects related to systemic administration. Therefore, intra-articular administration route has been a common technique for the treatment of joint related disorders. However, intra-articular administration of drug formulations has some drawbacks related to rapid degradation, impaction to patient's quality of life, frequent injections a high financial burden, and clearance of injected drugs from the joint cavity [50]. Furthermore, this treatment also increases the risk of infection due to numerous injections consequently and systemic toxicity due to the application of high dose [50].

To overcome the disadvantages of intra-articular drug administration, a number of micro- and nanocarrier-mediated drug delivery systems, including polymeric micro- and nanoparticles, liposome, and hydrogel, have been investigated for sustained release in joints [154]. More detailed information can be found in literature reviews [50, 154-156]. Microsphere types of drug delivery systems investigated for intra-articular route are summarized in Table 1.1. However, these studies have mostly been focused on the use of microspheres for intra-articular delivery of some NSAIDs and non-biologic DMARDs. There is only one study related with the delivery system of biologic DMARDs, in which anti-TNFα antibody (infliximab) was encapsulated into highly porous PLGA microspheres [157]. However, these microspheres were prepared and studied for the treatment of Crohn's Disease Fistulae instead of treatment of RA.

In active RA, intra-articular administration of a carrier involves its injection into a pathological environment; therefore, size, shape, and type of the carrier are important to avoid further formation of an inflammation or an immune response [50]. In the review article [50], various types of microspheres tested for intra-articular drug delivery were

reported and it has been proposed that a size range between 5 and 10 μm for microspheres provides a prolonged retention time for drugs in the joint cavity without inducing any inflammatory reactions.

Table 1.1. Some examples of intra-articular microsphere drug delivery studies

Therapeutic Material	Carrier Material	Reference
Celecoxib	Chitosan	[158]
	Albumin	[159]
Diclofenac	PLA, PLGA, poly(delta-valerolactone)	[160]
Diclofenac Sodium	PLGA	[161]
	Albumin	[162]
Flubiprofen	Gelatin	[163]
Ibuprofen	PLGA	[164]
Methotrexate	Poly (L-lactic acid) (PLLA)	[165-167]
Naproxen sodium	PLGA	[168]
Paclitaxel	PLGA, PLA, PCL, chitosan	[169]
Quercetin	PCL	[170]

1.7. Aim of the Study

RA is a chronic, autoimmune, systemic, and inflammatory joint disease and has many risks from disability to death. Anti-TNFα therapies have been shown to reduce progression of joint destruction and to have more extensive impact against inflammation than therapies against other pro-inflammatory cytokines. Systemic applications of TNFα blocking agents at frequent intervals are costly and have side effects. In recent years, local treatment approaches are attractive for delivery of anti-TNFα drugs with high concentrations at the main site of inflammation and for minimizing the side effects related to systemic administration. At this point, controlled drug delivery systems of anti-TNFα drugs will provide the advantages like; suppressing the inflammation effectively via longer term drug supply, reducing the adverse effects arising from the use of high doses, and providing protection on protein based drug over the treatment period.

In this study, it is aimed to develop intra-articularly injectable novel PCL and MPEG-PCL-MPEG microspheres for ETN delivery that will provide long term controlled release

of the drug for suppressing the inflammation in RA effectively (Figure 1.9). Human IgG was chosen as a model protein for optimization of ETN loaded microsphere preparation because ETN is a fusion protein of soluble TNFα receptor and Fc portion of the human IgG. Even though ETN has been used in the RA treatment, this is the first study for the development of intra-articular injectable microsphere formulation to achieve a local sustained anti-inflammatory treatment effect for chronic inflammatory arthritides. High treatment efficacy and clinical applicability are targeted with etanercept loaded PCL and MPEG-PCL-MPEG microspheres. The main objectives of this study are

- to provide high ETN encapsulation efficiency of microspheres,
- to produce a drug delivery system that provides a sustained-prolonged release of ETN for at least 3 months after intra-articular administration,
- to protect the bioactivity of ETN throughout the entire release period and to ensure sufficient amount of ETN release for suppressing the local inflammation,
- to obtain optimum particle size that should not cause any inflammatory response,
- to achieve adjustable release rates and released amounts of ETN according to selected polymer.
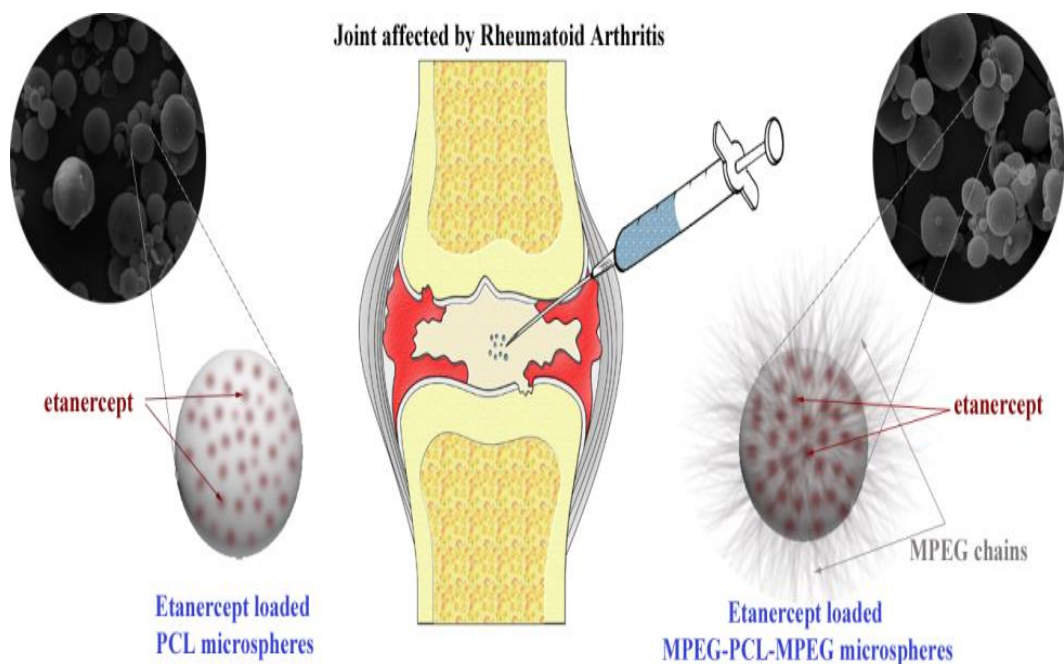
Figure 1.9. ETN loaded PCL and MPEG-PCL-MPEG microspheres

26

CHAPTER 2

MATERIALS AND METHODS

2.1. Materials

MPEG with a molecular weight of 2000 g mol^{-1} (Aldrich, Germany) was purified by re-crystallization in dichloromethane/diethyl ether system. Purification of ε-CL (Aldrich, Germany) was done by drying with calcium hydride (CaH$_2$) and distilled under reduced pressure. Dibutyltindilaurate (Aldrich, Germany), HMDI (Aldrich, Germany), dichloromethane (Merck, Germany), n-hexane (Sigma-Aldrich, Germany) were used without purification.

ETN (Enbrel®) was obtained from Wyeth Pharmaceuticals, England. Poly(ε-caprolactone) (Mw 65 000), Aldrich, Germany), IgG (Sigma, USA), PVA (Aldrich, Germany), chloroform (Sigma, Germany), Pluronic F-68 (PLF-68; Sigma, Germany), dimethyl sulfoxide (DMSO; AppliChem, Germany), sodium dodecyl sulfate (SDS; Bio-Rad, USA), copper sulfate pentahydrate solution (CuSO$_4$ 5H$_2$O; Sigma, USA), Tween 20 (Sigma, Germany), sodium azide (Sigma, Germany), bicinchoninic acid (BCA) reagent (Sigma, Germany) and ethylenediaminetetraacetic acid (EDTA, Sigma, USA) were used as received. Hydrophilic polyvinylidene difluoride (PVDF) membrane was obtained from Millipore (Ireland).

Dulbecco's Modified Eagle Medium (DMEM; Biochrom, Germany), DMEM medium without phenol red (Biochrom, Germany), fetal bovine serum (FBS; Biochrom, Germany), penicillin/streptomycin (PAA, Austria), trypsin-EDTA (PAA, Austria), cell culture inserts (ThinCert™, Greiner Bio-One, Belgium), Type IA collagenase (Sigma, USA), thiazolyl blue tetrazolium bromide (Sigma, USA), Hoechst dye (Invitrogen, USA), calf thymus DNA (Sigma, USA), tris (hydroxymethyl) aminomethane (TRIS, Bio-Rad, USA), BSA (PAA, Austria) and Alamar Blue reagent (Invitrogen, USA) were also used as received.

Human IgG enzyme-linked immunosorbent assay (ELISA) was purchased from RayBiotech (USA). Human TNFα, IL-6, IL-17, IFNγ, MMP-3, and MMP-13 ELISA kits and Q-ETA Etanercept ELISA kit were purchased from eBioscience (USA) and Matriks Biotek (Turkey), respectively. Wehi-164 var13 cell line was a kind gift of Prof. Dr. Atilla

Işık from Department of Virology of Faculty of Veterinary Medicine of Selçuk University.

Trizol (Invitrogen, USA), ImProm-II™ reverse transcriptase (Promega, USA), oligo(dT) 15 primer (Promega, USA), isopropanol (Applichem, Germany), diethyl pyrocarbonate (Applichem, Germany), and Jumpstart SYBR-Green ready mix (Sigma, USA) were purchased for real-time polymerase chain reaction (rtPCR) analysis.

All other chemicals were also of analytical grade and were used without further purification.

2.2. Methods

2.2.1. Synthesis of MPEG-PCL-MPEG Triblock Copolymer

MPEG-PCL-MPEG triblock copolymer was synthesized by ring-opening polymerization of ε-CL initiated by MPEG and the reaction scheme is given in Figure 2.1. Firstly, MPEG-PCL diblock copolymer was synthesized by ring-opening polymerization of ε-CL initiated by MPEG in the presence of catalyst (dibutyltindilaurate) [131]. Then, MPEG-PCL-MPEG triblock copolymer was synthesized by the reaction of synthesized MPEG-PCL diblock copolymer with coupling reagent (HMDI) [134, 171]. Briefly, pre-determined amounts of MPEG and ε-CL with 1:200 ([MPEG]/[ε-CL]) mole ratio were placed into 3-neck flask, and kept at 140ºC in an oil bath for 1h under vacuum. Then, dibutyltindilaurate with a concentration of 0.5% of total reactants was added, and it was stirred at 140°C for 9h under nitrogen atmosphere to synthesize MPEG-PCL. After 9h, HMDI with a concentration 10% of total reactants was added and the polymerization reaction was continued at 80°C for 6h under nitrogen atmosphere. After cooling to room temperature, the resultant MPEG-PCL-MPEG was dissolved in dichloromethane and n-hexane was added to the point of imminent precipitation. The solution was chilled at 4°C overnight. The precipitates were then filtered and washed with n-hexane several times before dried under reduced pressure at 40ºC for 3 days. MPEG and PCL homopolymers were also synthesized by using this polymerization condition to compare with the triblock copolymer.

The thermal properties of ε-CL and MPEG monomers and MPEG-PCL-MPEG triblock copolymer were characterized by differential scanning calorimetry (DSC, Perkin Elmer, USA) and thermogravimetric analysis (TGA, Perkin Elmer, USA). From DSC curves, degree of crystallinity of the homopolymers and triblock copolymer were calculated by using the Equation 6 given in a previous literature [172]:

$$\text{Percentage of crystallinity} = \frac{\Delta H_{sample}}{\Delta H_{100\% \text{ crystalline polymer}}} \times 100 \qquad (6)$$

Additionally, proton nuclear magnetic resonance (^{1}H NMR) spectroscopy (Bruker Biospin, Germany) and Fourier transform infrared (FT-IR) spectroscopy (Bruker IFS 66/S, FRA 106/S, Germany) were used to characterize chemical composition of monomers and copolymer. The macromolecular weight and mass distribution of monomers and copolymer were determined by using gel permeation chromatography (GPC, PL-GPC 220, Polymer Laboratories, USA). Calibration was done with polystyrene standards using tetrahydrofuran (THF) as the mobile phase.
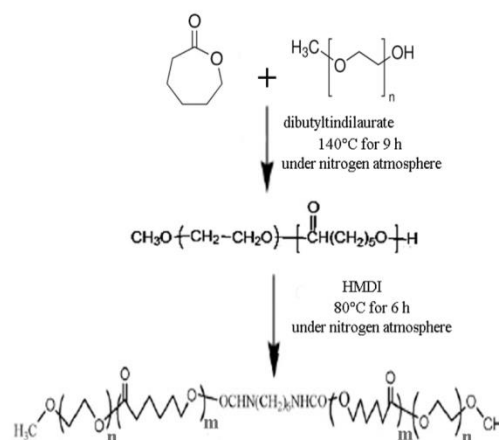
(A)   **(B)**

Figure 2.1. (A) Apparatus for MPEG-PCL-MPEG triblock copolymer synthesis **(B)** Reaction scheme of MPEG-PCL-MPEG triblock copolymer synthesis

2.2.2. Preparation and Characterization of IgG Loaded PCL and MPEG–PCL–MPEG Microspheres

2.2.2.1. Preparation of IgG Loaded PCL and MPEG–PCL–MPEG Microspheres

IgG loaded PCL and MPEG-PCL-MPEG microspheres with an initial loading 0.5% were prepared by double emulsion-solvent evaporation method. Briefly, 100 µl of the inner

aqueous phase (phosphate buffered saline; PBS, 10 mM sodium phosphate, 145 mM NaCl, pH 7.2) containing 10 mg/ml IgG and 1% PVA was added to 5% w/v PCL in dichloromethane or 2.5% w/v MPEG-PCL-MPEG solution in chloroform/DMSO mixture (1:1). The mixture was sonicated for 60 s on ice using Sonorex sonicator (Bandelin, Germany). The resulting primary emulsion was added into 1% w/v PVA solution to prepare PCL microspheres or to PLF-68 solution (3% w/v) for MPEG-PCL-MPEG microspheres. Obtained mixtures were stirred with a magnetic stirrer (Schott, Australia) at 1100 rpm for 15 min. The double emulsion (w/o/w) was poured into PVA solution and PLF-68 solution to prepare PCL and MPEG-PCL-MPEG microspheres, respectively. Then, these emulsions were stirred at 14000 rpm for 3 min in an ice bath with a homogenizer (Ultraturrax T-25, IKA, Germany) and stirred at 1100 rpm for 3h to evaporate the organic solvents. Finally, formed microspheres were collected by filtration through a 0.45 μm hydrophilic PVDF membrane, washed with distilled water and then vacuum-dried overnight .The microspheres were stored at 4°C until use.

IgG loaded PCL and MPEG-PCL-MPEG microspheres were sterilized by γ-irradiation with a typical sterilization dose (25 kGy) [173, 174] obtained from 60Co γ-source (Gamma- cell 220, MDS Nordion, Canada) at ambient temperature and at fixed dose rate (1.74 kGy/h) in Turkish Atomic Energy Authority.

2.2.2.2. Characterization of IgG loaded PCL and MPEG–PCL–MPEG Microspheres

2.2.2.2.1. Surface Morphology and Particle Size

The surface morphological properties of γ-irradiated and non-irradiated IgG loaded PCL and MPEG-PCL-MPEG microspheres were examined by scanning electron microscopy (SEM, JSM – 6400 Electron Microscope, Japan). Microspheres were mounted onto metal stubs using carbon tape, vacuum-coated with gold (25 nm) by using Hummle VII sputter coating device (Anatech, USA) for SEM analysis.

The mean particle sizes and particle size distribution of IgG loaded microspheres were determined before and after γ-irradiation from SEM images by measuring the diameters of 500 microspheres for each group using Image J analysis software (NIH, USA). The resulting size distribution of microspheres was plotted as a histogram with an equal number of bins between the largest and smallest values and as a cumulative percent arithmetic curve. Measure of the width of the distribution of particle size (SPAN) values of microspheres was obtained from cumulative (% undersize) microsphere size distribution curves by using the Equation 7.

$$\text{SPAN} = \frac{d[0.9] - d[0.1]}{d[0.5]} \tag{7}$$

where d[0.9], d[0.5], and d[0.1] are the particle diameters determined respectively at the 90th, 50th, and 10th percentiles of undersized particles.

2.2.2.2.2. Protein Loading and Encapsulation Efficiency

The protein loading and encapsulation efficiency of γ-irradiated and non-irradiated IgG loaded PCL and MPEG-PCL-MPEG microspheres were determined by modifying the method involving the hydrolysis of the microspheres by strong base and the extraction of the protein with SDS [175-177]. Briefly, microspheres (n= 6) were dissolved in DMSO at 37°C for 1 h. 0.25 N NaOH solution containing 0.5% SDS was then added and gently mixed in water bath (Nüve, Turkey) at 37°C for 4h. The mixture was then centrifuged (EBA-20, Hettich, Germany) at 3500 rpm for 5 min. The amount of protein was determined with μBCA assay. In this assay, equal amounts of aliquots and BCA working solution containing 50 parts BCA reagent and 1 part 4% copper sulfate pentahydrate solution were incubated with 15 min at 60°C. After cooling to room temperature, the amount of encapsulated protein was determined by measuring the optical density (OD) at 562 nm with a microplate reader (μQuant, Biotek, USA).

The calibration curve of μBCA assay was constructed with different concentrations of IgG (0-20 μg/ml) treated with DMSO and NaOH/SDS solution. The results of loading and encapsulation efficiency were obtained by the Equation 8 and 9, respectively.

$$\text{Protein loading } (\%) = \frac{\text{weight of protein in microspheres}}{\text{weight of microspheres}} \text{ X } 100 \tag{8}$$

$$\text{Encapsulation efficiency } (\%) = \frac{\text{actual IgG loading}}{\text{theoretical IgG loading}} \text{ X } 100 \tag{9}$$

The actual loading of IgG was determined as the amount of IgG recovered from microspheres divided by the weight of the hydrolyzed microspheres, and was expressed as percentage (w/w). The theoretical IgG loading was defined as the initial weight of IgG introduced in the process divided by the sum of the initial amounts of IgG and PCL or MPEG-PCL-MPEG.

2.2.2.2.3. *In vitro* Release of IgG From Microspheres

In vitro IgG release profiles from γ-irradiated and non-irradiated PCL and MPEG-PCL-MPEG microspheres were evaluated by immersing 5 mg microspheres in 2 ml of PBS (0.01M pH 7.4) containing 0.01% Tween 20 (to prevent particle aggregation [178]) and 0.05% sodium azide in a shaking water bath at 37°C for 90 days. At defined time intervals, all release medium was taken after centrifugation at 3500 rpm for 5 min and replaced by fresh medium. Total protein amount (biologically active and inactive) in the removed sample was determined by μBCA assay (n=4) as described in Section 2.2.2.2.2. The calibration curve for μBCA assay was constructed with different concentrations of IgG (0-20 μg/ml) in release medium to determine the released protein amount. Empty microspheres were used as blank.

Human IgG ELISA kit was used to measure the biologically active IgG released from γ-irradiated and non-irradiated PCL and MPEG-PCL-MPEG microspheres (n=3).For best fits, i*n vitro* release data of total and biologically active IgG were fitted with polynomial trendline (6th degree) and R^2 values and equations of related trend lines are given in Table C.1.

2.2.2.2.4. Kinetics of IgG Release

In order to evaluate the mechanism of IgG release from γ-irradiated and non-irradiated PCL and MPEG-PCL-MPEG microspheres, the release data were analyzed with the zero-, first order, Higuchi, and Korsmeyer-Peppas kinetic models [152].

The following plots were evaluated to determine the rate constants and correlation coefficients for respective kinetic models: cumulative % drug release vs. time (zero order kinetic model); log cumulative of % drug remaining vs. time (first order kinetic model); cumulative % drug release vs. square root of time (Higuchi model) and log cumulative % drug release vs. log time (Korsmeyer-Peppas model). Additionally, n values were also calculated from graphs of Korsmeyer-Peppas model.

2.2.2.2.5. IgG Stability

Stability of IgG encapsulated in γ-irradiated and non-irradiated PCL and MPEG-PCL-MPEG microspheres was examined with FT-IR spectroscopy after extraction [179]. IgG was extracted from microspheres by the hydrolysis of the microspheres with strong base

and extraction of the protein with SDS given in Section 2.2.2.2.2. After extraction, the aliquots of the clear supernatant were analyzed with FT-IR spectroscopy. The amide I region of the spectra (1700–1600 cm^{-1}) was used for analyzing protein secondary structure [180]. Therefore, the FT-IR spectrum of extracted samples, the standard IgG solution in extraction medium and control group (supernatants from the extraction of empty microspheres) were analyzed by second derivatization in the amide I band region for their peak frequencies using Opus 6 software (Bruker, Germany). Second derivative spectra were smoothed with a 9-point smooting function.

2.2.2.2.6. *In Vitro* Degradation Studies

Degradation studies for γ-irradiated and non-irradiated PCL and MPEG-PCL-MPEG microspheres loaded with IgG were conducted in PBS (pH 7.4) containing 0.05% sodium azide in a shaking water bath at 37°C for 6 months and the buffer medium was renewed every 3 days. At the end of degradation study, microspheres were collected by centrifugation, then washed with d-H$_2$O and dried at room temperature.

The surface morphology of the microspheres before and after degradation study was examined by SEM as given in Section 2.2.2.2.1. The mean particle size and particle size distribution of microspheres before and after degradation study were evaluated from SEM images by using Image J analysis software as described in Section 2.2.2.2.1. The chemical structure of the microspheres before and after degradation study was analyzed by FT-IR spectroscopy. The molecular weight of microspheres before and after degradation study was measured by using GPC. Average molecular weights were calculated using a series of polystyrene standards by using THF as the mobile phase.

The pH changes were monitored during degradation study and pH of microsphere-free release medium was measured as control group.

2.2.2.2.7. *In Vitro* Cytotoxicity Studies

In vitro cytotoxicity of the γ-irradiated empty PCL and MPEG-PCL-MPEG microspheres was evaluated according to the standards of ISO 10993-5. Empty PCL and MPEG-PCL-MPEG microspheres were incubated with 3T3 fibroblastic cell line (Sap Foot and Mouth Disease Institute, Turkey) for cytotoxicity tests and cells were evaluated in terms of morphological changes, cell viability and changes in cell number.

3T3 fibroblastic cells were cultured in high glucose DMEM, supplemented with 10% FBS and 100 units/ml penicillin/streptomycin, in 5% CO$_2$ at 37°C in a humidified carbon

dioxide incubator (5215 Shel Lab., USA). The doubling time of cells was 18 hours. The 3T3 cells grown to confluency was subcultured and seeded into 24-well plate at a density of 4 x 10^4 cells per 100 μl. The cells were incubated for 24 h for attachment of cells post-seeding at 37°C in 5% CO_2 atmosphere. After this incubation, γ-sterilized empty PCL or MPEG-PCL-MPEG microspheres were incubated with seeded 3T3 cells at passage 18 by using cell culture inserts for 2 days at 37°C in humidified environment of in carbon dioxide incubator (Figure 2.2). The 3T3 cells incubated without microspheres were used as control group. At the end of the incubation period, changes in the morphology, cell number and viability of cells were evaluated by microscopic examinations (Nikon Eclipse TS100, China), by MTT [3-(4, 5-dimetiltiazol-2-yl)-2, 5-difeniltetrazolyum bromide] assay and by fluorometric DNA quantitation, respectively.

In MTT assay, the cell culture insert with microspheres and the culture medium were removed and 500 μl of fresh MTT working solution (1:10 dilution of 5 mg/ml thiazolyl blue tetrazolium bromide in PBS solution with serum free DMEM medium) was added to each well and incubated for 4 h at 37°C. After MTT working solution was removed, 500 μl of DMSO was added to solubilize the formazan complex and the mixture was shaken at room temperature for 15 min. The OD was measured at 570 nm with a microplate reader (μQuant, Biotek, USA). The cells incubated without microspheres used as a control group for cellular viability. A control group was considered as 100% of cellular viability. The results are expressed as percentage cellular viability ± standard deviation from 5 different samples for each group.

The number of cells was assessed taking the amount of DNA per well as an index and quantified using a fluorometric DNA assay [181]. The fluorescence of the Hoechst reagent is enhanced after binding specifically to DNA and therefore allows a spectroscopic quantification of the DNA content after cell lysis. At the end of the incubation period, the supernatant of the corresponding cell culture was removed and treated hypotonically with 500 μL Millipore water for two hours at 37°C in 5% CO_2 atmosphere. Then, cell culture plate was placed at -80°C until frozen and was thawed to room temperature. After lysis, 1 ml TNE buffer (pH 7.4) containing TRIS, sodium chloride and EDTA was added to the wells. The supernatant samples were taken into a polystyrene cuvette and mixed with Hoechst dye solution prepared in TNE buffer at a 1:1 volume ratio. The fluorescence of the samples and control groups was measured by using Modulus Fluorometer (9200, Turner Biosytems, USA) equipped with an UV Fluorescence Optical Kit (Turner Biosytems, USA) excitation and emission filter centered at 350 nm and 450 nm, respectively. The calibration curve was constructed with measuring the fluorescence of different calf thymus DNA concentrations in TNE buffer. By using this calibration curve, the amount of DNA in the wells with or without microspheres was determined (n=5). Measured amounts of DNA per cells have been converted into the number of cells by using the ratio of the 7.2 pg DNA per mammalian cell.

34
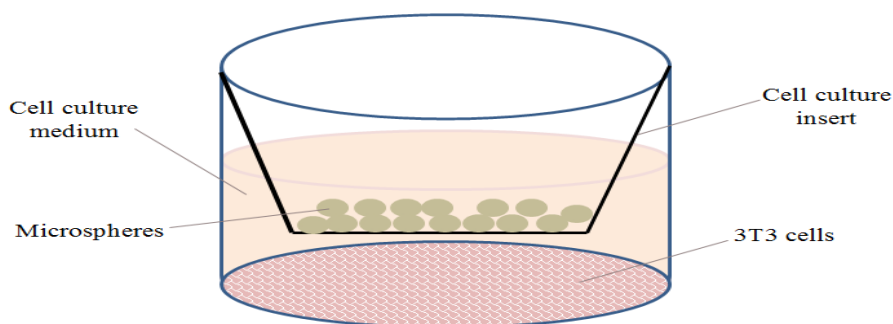
Figure 2.2. Experimental setup for incubation of PCL and MPEG-PCL-MPEG microspheres with 3T3 cells in same cell culture medium for the cytotoxicity tests

2.2.3. Preparation and Characterization of ETN Loaded PCL and MPEG–PCL–MPEG Microspheres

2.2.3.1. Preparation of ETN Loaded PCL and MPEG–PCL–MPEG Microspheres

ETN loaded PCL and MPEG-PCL-MPEG microspheres were prepared by the double emulsion-solvent evaporation method as given in Section 2.2.2.1. After preparation, ETN loaded PCL and MPEG-PCL-MPEG microspheres were sterilized by exposure to γ-irradiation as described in Section 2.2.2.1. The influences of different ETN concentrations (10, 25 and 50 mg/ml) on encapsulation efficiency and ETN release profile in PBS were evaluated.

2.2.3.2. Characterization of ETN Loaded PCL and MPEG–PCL–MPEG Microspheres

2.2.3.2.1. Surface Morphology and Particle Size

The surface morphology of γ-irradiated PCL and MPEG-PCL-MPEG microspheres loaded with ETN were examined by SEM as described in Section 2.2.2.2.1.

The mean particle size and particle size distribution of ETN loaded PCL and MPEG-PCL-MPEG microspheres were evaluated from SEM images by using Image J analysis software and size distributions of microspheres were plotted as histograms of as given in Section 2.2.2.2.1. In addition, SPAN values of microspheres were evaluated as written in Section 2.2.2.2.1.

2.2.3.2.2. Protein Loading and Encapsulation Efficiency

The protein loading and encapsulation efficiency of ETN loaded PCL and MPEG-PCL-MPEG microspheres were determined by modifying the method including the hydrolysis of the microspheres by strong base and the extraction of the protein with sodium dodecyl sulfate. Details of this method are given in Section 2.2.2.2.2.

2.2.3.2.3. Protein Adsorption Test

For protein adsorption test, synovial fluids of 5 RA patients and 1 healthy patient undergoing total knee replacements due to trauma were used. The study was approved by the Medical Ethics Committee of Hacettepe University, and informed consent was obtained from each patient. 5 mg empty PCL or MPEG-PCL-MPEG microspheres were placed in 200 μl of synovial fluids of healthy or RA patients for 14 days. At defined time intervals, all synovial fluid was removed and microspheres were washed with d-H_2O three times to remove physically attached proteins on the surface of microspheres. Adsorbed protein was dissolved from surface of microspheres by incubating microspheres in 3 ml 1% SDS solution in PBS (pH 7.4) in a shaking water bath at 37°C for 24 h [182]. At different time points, amounts of protein adsorbed on microspheres were determined by using μBCA assay as described in Section 2.2.2.2.2 (n=3). The calibration curve of μBCA assay was constructed with different concentrations of bovine serum albumin (BSA) (0-1.25 mg/ml) treated with 1% SDS solution in PBS (pH 7.4) in a shaking water bath at 37°C for 24 h.

2.2.3.2.4. *In Vitro* Release of ETN from Microspheres

In vitro ETN release profiles of PCL and MPEG-PCL-MPEG microspheres were evaluated by immersing microspheres in PBS (0.01M pH 7.4) as explained in Section 2.2.2.2.3. Total protein amount in the removed sample was determined by μBCA assay (n=3) as described in Section 2.2.2.2.3. Additionally, Q-ETA ELISA kit was used to

measure the bioactivity of etanercept released from γ-irradiated microspheres (n=3). For best fits, i*n vitro* release data were fitted with polynomial trendline (6th degree) and R^2 values and equations of related trend lines are given in Table D.1.

Release studies in cell culture medium (high glucose DMEM supplemented with 10% FBS and 100 units/ml penicillin/streptomycin) were also done for ETN loaded microspheres during 60 days. At defined time intervals, cell culture medium was completely removed and replaced by fresh medium. Amount of ETN released from microspheres (n=3) were determined at defined time intervals with Q-ETA ELISA. For best fits, i*n vitro* release data of total and biologically active IgG were fitted with polynomial trendline (6th degree) and R^2 values and equations of related trend lines are given in Table D.1.

ETN loaded PCL or MPEG-PCL-MPEG microspheres (5 mg) and free ETN (5 μg/ml) were incubated in healthy and RA synovial fluids at 37°C for 14 days for prediction of *in vivo* biological activity of free ETN and ETN released from microspheres. At defined time intervals, 20 μl samples were taken from the synovial fluids and free ETN concentration and the amount of etanercept released from microspheres were determined by Q-ETA ELISA (n=3).

2.2.3.2.5. Kinetics of ETN Release

The mechanism of ETN released from γ-irradiated PCL and MPEG-PCL-MPEG microspheres in different release media were evaluated by analyzing the obtained release data with kinetic models written in Section 2.2.2.2.4. Additionally, the rate constants and correlation coefficients for these kinetic models and n values were determined as described in Section 2.2.2.2.4.

2.2.3.2.6. *In Vitro* Cytotoxicity Studies

In vitro cytotoxicity of γ-irradiated PCL and MPEG-PCL-MPEG microspheres loaded with ETN was determined by Alamar Blue Assay using FLS obtained from 3 RA patients and 2 OA patients who were undergoing total joint replacement surgery. The study was approved by the Medical Ethics Committee of Hacettepe University and informed consent was obtained from each patient. Briefly, synovial membranes were minced and incubated with 0.4% (g/ml) Type IA collagenase in serum free high glucose DMEM supplemented with 100 units/ml penicillin/streptomycin for 1h at 37°C in 5% CO_2 atmosphere in carbon dioxide incubator (5215 Shel Lab., USA) [183]. FLS were cultured in high glucose DMEM supplemented with 10% FBS and 100 units/ml penicillin/streptomycin, in 5%

CO_2 at 37°C. The cell culture medium was changed every 3 days and the cells were subcultured in a 1:3 ratio using 0.1% trypsin-EDTA.

At passage 4, FLS were seeded in a 24-well plate at a density of 4×10^4 cells per 100 µl. 5 mg γ-sterilized ETN loaded PCL or MPEG-PCL-MPEG microspheres were placed in these wells using cell culture inserts and incubated at 37°C in carbon dioxide incubator for 14 days (n=3) (Figure 2.2). Additionally, the cells incubated in cell culture medium were used for control group. At predetermined time intervals, the culture medium was removed and fresh high glucose DMEM medium without phenol red containing 10% Alamar Blue reagent was added to each well. After 4h of incubation at 37°C in dark, media of cells were collected and their absorbance was read at 570 nm (reduced) and 600 nm (oxidized) with a microplate reader (µQuant, Biotek, USA).

To evaluate the percent difference in reduction of cell culture media by FLS incubated with etanercept loaded microspheres and by the control cells, the following absorbance equation given in Alamar Blue technical datasheet was used:

$$\% \text{ difference between test and control cells} = \frac{(O_{600} \times A_{570}) - (O_{570} \times A_{600})}{(O_{600} \times P_{570}) - (O_{570} \times P_{600})} \times 100 \quad (9)$$

Where
$O570$ = molar extinction coefficient (E) of oxidized Alamar Blue at 570 nm
$O600$ = E of oxidized Alamar Blue at 600 nm
$A570$ = absorbance of test wells at 570 nm
$A600$ = absorbance of test wells at 600 nm
$P570$ = absorbance of control well at 570 nm
$P600$ = absorbance of control well at 600 nm

2.2.4. Effects of ETN Loaded Microspheres on FLS

2.2.4.1. Isolation of FLS from RA Patients and Cell Culture

For this study, synovial tissues were obtained from 5 patients with RA (5 women, aged 24-67 years) (Table 2.1) and 4 patients with OA (4 women, aged 72-77 years) who were undergoing total joint replacement surgery. RA was diagnosed according to the 2010 ACR/EULAR (American College of Rheumatology/European League Against Rheumatism) classification criteria. The work described in this study has been carried out in accordance with The Code of Ethics of the World Medical Association (Declaration of Helsinki) for experiments involving humans. The study was approved by the Medical

Ethics Committee of Hacettepe University, and informed consent was obtained from each patient (Appendix A). Isolation of FLS from synovial membranes was explained in detail in Section 2.2.3.2.6. FLS at passage 4 were used in the experiments.

Table 2.1. Characteristics of RA patients

Patient Number	Code	CRP (mg/ml)	ESR (mm/h)	RF
1	H	<0.33	29	Not measured
2	M	2.6	56	36.20
3	C	3.72	37	9.69
4	S	<0.33	28	379
5	Z	1.92	45	Not measured

CRP, C-reactive protein; ESR, erythrocyte sedimentation rate; RF, rheumatoid factor

2.2.4.2. Study Design

FLS were seeded into 25 cm^2 flasks at a density of 2.5 x 10^5 and the following experimental groups used:

1. RA FLS (RA Control)
2. OA FLS (OA Control)
3. RA FLS + free ETN
4. RA FLS + ETN loaded PCL microspheres
5. RA FLS + ETN loaded MPEG-PCL-MPEG microspheres

For groups 1 and 2, FLS were cultivated with cell culture medium containing 5% FBS and cell culture medium was partially refreshed at pre-defined time periods.

For group 3, RA FLS were incubated for 4 days only with cell culture medium containing free ETN equal to the amount loaded in 10 mg microsphere (10 μg/ml). After 4 days, the fresh medium was added to existing medium. At day 7, half of medium was refreshed and this was repeated at defined time periods.

For groups 4 and 5, ETN loaded PCL or MPEG-PCL-MPEG MPEG microspheres (10 mg/per used flask) were incubated in cell culture medium containing 5% FBS in separate

flasks. After 3 days release, culture medium of RA FLS was replaced with 2.5 ml fresh medium containing 5% FBS and ETN released from microspheres. After 4 days, 2.5 ml culture medium containing 7 day release of ETN from microspheres was added to existing medium. After every 3 days, half of the culture medium was replaced with fresh medium and amount of the released ETN was determined at defined time periods.

For all experimental groups, changes in viability and numbers of FLS, levels of pro-inflammatory cytokines and MMPs released by FLS and changes in mRNA expression levels of IL-6, TNFα, MMP-3, and MMP-13 released by FLS were evaluated during 4 weeks.

2.2.4.3. Quantitation of ETN Concentration

Changes in ETN concentrations in free ETN group were monitored during 4 weeks. Additionally, *in vitro* ETN release from γ-irradiated PCL or MPEG-PCL-MPEG microspheres were evaluated in cell culture medium containing 5% FBS during 4 weeks. Q-ETA ELISA kit was used to determine the ETN amounts.

2.2.4.4. Viability and Cell Number of FLS

The cell numbers of FLS were determined by using a NucleoCounter (Chemometec, Denmark) at the end of 1st, 2nd, 3rd, and 4th weeks. The NucleoCounter is an integrated fluorescence microscope designed to detect signals from the fluorescent dye, propidium iodide (PI) bound to DNA. PI is immobilized in the interior of the disposable NucleoCassette. When the cassette has been loaded with the cell lysate the PI is dissolved and the cellular DNA is stained. At the end of each week, FLS in experimental groups were trypsinized with 0.1 % trypsin-EDTA. After trypsinization, 200 μl cell suspensions were taken and were first mixed with equal volumes of lysis/disaggregation buffer and then stabilizing buffer. The NucleoCassette was loaded with the lysate solution by immersing the tip of the cassette into the solution and cells were counted in the instrument.

Viability of RA FLS was assessed by Alamar Blue Assay which provides continuous monitoring of cultures over time. Details of Alamar Blue Assay are given in Section 2.2.3.2.6.

2.2.4.5. Levels of Pro-Inflammatory Cytokines and MMPs

Levels of TNFα, IL-6, IL-17, IFNγ, MMP-3, and MMP-13 released by RA FLS in experimental groups 3, 4 and 5 were compared with that of the control group (Group 1) for 4 weeks to examine the treatment efficacy of the delivery systems. Additionally, levels of pro-inflammatory cytokines and MMPs released by OA FLS (Group 2) were also compared with that of RA FLS (Group 1).

Levels of IL-6 IL-17, IFN-γ, MMP-3, and MMP-13 were determined by using ELISA. Levels of physiologically active TNFα released by FLS were determined by using a bioassay in which TNFα sensitive Wehi-164 var13 cell line was used. A calibration curve was obtained by measuring the viability of Wehi-164 cells incubated with predetermined amounts of human TNFα standard solutions by MTT test to determine the %production levels of physiologically active TNFα produced by FLS. The %production levels of physiologically active TNFα produced by FLS incubated with free ETN or ETN loaded PCL or MPEG-PCL-MPEG microspheres and by RA control FLS were compared. In addition, %production levels of physiologically active TNFα produced by RA FLS and OA FLS were compared.

2.2.4.6. Changes in mRNA Levels

Changes in mRNA expression levels of IL-6, TNFα, MMP-3, and MMP-13 of FLS were determined at each week for 4 weeks. The time course gene expression studies were conducted using reverse-transcriptase coupled rtPCR analysis. At first step, biological triplicates of cultured FLS were harvested in Trizol solution at the end of predetermined periods and stored at -80ºC until further processing. After the samples were thawed to room temperature, total RNA was extracted by using Trizol protocol upon manufacturer's recommendations and standard quality control measures were performed. Briefly, 200 μl chloroform was added to homogenized cell lysate. Then, the mixture was vortexed for 2-3 minutes and the samples were kept at room temperature. Later, sample was centrifuged at 12000 rpm for 15 minutes at 4ºC. The supernatant in which RNA was found was collected into 500 μl isopropanol in a new tube. This tube was mixed and kept at room temperature for 10 minutes. Again, sample was centrifuged at 12 000 rpm for 15 minutes at 4ºC. After supernatant was removed, 70% ethanol containing diethyl pyrocarbonate was added to the pellet and the mixture was vortexed. To avoid disrupting RNA, sample was centrifuged at lower speed (7500 rpm) for 10 minutes at 4ºC. After centrifugation, 70% ethanol was removed and RNA pellet was dried. According to the amount of pellet, 15 μl RNAse free water was added to pellet to dissolve it. Sample was kept at 60ºC for 10 minutes and stored at -20ºC until the analysis. After analysis, sample was stored at -80ºC. Quantity and

purity of RNA were determined spectrophotometrically by measuring the ODs at 230, 260 and 280 nm wavelengths, respectively. Denaturing agarose gel electrophoresis consisting 1% formaldehyde was used to determine the quality of isolated RNA by checking 18S and 28S ribosomal RNA bands.

Total RNA was reverse transcribed into cDNA by using ImProm-II™ reverse transcriptase enzyme and oligo(dT)15 primer. 1 μg RNA was used as a template and it was denatured at 70ºC for 5 minutes by adding 0.5 μg oligo(dT) 15 primer and RNAse free water with a total volume of 5 μl. After incubation, sample was kept in ice bath for 10 minutes.15 μl reverse transcription solution was prepared in a different tube. The transcription solution preparation protocol is given below:

	Final Concentration	Volume
RNAse free water		6.6 μl
Improm-IIтм buffer (5X)	1X	4 μl
MgCl2 (25mM)	3 mM	2.4 μl
dNTP mixture (10mM)	0.5 mM	1 μl
Improm-IIтм ReverseTranscriptase		1 μl
	Total:	**15 μl**

Real-time PCR analysis was conducted in Rotor-gene 6000 (Corbett Life Science, USA) using Jumpstart SYBR-Green ready mix and gene specific primers in experimental triplicates. Relative quantitation was achieved by normalizing the gene expression of the beta-actin housekeeping gene. After mixing 5 μl RNA + primer mixture with 15 μl reverse transcription solution, reverse transcription was conducted in Rotor-gene 6000as follows:

5 minutes at 25ºC
60 minutes at 42ºC
15 minutes at 70 ºC

At the end of this reaction, 20 μl cDNA was synthesized and cDNA samples were diluted with adding 60 μl d-water. Analysis was repeated 3 times for each sample. Volumes used in real time- PCR were as following:

2X SYBR Green mixture	5 μl
25 mM MgCl2	1.2 μl
Forward primer (10pmol/ μl)	0.4 μl
Reverse primer (10pmol/ μl)	0.4 μl
cDNA	2 μl
d-water	1 μl
Total:	**10 μl**

10 µl RT-PCR reaction was carried out at Rotor-gene 6000 device with the conditions given below:

2 minutes at 94ºC
2 seconds at 94ºC   x 40 cycles
20 seconds at 60 ºC   x 40 cycles

2.2.5. Statistical analysis

Statistical analyses were performed using the SPSS Software version 9 (SPSS Inc., USA). The results of the cell numbers, viability of FLS and levels of pro-inflammatory cytokines and MMPs released by FLS were expressed as the mean ± standard error of the mean (S.E.M.). Results of mean particle size measurements were given as mean ± standard error (S.E.). Other data were given as mean ± standard deviation (S.D.). For comparison of unpaired data, the Mann-Whitney U test was used. A p value ≤ 0.05 was considered significant.

CHAPTER 3

RESULTS AND DISCUSSION

3.1. Properties of Synthesized MPEG-PCL-MPEG Triblock Copolymer

In the optimization studies of MPEG-PCL-MPEG triblock copolymer synthesis, different [MPEG]/[ε-CL] monomer mol ratios (1:20, 1:100, and 1:200) and different copolymerization reaction times (from 4 to 9h) were used. A final monomer mol ratio of 1:200 and copolymerization reaction time (9h and 6h for diblock and triblock copolymer synthesis, respectively) were chosen to obtain a triblock copolymer, which is non-soluble in water and has a capability to form microspheres with homogeneous population.

The thermal properties of MPEG, PCL homopolymers and MPEG-PCL-MPEG triblock copolymer were characterized by DSC. DSC thermograms of homopolymers and MPEG-PCL-MPEG triblock copolymer are given in Figure 3.1. Melting temperature (T_m), enthalpy of melting (ΔH) and percentage of crystallinity of homopolymers and copolymer are presented in Table 3.1. MPEG-PCL-MPEG triblock copolymer showed higher T_m (66.64ºC) value with lower ΔH (49.88 J/g) compared to homopolymers. ΔH value of triblock copolymer was considerably lower than those of the homopolymers, probably due to phase mixing between MPEG and PCL blocks. During the triblock copolymer formation, amorphous regions increased and degree of crystallinity of MPEG and PCL segments decreased (Table 3.1).

Thermal stabilities of homopolymers and triblock copolymer were studied by TGA. TGA curves and differential thermogravimetric curves of MPEG-PCL-MPEG triblock copolymer and homopolymers are given in Figure 3.2. Additionally, the decomposition temperatures (T_d) of homopolymers and triblock copolymer are presented in Table 3.1. Two weight loss steps were observed in the differential thermogravimetric curve of MPEG-PCL-MPEG triblock copolymer, confirming the block structure of the copolymer. First weight-loss step reflected thermal degradation of the less stable PCL block chain and the second weight-loss stage was relevant to the degradation of the MPEG blocks. Similarly, in a previous study a series of PEG/PCL and PEG/PVL diblock copolymers were synthesized via ring-opening polymerization of ε-CL or γ-VL in the presence of novel aluminum alkoxide catalysts bearing Salen ligands and MPEG/PEG as the alkoxy moiety [184]. The group also observed two weight loss steps in TGA curves of diblock copolymers.
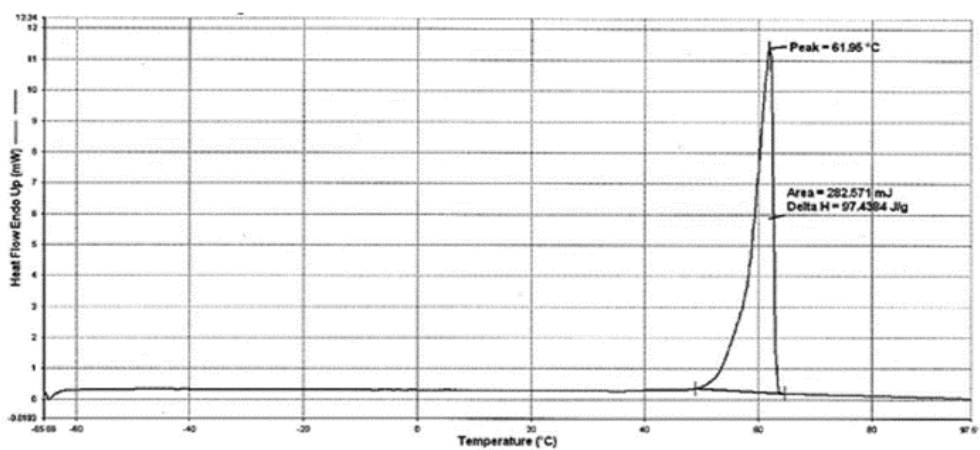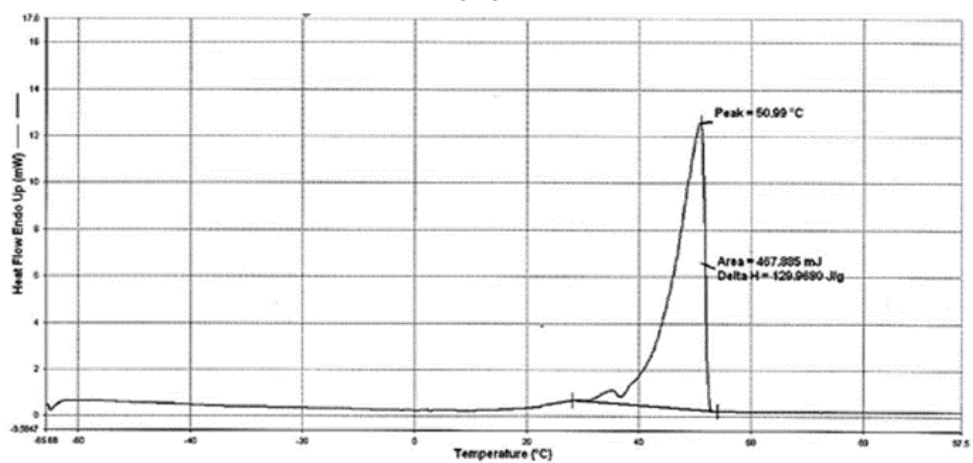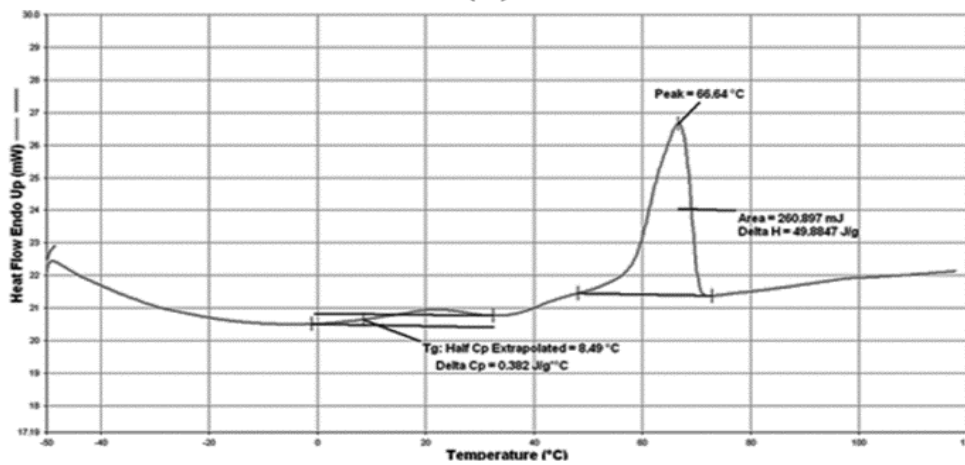
Figure 3.1. DSC thermograms of PCL **(A)** and MPEG **(B)** homopolymers and MPEG-PCL-MPEG triblock copolymer **(C)**
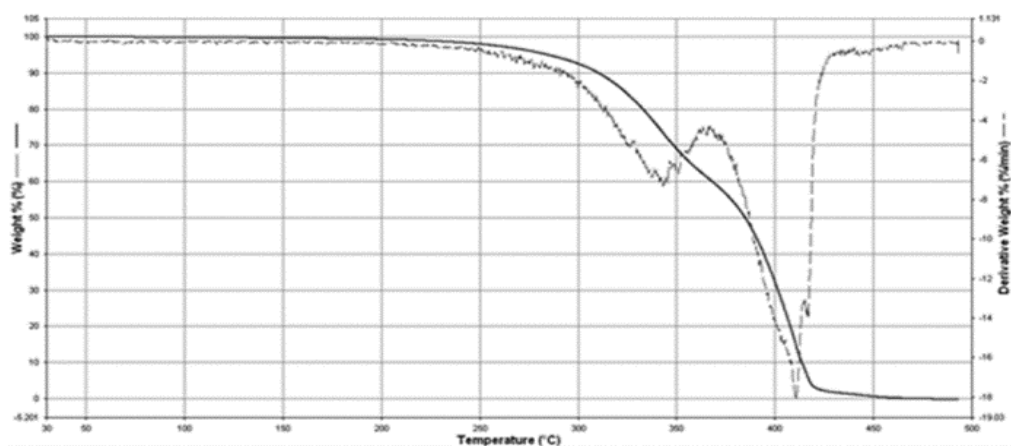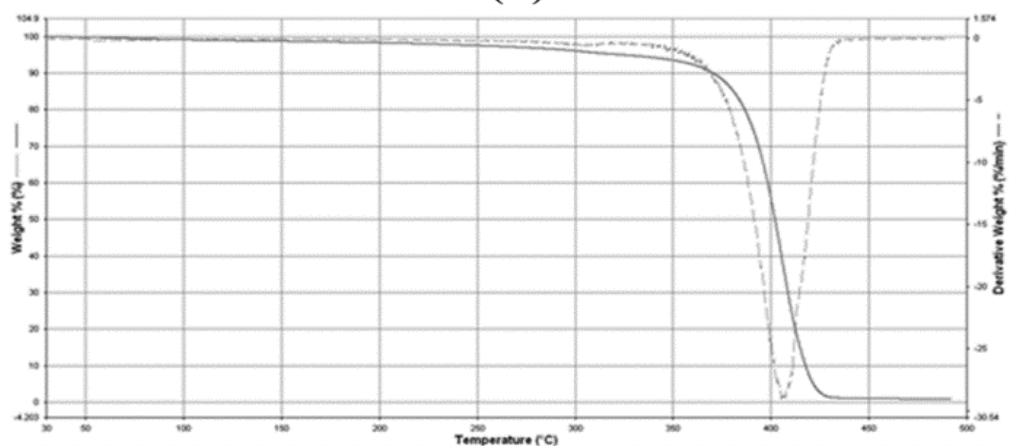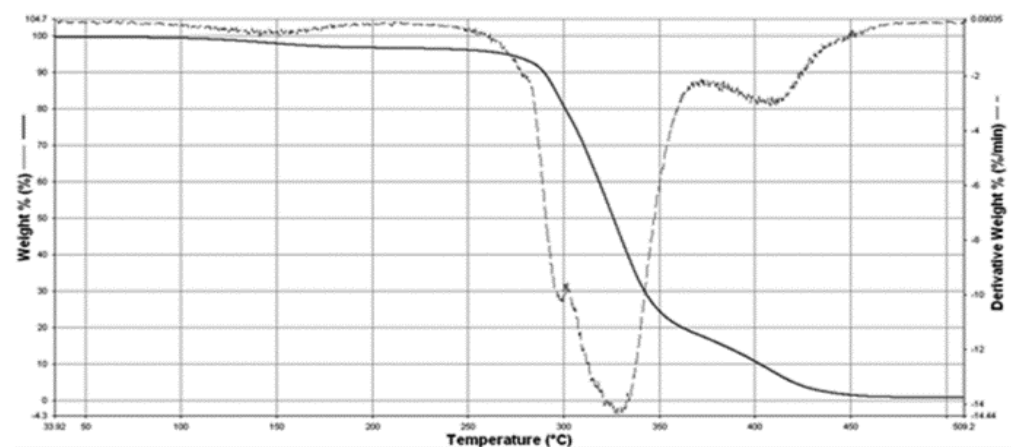
Figure 3.2. Thermogravimetry curve and differential thermogravimetric curve of of PCL **(A)** and MPEG **(B)** homopolymers and and MPEG-PCL-MPEG triblock copolymer **(C)**

Table 3.1. DSC and TGA data of synthesized MPEG and PCL homopolymers and MPEG-PCL-MPEG triblock copolymer

| Sample | T_m (°C) | ΔH (J/g) | % crystallinity | | | T_d(°C) |
			%PEG[a]	% PCL[b]	% total	
MPEG	50.99	129.97	68.5	-	-	407
PCL	61.95	97.44	-	72.2	-	343 and 410
MPEG-PCL-MPEG	66.64	49.88	26.9	37	35.1[c]	330 and 410

[a] **Degree of crystallinity of PEG segment calculated, based on the heat of melting of a 100% crystalline PEG (189.8 J/g)** [172]

[b] **Degree of crystallinity of PCL segment calculated, based on the heat of melting of a 100% crystalline PCL (134.9 J/g)** [172]

[c] **Total degree of crystallinity of the MPEG-PCL-MPEG copolymer, calculated by (degree of crystallinity (PEG) × wt% PEG in the copolymer) + (degree of crystallinity (PCL) × wt% PCL in the copolymer)** [172]

The chemical structure of MPEG-PCL-MPEG triblock copolymer was analyzed by using FT-IR and ^{1}H NMR spectroscopy. FT-IR spectra of MPEG and PCL homopolymers are given in Figure B.1. Both of the characteristic FT-IR peaks of MPEG and PCL segments were observed in the FT-IR spectra of triblock copolymer (Figure 3.3A). Existence of PCL segment was shown with the carbonyl stretching peak at 1721 cm^{-1} and asymmetric C-O-C stretching peak at 1238 cm^{-1}. Besides, the peaks related with MPEG segment such as CH stretching vibration at 2855 cm^{-1}, –CO stretching of -OCH2CH2 unit at 1106 cm^{-1}, C-O-C stretching at 1066 cm^{-1} and methylene stretching at 840 cm^{-1} were also observed in FT-IR spectra of triblock copolymer. Additionally, there is no absorption in 2250–2270 cm^{-1}, which indicates that the –NCO groups of coupling reagent (HMDI) disappeared completely due to coupling reaction of –NCO with –OH group. The absorption bands at 1577 cm^{-1} were attributed to N–H bending vibrations related with the HMDI, which confirmed the formation of MPEG-PCL-MPEG triblock copolymer. As seen in literature, existence of N-H bending vibration peak confirmed the MPEG-PCL-MPEG triblock copolymer formation [130, 171, 185].

^{1}H NMR spectra of MPEG and PCL homopolymers are given in Figure B.2 and ^{1}H NMR spectrum of triblock copolymer is given in Figure 3.3B. ^{1}H NMR spectrum of MPEG-PCL-MPEG triblock copolymer obtained in this study was very similar to the reported spectrum of MPEG-PCL-PEG triblock copolymer synthesized in the study of Fu *et al*. [171]. In ^{1}H NMR spectrum of triblock copolymer, both of the characteristic proton peaks of MPEG segment (3.4 and 3.8 ppm) and PCL segment (1.2-1.4, 1.5- 1.7, 2.3, and 4.1 ppm) were observed. The proton peaks (1.2–1.4 and 3.2 ppm) coming from the coupling

agent were also seen in the ^{1}H NMR spectrum of triblock copolymer. In the study of Hwang *et al.* [186], similar proton peaks were observed in the ^{1}H NMR spectrum of triblock copolymer and the peaks for the coupling agent confirmed the MPEG-PCL-MPEG triblock copolymer formation.
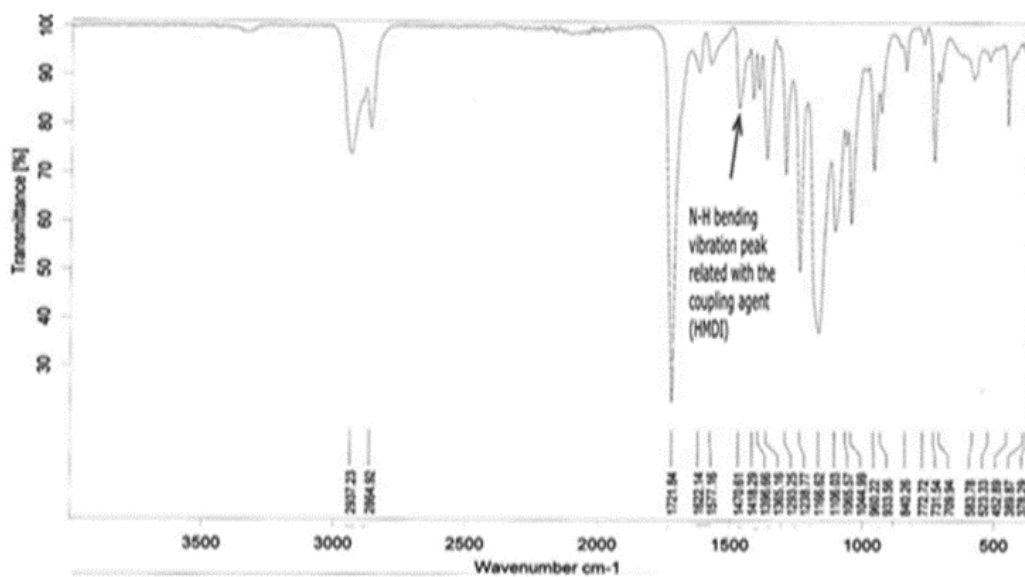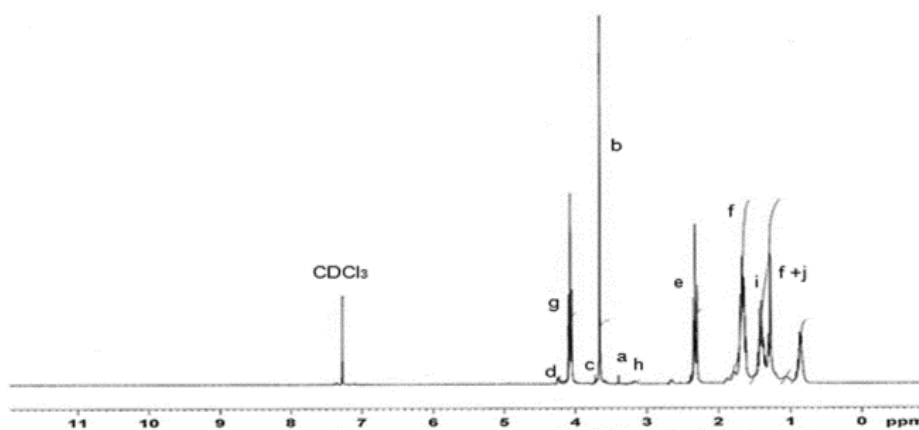
Figure 3.3. FT-IR **(A)** and ^{1}H NMR **(B)** spectrum of MPEG-PCL-MPEG triblock copolymer

The calculation of number average molecular weight (M_n), degree of polymerization and PCL/MPEG ratio of synthesized triblock copolymer was based on the integrity ratio of the ^{1}H NMR peaks at 4.1 ppm to methylene protons (-CH_2-) of PCL segment and 3.65 ppm (-CH_2-) to MPEG segments (Table 3.2).

GPC was used to determine the number average molecular weight (M_n), weight average molecular weight (M_w) and polydispersity index of MPEG-PCL-MPEG triblock copolymer. In Table 3.2, all the quantitative data on number average molecular weight (M_n), weight average molecular weight (M_w) and polydispersity of the copolymer are listed. The PDI is a measure of the distribution of molecular mass in polymer sample and unity for a polymer of uniform molecular weight and becomes larger as the distribution becomes broader. Typical commercial polymers used in biomaterials have polydispersity indices of 1.5 – 50, although polymers with polydispersity indices of less than 1.1 can be synthesized with special techniques [187]. PDI value of MPEG-PCL-MPEG had a higher PDI value than 1.5, indicating that triblock copolymer had a broader molecular mass distribution.

Table 3.2. Molecular weight of synthesized MPEG–PCL–MPEG triblock copolymer

PCL/MPEG (theoretical mol, %)[a]	99.5 : 0.5
M_n (theoretical)[a]	24 800
PCL/MPEG (calculated mol, %)[b]	98.6 : 1.4
M_n[c]	19 199
M_n[d]	14 051
M_w[d]	47 038
PDI[e]	3.35

[a] **Calculated based on feed ratio**

[b] **Calculated based on the ^{1}H NMR spectrum**

[c] **The number average molecular weight as calculated from the ^{1}H NMR spectrum**

[d] **The number average and weight average molecular weight as measured by GPC analysis (calibrated with polystyrene standards)**

[e] **Polydispersity index (M_w/M_n) as measured by the GPC analysis**
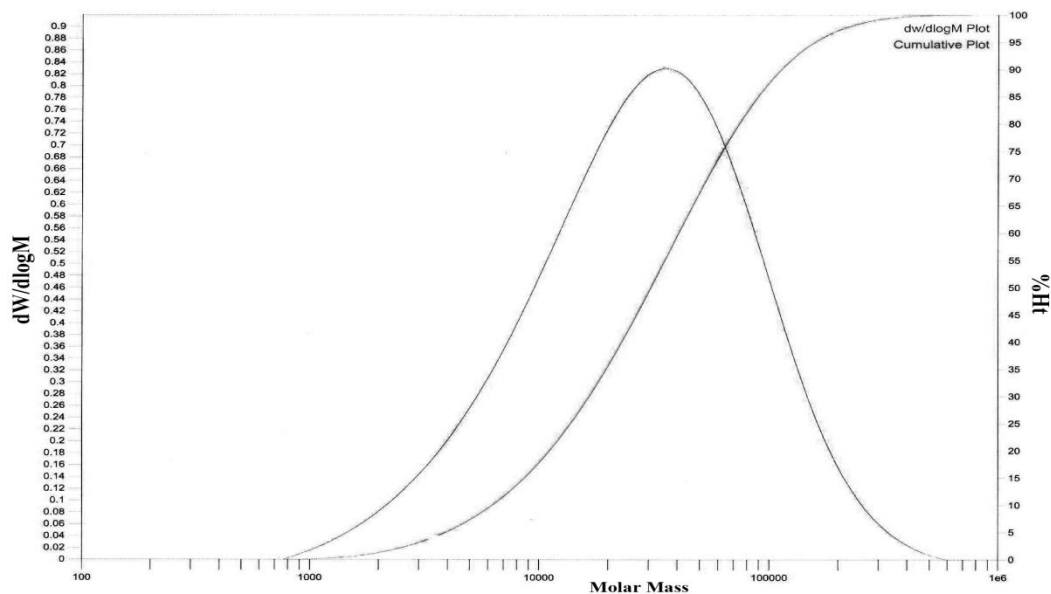
Figure 3.4. GPC chromatogram of MPEG-PCL-MPEG triblock copolymer

3.2. Properties of IgG Loaded PCL and MPEG-PCL-MPEG Microspheres

In microencapsulation process, the properties of the final products notably depend on a number of factors which are associated with the technique used. Some of the most important factors to be considered in designing protein delivery systems are reasonable encapsulation efficiency, stability of the protein, retention of biological function of the protein formulation and required dosage of the protein for therapeutic efficiency.

In literature, polymeric protein delivery systems with high encapsulation efficiencies (63-99.6%) and small sizes (5-21 µm) were obtained by using high speed homogenizers (8000-14 000 rpm) [176, 188, 189]. Besides, stability of the primary emulsion (water-in-oil) is a critical factor for increasing the encapsulation efficiency in the double emulsion-solvent evaporation method [190]. When the primary emulsion is unstable, encapsulation efficiency is low because the internal aqueous phase tends to merge with the external aqueous phase. Therefore, some emulsifying agents such as BSA, PVA, Tween-80, or Span-80 are added into the internal aqueous phase or into the polymer phase to enhance the stability of the primary emulsion [190]. For these reasons, PVA solution in the internal aqueous phase and homogenization step after secondary emulsion step were used in this study. In preliminary studies, the composition of outer aqueous phase (1% or 2% PVA), the concentration of encapsulated protein (2-10 mg/ml IgG) and outer aqueous phase parameters such as volume and components (NaCl addition to PVA solution) were

51

changed separately to obtain IgG loaded microspheres with high encapsulation efficiency and homogeneous particle size distribution.

3.2.1. Surface Morphology and Particle Size

The surface morphology of IgG loaded PCL and MPEG-PCL-MPEG microspheres before and after γ-irradiation was examined by SEM. SEM micrographs of IgG loaded microspheres are presented in Figures 3.5 and 3.6. The microspheres possessed a spherical shape with a mostly smooth surface without observable pores. There were no difference between γ-irradiated and non-irradiated microspheres of both polymers in surface morphology (Figure 3.5B-C and Figure 3.6B-C). Similar result was observed in the study of Carrascosa *et al.* [173] in which they sterilized insulin like growth factor (IGF-I) loaded PLGA microspheres with γ-irradiation. Likewise, in another study, the surface morphology of ibuprofen loaded PLGA microparticles did not change after γ-irradiation [164].

(A)   **(B)**
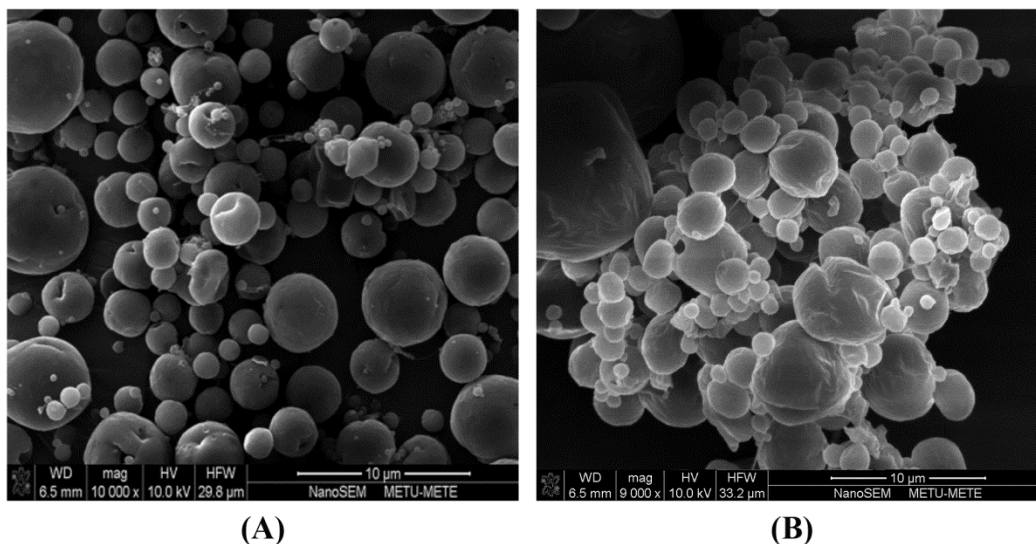
Figure 3.5. SEM images of IgG loaded microspheres: General view of PCL **(A)** and MPEG-PCL-MPEG **(B)** microspheres
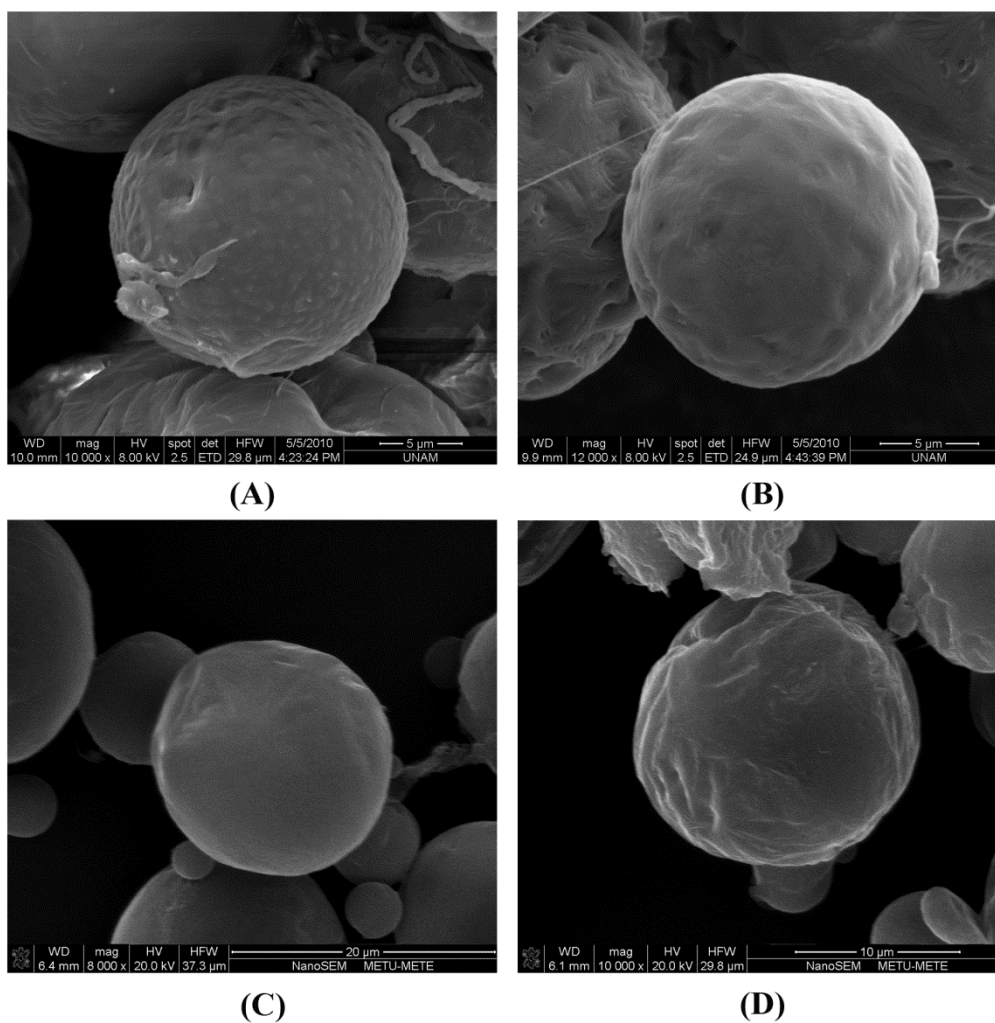
Figure 3.6. SEM images of IgG loaded microspheres: Surface of non-irradiated PCL (**A**), γ-irradiated PCL (**B**), non-irradiated MPEG-PCL-MPEG (**C**) and γ-irradiated MPEG-PCL-MPEG (**D**) microspheres

The particle size distributions of IgG loaded microspheres before and after γ-irradiation were plotted as a histogram as a total cumulative percent arithmetic curve (Figures C.1 and C.2). Accordingly, mean particle size, particle size values that involve particle sizes at 10th, 50th, and 90th percentiles and SPAN values of IgG loaded PCL and MPEG-PCL-MPEG microspheres are given in Table 3.3. No significant change in mean particle size of microspheres was observed after γ-sterilization. Similar result was given in a previous study in which the size of IGF-I loaded PLGA microspheres did not change after γ-irradiation [173]. Non-irradiated and γ-irradiated PCL microspheres had higher SPAN

53

values compared to that of non-irradiated and γ-irradiated MPEG-PCL-MPEG microspheres, which indicated broader size distribution for PCL microspheres.

Table 3.3. Comparision of particle size analysis results of IgG loaded PCL and MPEG-PCL-MPEG microspheres

	Particle Size (µm)	d[0.1] (µm)	d[0.5] (µm)	d[0.9] (µm)	Span
Non-irradiated PCL microspheres	5.99 ± 0.12	2.88	5.46	9.69	1.25
γ-irradiated PCL microspheres	5.79 ± 0.12	3.02	5.19	9.26	1.20
Non-irradiated MPEG-PCL-MPEG microspheres	6.05 ± 0.11	3.35	5.55	9.35	1.08
γ-irradiated MPEG-PCL-MPEG microspheres	5.84 ± 0.10	3.34	5.36	8.88	1.03

Data are given as mean ± S.E.
d[0.1] is the particle diameters determined respectively at the 10th percentiles of undersized particles.
d[0.5] is the particle diameters determined respectively at the 50th percentiles of undersized particles.
d[0.9] is the particle diameters determined respectively at the 90th percentiles of undersized particles.

3.2.2. Protein Loading and Encapsulation Efficiency

The protein loading and encapsulation efficiency are essential parameters, indicating the quality of the process, which is better or more efficient when a larger fraction of the drug is encapsulated. Furthermore, the knowledge of the amount of encapsulated protein is essential for calculating the cumulative amount of protein released under *in vitro* experimental conditions and in dosing the amount of protein for *in vivo* use. Evaluation of these outcomes was done using the calibration curve of IgG treated with DMSO and NaOH/SDS similar to the extraction of microspheres (Figure C.3).

IgG encapsulation efficiency and loading results of PCL and MPEG-PCL-MPEG microspheres are given in Table 3.4. Results showed that neither IgG-loading nor encapsulation efficiency did change after γ-irradiation. This result was in agreement with literature [164, 173, 174]. Another important finding was higher loading and

encapsulation efficiency values for MPEG-PCL-MPEG microspheres than those of PCL (Table 3.4). This was thought to be caused by the presence of hydrophilic MPEG segments in polymer matrix, which enhanced the affinity of IgG to the polymeric core. In a similar study, human serum albumin loaded PEG-PCL and PCL microspheres had encapsulation efficiencies of between 35.4-50.1% and 25.8% for two polymer types, respectively [122]. In another study, cytarabine loaded-microparticles were prepared by using PCL polymer alone or with MPEG-PCL diblock copolymers [191]. It was reported that use of MPEG-PCL has considerably enhanced cytarabine encapsulation efficiency (1.57% -13%) when compared to homopolymer microparticles (1.3%). These studies also explained this outcome as the increased affinity of the hydrophilic drug to the more hydrophilic polymer core in the presence of MPEG blocks.

Table 3.4. IgG-loading and encapsulation efficiency results of PCL and MPEG-PCL-MPEG microspheres before and after γ-irradiation

	Encapsulation Efficiency (%)	Loading (%)
Non-irradiated PCL microspheres	54.00 ± 1.30^a	0.27 ± 0.01^a
γ-irradiated PCL microspheres	54.23 ± 0.80^b	0.25 ± 0.02^b
Non-irradiated MPEG-PCL-MPEG microspheres	74.32 ± 3.40^a	0.35 ± 0.01^a
γ-irradiated MPEG-PCL-MPEG microspheres	74.64 ± 3.81^b	0.37 ± 0.02^b

Data are given as mean ± S.D.
[a] Statistically significant differences between non-irradiated microspheres ($p \leq 0.05$).
[b] Statistically significant differences between γ-irradiated microspheres ($p \leq 0.05$).

3.2.3. *In Vitro* Release of IgG

Release profiles of drugs from microspheres are important for evaluation of delivery systems in the respect of a therapeutic effectiveness. The *in vitro* release studies give in advance information for *in vivo* use of the delivery system. In this study, release experiments were conducted for 3 months as it is aimed to develop a controlled delivery system that will provide sustained release of a protein for at least 3 months *in vivo*. In addition, the influence of γ-sterilization on release rate and on bioactivity of released IgG was also studied to evaluate therapeutic effectiveness of the system. The calibration curve for μBCA assay used in calculations of total IgG was constructed with different concentrations of IgG (0-20 μg/ml) in release medium (Figure C.4). For biologically

active IgG, ELISA method was applied in the calibration curve which was constructed with different concentration of IgG (0-4.44 ng/ml) (Figure C.5).

The cumulative release profiles of microspheres are given in Figures 3.7A and B for total and biologically active IgG amounts, respectively. Moreover, these amounts of IgG release from non-irradiated microspheres were also compared with those of γ-irradiated microspheres specifically at 6h, 20-day, and 90-day release periods (Table 3.5). The cumulative total IgG release profiles of γ-irradiated and non-irradiated PCL and MPEG-PCL-MPEG microspheres were similar (Figure 3.7A). When γ-irradiated and non-irradiated PCL microspheres were compared, no significant difference between groups was observed in total amounts of IgG release at the end of 20 day. However, a significant increase in the cumulative amount of IgG released from γ-irradiated MPEG-PCL-MPEG microspheres was observed compared to non-irradiated MPEG-PCL-MPEG microspheres at the end of 20 day (Table 3.5). Furthermore, total amounts of IgG released from γ-irradiated PCL microspheres were found significantly lower than that of IgG released from γ-irradiated and non-irradiated MPEG-PCL-MPEG microspheres. At the end of 90 day release, no significant difference was observed for the released total amounts of IgG among groups. When the amounts of IgG released from non-irradiated microspheres were compared, presence of MPEG segment in PCL matrix did not change the total amount of IgG released. However, γ-irradiated PCL microspheres showed a slower release profile compared to γ-irradiated MPEG-PCL-MPEG microspheres. In a previous study, the group synthesized MPEG-PLA copolymer and prepared paclitaxel loaded nanoparticles [192]. They observed that MPEG-PLA nanoparticles exhibited a much faster release rate compared to that of PLGA nanoparticles. During first 7 days, 85% paclitaxel was released from MPEG-PLA nanoparticles whereas only 30% paclitaxel was released from PLGA nanoparticles in 1 month. In the study of Li *et al.* [143], MPEG-PCL di-block and PCL-PEG-PCL triblock copolymers with different MPEG/PCL ratio were used to prepare nanoparticles for local delivery of tetradrine, a bis-benzylisoquinoline alkaloid with an anti-tumor effect *in vitro* and *in vivo*. The nanoparticles prepared from triblock copolymers exhibited a more sustained-release pattern compared to their diblock counterparts due to the differences between the "brush" structure for diblock copolymers and "mushroom" structure for triblock copolymers in aqueous solution. For obtaining more prolonged and sustained delivery of IgG, MPEG-PCL-MPEG triblock copolymer which is more hydrophilic than PCL-PEG-PCL triblock copolymer was chosen to prepare IgG loaded microspheres instead of their diblock counterparts in this study.

The amounts of biologically active IgG released from γ-irradiated and non-irradiated microspheres (Figure 3.7B) were found to be lower than the total amount released from the γ-irradiated and non-irradiated microspheres (Figure 3.7A). ELISA depends on the specific antigen-antibody binding and therefore, measures only the amount of biologically active proteins. Therefore, the released amounts of IgG determined by ELISA were found lower than amounts determined by μBCA which measures both active and inactive proteins. When the amounts of biologically active IgG released from non-irradiated

56

microspheres were compared, total amount of biologically active IgG released from MPEG-PCL-MPEG microspheres was found significantly higher than that of biologically active IgG released from PCL microspheres at all time periods (Figure 3.7 and Table 3.5). This result showed that MPEG segment of copolymer provides further protection on protein during microsphere preparation. In a previous study, they encapsulated nerve growth factor with PEG 400 in PLGA microspheres to protect the stability of nerve growth factor [193]. PEG 400 displaced the protein from the w/o interface and protected it from denaturation upon contact with the organic phase.

The total amount of biologically active IgG released from γ-irradiated PCL microspheres was significantly lower than that of IgG released from other microsphere groups at all time periods. Total amount of biologically active IgG released from non-irradiated and γ-irradiated MPEG-PCL-MPEG microspheres were found significantly higher than that of IgG released from non-irradiated and γ-irradiated PCL microspheres at all-time points. These results were thought to be also related with total crystallinity of the PCL being about two times the crystallinity of MPEG-PCL-MPEG shown in DSC results.

The ratios of the amount of biologically active IgG released from microspheres to the total amount of IgG released from microspheres are given in Table 3.6. Bioactivity of IgG released from non-irradiated PCL and MPEG-PCL-MPEG microspheres was protected completely at the end of 6 h. As mentioned before, PVA addition to the inner phase during microsphere preparation improved the primary emulsion stability and prevented the deleterious effects on protein stability originating from the presence of the water/organic solvent interface. Moreover, presence of MPEG segment at MPEG-PCL-MPEG microspheres provided further protection on IgG when microspheres were exposed to γ-irradiation.

At the end of 90 day release study, 30±2% and 57±3% of the bioactivity of IgG released from non-irradiated PCL and MPEG-PCL-MPEG microspheres were protected, respectively. On the other hand, 20±3% and 49±2% of the bioactivity of IgG released from γ-irradiated PCL and MPEG-PCL-MPEG microspheres were protected, respectively. In a previous study, IgG was encapsulated into PLGA microspheres by using double emulsion or solid-in-oil-in-water (s/o/w) method without adding any excipient and evaluated the ratios of IgG detected by ELISA to IgG detected by high-performance liquid chromatography (HPLC) to determine the changes in the bioactivity of IgG [194]. They observed only 37% bioactivity in the initial release samples from s/o/w microspheres and 20% bioactivity from double emulsion microspheres. However, in this study, loss of bioactivity of IgG released from non-irradiated and γ-irradiated MPEG-PCL-MPEG (57% and 49%, respectively) at the end of 90 days was found lower than that observed for IgG released from non-sterilized PLGA microspheres at the end of 2 h in the study of Wang *et al*. prepared by (s/o/w) method (63%) and by double emulsion (80%).
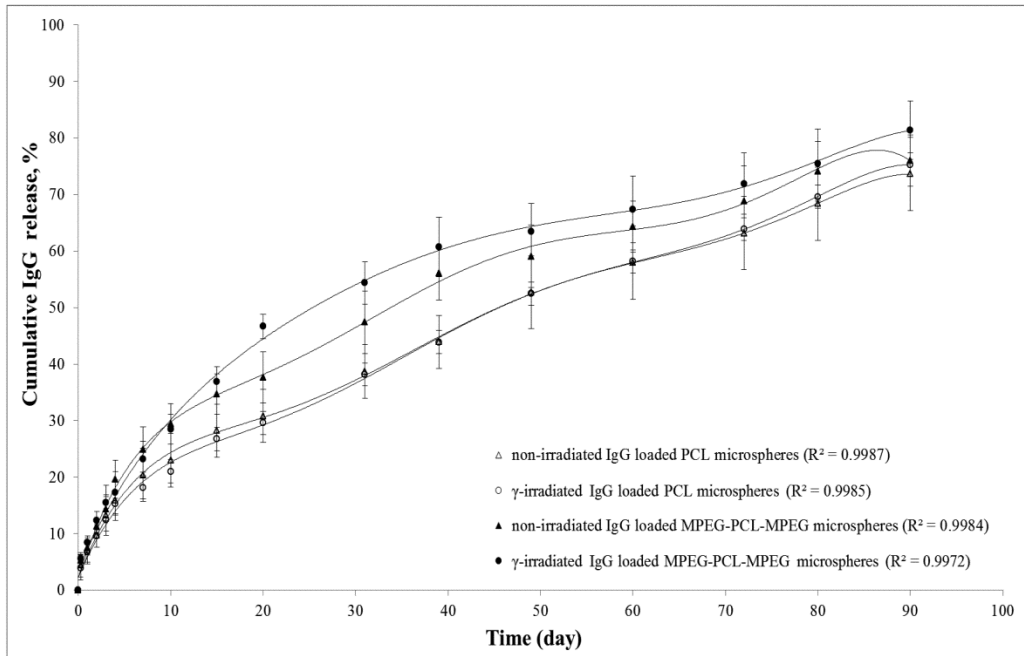
(A)
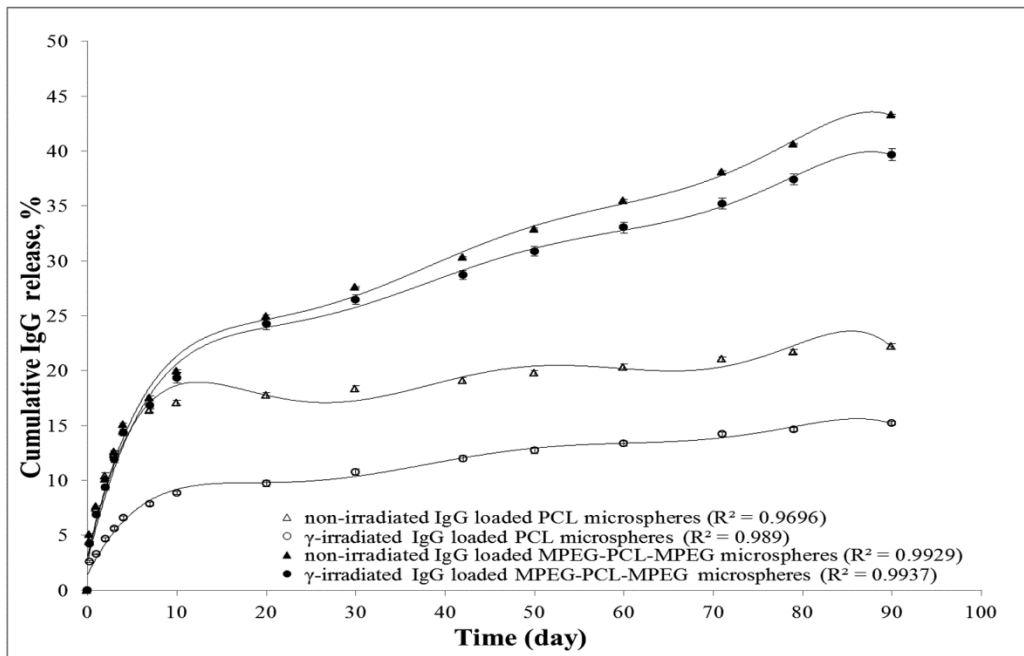
(B)

Figure 3.7. Cumulative release profile of IgG loaded PCL and MPEG-PCL-MPEG microspheres in release medium for 90 days determined by μBCA assay **(A)** and ELISA **(B)** (Data were as mean ± S.D.)

Table 3.5. Cumulative % IgG release from γ-irradiated and non-irradiated PCL and MPEG-PCL-MPEG microspheres determined by µBCA assay and ELISA at the end of 6 h, 20 and 90 days

	Non-irradiated PCL microspheres	γ-irradiated PCL microspheres	Non-irradiated MPEG-PCL-MPEG microspheres	γ-irradiated MPEG-PCL-MPEG microspheres
µBCA Assay				
6h	4.5 ± 2.2	3.9 ± 2.0	5.3 ± 1.1	5.6 ± 0.6
20 day	30.8 ± 4.7	29.6 ± 2.0^{a}	37.7 ± 4.5^{b}	$46.7 \pm 2.2^{a,b}$
90 day	73.9 ± 6.5	75.3 ± 2.1	76.0 ± 4.5	81.4 ± 5.1
ELISA				
6h	4.4 ± 0.03^{c}	$2.6 \pm 0.1^{a,c}$	5.1 ± 0.1^{b}	$4.2 \pm 0.1^{a,b}$
20 day	17.5 ± 0.3^{c}	$9.7 \pm 0.3^{a,c}$	25.0 ± 0.1^{b}	$24.2 \pm 0.5^{a,b}$
90 day	22.2 ± 0.3^{c}	$15.2 \pm 0.2^{a,c}$	43.3 ± 0.1^{b}	$39.7 \pm 0.5^{a,b}$

Data were as mean ± S.D.

[a]Statistical significances between the % IgG released from γ-irradiated PCL and γ-irradiated MPEG-PCL-MPEG microspheres by using same protein determination method at the same time period ($p \leq 0.05$).

[b] Statistical significances between the % IgG released from non-irradiated and γ-irradiated MPEG-PCL-MPEG microspheres by using same protein determination method at the same time period ($p \leq 0.05$).

[c] Statistical significances between the % IgG released from non-irradiated and γ-irradiated PCL microspheres by using same protein determination method at the same time period ($p \leq 0.05$).

Table 3.6. The ratio of the amount of biologically active IgG released from γ-irradiated and non-irradiated PCL and MPEG-PCL-MPEG microspheres to the total amount of IgG released

	Ratio of the amount of biologically active released protein to the amount of total released protein		
	6 h	20 day	90 day
Non-irradiated PCL microspheres	0.99 ± 0.06 [a]	0.58 ± 0.02 [a,c]	0.30 ± 0.02 [a,c]
γ-irradiated PCL microspheres	0.67 ± 0.02 [a,b]	0.33 ± 0.01 [a,b]	0.20 ± 0.03 [a,b]
Non-irradiated MPEG-PCL-MPEG microspheres	0.97 ± 0.04	0.66 ± 0.03 [c,d]	0.57 ± 0.03 [c,d]
γ-irradiated MPEG-PCL-MPEG microspheres	0.75 ± 0.03 [b]	0.52 ± 0.01 [b,d]	0.49 ± 0.02 [b,d]

Data were as mean ± S.D.
[a] Statistical significances between the value of non-irradiated and γ-irradiated PCL microspheres at the same time period ($p \leq 0.05$).
[b] Statistical significances between the value of γ-irradiated PCL and γ-irradiated MPEG-PCL-MPEG microspheres at the same time period ($p \leq 0.05$).
[c] Statistical significances between the value of non-irradiated PCL and non-irradiated MPEG-PCL-MPEG microspheres at the same time period ($p \leq 0.05$).
[d] Statistical significances between the value of non-irradiated and γ-irradiated MPEG-PCL-MPEG microspheres at the same time period ($p \leq 0.05$).

3.2.4. Kinetics of IgG Release

In vitro release data of PCL or MPEG-PCL-MPEG microspheres in PBS were fitted to Higuchi, Korsmeyer–Peppas, first, and zero-order release models to find out the mechanism of total IgG release from microspheres. The coefficient of determination (R^2), rate constants (k_0, k_1, k_H and k_P) and n values obtained after linear regression on mathematical models are presented in Table 3.7. R^2 values showed that the best-fits were generally obtained in Higuchi and Korsmeyer-Peppas models rather than zero-order and first-order models. In Higuchi approach, the cumulative amounts of IgG released from microspheres were proportional to square root of time, indicating that release from microspheres was governed by diffusion. Diffusion controlled release was also confirmed by fitting the release data to Korsmeyer–Peppas model, a generalized formula derived from the Higuchi equation. Korsmeyer–Peppas model is limited to the first 60% of the cumulative amount of drug release and the release exponent (n) is used to characterize

release mechanism. If n is 0.43, it means that release mechanism follows Fickian diffusion, and higher values for mass transfer ($0.43 < n < 0.85$) shows that release follows a non-Fickian model which is denominated as anomalous transport [150]. For the values of n higher than 0.85, polymer swelling is solely the release rate controlling mechanism and zero order drug release kinetics is observed [150]. n values for both γ-irradiated and non-irradiated microsphere groups were above 0.43 indicating IgG release was governed by an anomalous transport. This revealed that the water transport mechanism was mainly due to the combination of both diffusion through polymeric matrix and surface erosion of PCL and MPEG-PCL-MPEG microspheres incubated in PBS for 90 days.

Table 3.7. *In vitro* release kinetic parameters of IgG loaded PCL and MPEG-PCL-MPEG microspheres before and after γ-sterilization

		Non-irradiated PCL microspheres	γ-irradiated PCL microspheres	Non-irradiated MPEG-PCL-MPEG microspheres	γ-irradiated MPEG-PCL-MPEG microspheres
µBCA Assay					
Zero order					
	k_0	0.031	0.033	0.033	0.035
	R^2	0.96	0.97	0.91	0.89
First order					
	k_1	0.0006	0.0006	0.0006	0.0006
	R^2	0.99	0.99	0.98	0.98
Higuchi					
	k_H	1.54	1.58	1.66	1.77
	R^2	1.00	0.99	0.99	0.99
Korsmeyer-Peppas					
	k_p	1.32	1.21	1.46	1.49
	n	0.52	0.53	0.52	0.54
	R^2	0.99	1.00	0.98	0.98

Protein release from biodegradable polymeric microspheres can be controlled by two main mechanisms: diffusion of the protein out of microsphere and erosion of the polymer matrix surface. However, polymer hydrolysis and polymeric matrix erosion of PCL is

slower than that of MPEG-PCL-MPEG. Therefore, diffusion can be the more dominant factor affecting IgG release kinetics from PCL microspheres. On the other hand, release of IgG from MPEG-PCL-MPEG microspheres was controlled by diffusion and polymer erosion during 90 days, which is in agreement with the results of SEM analysis after degradation study given in Figure 3.8. Significant defects were observed on the surface of IgG loaded MPEG-PCL-MPEG microspheres compared to the surface of IgG loaded PCL microspheres at the end of 6 month PBS incubation. Moreover, k_H values for IgG release from γ-irradiated and non-irradiated PCL microspheres were found lower than that for IgG release from MPEG-PCL-MPEG microspheres (Table 3.7). This correlated well with the *in vitro* release profile of IgG from microspheres, in which IgG release from γ-irradiated and non-irradiated PCL microspheres showed a slower release profile compared to that from γ-irradiated and non-irradiated MPEG-PCL-MPEG microspheres.

3.2.5. IgG Stability

Most proteins fold into unique 3-dimensional structure and this structure is organized hierarchically from so-called primary structure to quaternary structure. Denaturation of proteins involves the disruption and possible destruction of both the secondary and tertiary structures. In secondary structure loss, protein loses all regular repeating patterns as alpha-helices and beta-pleated sheets, and adopts a random coil configuration. Loss of tertiary structure involves the disruption of covalent, noncovalent dipole-dipole and van der Waals interactions between amino acid side chains. If only tertiary structure is destroyed and primary and secondary structures are protected, this denaturation is reversible (proteins can regain their native state). If both secondary and tertiary structures are destroyed, this denaturation is irreversible and protein loses its bioactivity. When encapsulating proteins in polymeric microspheres, the protein must maintain its three-dimensional structure to exhibit its biological activity for an effective treatment.

The changes in secondary structure of IgG encapsulated in PCL and MPEG-PCL-MPEG microspheres before and after γ-irradiation were evaluated by FT-IR spectroscopy after extraction of IgG from microspheres as done by Emami *et al*. [179] and the amide I region of the spectra (1700–1600 cm^{-1}) was used for analyzing protein secondary structure [180]. Besides, the standard IgG solution and the supernatants from the extraction of empty PCL and MPEG-PCL-MPEG microspheres were also examined by FT-IR spectroscopy. The FT-IR spectra of standards and samples are given in Figure C.6. The bands at around 1656 cm^{-1} in the amide I region has been identified as carbonyl stretching of α-helices in secondary structure [195]. When supernatants from the extraction of empty microspheres were examined, C=O stretching vibrations of the PCL and MPEG-PCL-MPEG polymers at about 1720 cm^{-1} were distinctly separated from the amide I vibration region 1600–1700 cm^{-1} and no peaks were observed at this region. No shifts were observed at the

wavelength of FT-IR bands related with α-helices structure of IgG released from γ-irradiated and non-irradiated PCL and MPEG-PCL-MPEG microspheres. The stability of IgG has been protected during the microsphere preparation steps. However, a decrease was observed in the intensity of FT-IR bands of samples compared to the IgG standard. It was thought that the extraction medium containing DMSO and strong alkaline base could have affected the secondary structure of released IgG and caused a decrease in the intensity of FT-IR bands of samples.

The α-helix contents of IgG released from PCL or MPEG-PCL-MPEG microspheres before and after γ-irradiation were also compared with the α-helix content of IgG standard solution in Table 3.8. FT-IR analysis showed that IgG has an α-helix content of $12.58 \pm 0.12\%$. This result is in agreement with the result obtained in a previous study, in which they prepared IgG loaded PLGA microspheres and examined the secondary structure of IgG with FT-IR analysis [194]. They observed that IgG has an α-helix content of $12.4 \pm 0.6\%$. No significant changes between the α-helix content of IgG encapsulated in microspheres before γ-irradiation were observed (Table 3.8). When the results of non-irradiated microspheres were compared with that of IgG standard solution, the stability of IgG has been protected during the microsphere preparation steps. On the other hand, after γ-irradiation there was a significant decrease at the % of α-helix content of encapsulated IgG in both groups. These results were in agreement with the results of ELISA given in Table 3.6. Decrease in % of α-helix content of IgG encapsulated in PCL microspheres was significantly higher than that of IgG encapsulated in MPEG-PCL-MPEG microspheres after γ-irradiation. This showed that IgG stability was protected more efficiently in MPEG-PCL-MPEG microspheres compared to PCL microspheres during γ-irradiation.

Table 3.8. Secondary structure of IgG standard solution and IgG in PCL or MPEG-PCL-MPEG microspheres

Formulations	α-Helix Content in Amide I region (%)
Standard IgG Solution	12.58 ± 0.12[a,c]
IgG in non-irradiated PCL microspheres	12.72 ± 0.30[b,d]
IgG in γ-irradiated PCL microspheres	9.32 ± 0.11[a,b,f,g]
IgG in non-irradiated MPEG-PCL-MPEG microspheres	12.66 ± 0.26[e,g]
IgG in γ-irradiated MPEG-PCL-MPEG microspheres	10.52 ± 0.13[c,d,e,f]

Data were as mean ± S.D.
[a,b,c,d,e,f,g] **Statistically significant differences between groups.**

3.2.6. *In Vitro* Degradation

The knowledge of the degradation properties of the biodegradable polymers is important to prepare microparticulate delivery systems with suitable drug release rates. The degradation studies of γ-irradiated and non-irradiated IgG loaded PCL and MPEG-PCL-MPEG microspheres were conducted in PBS over a period of 6 months.

At the end of PBS incubation for 6 months, surface morphologies of microspheres (Figure 3.8A-D) were compared with those of microspheres that were not incubated in PBS (Figure 3.5B-C and 3.6B-C). Non-irradiated and γ-irradiated PCL and MPEG-PCL-MPEG microspheres possessed a spherical shape with a rough surface before the degradation study. At the end of degradation study, it was observed that microspheres maintained their spherical shape, but their surfaces were rougher with some defects. Especially, significant defects were observed at the surface of γ-irradiated MPEG-PCL-MPEG microspheres loaded with IgG at the end of incubation.
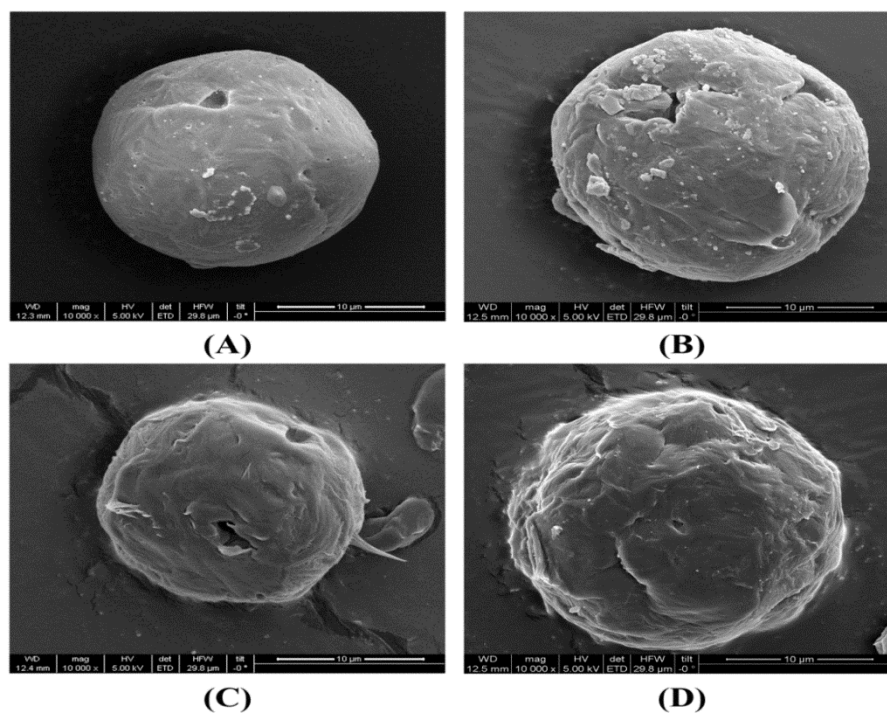
Figure 3.8. SEM images of IgG loaded PCL and MPEG-PCL-MPEG microspheres after degradation study**:** Surfaces of **A)** non-irradiated PCL microsphere, **B)** γ-irradiated PCL microsphere, **C)** non-irradiated MPEG-PCL-MPEG microsphere, **D)** γ-irradiated MPEG-PCL-MPEG microsphere

The particle size distributions of IgG loaded microspheres before and after degradation study were plotted as a histogram as a total cumulative percent arithmetic curve (Figures C.1, C.2, C.7, and C.8). At the end of 6 month incubation, no significant changes were observed in the particle sizes of non-irradiated and γ-irradiated MPEG-PCL-MPEG and PCL microspheres loaded with IgG (Table 3.3 and 3.9). Before degradation study non-irradiated and γ-irradiated MPEG-PCL-MPEG microspheres loaded with IgG showed narrower (homogeneous) size distributions compared to PCL microsphere counterparts. After degradation study, SPAN values of all groups were found lower than 1, indicating narrow (homogeneous) size distributions for all microsphere groups.

Table 3.9. Mean particle sizes of non-irradiated and γ-irradiated PCL and MPEG-PCL-MPEG microspheres loaded with IgG after degradation study

	Particle Size (µm)	d[0.1] (µm)	d[0.5] (µm)	d[0.9] (µm)	Span
Non-irradiated PCL microspheres	5.91 ± 0.10	3.06	5.84	8.39	0.91
γ-irradiated PCL microspheres	5.94 ± 0.09	3.44	5.63	8.94	0.98
Non-irradiated MPEG-PCL-MPEG microspheres	5.78 ± 0.09	3.19	5.59	8.73	0.99
γ-irradiated MPEG-PCL-MPEG microspheres	5.61 ± 0.08	3.43	5.29	8.34	0.93

Data are given as mean ± S.E.
d[0.1] is the particle diameters determined respectively at the 10th percentiles of undersized particles.
d[0.5] is the particle diameters determined respectively at the 50th percentiles of undersized particles.
d[0.9] is the particle diameters determined respectively at the 90th percentiles of undersized particles.

The changes in the chemical structure of γ-irradiated and non-irradiated microspheres before and after degradation study were also examined by FT-IR analysis (Figures C.9 and B.10). Generally, no significant difference was found between the FT-IR spectra of γ-irradiated and non-irradiated microspheres before and after degradation. However, a band at 3329.47 cm^{-1} was more pronounced in the FT-IR spectrum of γ-irradiated MPEG-PCL-MPEG microspheres loaded with IgG compared to that of other groups at the end of degradation study. This band could be related with hydroxyl and carboxyl end groups formed after chain breaking. In the study of Li *et al.* [196], degradation of PEO-PCL multiblock copolymers was investigated at 37ºC in a phosphate buffer. Similarly, they

observed that FT-IR band at 3520 cm^{-1} related with hydroxyl and carboxyl end groups formed after chain breaking of PCL segment was more pronounced after 11 weeks.

The changes in the molecular weights of non-irradiated and γ-irradiated microspheres before and after degradation study were determined with GPC analysis. The number average molecular weight (M_n) and weight average molecular weight (M_w) values of microspheres are given in Table 3.10. According to the GPC results, M_n value of IgG loaded PCL microspheres decreased after γ-irradiation while M_w value of these microspheres increased. The decrease in the M_n value can be explained by chains being broken and the increase in the M_w value can be due to cross-linking. In a previous study, the effects of γ-sterilization on PCL properties were evaluated and it was observed that γ-sterilization caused an increase in M_w and decrease in M_n [197]. γ-irradiation could induce the polymer chain scission reactions, preferentially in the amorphous regions and the cross-linking of chains [197, 198]. After γ-irradiation, M_n value of IgG loaded MPEG-PCL-MPEG microspheres decreased while M_w value of these microspheres did not change. In the study of Dorati *et al*. [199], the effects of different γ-irradiation doses (5, 15, 25 and 50 kGy) on poly(ethylene glycol)-co-poly(d,l lactide) (PEGd,lPLA) and PEG-PLGA polymers were studied and it was observed that M_n reduction (%) of multiblock copolymers was bigger than M_w reduction at all the γ-irradiation doses. They concluded that degradation reaction induced by γ-irradiation is predominantly based on unzipping mechanism. This unzipping mechanism which primary affected the terminal groups of polymer chains causes a faster decay of the M_n value compared to M_w value.

No changes in M_n and M_w values of non-irradiated and γ-irradiated PCL microspheres were observed at the end of 6 months. This was an expected outcome for the known long degradation time of PCL due to its high degree of crystallinity and hydrophobicity.Although, no changes were observed in M_n and M_w values of non-irradiated MPEG-PCL-MPEG microspheres, higher decreases were observed at these values of γ-irradiated form of these microspheres at the end of 6 months. This was due to the presence of MPEG segments which was more sensitive to oxidative degradation during γ-irradiation [200]. In a previous study, the nature and the concentration of free radicals formed upon exposure of PEGd,lPLA and PEG-PLGA multiblock copolymers to 25 kGy γ-irradiation dose were evaluated [201]. They reported that when oxygen molecules enter into the amorphous region of polymer, they react with free hydrogen atoms which increase amorphous regions and create cracks thereby leading to a reduction in Mw and Mn values during γ-irradiation.

Changes in pH of release medium affect both polymer degradation rate and stability of the protein released from the polymer matrix [202]. Acidic and alkaline media are known to accelerate polymer degradation. Also, pH of solution has a great influence on protein conformation and acidic pH may aggregate some proteins. For these reasons, pH of release medium containing γ-irradiated or non-irradiated microspheres was measured at regular intervals. During 6 months, no significant pH changes were observed and pH

values were in the range of 7.38 – 7.41 (Figure 3.9). PCL and MPEG-PCL-MPEG microspheres can be considered suitable for protein delivery due to not generating an acidic environment.

Table 3.10. Number average molecular weight (M_n) and weight average molecular weight (M_w) of non-irradiated and γ-irradiated PCL and MPEG-PCL-MPEG microspheres loaded with IgG before and after degradation study

	M_n (g/mol)	M_w (g/mol)
BEFORE DEGRADATION		
Non-irradiated PCL microspheres	29 250	69 702
γ-irradiated PCL microspheres	10 072	73 866
Non-irradiated MPEG-PCL-MPEG microspheres	20 007	56 089
γ-irradiated MPEG-PCL-MPEG microspheres	16 275	55 349
AFTER DEGRADATION		
Non-irradiated PCL microspheres	27 350	65 702
γ-irradiated PCL microspheres	9678	70 678
Non-irradiated MPEG-PCL-MPEG microspheres	17 784	51 686
γ-irradiated MPEG-PCL-MPEG microspheres	10 978	46 920
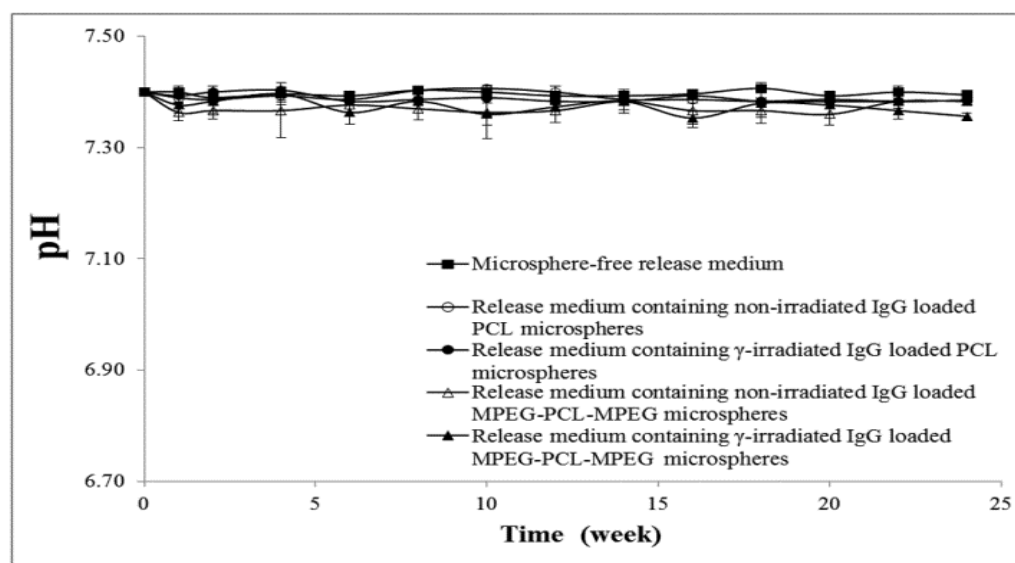
Figure 3.9. pH changes of microsphere-free release medium and release medium of microspheres during 6 months (Values are shown as mean ± S.D.)

3.2.7. *In Vitro* Cytotoxicity

Solvents commonly used in the double emulsion-solvent evaporation method, such as methylene chloride or chloroform, may remain at trace amounts in the microspheres, and may cause some toxic effects [191, 203]. Therefore, *in vitro* cytotoxicity experiments were carried out to investigate the cytotoxic effects arising from the microsphere preparation method.

The morphological changes in 3T3 cells were studied with microscopic examination. 20x phase contrast images of control cells and cells incubated with γ-irradiated empty PCL and MPEG-PCL-MPEG microspheres for 2 days are given in Figure 3.10. No morphological differences were observed between control group cells and cells incubated with microspheres.

(A)

(B)

(C)
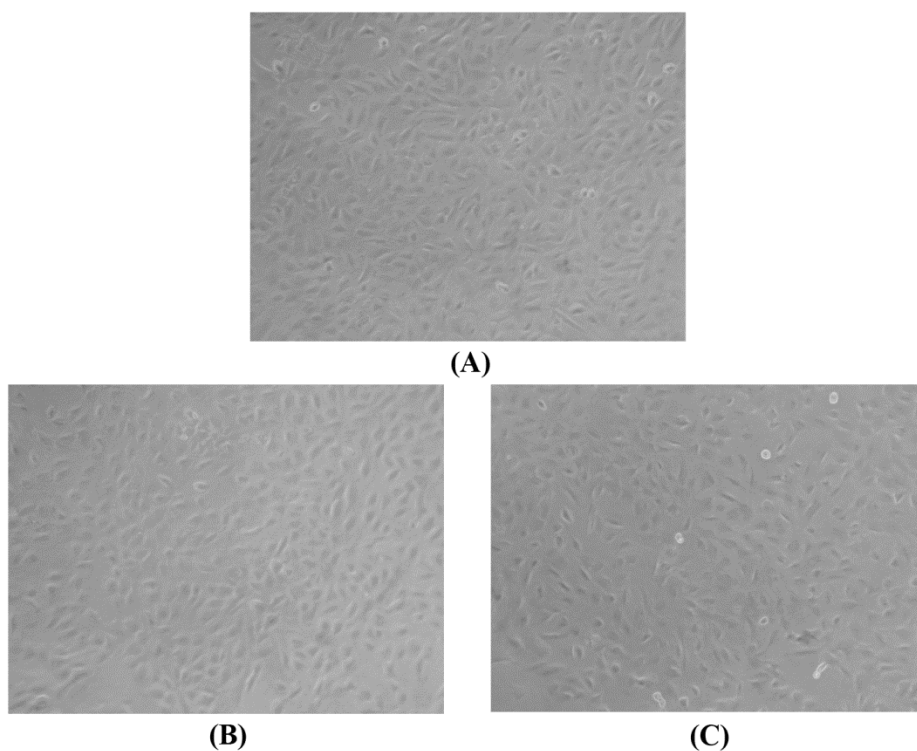
Figure 3.10. Phase contrast micrographs of **(A)** control group 3T3 cells **(B)** cells incubated with PCL microspheres **(C)** cells incubated with MPEG-PCL-MPEG microspheres for 2 days (20x magnification)

To evaluate the cytotoxicity of PCL and MPEG-PCL-MPEG microspheres, the MTT viability assay was also performed using 3T3 fibroblast cell line. The viability of the cells incubated with γ-irradiated empty PCL and MPEG-PCL-MPEG microspheres was compared with that of control group (Figure 3.11). The MTT assay results showed that microspheres did not present cytotoxic effect to cells as all showed cellular viability near to that of the control group.
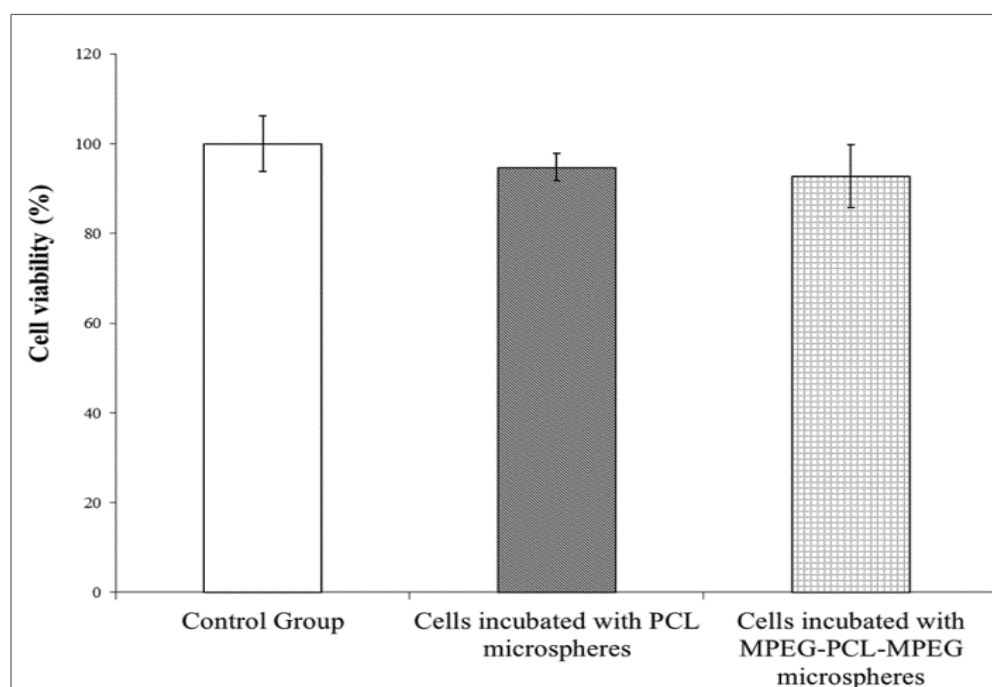
Figure 3.11. Relative cell viability after incubation with PCL or MPEG-PCL-MPEG microspheres for 2 days compared to control group (Values are shown as mean ± S.D.)

The cytotoxic effects were also evaluated by determining the changes in cell number after incubation of 3T3 cells with microspheres for 2 days. The cell numbers of control group and microsphere groups were determined by fluorometric quantitation of DNA. A calibration curve was constructed with measuring the fluorescence of different concentrations of calf thymus DNA in TNE buffer to determine the amounts of DNA in all groups (Figure C.11). Measured amounts of total DNA/well were then converted into cell number using the ratio of 7.2 pg DNA per mammalian cell (Figure 3.12). The fluorometric assay results showed that there was no significant difference between cell numbers of control and 3T3 cells incubated with γ-irradiated empty PCL and MPEG-

PCL-MPEG microspheres. In agreement with the MTT results and microscopic examinations, fluorometric assay results showed that microspheres did not present cytotoxic effect on cells.
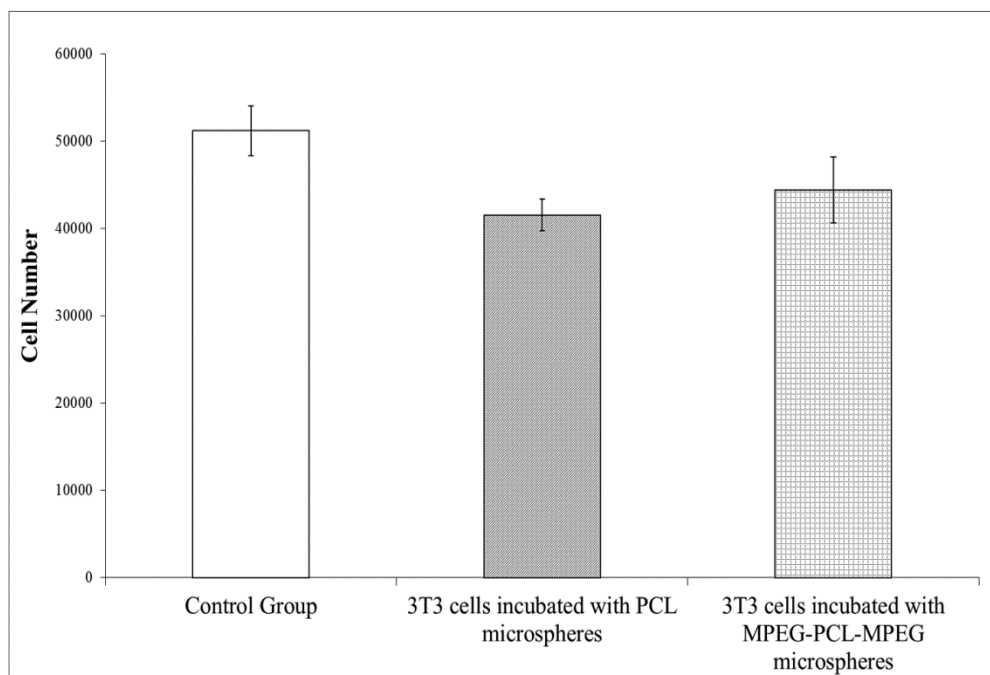
Figure 3.12. Cell numbers of 3T3 cells in control group and PCL and MPEG-PCL-MPEG microsphere groups after 2 day incubation (Data were as mean ± S.D.)

3.3. Properties of ETN Loaded PCL and MPEG-PCL-MPEG Microspheres

In preliminary studies, three alternative concentrations (10, 25 and 50 mg/ml) of ETN were used to prepare ETN loaded PCL microspheres. After preparation of these microspheres, the influence of different initial ETN concentrations on encapsulation efficiency, loading, and ETN release profile in PBS were evaluated.

PCL microspheres with prepared 25 or 50 mg/ml initial concentrations of ETN had significantly higher encapsulation efficiencies and loading values compared to microspheres with 10 mg/ml initial concentration of ETN (Table 3.11). This trend was also present between PCL microspheres prepared with 50 mg/ml and 25 mg/ml ETN for

the loading outcomes. However, no significant difference was observed between encapsulation efficiencies of PCL microspheres loaded with 25 or 50 mg/ml ETN.

Table 3.11. ETN-loading and encapsulation efficiencies of PCL microspheres with different concentrations of ETN solution

	Encapsulation Efficiency (%)	Loading (%)
10 mg/ml ETN loaded PCL microspheres	$50.29 \pm 3.03^{a, b}$	$0.26 \pm 0.02^{a,b}$
25 mg/ml ETN loaded PCL microspheres	65.37 ± 1.80^{a}	$0.82 \pm 0.01^{a,c}$
50 mg/ml ETN loaded PCL microspheres	60.09 ± 4.56^{b}	$1.53 \pm 0.13^{b,c}$

Data are given as mean ± S.D.
[a,b,c] Statistically significant differences between groups for same properties ($p \leq 0.05$).

In vitro ETN release profiles of PCL microspheres prepared with different protein concentrations (10, 25 and 50 mg/ml) were evaluated in PBS and cell culture medium. ETN release study in PBS was conducted for 7 days using non-irradiated PCL microspheres prepared with different ETN concentrations and amounts of ETN released from microspheres were determined by μBCA assay and ELISA (Figure 3.13). ETN release profiles of all groups were similar and the result was in accordance with loading encapsulation efficiency outcomes. The total and biologically active amount of ETN released from microspheres of the two high concentrations (25 mg/ml and 50 mg/ml) was significantly higher than that of microspheres loaded with 10 mg/ml ETN for 7-day period. However, no significant differences were observed between the total and biologically active amounts of ETN released from microspheres loaded with 25 and 50 mg/ml ETN at the end of 7 days.

According to these results, 25 mg/ml ETN concentration was chosen to prepare the ETN loaded PCL and MPEG-PCL-MPEG microspheres because they had the highest encapsulation efficiency and loading among groups and the total and biologically active amounts of ETN released from these microspheres were also high.
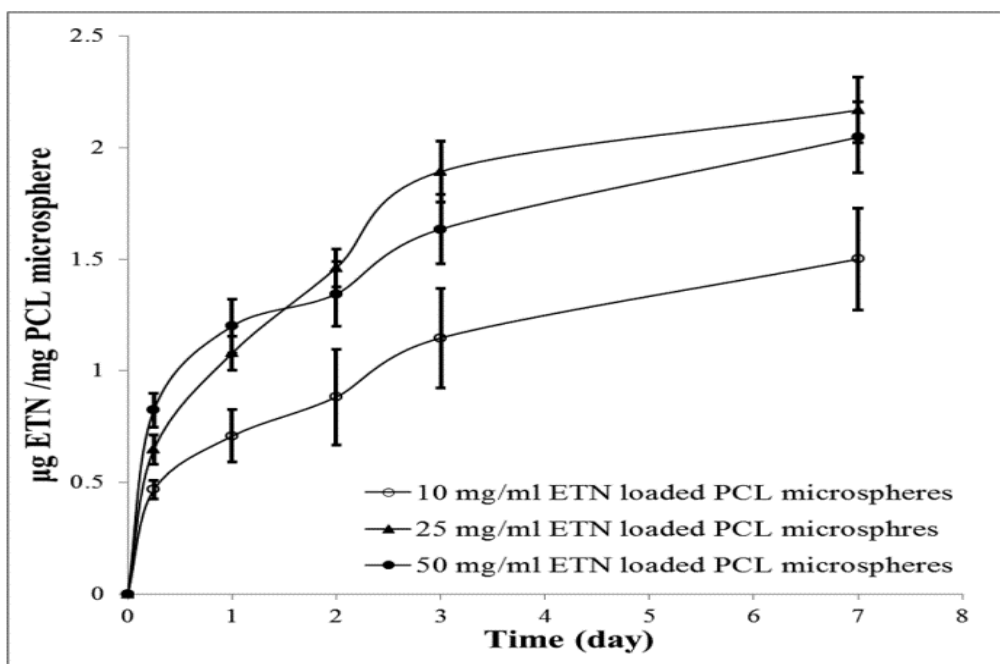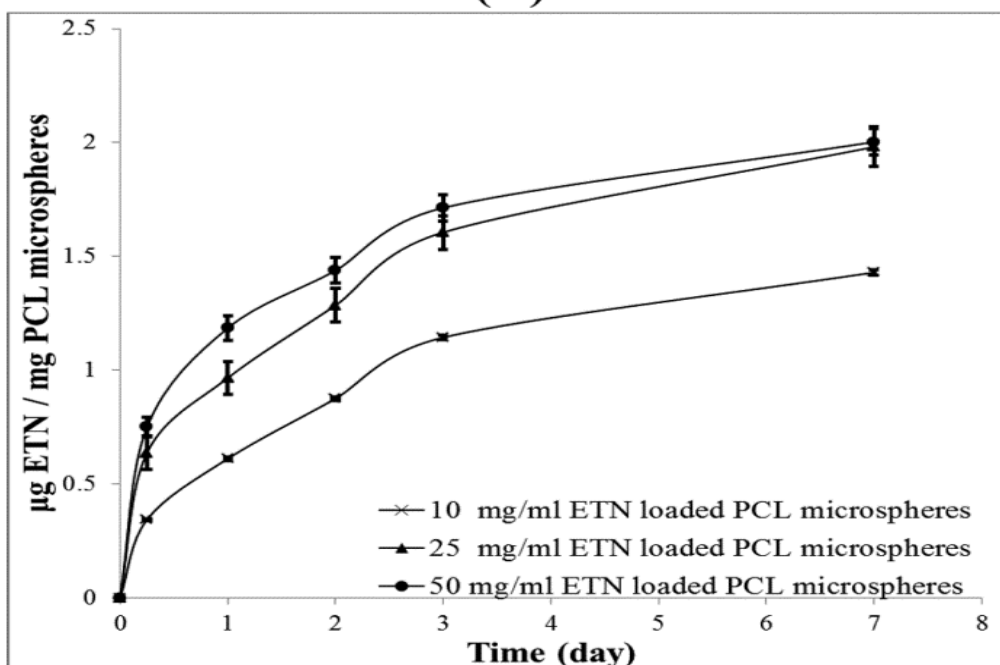
Figure 3.13. 7-day cumulative release profiles of ETN loaded PCL microspheres loaded with different protein concentrations (10, 25 and 50 mg/ml) in PBS determined by μBCA assay **(A)** and ELISA **(B)** (Data were as mean ± S.D.)

3.3.1. Surface Morphology and Particle Size

The surface morphologies of ETN loaded PCL or MPEG-PCL-MPEG microspheres were examined by SEM after γ-sterilization (Figure 3.14). Both microsphere groups possessed spherical shape with smooth surface and without observable pores.

The particle size distributions of γ-irradiated PCL and MPEG-PCL-MPEG microspheres loaded with ETN were plotted as a histogram (Figure D.1). In addition, mean particle sizes, particle sizes at 10th, 50th, and 90th percentiles and SPAN values of ETN loaded microspheres are given in Table 3.12. No significant difference was observed between mean particle sizes of microsphere groups. Mean particle sizes of γ-irradiated PCL and MPEG-PCL-MPEG microspheres loaded with ETN loaded (5.24±0.17 and 4.98±0.09 μm, respectively) were significantly smaller than those of γ-irradiated PCL and MPEG-PCL-MPEG microspheres loaded with IgG (5.79±0.12 and 5.84±0.10 μm, respectively) given in Section 3.2.1, although the values were very close.

PCL microspheres had higher SPAN value compared to MPEG-PCL-MPEG microspheres, indicating broader size distribution for PCL microspheres as was observed for IgG loaded PCL and MPEG-PCL-MPEG microspheres given in Section 3.2.1.

For intra-articularly applied carrier systems, size, shape, and type of the carrier are important to avoid induction of inflammation or an immune response at injection site, which is an already pathological environment in active RA [50]. Various types of microspheres tested for intra-articular drug delivery were reviewed and it was reported that a size range between 5 and 10 μm for microspheres provides a prolonged retention time for drugs in the joint cavity without inducing any inflammatory reactions [50]. In our study, 90% of particle size of ETN loaded PCL and MPEG-PCL-MPEG microspheres were found in this range and both microsphere formulations are suitable for intra-articular applications.
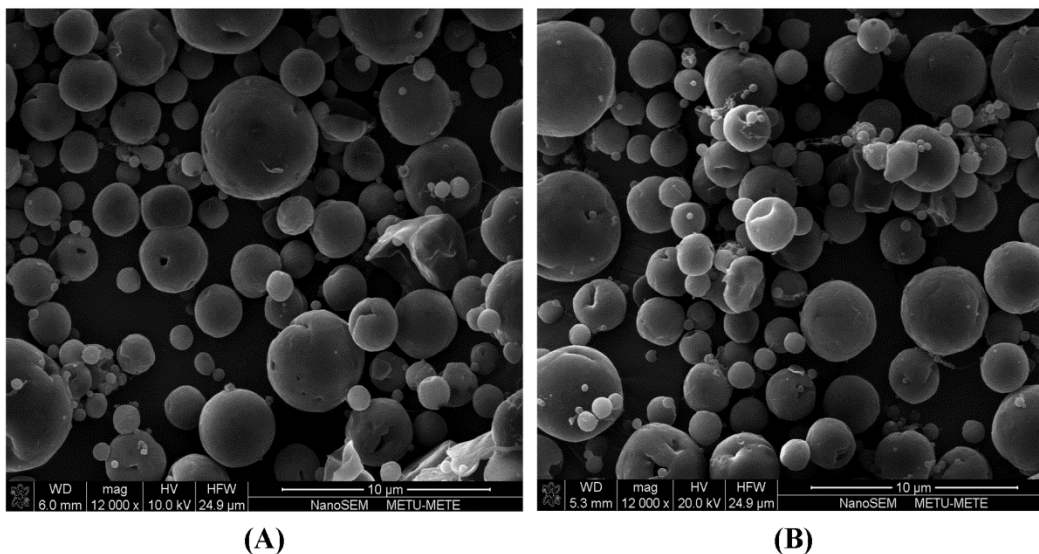
Figure 3.14. SEM images of ETN loaded A) PCL, B) MPEG-PCL-MPEG microspheres

Table 3.12. Comparision of particle size analysis results of ETN loaded PCL and MPEG-PCL-MPEG microspheres

	Particle Size (μm)	d[0.1] (μm)	d[0.5] (μm)	d[0.9] (μm)	Span
PCL microspheres	5.24 ± 0.17	2.15	4.24	10.12	1.88
MPEG-PCL-MPEG microspheres	4.98 ± 0.09	2.88	4.74	7.26	0.92

Data are given as mean ± S.E.

3.3.2. ETN Loading and Encapsulation Efficiency

The ETN contents of PCL and MPEG-PCL-MPEG microspheres were measured with μBCA assay after the hydrolysis of microspheres and subsequent extraction of the protein. The calibration curve was constructed with different concentrations of ETN treated with same solvent (Figure D.2).

The ETN encapsulation efficiency and loading for γ-irradiated PCL and MPEG-PCL-MPEG microspheres are given in Table 3.13. MPEG-PCL-MPEG microspheres showed higher ETN loading and encapsulation efficiency than PCL microspheres. This result is in

agreement with the result observed for the IgG loading and encapsulation efficiency of PCL and MPEG-PCL-MPEG microspheres (Section 3.2.2). As explained in Section 3.2.2, the presence of hydrophilic MPEG segments in polymer matrix improved the hydrophilicity of the polymeric matrix and thereby enhanced the affinity of ETN to the polymeric core.

Table 3.13. ETN-loading and encapsulation efficiency of γ-irradiated PCL and MPEG-PCL-MPEG microspheres

	Encapsulation efficiency (%)	Loading (%)
γ-irradiated PCL microspheres	65.06 ± 1.85^{a}	1.62 ± 0.03^{a}
γ-irradiated MPEG-PCL-MPEG microspheres	75.64 ± 1.78^{a}	1.84 ± 0.04^{a}

Data are given as mean ± S.D.
[a] Statistically significant difference between groups for same properties (p ≤ 0.05).

3.3.3. Protein Adsorption Test

One of the most important issues to be considered is the adsorption of plasma proteins on the surfaces of carrier systems, which is the first step in the acute biological response. Adsorption of plasma proteins mediates cell adhesion, including platelet activation and leukocyte binding in the clotting and inflammation cascades, respectively. Synovial fluid is a plasma lysate containing high amount of plasma proteins, therefore protein adsorption is also an important issue for intra-articular applications. Moreover, non-specific protein adsorptions on surfaces of polymeric microspheres limit the release of proteins and result in slower release profiles [204-206]. Because of these reasons, the amounts of protein adsorbed to the γ-irradiated empty PCL and MPEG-PCL-MPEG microspheres incubated in healthy or RA synovial fluids was determined at certain time intervals (Figure 3.15). The calibration curve of μBCA assay was also constructed with different concentrations of BSA (0-1.25 mg/ml) treated with 1% SDS solution in PBS to determine the protein amount adsorbed on empty microspheres (Figure D.3).

After 1 day incubation, no significant difference was observed between both groups in same type of synovial fluid. However, a significant increase in the amount of protein adsorbed on PCL microspheres was seen after 1st and 2nd day for RA and healthy synovial fluid incubations, respectively. Proteins mainly adsorb on surfaces by hydrophobic, van der Waals, and electrostatic interactions. More protein adsorb on hydrophobic surfaces

compared to the hydrophilic ones [207]. PEG can minimize the adsorption of plasma proteins by steric repulsion and there is also a direct correlation between the PEG chain-length and minimization of protein adsorption [207]. In the study of Cho *et al.* [182], they prepared blend films based on PCL and PEG grafted PCL with different blend ratios and studied protein adhesion on these films. They observed that the level of the protein adsorption decreased when PEG component was introduced.

For first two days, protein adsorption on PCL microspheres incubated in RA synovial fluid was significantly higher than that of PCL microspheres incubated in healthy synovial fluid. However, no significant difference was observed between the amounts of protein adsorbed on PCL microspheres incubated in healthy and RA synovial fluid after 2nd day. Healthy synovial fluid contains high amount of blood plasma proteins such as albumin (ca 11 mg/ml) and globulins (ca 7 mg/ml) and also synovial fluids of RA patients have a higher albumin concentration compared to those of healthy individuals [6]. In agreement with literature, total protein concentration of RA synovial fluid was higher (30.34 ± 1.25 mg/ml) than that of healthy synovial fluid (19.76 ± 1.44 mg/ml). Thus, higher amount of protein was adsorbed on PCL microspheres incubated in RA synovial fluid compared to incubation in healthy synovial fluid. On the other hand, no significant difference was observed in amounts of adsorbed protein on MPEG-PCL-MPEG microspheres for incubations in healthy or RA synovial fluids during 14 days. MPEG segment in MPEG-PCL-MPEG minimized the protein adsorption on surfaces of microspheres by increasing surface negativity and thereby decreasing the hydrophobic or electrostatic interactions mentioned above.
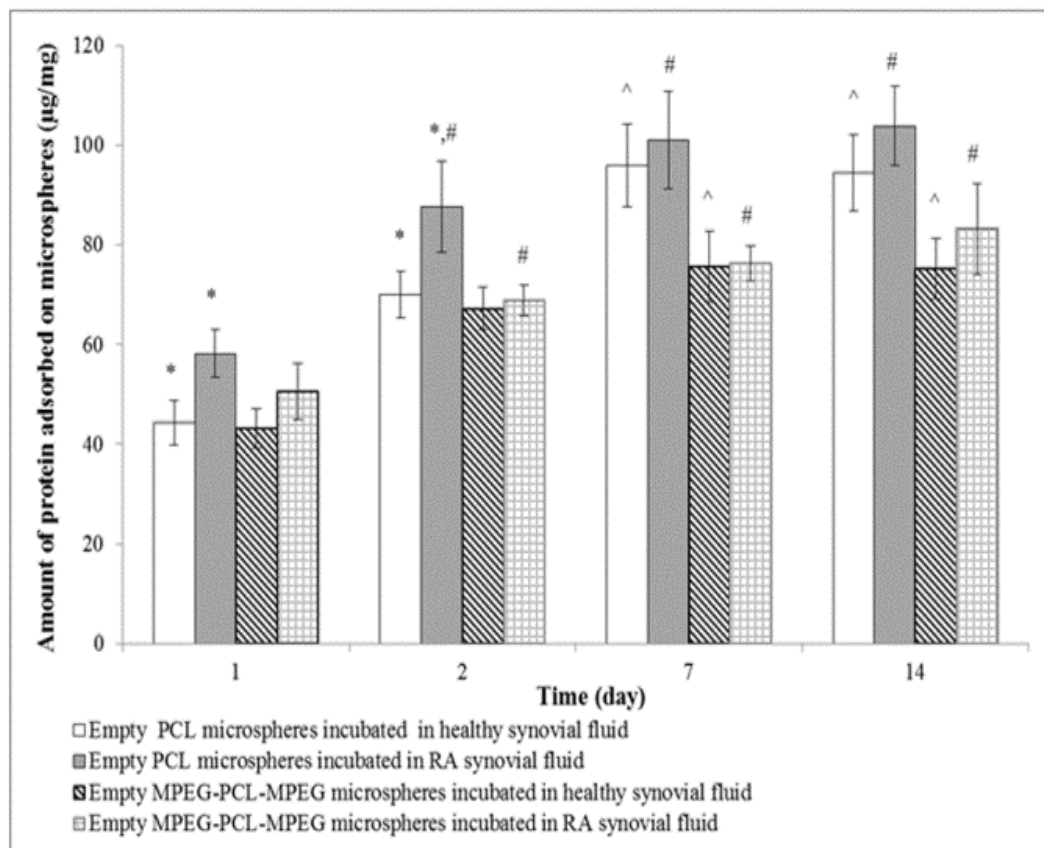
Figure 3.15. Amount of protein absorbed on empty PCL or MPEG-PCL-MPEG microspheres incubated in synovial fluids of healthy and RA patients for 14 days. Data are given as mean ± S.D. * Statistically significant differences between PCL microspheres incubated in synovial fluids of healthy and RA patients at the same time period and ^, # Statistically significant differences between different types of microspheres incubated in synovial fluids of healthy and RA, respectively.

3.3.4. *In Vitro* Release of ETN From Microspheres

The amount of ETN released from PCL and MPEG-PCL-MPEG microspheres was determined by the same approaches with IgG release studies. The calibration curves for µBCA assay was constructed with different concentrations of ETN (0-15 µg/ml) in release medium (Figure D.4). For ELISA method, the calibration curve constructed with different concentrations of ETN (0-2 µg/ml) is also presented in Figure D.5.

The cumulative release profiles of total and biologically active ETN from γ-irradiated PCL and MPEG-PCL-MPEG microspheres incubated in PBS are given in Figure 3.16A and B, respectively. The cumulative release profiles of ETN from PCL and MPEG-PCL-MPEG microspheres showed similar trends during 90 days. ETN release from PCL microspheres showed a slower release profile compared to that from MPEG-PCL-MPEG microspheres as in the case of IgG release (Figure 3.7 in Section 3.2.3). The presence of hydrophilic MPEG segment in microspheres enhanced ETN release. In the study of Kim *et al.* [145], BSA loaded PEG-PCL and PEG-PLLA microspheres were prepared by using $(AB)_n$ type amphiphilic multiblock copolymers with various compositions. They examined that the rate and amount of BSA release increased with increasing the ratio of PEG segment.

When the results of μBCA assay and ELISA were compared, no significant difference was observed between the amounts of total and biologically active ETN released from γ-irradiated MPEG-PCL-MPEG during 90 days (Figure 3.16A and B). However, the amount of biologically active ETN released from γ-irradiated PCL microspheres was found significantly lower than the total amount released from the γ-irradiated MPEG-PCL-MPEG microspheres. For IgG loaded PCL and MPEG-PCL-MPEG microspheres, same result was observed as given in Section 3.2.3. These results showed that the presence of MPEG segment in microspheres protects the stability of protein during the preparation step.

To examine the loss of the bioactivity of released ETN, the ratios of the amount of biologically active ETN released from microspheres to the total amount of ETN released from microspheres were given in Table 3.14. When the results given in Table 3.14 were compared with those in Table 3.6, the bioactivity of ETN released from γ-irradiated PCL and MPEG-PCL-MPEG microspheres were completely protected for 20 days whereas only $33 \pm 1\%$ and $52 \pm 1\%$ of the bioactivity of the IgG released from γ-irradiated PCL and MPEG-PCL-MPEG microspheres were protected for this time period, respectively. As described in Enbrel®, etanercept US Prescribing Information of Wyeth, the ETN formulation also contains some additives such as mannitol, sucrose, and trometamol to protect the bioactivity of ETN. This was thought as the reason for bioactivity of ETN being completely protected during 20 days. Furthermore, at the end of 90 day release study, $91.16 \pm 1.22\%$ bioactivity of ETN released from PCL microspheres and $98.38 \pm 2.11\%$ ETN released from MPEG-PCL-MPEG microspheres were protected. Protection of ETN bioactivity for MPEG-PCL-MPEG microspheres was statistically higher than that of for PCL microspheres at the end of 90 days. Hence, besides additives in drug formulation, MPEG segment at polymer matrix also improved the protection of ETN from denaturation as mentioned in Section 3.2.3.
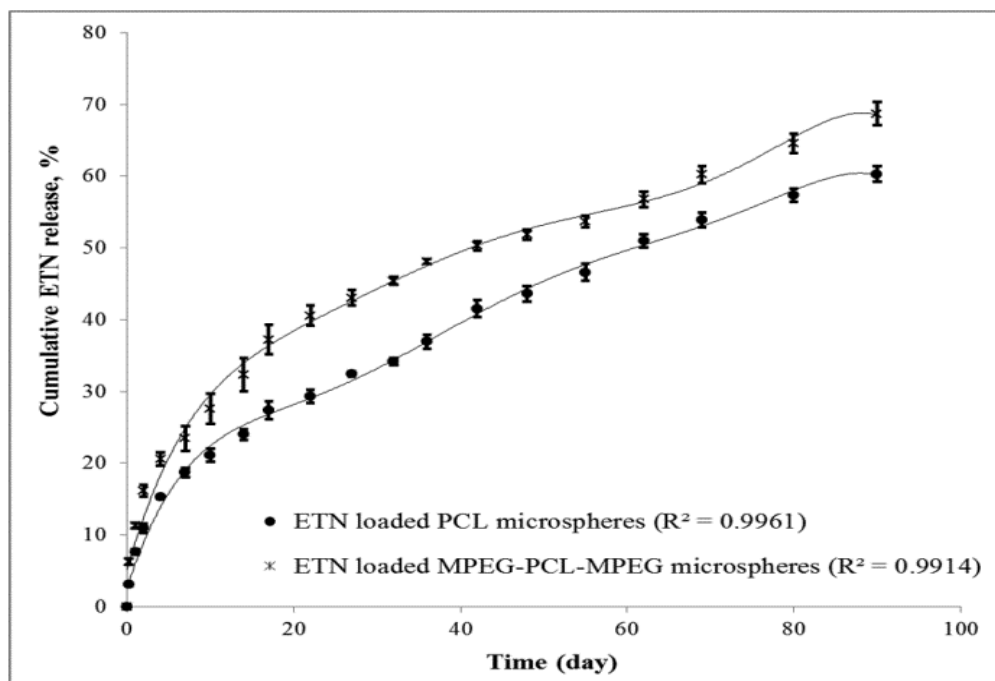
(A)
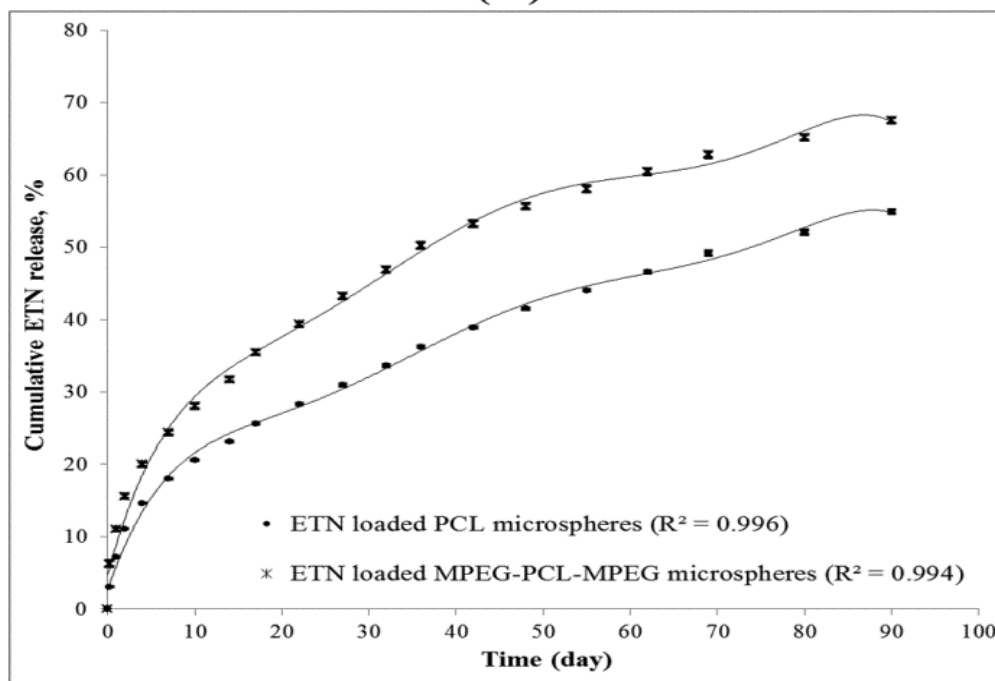
(B)

Figure 3.16. Cumulative release profile of ETN loaded PCL and MPEG-PCL-MPEG microspheres in PBS for 90 days determined by μBCA assay **(A)** and ELISA **(B)** (Data are given as mean ± S.D.)

Table 3.14. The ratio of the amount of biologically active ETN released to the total amount of ETN released from γ-irradiated PCL and MPEG-PCL-MPEG microspheres

	Ratio of the amount of biologically active released ETN to the total amount released		
	6 h	20 day	90 day
PCL microspheres	1.00 ± 0.08	0.97 ± 0.03	0.91 ± 0.01[a]
MPEG-PCL-MPEG microspheres	1.00 ± 0.004	0.97 ± 0.03	0.98 ± 0.02[a]

Data are given as mean ± S.D.
[a] Statistically significant difference between groups at 90 day ($p \leq 0.05$).

The percent cumulative amounts of biologically active ETN released from γ-irradiated PCL and MPEG-PCL-MPEG microspheres were also evaluated by incubating microspheres in cell culture medium containing 10% FBS for 60 days. The calibration curve constructed with different concentration of ETN (0-2 μg/ml) (Figure D.6) are used for released drug amount determinations.

The cumulative release profiles of biologically active ETN from γ-irradiated microspheres incubated in cell culture medium containing 10% FBS are presented in Figure 3.17. As observed in PBS, PCL microspheres showed a slower release profile for biologically active ETN compared to MPEG-PCL-MPEG microspheres. Presence of hydrophilic MPEG segment caused more release of ETN from MPEG-PCL-MPEG microspheres owing to enhanced diffusion of water into microspheres as explained before. In addition, MPEG segments might have resulted in more ETN release from these microspheres by decreasing the adsorption of serum proteins in cell culture medium. In a previous study, the effect of various additives (i.e., PEGs, BSA and poloxamer 188) on lysozyme release from PLGA microspheres has been studied in TRIS-HCL buffer medium containing 0.1% w/v BSA [206]. They observed that BSA in release medium tended to be adsorbed on PLGA microspheres when there is no additive and limited the release of lysozyme.

In vitro release studies in PBS and cell culture medium showed that ETN loaded PCL and MPEG-PCL-MPEG microspheres can provide a sustained-prolonged release of biologically active ETN for at least 90 days after intra-articular administration. Therefore, once weekly or twice weekly administration period of ETN in conventional treatment can be extended to longer periods with this microcarrier approach.
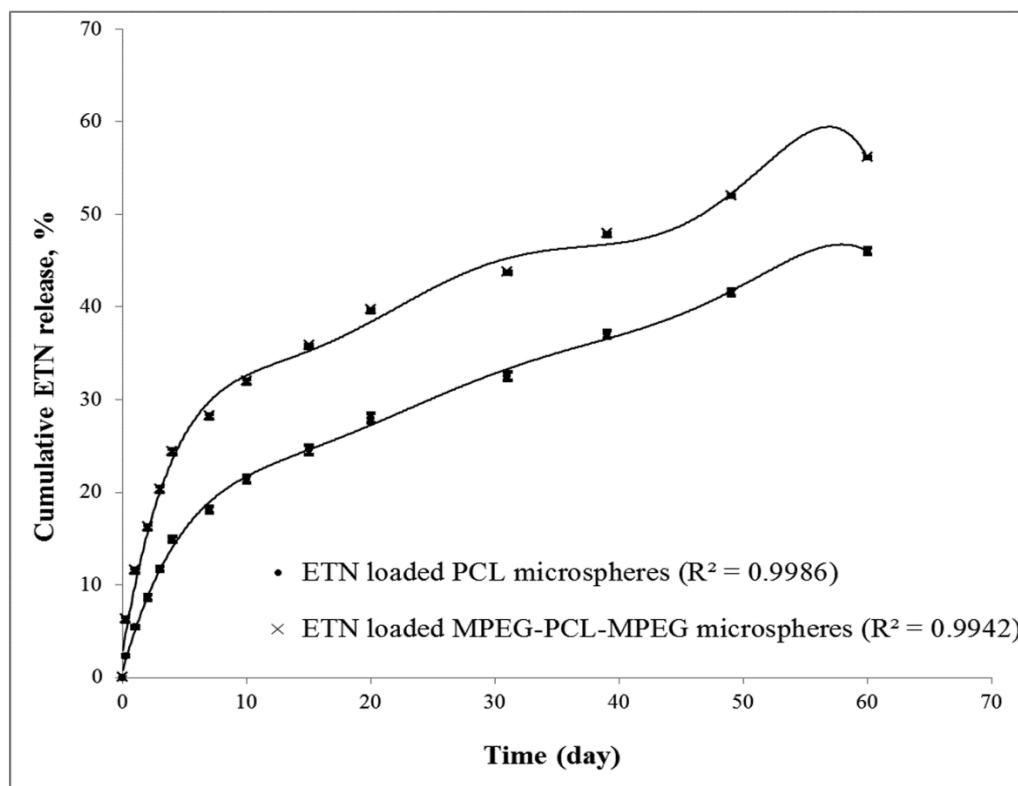
Figure 3.17. Cumulative release profiles of ETN loaded PCL and MPEG-PCL-MPEG microspheres in cell culture medium for 60 days determined by ELISA (Data are given as mean ± S.D.)

The cumulative amount of biologically active ETN released from γ-irradiated PCL and MPEG-PCL-MPEG microspheres were also evaluated in healthy and RA synovial fluids for 14 days. The cumulative release profiles of biologically active ETN released from PCL and MPEG-PCL-MPEG microspheres incubated in healthy and RA synovial fluids are presented in Figure 3.18. ETN loaded PCL and MPEG-PCL-MPEG microspheres showed slower release profiles in healthy synovial fluid compared to their counterparts incubated in RA synovial fluid during 14 days. As mentioned in Section 1.1, synovial fluid is very viscous because of its high concentration of hyaluronic acid. In degenerative joint disease such as OA and RA, the molecular weight and concentration of hyaluronic acid are reduced resulting in a decrease in viscosity of synovial fluids [7, 208]. Therefore, it was thought that the ETN released from microspheres in RA synovial fluid was significantly higher than that in healthy synovial fluid because of the lower viscosity in RA state. Even though more protein adsorption on PCL microspheres was observed in RA synovial fluid compared to healthy synovial fluid, a slower release of ETN was obtained

81

in healthy synovial fluid. This observation suggests that the viscosity of synovial fluid is a more predominant factor than protein adsorption on microspheres for determining ETN release from microspheres. This finding can be supported with MPEG-PCL-MPEG results. According to the results of protein adsorption test, no significant differences were found between the amounts of protein adsorbed on empty MPEG-PCL-MPEG microspheres incubated in RA or healthy synovial fluids. However, ETN loaded MPEG-PCL-MPEG microspheres also showed slower release profiles in healthy synovial fluid compared to their counterparts incubated in RA synovial fluid. Besides, the cumulative release amounts of ETN in synovial fluids were also observed to be considerably (about three fold) lowers than the release amounts in PBS and cell culture medium. This was probably related with lower viscosity properties of PBS and cell culture medium compared to the synovial fluid.

For each synovial fluid type, percent cumulative amount of biologically active ETN released from MPEG-PCL-MPEG microspheres was found significantly higher than that from PCL microspheres at each time point. As mentioned before, presence of hydrophilic MPEG segment causes more release of ETN from MPEG-PCL-MPEG microspheres. In addition to the ETN release study in synovial fluids, free ETN was also incubated in healthy and RA synovial fluids for 14 days to examine the changes in bioactivity of free drug. No significant changes were observed in the concentration of free ETN in synovial fluids (Figure D.7) suggesting that ETN was stable for 14 day-period in synovial environment.

The cumulative amounts of ETN released from PCL or MPEG-PCL-MPEG microspheres in PBS, cell culture medium containing 10% FBS, healthy and RA synovial fluids are compared in Table 3.15. In all release media, amounts of ETN released from MPEG-PCL-MPEG microspheres was significantly higher than those from PCL microspheres. For both PCL and MPEG-PCL-MPEG microspheres, percent cumulative release in cell culture medium was significantly higher than those observed in healthy and RA synovial fluids. However, percent cumulative releases in cell culture medium and synovial fluids were significantly lower than that observed in PBS. In a previous study, the release profiles of 5-fluorouracil-hexyl-carbamoyl fluorouracil loaded N-isopropylacrylamide and vinyl pyrrolidone copolymer nanospheres were examined in PBS and diluted serum media [209]. They observed a slower release in serum due to the absorption of complement proteins present in serum. The percent cumulative amounts of biologically active ETN released from microspheres in healthy and RA synovial fluids were found significantly lower than those of in PBS and cell culture medium because of higher viscosity of synovial fluids compared to PBS and cell culture medium. This lower protein release from microspheres in synovial fluids can be attributed to adsorption of proteins on the surface of microspheres or to viscosity difference of the release environments, which affects diffusion process.
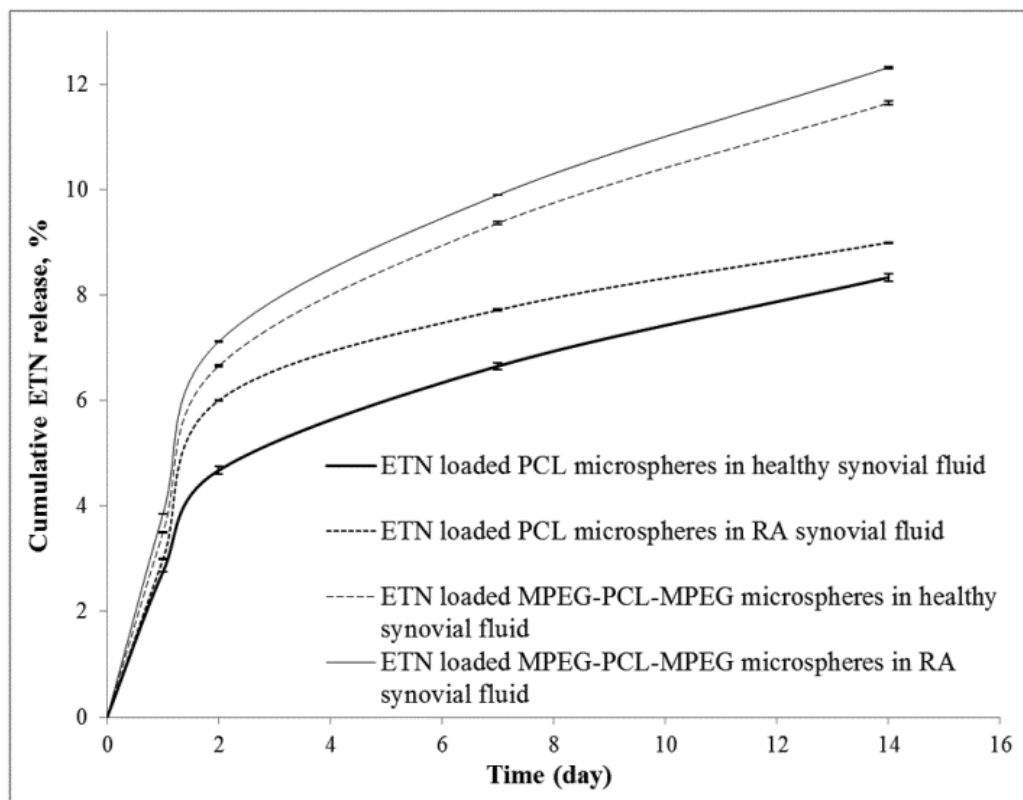
Figure 3.18. Cumulative release profiles of ETN loaded PCL and MPEG-PCL-MPEG microspheres in healthy and RA synovial fluids for 14 days (Data are given as mean ± S.D.)

Table 3.15. Comparison of cumulative (%) ETN release from γ-irradiated PCL and MPEG-PCL-MPEG microspheres in different release media

Release Medium	PCL microspheres	MPEG-PCL-MPEG microspheres
PBS	23.17 ± 0.06	31.74 ± 0.31
cell culture medium with 10% FBS	24.59 ± 0.47	35.74 ± 0.19
RA synovial fluid	9.00 ± 0.01	12.32 ± 0.02
Healthy synovial fluid	8.34 ± 0.07	11.64 ± 0.03

Data are given as mean ± S.D.
All groups were significantly different from each other ($p \leq 0.05$).

3.3.5. Kinetics of ETN Release

In vitro release data of PCL or MPEG-PCL-MPEG microspheres in different release media were fitted to Higuchi, Korsmeyer–Peppas, first, and zero-order release models to find out the mechanism of ETN release from microspheres. The coefficient of determination (R^2), rate constants (k_0, k_1, k_H and k_P) and n values obtained after linear regression on mathematical models are presented in Table 3.16.

R^2 values showed that the best-fits were obtained in Higuchi and Korsmeyer-Peppas models rather than zero-order and first-order models. ETN release from PCL and MPEG-PCL-MPEG microspheres was found diffusion controlled due to the fitting well to Higuchi model as observed for IgG loaded microspheres given in Section 3.2.4. This observation was also confirmed by fitting the release data to Korsmeyer–Peppas model. For *in vitro* release studies evaluated in PBS and cell culture medium, n values for both microsphere formulations were above 0.43 indicating ETN release was governed by an anomalous transport mechanism. This revealed that the water transport mechanism was mainly due to the combination of both diffusion through and surface erosion from PCL and MPEG-PCL-MPEG microspheres incubated in PBS and cell culture medium during 90 and 60 days, respectively. In agreement with these results, significant defects were observed on the surface of γ-irradiated MPEG-PCL-MPEG microspheres loaded withIgG loaded at the end of 6-month PBS incubation (Figure 3.8 in Section 3.2.6). However, for release studies in healthy and RA synovial fluids n values for both microsphere formulations were near 0.43 suggesting that ETN release in synovial fluid was mainly diffusion controlled.

Two main mechanisms can control the protein release from biodegradable polymeric microspheres: diffusion of the protein from microsphere and erosion of the polymer matrix surface. However, polymer hydrolysis and polymeric matrix erosion of PCL and MPEG-PCL-MEG are very slow. As given in Table 3.10 in Section 3.2.6, decrease in molecular weight (M_w) of γ-irradiated PCL and MPEG-PCL-MPEG microspheres loaded with IgG were not high at the end of 6-month PBS incubation. Therefore, diffusion can be the more dominant factor affecting ETN release kinetics for the early stages of *in vitro* release as observed in 14-day synovial fluid release study. On the other hand, release of ETN from microspheres was controlled by diffusion and polymer erosion during the later stages as seen in the 60 day cell culture medium and 90 day PBS release studies. Rate constants for ETN release from MPEG-PCL-MPEG microspheres were found higher than that for PCL microspheres (Table 3.16). *In vitro* release profile of ETN from microspheres correlated well with this observation. ETN release from PCL microspheres showed a slower release profile compared to that from MPEG-PCL-MPEG microspheres.

Table 3.16. *In vitro* release kinetic parameters of ETN loaded PCL and MPEG-PCL-MPEG microspheres after γ-sterilization incubated in different release media

	Zero Order		First order		Higuchi		Korsmeyer-Peppas		
	R^2	k_0	R^2	k_1	R^2	k_H	R^2	k_p	n
PBS (µBCA Assay)									
PCL	0.93	0.026	0.98	0.0004	1.00	1.27	0.99	1.28	0.51
MPEG-PCL-MPEG	0.87	0.027	0.95	0.0005	0.99	1.39	0.96	1.92	0.48
PBS (ELISA)									
PCL	0.91	0.023	0.96	0.0003	1.00	1.16	0.99	1.30	0.50
MPEG-PCL-MPEG	0.87	0.029	0.95	0.0005	0.99	1.45	0.96	1.86	0.49
Cell Culture Medium									
PCL	0.90	0.029	0.94	0.0004	0.99	1.20	0.99	1.06	0.53
MPEG-PCL-MPEG	0.82	0.033	0.90	0.0005	0.96	1.40	0.94	1.94	0.49
RA Synovial Fluid									
PCL	0.71	0.0220	0.72	0.0002	0.91	0.49	0.97	1.01	0.39
MPEG-PCL-MPEG	0.79	0.0210	0.80	0.0003	0.96	0.67	0.98	1.03	0.44
Healthy Synovial Fluid									
PCL	0.80	0.021	0.81	0.0002	0.96	0.45	0.99	0.98	0.37
MPEG-PCL-MPEG	0.80	0.03	0.81	0.0003	0.96	0.63	0.98	1.01	0.43

3.3.6. *In Vitro* Cytotoxicity Studies

In vitro cytotoxicity of ETN loaded PCL and MPEG-PCL-MPEG microspheres was evaluated by Alamar Blue assay using FLS of OA and RA patients. Alamar Blue is an indicator dye which incorporates an oxidation – reduction indicator that both fluoresces and changes color in response to the chemical reduction of growth medium, resulting from cell metabolism. As this dye is extremely stable and non-toxic to the cells, continuous monitoring of cultures over time is possible [210]. For this reason, Alamar Blue Assay has been considered superior to MTT test for cell viability [211].

Cell viability difference of OA or RA FLS incubated with γ-irradiated PCL or MPEG-PCL-MPEG microspheres loaded with ETN from control OA or RA FLS is given in Figure 3.19. The results showed that there were no toxic effects on the viability and proliferation of synovial fibroblast cells. In agreement with the MTT and fluorometric assay results and microscopic examinations, the preparation method of microspheres did not produce any toxic effect on the viability and proliferation of cells.
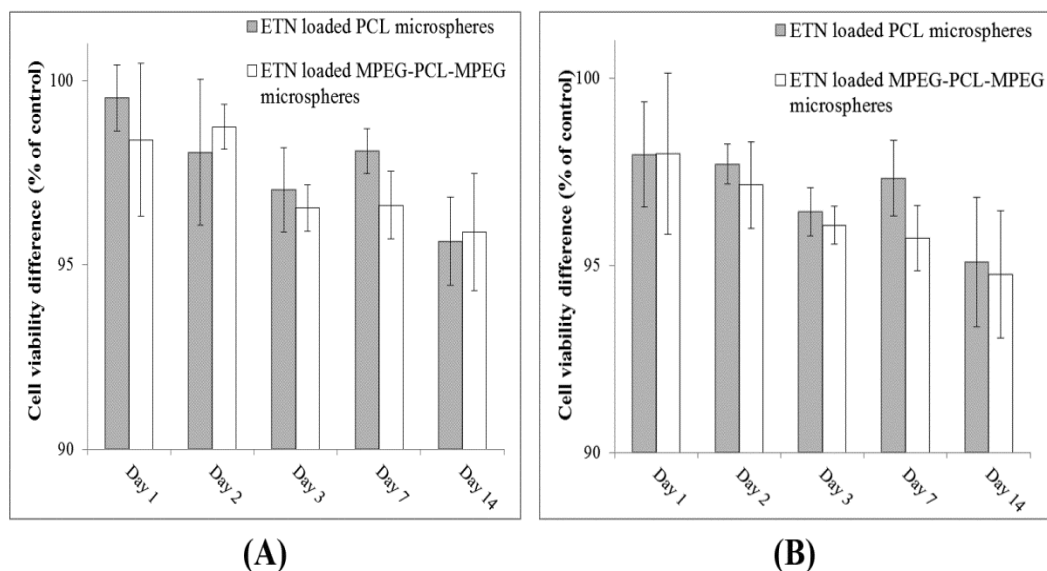

Figure 3.19. Relative cell viability of FLS obtained from OA **(A)** and RA **(B)** patients after incubation with PCL or MPEG-PCL-MPEG microspheres for 14 days compared to control groups (Values are shown as mean ± S.D., n=3)

86

3.4.   Effects of ETN Loaded Microspheres on FLS

3.4.1.   *In Vitro* RA Model Establishment Using RA FLS

Changes in TNFα levels at different passages of FLS were determined by ELISA and compared with each other and with the TNFα level in RA synovial fluid. The calibration curve used in this analysis was constructed with different concentrations of TNFα (0-500 pg/ml) (Figure E.1).TNFα levels in RA synovial fluid and cell culture media of RA FLS at different passages are given in Figure 3.20. TNFα concentration of RA synovial fluid (90.34±9.06 pg/ml) was found significantly higher among the groups. However, no significant differences were observed between the TNFα levels at different passages. In a previous study, TNFα concentration of synovial fluid of RA patients was found as 93.53±25.21 pg/ml and this group also observed a decrease in TNFα levels in the cell culture media compared to that of synovial fluid [212]. Moreover, FLS of RA patients at higher passages were generally used in the previous studies [213-215]. In a previous study, they observed that after the isolated synovial cells were cultured for a long time (passaged at least 4 times), the percentage of macrophage-like cells decreased whereas the percentage of fibroblast-like cells was increased [216]. For these reasons, RA FLS at passage 4 were used to evaluate the treatment efficacy of ETN loaded PCL and MPEG-PCL-MPEG microspheres. Phase contrast images of RA FLS at passage 4 are given in Figure 3.21. Morphological properties of these cells were found similar to the synovial fibroblast cells isolated from the synovial membrane of RA patients in literature [217, 218].

In preliminary studies, the effects of single stimulation of FLS with different concentration of IL-1β (0.1, 1, and 10 ng/ml) and with the combination of IL-1β and TNFα were also investigated by comparing the TNFα levels of FLS before and after stimulation (Figure E.2, E.3, and E.4). When TNFα levels of IL-1β stimulated FLS were compared with that of non-stimulated FLS, only at day 7 a significant difference was observed between TNFα levels of stimulated and non-stimulated cells (Figure E.2). However, no significant difference was observed between 0.1, 1 and 10 ng/ml IL-1β stimulated cell groups. Besides, no significant difference was observed between stimulated and non-stimulated cell groups at other time points. TNFα level of the synovial fibroblast cells stimulated with the combination of IL-1β and TNFα showed an extremely higher value compared to other cell groups at 1st day due to the addition of external TNFα (Figure E.3). However, no significant difference was observed between the TNFα levels of FLS stimulated with the combination of IL-1β and TNFα and non-stimulated FLS after 1st day.

In another preliminary study, the effects of continuous stimulation of FLS with different concentration of IL-1β (0.1 and 1 ng/ml) were examined by comparing the TNFα levels of

FLS before and after stimulation for 12 days (Figure E.5). No significant difference was observed between TNFα levels of stimulated and non-stimulated RA FLS. After 6 days incubation, FLS stimulated with 1 ng/ml IL-1β were detached from well surface and thus TNFα levels of these cells could not be determined. According to results of these preliminary studies, IL-1β and TNFα stimulation did not cause any significant difference in TNFα levels of RA FLS. Therefore, non-stimulated RA FLS were used at the last stage of this study.

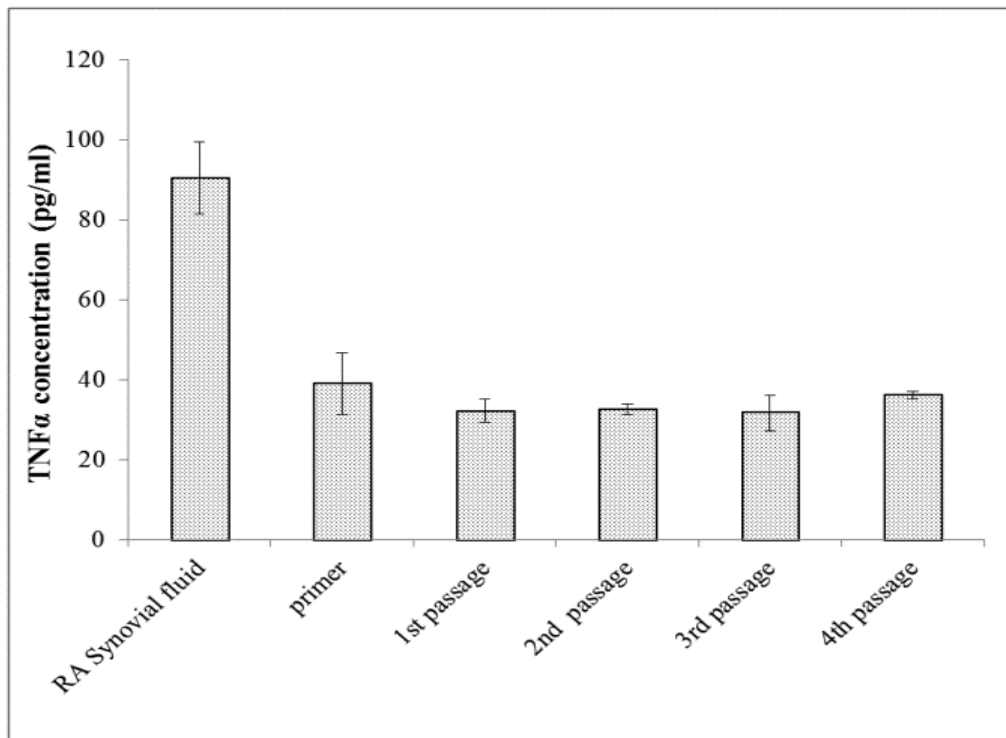**Figure 3.20.** TNFα levels of RA synovial fluid and cell culture media of RA FLS at different passages (Values are shown as mean ± S.D., n=2)
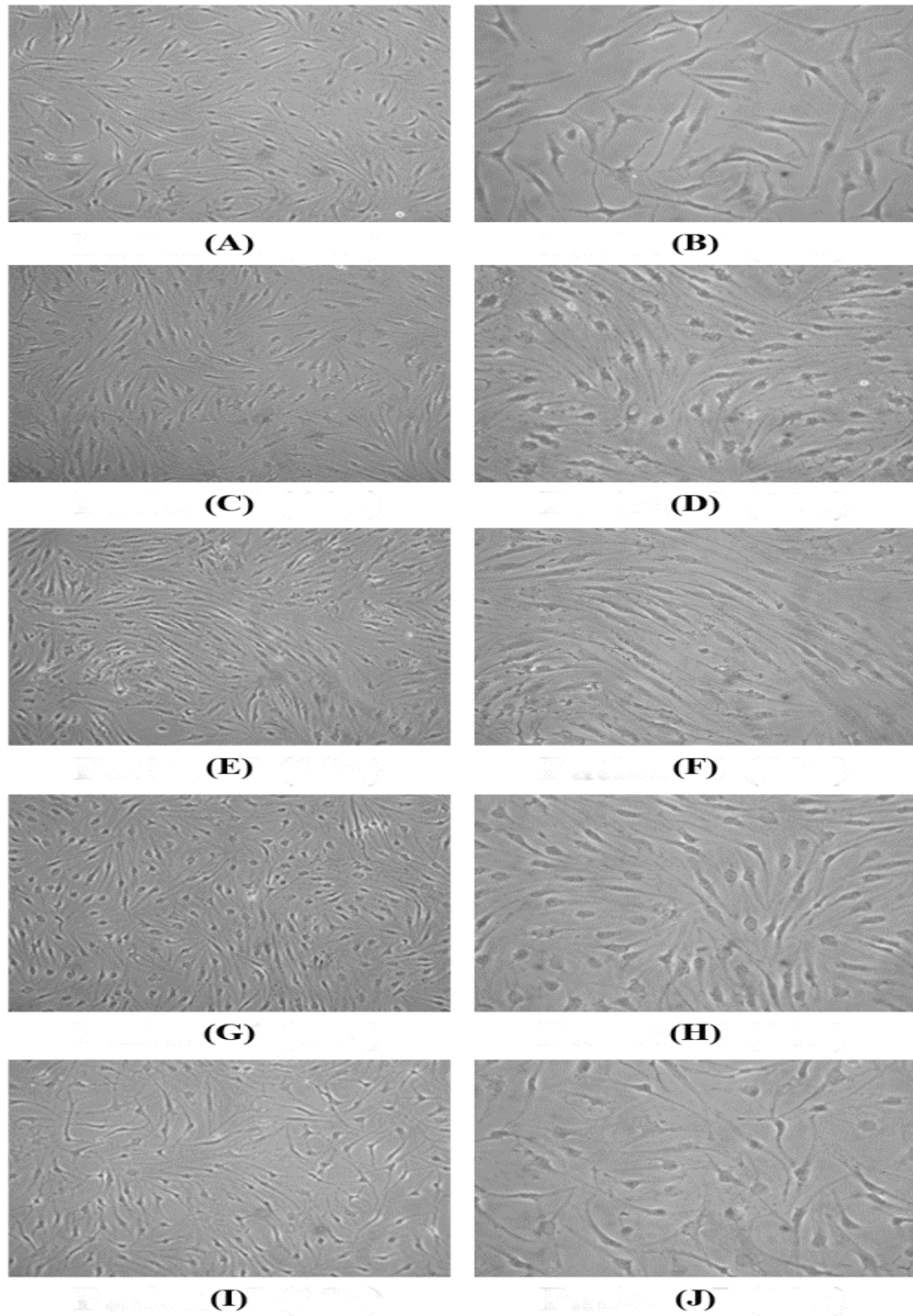
Figure 3.21. Phase contrast micrographs of the FLS isolated from the synovial membrane of RA patient 1,2,3,4 and 5 at 10x magnification ((**A), (C), (E), (G)** and **(I),** respectively) and at 20x magnification ((**B), (D), (F), (H)** and **(J),** respectively)

3.4.2. Quantitation of ETN Concentration

Changes in ETN concentrations in free ETN group and *in vitro* ETN release from PCL and MPEG-PCL-MPEG microspheres were evaluated for 4 weeks in cell culture media. To quantitate ETN concentrations, a calibration curve was constructed with different concentration of ETN (0-4 μg/ml) and it is given in Figure E.6.

Amount of biologically active ETN released from microspheres in cell culture medium containing 5% FBS was determined before addition to FLS and the cumulative ETN release profiles of microspheres are presented in Figure 3.22A. Total amounts of biologically active ETN released from MPEG-PCL-MPEG microspheres were significantly higher than that from PCL microspheres at each time point as observed in Section 3.3.4. Additionally, changes in ETN concentrations for free ETN and microspheres groups were also compared (Figure 3.22B). ETN concentration of the free drug group decreased shortly whereas ETN concentration increased with sustained release from microspheres.

The free drugs dissolved in synovial fluid are rapidly eliminated from the joint ($t_{1/2}$ of about 0.1-6 h). Therefore, maintenance of therapeutic concentration for an extended period of time necessitates the administration of the drug in the form of repeated intra-articular injections or an injectable depot formulation [156]. Results showed that PCL and MPEG-PCL-MPEG microspheres can provide sustained drug release which might be a better alternative for free drug applications.
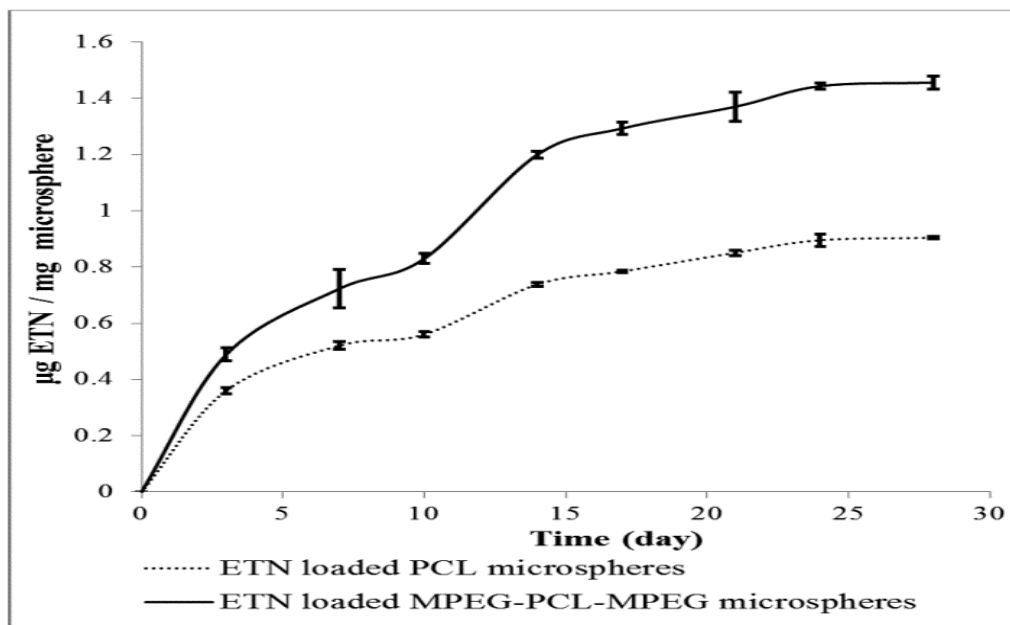
(A)
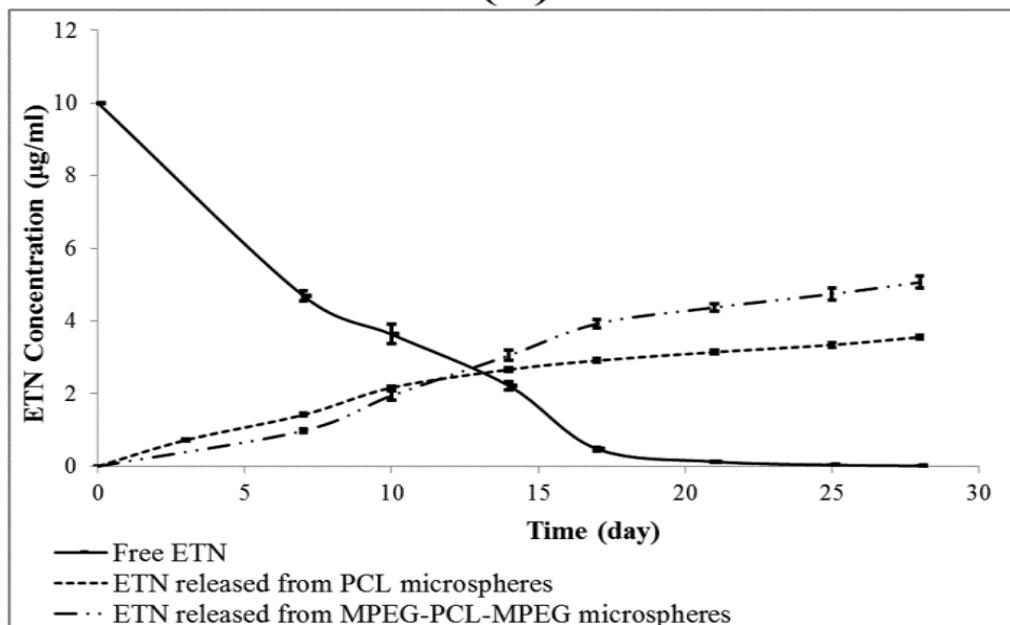
(B)

Figure 3.22. (A) Cumulative ETN release profile of ETN loaded PCL and MPEG-PCL-MPEG microspheres incubated in cell culture medium for 4 weeks, **(B)** Changes in ETN concentration in free drug and PCL or MPEG-PCL-MPEG microsphere groups (Values are shown as mean ± S.D., n=3)

3.4.3. Viability and Cell Number of FLS

Changes in viability and numbers of FLS of all experimental groups were evaluated during 4 weeks of incubation and the results are given in Figure 3.23A and B. In all time points, no significant differences were observed in cell numbers among RA cell groups (Figure 3.23A). Incubation of RA FLS with free ETN or cell culture medium containing ETN released from microspheres did not cause any changes at cell numbers. When the cell numbers of RA groups and OA control group were compared, cell numbers among RA groups were found significantly higher than that of OA control group at each time point. In a previous study, it was shown that RA FLS had a 25% higher rate of proliferation than OA FLS [219]. The proliferation markers such as proliferating cell nuclear antigen, c-myc, and nucleolar organizing region are present in high amount in RA FLS than in OA FLS [220]. Therefore, higher cell numbers were observed among RA groups compared to the OA control group.

Viability of RA FLS incubated with or without free ETN or cell culture medium containing ETN released from ETN loaded PCL or MPEG-PCL-MPEG microspheres were determined at the end of each week for 4 weeks. Ratios of the percent cell viability of RA FLS incubated with free ETN or cell culture medium containing ETN released from microspheres to the percent cell viability of control RA FLS are given in Figure 3.23B. Viability of FLS incubated with free ETN was found significantly lower than that of FLS incubated with ETN released from microspheres at first week. This result indicates that high levels of the free ETN caused a decrease in cell viability in group 3 at first week. However, after changing half of the medium, with a reduction in free ETN level, cell viability increased and no significant differences were observed between all groups at other time periods. These results were in accordance with cytotoxicity results in which cell response depends on the applied dose used [221]. Problems such as toxicity, decrease in the patient's quality of life and pain, loss of function at injection site related with a high dose drug application in clinic are observed [222, 223]. During 4 week, no decrease in cell viability was observed in groups 4 and 5, probably due to the slow release of ETN from the microspheres. Therefore, microspheres can provide an advantage in preserving viability by conservation of the safe environment in the joint. Even in the case of high total amounts of ETN release from MPEG-PCL-MPEG microspheres no decrease in cell viability was observed compared to free ETN group, owing to gradual delivery of drug.
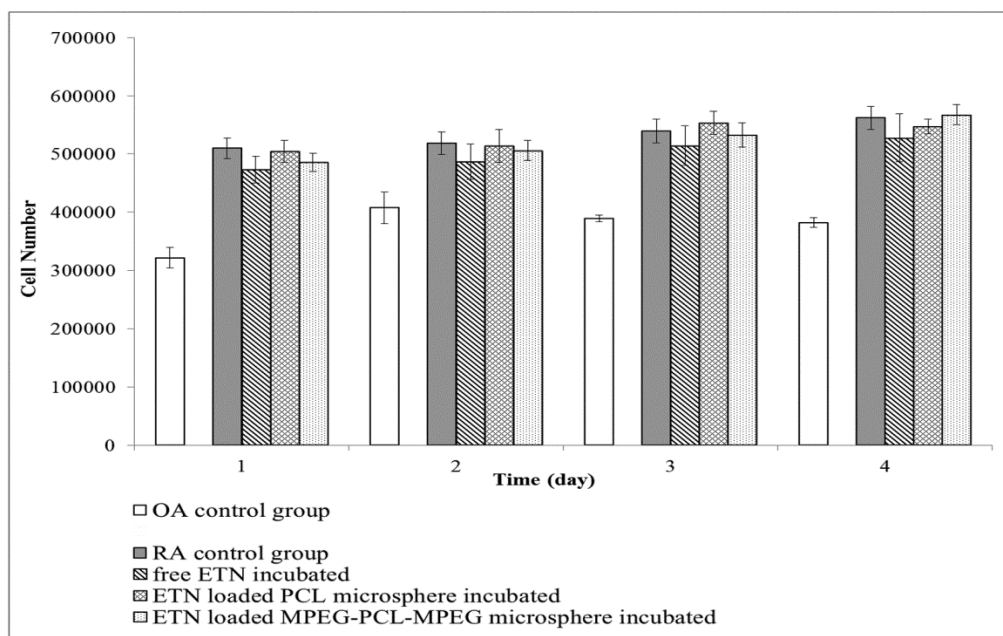
(A)
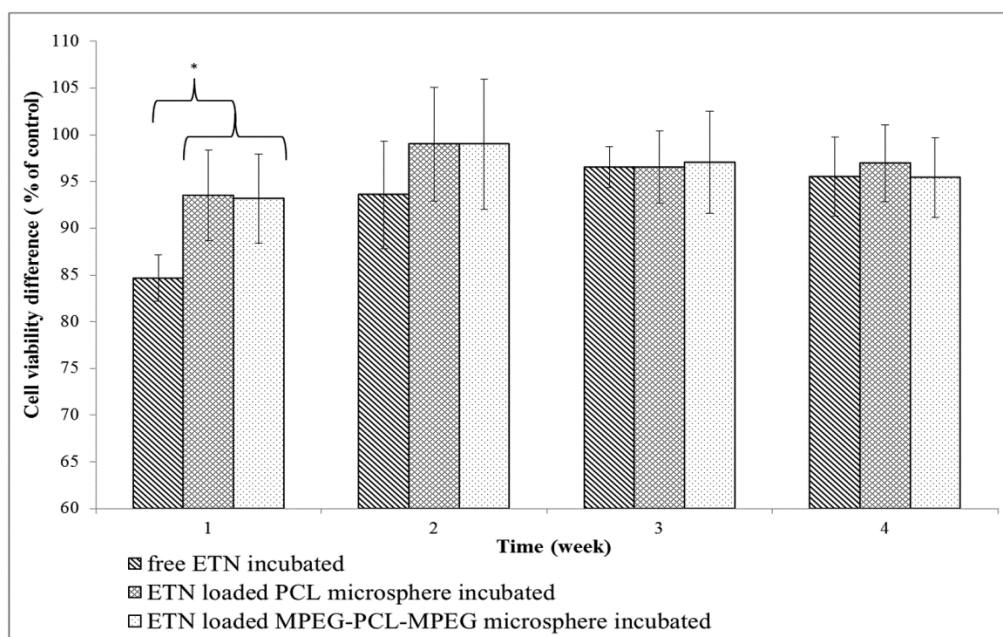
(B)

Figure 3.23. A) Cell numbers **(B)** Relative viability of FLS upon incubation with free ETN or ETN released from microspheres. RA FLS without exposure to drug served as control for determination of cell viability (Values are shown as mean ± S.E.M.)

3.4.4. Levels of Pro-Inflammatory Cytokines and MMPs

Changes in levels of pro-inflammatory cytokines and MMPs released by the FLS were determined by ELISA during 4 weeks to examine the treatment efficacy of the ETN loaded PCL and MPEG-PCL-MPEG microspheres. For ELISA examinations, calibration curves were constructed with using different concentrations of TNFα (0-1000 pg/ml), IL-6 (0-100 pg/ml), IL-17 (0-100 pg/ml), IFN-γ (0-100 pg/ml), MMP-3 (0-4 ng/ml) and MMP-13 (0-20 pg/ml) and they are given in Figure E.1, E.7-11, respectively. Additionally, levels of physiologically active TNFα released by RA FLS were determined by using TNFα sensitive Wehi-164 cells and the calibration curve was obtained by measuring the viability of cells incubated with predetermined amounts of human TNFα standard solutions (0-120 pg/ml) (Figure E.12).

Comparison of production levels of total and physiologically active TNFα produced by FLS in experimental groups 3, 4 and 5 were compared with that of the RA control (Group 1) at the end of each week for 4 weeks (Figure 3.24A and B). No significant differences were observed for TNFα among groups probably because both ETN bound and unbound TNFα were quantitated by ELISA (Figure 3.24A). Etanercept is a neutralizing biologic that does not remove TNF-α molecule from the solution [224]. The presence of the etanercept-bound TNFα was still able to bind to the antibodies utilized in the ELISA and so therefore resulted in high measurements. For this reason, a bioassay was used to measure the levels of physiologically active TNFα released from FLS. The comparison of %-production levels of physiologically active TNFα among RA groups are given in Figure 3.24B. After 2 weeks, percentages of biologically active TNFα released from RA FLS decreased by 35% in microsphere groups while it decreased only by 10-25% in the free ETN group. A decrease of TNFα levels was observed after 2 week incubation due to continuous release of ETN from microspheres. However, no significant decrease was observed in physiologically active TNFα amounts in cell culture medium due to decrease of amount of free ETN in culture medium with each medium change.

Figure 3.25A is a graphical presentation of the comparison of %-production levels of IL-6 among RA groups. %-production levels of IL-6 decreased by 25-30% in microsphere groups, whereas only a 10-15% decrease was observed in the free ETN group after 2 weeks. However, no difference was observed between %-production levels of IL-6 in microsphere groups. IL-6 is indeed a crucial element of inflammation and pro-inflammatory cytokines produced in RA affect the production of IL-6 [13]. Therefore, decrease in %-production levels of IL-6 and physiologically active TNFα in microsphere groups were in parallel.

The comparison of %-production levels of IL-17 among RA groups are given in Figure 3.25B. At the end of 2nd week, %-production levels of IL-17 were significantly lower only in MPEG-PCL-MPEG microsphere group when compared to the free ETN group.

However, %-production levels of IL-17 in both microsphere groups were significantly lower than that of the free ETN group at the end of 4th week. A significant decrease in IL-17 levels of RA FLS in microsphere groups was not observed after 2 weeks whereas significant decreases were observed in TNFα and IL-6 levels of RA FLS in microsphere groups compared to those of RA FLS in free ETN group.

Figure 3.25C is a graphical presentation of the comparison of %-production levels of IFN-γ among RA groups. %-production levels of IFN-γ in both microsphere groups were significantly lower than that of the free ETN group at the end of 4 weeks.
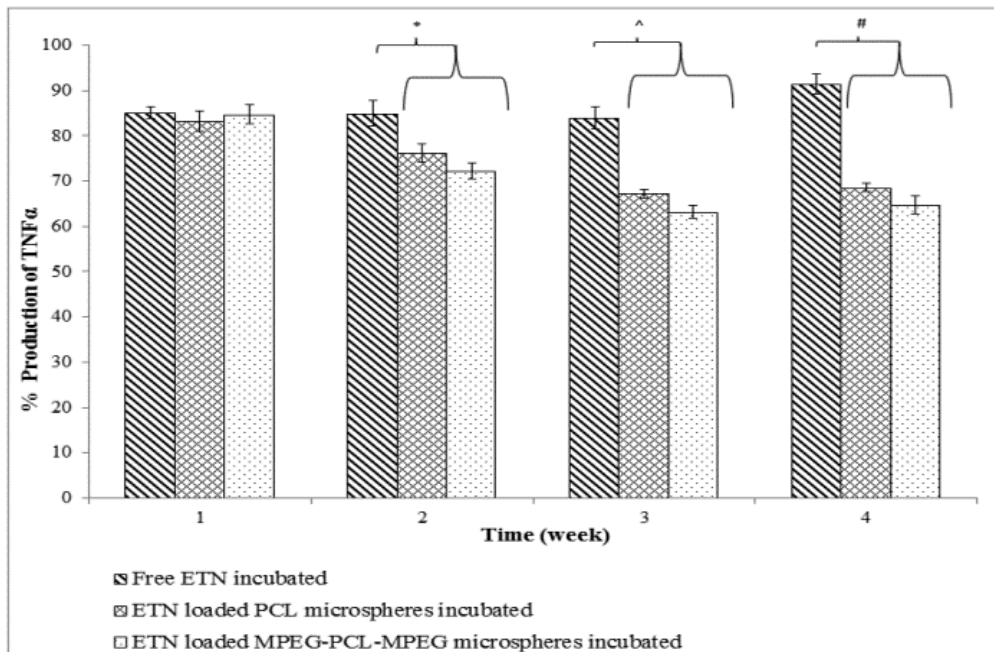
The comparison of %-production levels of MMP-3 and MMP-13 among RA groups are given in Figure 3.26A and B. %-production levels of MMP-3 measured at 2nd, 3rd, and 4th weeks were significantly lower in the microsphere groups compared to the free ETN group. %-production levels of MMP-3 decreased by 30% in microsphere groups, whereas only a 10% decrease was observed in the free ETN group at the end of 3 weeks. Similarly, %-production levels of MMP-13 were significantly lower in the microsphere groups after 1 week. In adult RA, MMP-1 and MMP-3 are shown to be important for cartilage loss. TNFα also stimulates the release of MMP from fibroblast and chondrocytes [13].

Significant decreases in the protein levels of pro-inflammatory cytokines and MMPs secreted by FLSs incubated with microspheres generally started at the end of 2nd week when the concentration of ETN released from microspheres was higher than that of free ETN (Figure 3.22B). Microspheres provide therapeutic level of ETN for an extended period of time compared to free ETN. These results demonstrated that the ETN loaded microspheres have efficiently decreased the protein levels of TNFα, IFNγ, IL-6, IL-17, MMP-3, and MMP-13 for a longer period of time, in a sustained manner.

Levels of pro-inflammatory cytokines and MMPs produced by FLS in OA and RA controls were also compared during 4 weeks (Figure 3.27). The levels of pro-inflammatory cytokines and MMPs in cultural supernatants of RA controls were found higher than that in the cultural supernatants of OA as expected.
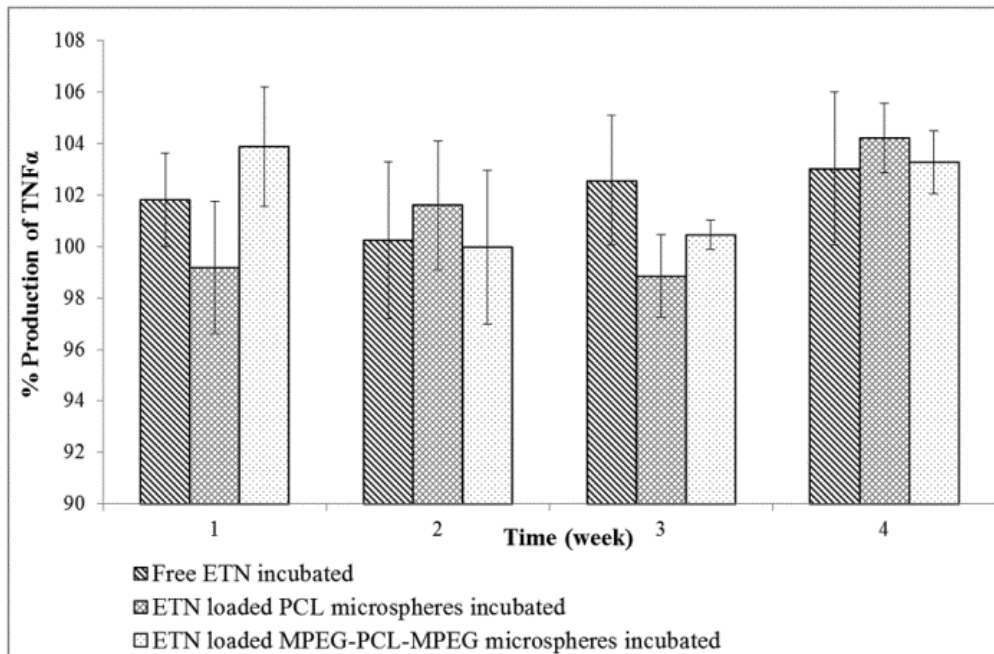
(A)

(B)

Figure 3.24. Comparison of production levels of total TNFα **(A)** and physiologically active TNFα **(B)** produced by FLS among treatment groups with respect to control group (Values are shown as mean ± S.E.M., n=5)
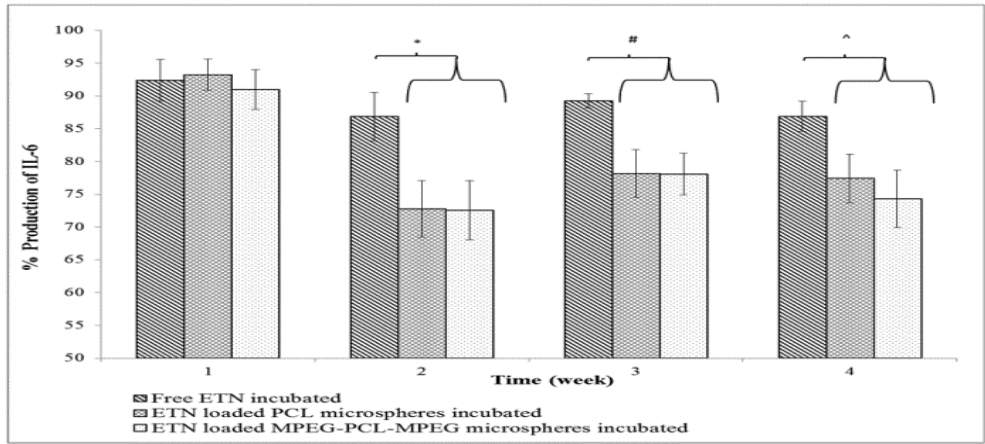
(A)
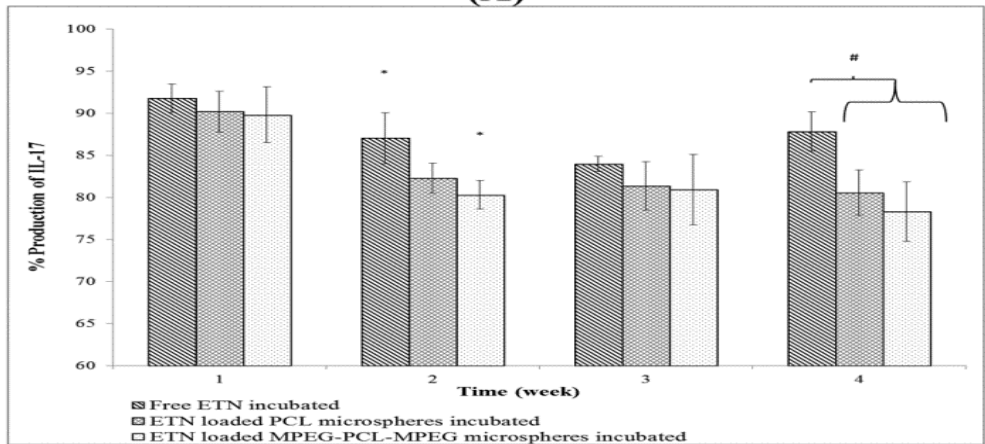
(B)
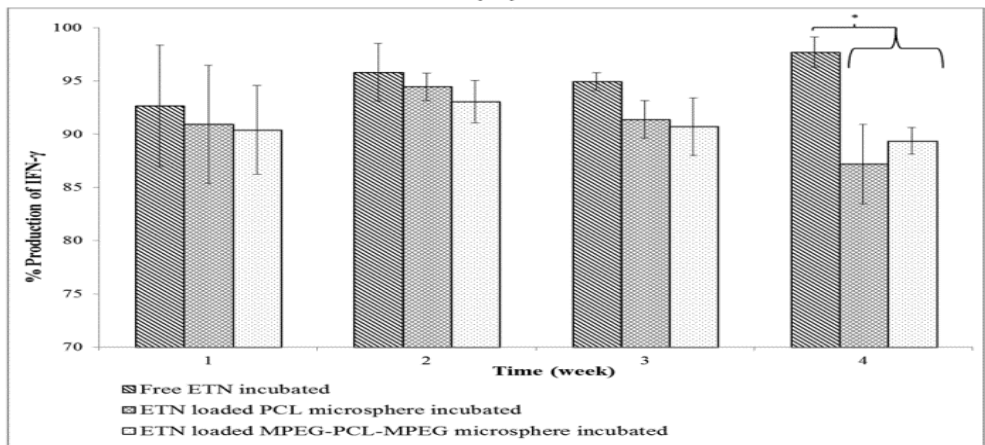
(C)

Figure 3.25. Comparison of production levels of IL-6 (**A**), IL-17 (**B**), IFNγ (**C**) produced by FLS among treatment groups with respect to control group (Values are shown as mean ± S.E.M., n=5)
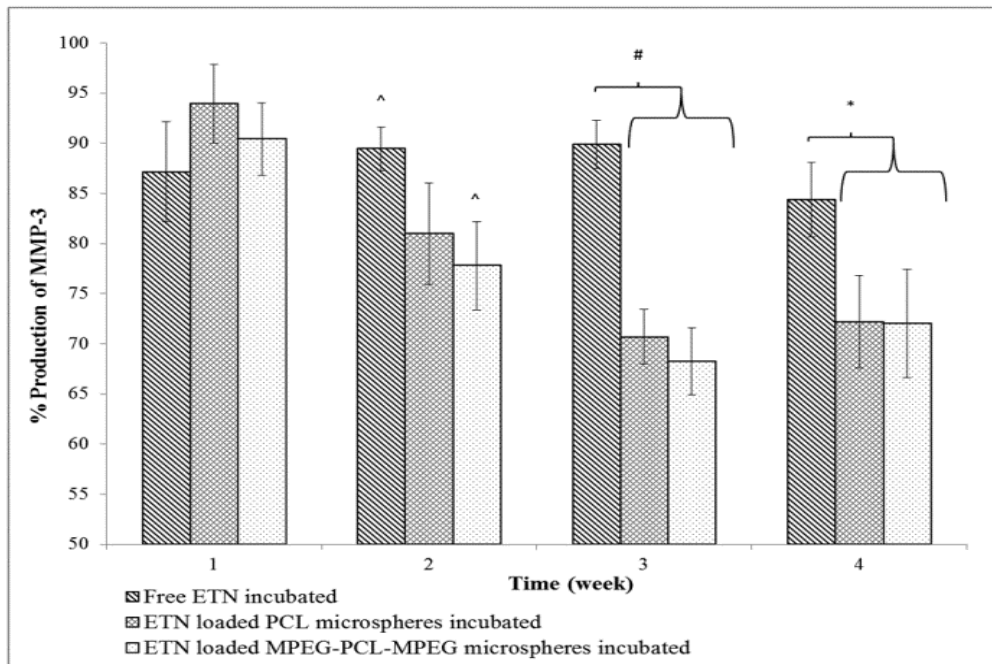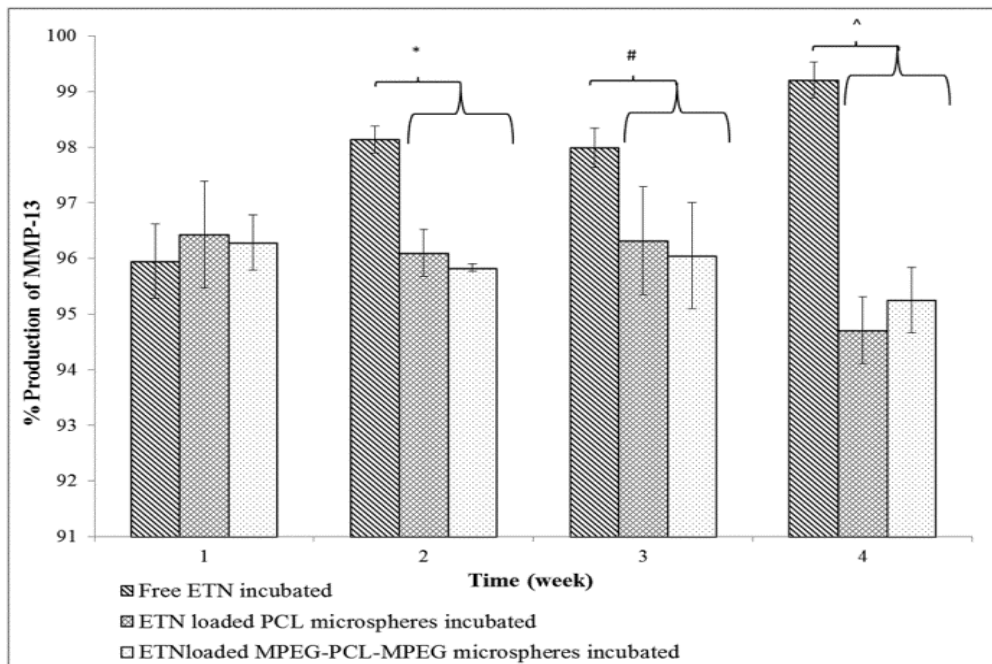
Figure 3.26. Comparison of production levels of MMP-3 **(A)** and MMP-13 **(B)** produced by FLS among treatment groups with respect to control group (Values are shown as mean ± S.E.M., n=5)
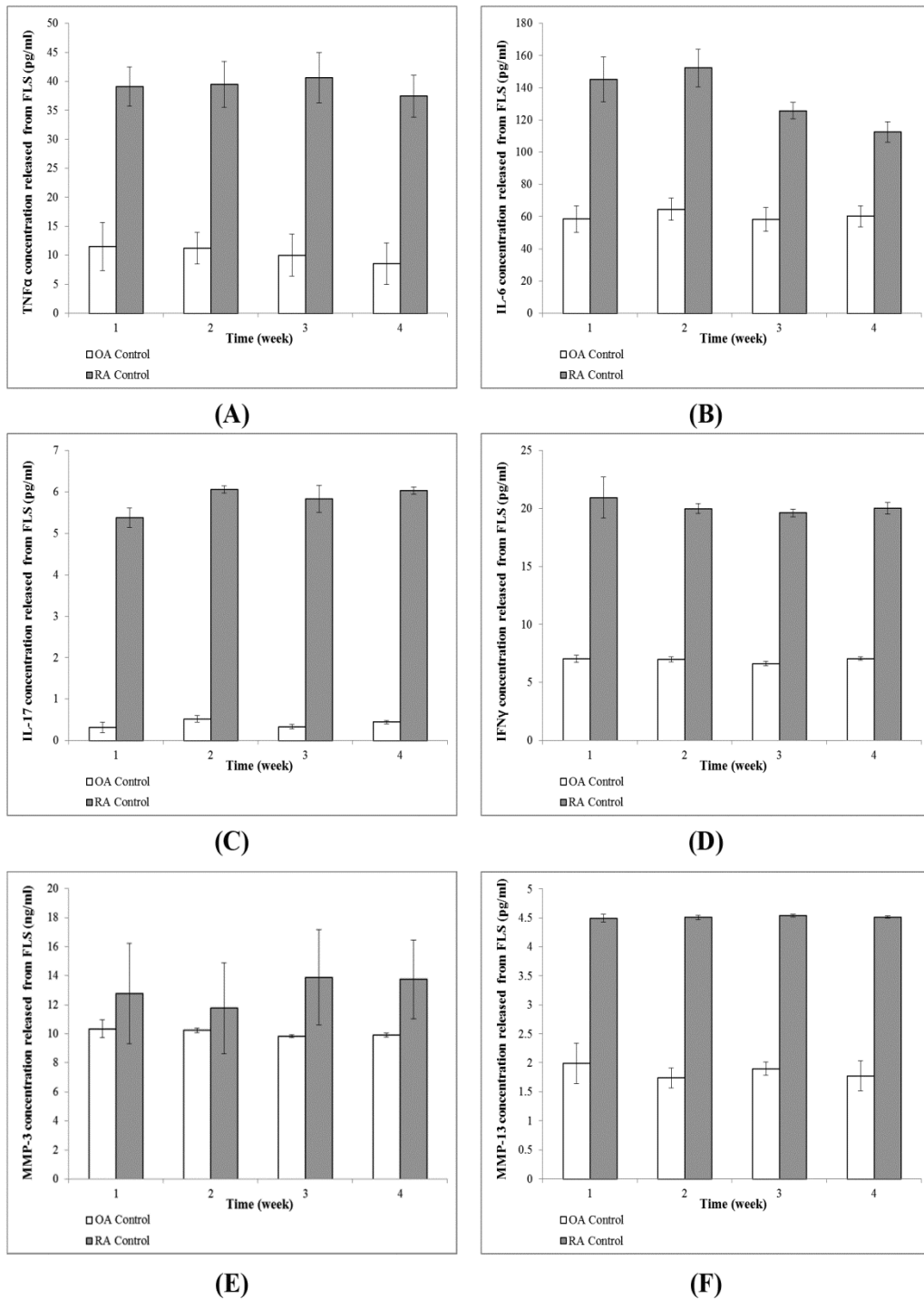
Figure 3.27. Comparison of production levels of TNFα **(A)**, IL-6 **(B)**, IL-17 **(C)**, IFN-γ **(D)**, MMP-3 **(E)**, MMP-13 **(F)** produced by FLS among RA and OA control groups (Values are shown as mean ± standard error of the mean, n=5 for RA control group and n=4 for OA control group)

3.4.5. Changes in mRNA Levels

Changes in mRNA expression levels of IL-6, TNFα, MMP-3, and MMP-13 of FLS were determined at each week for 4 weeks.

TNFα expression was relatively low with a PCR amplification yielding Ct values higher than 30 across all samples. Thus, TNFα expression was designated as "unquantitable". Changes in TNFα gene expressions for each patient were compared at each time according to their intensity in Table 3.17. Values of TNFα gene expressions showed periodical rise and decrease and sometimes values of TNFα gene expressions could not be measured. Therefore, it was thought that TNFα gene expressions changed depending on time. In literature, *in vitro* studies were conducted between 24-72 hours to examine the effects of anti-TNFα drugs on different cells by using ELISA [213, 224]. Additionally, studies in which the effects of different agents on IL-6, MMP-3, MMP-1 and other pro-inflammatory cytokine gene expressions of synovial fibroblast cells were also done between 24-72 hours [225, 226]. In this thesis, *in vitro* study in which the effects of ETN loaded microspheres on FLS were investigated was a long term study compared to the studies in literature. Therefore, it was thought that some changes of FLS behavior might occur during 4 week and values of TNFα gene expressions measured considerably low.

The relative expressions of IL-6, MMP-3, and MMP-13 are presented in Figure 3.28A, B, and C. The gene expression among experiment groups exhibited an inconsistent variation between 0.2 to 3 folds with a relatively high standard deviation. These observed variations in gene expression did not meet statistical significance and were interpreted as a background fluctuation. No significant variation in IL-6, TNFα, MMP-3, and 13 gene expressions in OA or RA samples was observed. Even though the mechanism of action of ETN is devoid of any impact on gene expression, a number of sights may further explain this observation. OA and RA FLS were at passage 4 and they have been maintained in cell culture conditions supplemented with FBS that is constantly propelling them to replicate. This supra-physiologic environment and conditions which are devoid of any host elements and resembling a fetal environment is likely to exert a "reset" to the cellular transcriptional program. In tissue culture, FLS are constantly under the influence of growth factors, thus constantly proliferating and lacking the immunological impact of humoral and cellular host immunity as well as other mediators. They are not surrounded by the inflammatory microenvironment as in the case in the inflamed joint. Considering this strikingly different state in tissue culture, they could not reflect the transcriptional program that is present inside the inflamed joint. Considering the significant impact of fetal calf serum concentrations on the expression of house-keeping genes (PMID: 11086195), it is likely that these cells are far from their *in vivo* state, thus do not induce TNFα or other inflammatory mediators unless they are stimulated. Stimulating FLS cells via soluble immunomodulators such as IFN-γ or LPS is likely to create an extensively acute reaction that is further far from the chronic inflammatory state of the rheumatoid

joint. Thus, ETN is suppressing the protein levels of TNFα, IL-6 and MMP-13 but is not affecting their transcription as discussed above.

Table 3.17. Changes in TNFα gene expressions for each patient at each time point

| | **TNFα gene expression** | | | | |
	H	M	C	S	Z
DAY ZERO	0	0	0	++	0
1st WEEK					
RA FLS (Control)	0	0	0	0	0
RA FLS + Free ETN	0	++	+	0	0
RA FLS + ETN loaded PCL microspheres	+	0	++	0	+
RA FLS + ETN loaded MPEG-PCL-MPEG microspheres	0	++	+	+	++
2nd WEEK					
RA FLS (Control)	++	++	+	0	++
RA FLS + Free ETN	-	+	++	+	0
RA FLS + ETN loaded PCL microspheres	0	0	+	++	++
RA FLS + ETN loaded MPEG-PCL-MPEG microspheres	+	+	++	++	++
3rd WEEK					
RA FLS (Control)	0	+	++	+	+
RA FLS + Free ETN	-	0	0	0	++
RA FLS + ETN loaded PCL microspheres	0	0	0	0	+
RA FLS + ETN loaded MPEG-PCL-MPEG microspheres	0	+	0	0	0
4th WEEK					
RA FLS (Control)	0	0	0	+	+
RA FLS + Free ETN	-	0	0	+	+
RA FLS + ETN loaded PCL microspheres	0	+	0	0	+
RA FLS + ETN loaded MPEG-PCL-MPEG microspheres	0	0	0	++	0

0 could not be measured
+ increase
++ significant increase
- no sample

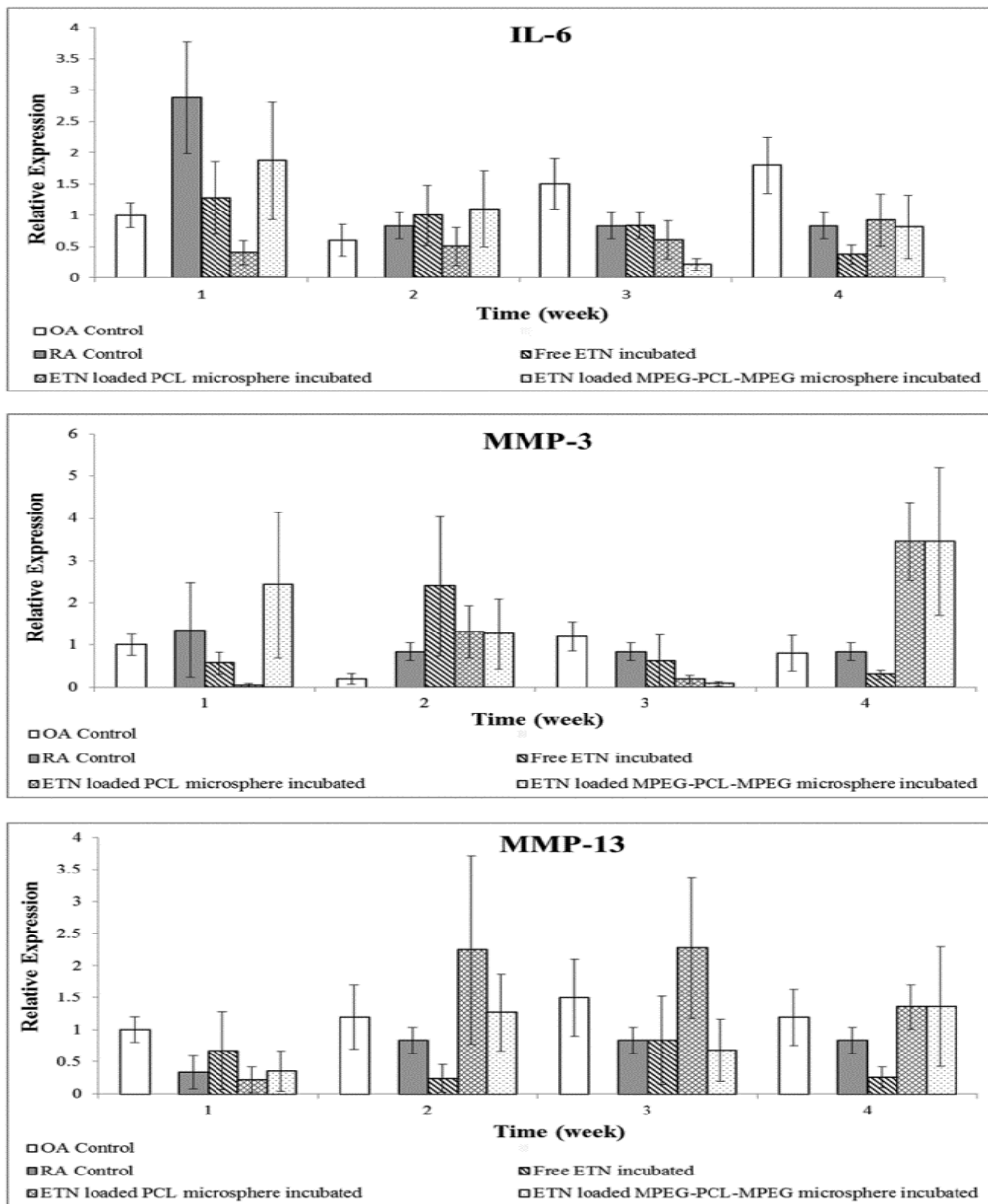**Figure 3.28.** The average relative expression of IL-6 and MMP-3 and 13 levels of OA and RA patients are presented in time-course. The relative suppression of IL-6 levels in OA group over the time did not meet statistical significance. Likewise the fluctuating expression of MMP-3 and MMP-13 transcripts exhibited a two fold alternating fluctuation between the groups (Values are shown as mean ± S.D., n=5 for RA FLS and n=4 for OA FLS).

CHAPTER 4

CONCLUSION

Rheumatoid arthritis (RA) is a common chronic inflammatory disease of the joints characterized by synovial inflammation. If untreated, this disease can result in progressive joint destruction, significant disability, systemic manifestations, and premature mortality. Anti-TNFα drugs show comprehensive effect against the treatment of inflammation due to their ability to reduce the production of TNFα as well as the other pro-inflammatory cytokines, significantly. However, systemic application of anti-TNFα at frequent intervals is costly and has side effects such as infection and injection-site reactions. In recent years, local treatment approaches are attractive for delivery of anti-TNFα drugs with high concentrations at the main site of inflammation. Controlled drug delivery systems of anti-TNFα drugs will provide the advantages like; suppressing the inflammation effectively via longer term drug supply, reducing the adverse effects arising from the use of high doses, and providing protection on protein based drug over the treatment period.

In this study, an intra-articularly injectable microsphere delivery system for one of the most widely used anti-rheumatic drug, namely etanercept (ETN) has been developed for the first time in literature to provide long term controlled release of the drug for suppressing the inflammation in RA. Two biocompatible polymers, PCL and MPEG-PCL-MPEG triblock copolymer, were used in microsphere preparation. PCL and MPEG-PCL-MPEG microspheres developed in this dissertation are patent pending for the manufacture and use for intra-articular delivery of anti-TNFα drugs used in the treatment of rheumatic diseases (PCT/TR2012/000148).

MPEG-PCL-MPEG triblock copolymer was synthesized by ring-opening polymerization of ε-CL initiated by MPEG considering the advantage of hydrophilic MPEG segment at both ends of the copolymer. ETN loaded PCL and MPEG-PCL-MPEG microspheres have been successfully formulated with spherical morphology with a suitable size (around 5 μm) for intra-articular applications. Introducing MPEG segment into PCL chains significantly improved the encapsulation efficiency of microspheres as well as loading of ETN. MPEG-PCL-MPEG microspheres enhanced protection of ETN bioactivity compared to their PCL counterpart. Additionally, MPEG segment minimized the protein adsorption on surfaces of microspheres by increasing surface negativity and therefore, in vivo use of MPEG-PCL-MPEG microspheres can be more beneficial compared to PCL microspheres. MPEG-PCL-MPEG microspheres showed increased release rate of ETN in all release media. Beside, MPEG segment improved the degradation properties of PCL

matrix. No toxic effect on cells with PCL and MPEG-PCL-MPEG microspheres was observed. PCL and MPEG-PCL-MPEG microspheres were able to release biologically active ETN for a prolonged time period, which will be superior to the conventional treatment applied at frequent intervals. Sustained ETN release from microspheres resulted with a significant decrease in pro-inflammatory cytokines (TNFα, IFNγ, IL-6, IL-17) and MMP levels (MMP-3, and MMP-13) while conserving the viability of fibroblast–like synoviocytes of RA patients compared to bolus administration of the free drug.

As a conclusion, it can be stated that MPEG-PCL-MPEG microspheres may be considered as a promising intra-articular ETN delivery system that will provide ETN in bioactive form for at least 3 months at the site without significant degradation of the system. Hence, it may be suggested as a new approach for treatment of RA, especially for cases with inflammation in few numbers of joints. However, further in vivo studies are necessary to investigate the treatment efficacy of etanercept ETN loaded microspheres.

REFERENCES

1. Edwards, J.C. The nature and origins of synovium: Experimental approaches to the study of synoviocyte differentiation. J Anat. 1994; 184 (Pt 3): 493-501.

2. Bartok, B. and G.S. Firestein. Fibroblast-like synoviocytes: Key effector cells in rheumatoid arthritis. Immunol Rev. 2010; 233(1): 233-55.

3. Iwanaga, T., M. Shikichi, H. Kitamura, H. Yanase, and K. Nozawa-Inoue. Morphology and functional roles of synoviocytes in the joint. Arch Histol Cytol. 2000; 63(1): 17-31.

4. Mundt, L.A. and K. Shanahan. Synovial fluid. in Graff's textbook of routine urinalysis and body fluids. 2011; Lippincott Williams & Wilkins: Philadelphia. p. 253-263.

5. Lipowitz, A.J. Synovial fluid. in Textbook of small animal orthopaedics, C.D. Newton and D.M. Nunamaker, Editors. 1985; International Veterinary Information Service: ABD.

6. Oates, K.M., W.E. Krause, R.L. Jones, and R.H. Colby. Rheopexy of synovial fluid and protein aggregation. J R Soc Interface. 2006; 3(6): 167-74.

7. Rinaudo, M., Y. Rozand, P. Mathieu, and T. Conrozier. Role of different pre-treatments on composition and rheology of synovial fluids. Polymers. 2009; 1: 16-34.

8. Tadmor, R., N. Chen, and J.N. Israelachvili. Thin film rheology and lubricity of hyaluronic acid solutions at a normal physiological concentration. J Biomed Mater Res. 2002; 61(4): 514-23.

9. Jay, G.D. Characterization of a bovine synovial fluid lubricating factor. I. Chemical, surface activity and lubricating properties. Connect Tissue Res. 1992; 28(1-2): 71-88.

10. Swann, D.A., S. Sotman, M. Dixon, and C. Brooks. The isolation and partial characterization of the major glycoprotein (lgp-i) from the articular lubricating fraction from bovine synovial fluid. Biochem J. 1977; 161(3): 473-85.

11. Jay, G.D., J.R. Torres, M.L. Warman, M.C. Laderer, and K.S. Breuer. The role of lubricin in the mechanical behavior of synovial fluid. Proc Natl Acad Sci U S A. 2007; 104(15): 6194-9.

12. Rogers, J., L. Shepstone, and P. Dieppe. Is osteoarthritis a systemic disorder of bone? Arthritis Rheum. 2004; 50(2): 452-7.

13. Choy, E.H. and G.S. Panayi. Cytokine pathways and joint inflammation in rheumatoid arthritis. N Engl J Med. 2001; 344(12): 907-16.

14. Firestein, G.S. Evolving concepts of rheumatoid arthritis. Nature. 2003; 423(6937): 356-61.

15. Doan, T. and E. Massarotti. Rheumatoid arthritis: An overview of new and emerging therapies. J Clin Pharmacol. 2005; 45(7): 751-62.

16. Basra, G., P. Jajoria, and E. Gonzalez. Rheumatoid arthritis and swine influenza vaccine: A case report. Case Reports in Rheumatology. 2012; 2012(Article ID 785028): 1-3.

17. Lokwani, P., Y. Upadhyay, P. Kumar, S. Gupta, R. Kalyanwat, and R.K. Songara. Review on: Ankylosing spondylitis. Pharmacie Globale (IJCP). 2011; 8(02).

18. Cantini, F., L. Niccoli, C. Nannini, O. Kaloudi, M. Bertoni, and E. Cassara. Psoriatic arthritis: A systematic review. Int J Rheum Dis. 2010; 13: 300-317.

19. Hashkes, P.J. and R.M. Laxer. Medical treatment of juvenile idiopathic arthritis. JAMA. 2005; 294(13): 1671-84.

20. Weiss, J.E. and N.T. Ilowite. Juvenile idiopathic arthritis. Rheumatic Disease Clinics of North America. 2007; 33(3): 441-+.

21. Eyre, S., J. Bowes, D. Diogo, A. Lee, A. Barton, P. Martin, A. Zhernakova, E. Stahl, S. Viatte, K. McAllister, C.I. Amos, L. Padyukov, R.E. Toes, T.W. Huizinga, C. Wijmenga, G. Trynka, L. Franke, H.J. Westra, L. Alfredsson, X. Hu, C. Sandor, P.I. de Bakker, S. Davila, C.C. Khor, K.K. Heng, R. Andrews, S. Edkins, S.E. Hunt, C. Langford, D. Symmons, P. Concannon, S. Onengut-Gumuscu, S.S. Rich, P. Deloukas, M.A. Gonzalez-Gay, L. Rodriguez-Rodriguez, L. Arlsetig, J. Martin, S. Rantapaa-Dahlqvist, R.M. Plenge, S. Raychaudhuri, L. Klareskog, P.K. Gregersen, and J. Worthington. High-density genetic mapping identifies new susceptibility loci for rheumatoid arthritis. Nat Genet. 2012; 44(12): 1336-40.

22. Lipsky, P.E. Rheumatoid arthritis. in Harrison's rheumatology, A. Fauci and C.M. Langford, Editors. 2010; McGraw-Hill: United States. p. 82-99.

23. Khuder, S.A., A.Z. Peshimam, and S. Agraharam. Environmental risk factors for rheumatoid arthritis. Rev Environ Health. 2002; 17(4): 307-15.

24. Lee, D.M. and M.E. Weinblatt. Rheumatoid arthritis. Lancet. 2001; 358(9285): 903-11.

25. Juarez, M., A. Filer, and C.D. Buckley. Fibroblasts as therapeutic targets in rheumatoid arthritis and cancer. Swiss Med Wkly. 2012; 142: w13529.

26. Pap, T., U. Muller-Ladner, R.E. Gay, and S. Gay. Fibroblast biology. Role of synovial fibroblasts in the pathogenesis of rheumatoid arthritis. Arthritis Res. 2000; 2(5): 361-7.

27. Kinne, R.W., B. Stuhlmuller, and G.R. Burmester. Cells of the synovium in rheumatoid arthritis. Macrophages. Arthritis Res Ther. 2007; 9(6): 224.

28. Cope, A.P. T cells in rheumatoid arthritis. Arthritis Res Ther. 2008; 10 Suppl 1: S1.

29. Mauri, C. and M.R. Ehrenstein. Cells of the synovium in rheumatoid arthritis. B cells. Arthritis Res Ther. 2007; 9(2): 205.

30. Otero, M. and M.B. Goldring. Cells of the synovium in rheumatoid arthritis. Chondrocytes. Arthritis Res Ther. 2007; 9(5): 220.

31. Schett, G. Cells of the synovium in rheumatoid arthritis. Osteoclasts. Arthritis Res Ther. 2007; 9(1): 203.

32. Gajewski, M., P. Rzodkiewicz, and S. Maslinski. The role of neutrophils in rheumatoid arthritis – experiments in vitro: A change of conception? in Rheumatoid arthritis - etiology, consequences and co-morbidities, A.B. Lemmey, Editor. 2012; InTech: Croatia. p. 59-72.

33. Middleton, J., L. Americh, R. Gayon, D. Julien, L. Aguilar, F. Amalric, and J.P. Girard. Endothelial cell phenotypes in the rheumatoid synovium: Activated, angiogenic, apoptotic and leaky. Arthritis Res Ther. 2004; 6(2): 60-72.

34. Wang, W., S. Shao, Z. Jiao, M. Guo, H. Xu, and S. Wang. The th17/treg imbalance and cytokine environment in peripheral blood of patients with rheumatoid arthritis. Rheumatol Int. 2012; 32(4): 887-93.

35. Boissier, M.C., E. Assier, G. Falgarone, and N. Bessis. Shifting the imbalance from th1/th2 to th17/treg: The changing rheumatoid arthritis paradigm. Joint Bone Spine. 2008; 75(4): 373-5.

36. Zhu, J. and W.E. Paul. Cd4 t cells: Fates, functions, and faults. Blood. 2008; 112(5): 1557-69.

37. Chen, J., J. Li, H. Gao, C. Wang, J. Luo, Z. Lv, and X. Li. Comprehensive evaluation of different t-helper cell subsets differentiation and function in rheumatoid arthritis. J Biomed Biotechnol. 2012; 2012: 535361.

38. Brentano, F., D. Kyburz, O. Schorr, R. Gay, and S. Gay. The role of toll-like receptor signalling in the pathogenesis of arthritis. Cell Immunol. 2005; 233(2): 90-6.

39.   Crome, S.Q., A.Y. Wang, and M.K. Levings. Translational mini-review series on th17 cells: Function and regulation of human t helper 17 cells in health and disease. Clin Exp Immunol. 2010; 159(2): 109-19.

40.   Annunziato, F., L. Cosmi, F. Liotta, E. Maggi, and S. Romagnani. Type 17 t helper cells-origins, features and possible roles in rheumatic disease. Nat Rev Rheumatol. 2009; 5(6): 325-31.

41.   Fossiez, F., O. Djossou, P. Chomarat, L. Flores-Romo, S. Ait-Yahia, C. Maat, J.J. Pin, P. Garrone, E. Garcia, S. Saeland, D. Blanchard, C. Gaillard, B. Das Mahapatra, E. Rouvier, P. Golstein, J. Banchereau, and S. Lebecque. T cell interleukin-17 induces stromal cells to produce proinflammatory and hematopoietic cytokines. J Exp Med. 1996; 183(6): 2593-603.

42.   Isaacs, J.D. The changing face of rheumatoid arthritis: Sustained remission for all? Nat J Rev Immunol. 2010; 10(8): 605-611.

43.   McInnes, I.B. and G. Schett. Cytokines in the pathogenesis of rheumatoid arthritis. Nat Rev Immunol. 2007; 7(6): 429-42.

44.   Feldmann, M., F.M. Brennan, and R.N. Maini. Role of cytokines in rheumatoid arthritis. Annu Rev Immunol. 1996; 14: 397-440.

45.   Meyer, L.H., L. Franssen, and T. Pap. The role of mesenchymal cells in the pathophysiology of inflammatory arthritis. Best Pract Res Clin Rheumatol. 2006; 20(5): 969-81.

46.   Bottini, N. and G.S. Firestein. Duality of fibroblast-like synoviocytes in ra: Passive responders and imprinted aggressors. Nat Rev Rheumatol. 2013; 9(1): 24-33.

47.   Burger, J.A., N.J. Zvaifler, N. Tsukada, G.S. Firestein, and T.J. Kipps. Fibroblast-like synoviocytes support b-cell pseudoemperipolesis via a stromal cell-derived factor-1- and cd106 (vcam-1)-dependent mechanism. J Clin Invest. 2001; 107(3): 305-15.

48.   Muller-Ladner, U. and S. Gay. Mmps and rheumatoid synovial fibroblasts: Siamese twins in joint destruction? Ann Rheum Dis. 2002; 61(11): 957-9.

49.   Pap, T., I. Meinecke, U. Muller-Ladner, and S. Gay. Are fibroblasts involved in joint destruction? Ann Rheum Dis. 2005; 64 Suppl 4: iv52-4.

50.   Butoescu, N., O. Jordan, and E. Doelker. Intra-articular drug delivery systems for the treatment of rheumatic diseases: A review of the factors influencing their performance. Eur J Pharm Biopharm. 2009; 73(2): 205-18.

51.   Fries, J.F. Current treatment paradigms in rheumatoid arthritis. Rheumatology (Oxford). 2000; 39 Suppl 1: 30-5.

52.   Rindfleisch, J.A. and D. Muller. Diagnosis and management of rheumatoid arthritis. Am Fam Physician. 2005; 72(6): 1037-47.

53.   Sigurdardottir, S.L., J. Freysdottir, T. Vikingsdottir, H. Valdimarsson, and A. Vikingsson. Do non-steroidal anti-inflammatory drugs influence chronic inflammation? The effects of piroxicam on chronic antigen-induced arthritis in rats. Scand J Rheumatol. 2008; 37(6): 469-76.

54.   O'Dell, J.R. Therapeutic strategies for rheumatoid arthritis. N Engl J Med. 2004; 350(25): 2591-602.

55.   van der Heide, A., J.W. Jacobs, J.W. Bijlsma, A.H. Heurkens, C. van Booma-Frankfort, M.J. van der Veen, H.C. Haanen, D.M. Hofman, G.A. van Albada-Kuipers, E.J. ter Borg, H.L. Brus, H.J. Dinant, A.A. Kruize, and Y. Schenk. The effectiveness of early treatment with "second-line" antirheumatic drugs. A randomized, controlled trial. Ann Intern Med. 1996; 124(8): 699-707.

56.   Verstappen, S.M., J.W. Jacobs, J.W. Bijlsma, A.H. Heurkens, C. van Booma-Frankfort, E.J. Borg, D.M. Hofman, and M.J. van der Veen. Five-year followup of rheumatoid arthritis patients after early treatment with disease-modifying antirheumatic drugs versus treatment according to the pyramid approach in the first year. Arthritis Rheum. 2003; 48(7): 1797-807.

57.   Fan, P.T. and K.H. Leong. The use of biological agents in the treatment of rheumatoid arthritis. Ann Acad Med Singapore. 2007; 36(2): 128-34.

58.   Quan, L.D., G.M. Thiele, J. Tian, and D. Wang. The development of novel therapies for rheumatoid arthritis. Expert Opin Ther Pat. 2008; 18(7): 723-738.

59.   Choy, E.H., A.F. Kavanaugh, and S.A. Jones. The problem of choice: Current biologic agents and future prospects in ra. Nat Rev Rheumatol. 2013; 9(3): 154-63.

60.   Breedveld, F.C., M.H. Weisman, A.F. Kavanaugh, S.B. Cohen, K. Pavelka, R. van Vollenhoven, J. Sharp, J.L. Perez, and G.T. Spencer-Green. The premier study: A multicenter, randomized, double-blind clinical trial of combination therapy with adalimumab plus methotrexate versus methotrexate alone or adalimumab alone in patients with early, aggressive rheumatoid arthritis who had not had previous methotrexate treatment. Arthritis Rheum. 2006; 54(1): 26-37.

61.   St Clair, E.W., D.M. van der Heijde, J.S. Smolen, R.N. Maini, J.M. Bathon, P. Emery, E. Keystone, M. Schiff, J.R. Kalden, B. Wang, K. Dewoody, R. Weiss, and D. Baker. Combination of infliximab and methotrexate therapy for early rheumatoid arthritis: A randomized, controlled trial. Arthritis Rheum. 2004; 50(11): 3432-43.

62.   Emery, P., F.C. Breedveld, S. Hall, P. Durez, D.J. Chang, D. Robertson, A. Singh, R.D. Pedersen, A.S. Koenig, and B. Freundlich. Comparison of methotrexate monotherapy with a combination of methotrexate and etanercept in active, early,

moderate to severe rheumatoid arthritis (comet): A randomised, double-blind, parallel treatment trial. Lancet. 2008; 372(9636): 375-82.

63.   Dayer, J.M. Interleukin 1 or tumor necrosis factor-alpha: Which is the real target in rheumatoid arthritis? J Rheumatol Suppl. 2002; 65: 10-5.

64.   Butler, D.M., R.N. Maini, M. Feldman, and F.M. Brennan. Modulation of proinflammatory cytokine release in rheumatoid synovial membrane cell cultures: Comparison of monoclonal anti tnf-α antibody with interleukin-1 receptor antagonist. Eur Cytokine Netw. 1995; 6: 225-30.

65.   Geyer, M. and U. Muller-Ladner. Rationale of using different biological therapies in rheumatoid arthritis. Arthritis Res Ther. 2010; 12(4): 214.

66.   Jarvis, B. and D. Faulds. Etanercept: A review of its use in rheumatoid arthritis. Drugs. 1999; 57(6): 945-66.

67.   Mohler, K.M., D.S. Torrance, C.A. Smith, R.G. Goodwin, K.E. Stremler, V.P. Fung, H. Madani, and M.B. Widmer. Soluble tumor necrosis factor (tnf) receptors are effective therapeutic agents in lethal endotoxemia and function simultaneously as both tnf carriers and tnf antagonists. J Immunol. 1993; 151(3): 1548-61.

68.   Dhillon, S., K.A. Lyseng-Williamson, and L.J. Scott. Etanercept: A review of its use in the management of rheumatoid arthritis. Drugs. 2007; 67(8): 1211-41.

69.   Bathon, J.M., R.W. Martin, R.M. Fleischmann, J.R. Tesser, M.H. Schiff, E.C. Keystone, M.C. Genovese, M.C. Wasko, L.W. Moreland, A.L. Weaver, J. Markenson, and B.K. Finck. A comparison of etanercept and methotrexate in patients with early rheumatoid arthritis. N Engl J Med. 2000; 343(22): 1586-93.

70.   Seriolo, B., S. Paolino, A. Sulli, V. Ferretti, and M. Cutolo. Bone metabolism changes during anti-tnf-alpha therapy in patients with active rheumatoid arthritis. Ann N Y Acad Sci. 2006; 1069: 420-7.

71.   Korth-Bradley, J.M., A.S. Rubin, R.K. Hanna, D.K. Simcoe, and M.E. Lebsack. The pharmacokinetics of etanercept in healthy volunteers. Ann Pharmacother. 2000; 34(2): 161-4.

72.   Lyseng-Williamson, K.A. and G.L. Plosker. Etanercept: A pharmacoeconomic review of its use in rheumatoid arthritis. Pharmacoeconomics. 2004; 22(16): 1071-95.

73.   Giles, J.T. and J.M. Bathon. Serious infections associated with anticytokine therapies in the rheumatic diseases. J Intensive Care Med. 2004; 19(6): 320-34.

74.   Bongartz, T., A.J. Sutton, M.J. Sweeting, I. Buchan, E.L. Matteson, and V. Montori. Anti-tnf antibody therapy in rheumatoid arthritis and the risk of serious infections and malignancies: Systematic review and meta-analysis of rare harmful effects in randomized controlled trials. JAMA. 2006; 295(19): 2275-2285.

75. Fisher, B.A.C. and A. Keat. Should we be using intraarticular tumor necrosis factor blockade in inflammatory monoarthritis? J Rheumatol. 2006; 33: 1934-1935.

76. Nikas, S.N., T.I. Temekonidis, A.K. Zikou, M.I. Argyropoulou, S. Efremidis, and A.A. Drosos. Treatment of resistant rheumatoid arthritis by intra-articular infliximab injections: A pilot study. Ann Rheum Dis. 2004; 63(1): 102-3.

77. Conti, F., R. Priori, M.S. Chimenti, G. Coari, A. Annovazzi, G. Valesini, and A. Signore. Successful treatment with intraarticular infliximab for resistant knee monarthritis in a patient with spondylarthropathy: A role for scintigraphy with 99mtc-infliximab. Arthritis Rheum. 2005; 52(4): 1224-6.

78. Bliddal, H., L. Terslev, E. Qvistgaard, M. Konig, C.C. Holm, H. Rogind, M. Boesen, B. Danneskiold-Samsoe, and S. Torp-Pedersen. A randomized, controlled study of a single intra-articular injection of etanercept or glucocorticosteroids in patients with rheumatoid arthritis. Scand J Rheumatol. 2006; 35(5): 341-5.

79. Bliddal, H., L. Terslev, E. Qvistgaard, P. Recke, C.C. Holm, B. Danneskiold-Samsoe, A. Savnik, and S. Torp-Pedersen. Safety of intra-articular injection of etanercept in small-joint arthritis: An uncontrolled, pilot-study with independent imaging assessment. Joint Bone Spine. 2006; 73(6): 714-7.

80. Boesen, M., L. Boesen, K.E. Jensen, M.A. Cimmino, S. Torp-Pedersen, L. Terslev, M. Koenig, B. Danneskiold-Samsoe, H. Rogind, and H. Bliddal. Clinical outcome and imaging changes after intraarticular (ia) application of etanercept or methylprednisolone in rheumatoid arthritis: Magnetic resonance imaging and ultrasound-doppler show no effect of ia injections in the wrist after 4 weeks. J Rheumatol. 2008; 35(4): 584-91.

81. Roux, C.H., O. Brocq, L. Valerio, N. Amoretti, V. Breuil, C. Albert-Sabonnadiere, C. Grisot, Y. Allam, P. Chevalier, C. pradier, and L. Euller-Ziegler. Etanercept versus glucocorticosteroids intra-articular (ia) injections in rheumatoid arthritis (ra): A randomized double blind study. Ann Rheum Dis. 2008; 67: 329.

82. Bouysset, M., F. Coury, T. Tavernier, M. Bonnin, J. Damiano, C. Nemoz, and J.G. Tebib. Intraarticular injection of adalimumab in localized psoriatic arthritis. Medecine Et Chirurgie Du Pied. 2009; 25(4): 133-135.

83. Ayral, X. Injections in the treatment of osteoarthritis. Best Pract Res Clin Rheumatol. 2001; 15(4): 609-26.

84. Jain, K.K. Drug delivery systems - an overview. Methods Mol Biol. 2008; 437: 1-50.

85. Allen, T.M. and P.R. Cullis. Drug delivery systems: Entering the mainstream. Science. 2004; 303(5665): 1818-22.

86. Verma, R.K. and S. Garg. Current status of drug delivery technologies and future directions. Pharm Technol On-line. 2001; 25(2): 1-14.

87. Stevenson, C.L., J.T. Santini, Jr., and R. Langer. Reservoir-based drug delivery systems utilizing microtechnology. Adv Drug Deliv Rev. 2012; 64(14): 1590-602.

88. Paolino, D., P. Sinha, and M. Ferrari. Drug deliverry sytems. in Encyclopedia of medical devices and instrumentation, J.G. Webster, Editor. 2006; John Wiley & Sons, Inc. p. 437-495.

89. Zhang, L., D. Pornpattananangku, C.M. Hu, and C.M. Huang. Development of nanoparticles for antimicrobial drug delivery. Curr Med Chem. 2010; 17(6): 585-94.

90. Nieh, M.P., J. Katsaras, and X. Qi. Controlled release mechanisms of spontaneously forming unilamellar vesicles. Biochim Biophys Acta. 2008; 1778(6): 1467-71.

91. Alsaleh, F.M., F.J. Smith, S. Keady, and K.M. Taylor. Insulin pumps: From inception to the present and toward the future. J Clin Pharm Ther. 2010; 35(2): 127-38.

92. Wessely, R., J. Hausleiter, C. Michaelis, B. Jaschke, M. Vogeser, S. Milz, B. Behnisch, T. Schratzenstaller, M. Renke-Gluszko, M. Stover, E. Wintermantel, A. Kastrati, and A. Schomig. Inhibition of neointima formation by a novel drug-eluting stent system that allows for dose-adjustable, multiple, and on-site stent coating. Arterioscler Thromb Vasc Biol. 2005; 25(4): 748-53.

93. Colilla, M., M. Manzano, and M. Vallet-Regi. Recent advances in ceramic implants as drug delivery systems for biomedical applications. Int J Nanomedicine. 2008; 3(4): 403-14.

94. Coelho, J.F., P.C. Ferreira, P. Alves, R. Cordeiro, A.C. Fonseca, J.R. Gois, and M.H. Gil. Drug delivery systems: Advanced technologies potentially applicable in personalized treatments. EPMA J. 2010; 1(1): 164-209.

95. Frokjaer, S. and D.E. Otzen. Protein drug stability: A formulation challenge. Nat Rev Drug Discov. 2005; 4(4): 298-306.

96. Malik, N.N. Drug discovery: Past, present and future. Drug Discov Today. 2008; 13(21-22): 909-12.

97. Malik, D.K., S. Baboota, A. Ahuja, S. Hasan, and J. Ali. Recent advances in protein and peptide drug delivery systems. Curr Drug Deliv. 2007; 4(2): 141-51.

98. Gupta, H. and A. Sharma. Recent trends in protein and peptide drug delivery systems. Asian J Pharm. 2009; 4(2): 141-151.

99. Pisal, D.S., M.P. Kosloski, and S.V. Balu-Iyer. Delivery of therapeutic proteins. J Pharm Sci. 2010; 99(6): 2557-75.

100. Ye, M., S. Kim, and K. Park. Issues in long-term protein delivery using biodegradable microparticles. J Control Release. 2010; 146(2): 241-60.

101. Sinha, V.R. and A. Trehan. Biodegradable microspheres for protein delivery. J Control Release. 2003; 90(3): 261-80.

102. Vilar, G., J. Tulla-Puche, and F. Albericio. Polymers and drug delivery systems. Curr Drug Deliv. 2012; 9(4): 367-94.

103. Panyam, J., S.K. Sahoo, S. Prabha, T. Bargar, and V. Labhasetwar. Fluorescence and electron microscopy probes for cellular and tissue uptake of poly(d,l-lactide-co-glycolide) nanoparticles. Int J Pharm. 2003; 262(1-2): 1-11.

104. Yang, W.W. and E. Pierstorff. Reservoir-based polymer drug delivery systems. J Lab Autom. 2012; 17(1): 50-8.

105. Kim, K.K. and D.W. Pack. Microspheres for drug delivery in Biomems and biomedical nanotechnology, M. Ferrari, A.P. Lee, and L.J. Lee, Editors. 2006; Springer US. p. 19-50.

106. BBC-Research, Microspheres: Technologies and global markets. 2010, BCC p. 210.

107. Pillai, O. and R. Panchagnula. Polymers in drug delivery. Curr Opin Chem Biol. 2001; 5(4): 447-51.

108. Sinha, V.R., K. Bansal, R. Kaushik, R. Kumria, and A. Trehan. Poly-epsilon-caprolactone microspheres and nanospheres: An overview. Int J Pharm. 2004; 278(1): 1-23.

109. Woodruff, M.A. and W. Dietmar. The return of a forgotten polymer: Polycaprolactone in the 21st century. Prog Polym Sci. 2010; 35(10): 1217-1256.

110. Erdemli, O., O. Captug, H. Bilgili, D. Orhan, A. Tezcaner, and D. Keskin. In vitro and in vivo evaluation of the effects of demineralized bone matrix or calcium sulfate addition to polycaprolactone-bioglass composites. J Mater Sci Mater Med. 2010; 21(1): 295-308.

111. Luciani, A., V. Coccoli, S. Orsi, L. Ambrosio, and P.A. Netti. Pcl microspheres based functional scaffolds by bottom-up approach with predefined microstructural properties and release profiles. Biomaterials. 2008; 29(36): 4800-7.

112. Izquierdo, R., N. Garcia-Giralt, M.T. Rodriguez, E. Caceres, S.J. Garcia, J.L. Gomez Ribelles, M. Monleon, J.C. Monllau, and J. Suay. Biodegradable pcl scaffolds with an interconnected spherical pore network for tissue engineering. J Biomed Mater Res A. 2008; 85(1): 25-35.

113. Lin, W.J. and L.I. Huang. Fabrication of porous poly(epsilon-caprolactone) microparticles for protein release. J Microencapsul. 2001; 18(5): 577-84.

114. Coccoli, V., A. Luciani, S. Orsi, V. Guarino, F. Causa, and P.A. Netti. Engineering of poly(epsilon-caprolactone) microcarriers to modulate protein encapsulation capability and release kinetic. J Mater Sci Mater Med. 2008; 19(4): 1703-11.

115. Dash, T.K. and V.B. Konkimalla. Poly-caprolactone based formulations for drug delivery and tissue engineering: A review. J Control Release. 2012; 158(1): 15-33.

116. Pitt, C.G. Poly-ε-caprolactone and its copolymers. in Biodegradable polymers as drug delivery systems, M. Chasin and R. Langer, Editors. 1990; Marcel-Dekker: New York. p. 71-120.

117. Tay, B.Y., S.X. Zhang, M.H. Myint, F.L. Ng, M. Chandrasekaran, and L.K.A. Tan. Processing of polycaprolactone porous structure for scaffold development. J Mater Process Tech. 2007; 182: 117-121.

118. Ciardelli, G., V. Chiono, G. Vozzi, M. Pracella, A. Ahluwalia, N. Barbani, C. Cristallini, and P. Giusti. Blends of poly-(epsilon-caprolactone) and polysaccharides in tissue engineering applications. Biomacromolecules. 2005; 6(4): 1961-76.

119. Ramesh, D.V., N. Medlicott, M. Razzak, and I.G. Tucker. Microencapsulation of fitc-bsa into poly(ε-caprolactone) by a water-in-oil-in-oil solvent evaporation technique. Trends Biomater Artif Organs. 2002; 15: 31-36.

120. Wei, X., C. Gong, M. Gou, S. Fu, Q. Guo, S. Shi, F. Luo, G. Guo, L. Qiu, and Z. Qian. Biodegradable poly(epsilon-caprolactone)-poly(ethylene glycol) copolymers as drug delivery system. Int J Pharm. 2009; 381(1): 1-18.

121. Kim, M.S., K.S. Seo, H. Hyun, G. Khang, and S.H. Cho. Controlled release of bovine serum albumin using mpeg-pcl diblock copolymers as implantable protein carriers. J Appl Polym Sci. 2006; 102: 1561-1567.

122. Zhou, S., X. Deng, and H. Yang. Biodegradable poly(epsilon-caprolactone)-poly(ethylene glycol) block copolymers: Characterization and their use as drug carriers for a controlled delivery system. Biomaterials. 2003; 24(20): 3563-70.

123. Knop, K., R. Hoogenboom, D. Fischer, and U.S. Schubert. Poly(ethylene glycol) in drug delivery: Pros and cons as well as potential alternatives. Angew Chem Int Ed Engl. 2010; 49(36): 6288-308.

124. Ryu, J.G., Y.I. Jeong, Y.H. Kim, I.S. Kim, D.H. Kim, and S.H. Kim. Preparation of core-shell type nanoparticles of poly(ε-caprolactone/poly(ethylene glycol)/poly(ε-caprolactone) triblock copolymers. Bull. Korean Chem. Soc. 2001; 22(5): 467.

125. Liu, M.J., K. Kono, and J.M.J. Frechet. Water-soluble dendrimer-poly(ethylene glycol) starlike conjugates as potential drug carriers. Journal of Polymer Science Part a-Polymer Chemistry. 1999; 37(17): 3492-3503.

126. Wattendorf, U. and H.P. Merkle. Pegylation as a tool for the biomedical engineering of surface modified microparticles. J Pharm Sci. 2008; 97(11): 4655-69.

127. Sinha, V.R., A. Aggarwal, and A. Trehan. Biodegradable pegylated microspheres and nanospheres. Am J Drug Deliv. 2004; 2(3): 157-171.

128. Bonacucina, G., M. Cespi, G. Mencarelli, G. Giorgioni, and G.F. Palmieri. Thermosensitive self-assembling block copolymers as drug delivery systems. Polymers. 2011; 3(2): 779-811.

129. Lemmouchi, Y., M.C. Perry, A.J. Amass, K. Chakraborty, and E. Schacht. Novel synthesis of biodegradable amphiphilic linear and star block copolymers based on poly(epsilon-caprolactone) and poly(ethylene glycol). Journal of Polymer Science Part a-Polymer Chemistry. 2007; 45(17): 3975-3985.

130. Gong, C.Y., Z.Y. Qian, C.B. Liu, M.J. Huang, Y.C. Gu, Y.J. Wen, B. Kan, K. Wang, M. Dai, X.Y. Li, M.L. Gou, M.J. Tu, and Y.Q. Wei. A thermosensitive hydrogel based on biodegradable amphiphilic poly(ethyleneglycol)–polycaprolactone–poly(ethyleneglycol) block copolymers. Smart Mater Struct. 2007; 16: 927-933.

131. Nikles, S.M., J.A. Nikles, J.S. Hudson, and D.E. Nikles. Diblock copolymers for magnetically triggered drug delivery systems. JOSHUA. 2010; 7: 35-38.

132. Cuong, N.-V., J.-L. Jiang, Y.-L. Li, J.-R. Chen, S.-C. Jwo, and M.-F. Hsieh. Doxorubicin-loaded peg-pcl-peg micelle using xenograft model of nude mice: Effect of multiple administration of micelle on the suppression of human breast cancer. Cancers. 2011; 3: 61-78.

133. Diao, Y.Y., H.Y. Li, Y.H. Fu, M. Han, Y.L. Hu, H.L. Jiang, Y. Tsutsumi, Q.C. Wei, D.W. Chen, and J.Q. Gao. Doxorubicin-loaded peg-pcl copolymer micelles enhance cytotoxicity and intracellular accumulation of doxorubicin in adriamycin-resistant tumor cells. Int J Nanomedicine. 2011; 6: 1955-62.

134. Gong, C., S. Shi, P. Dong, B. Kan, M. Gou, X. Wang, X. Li, F. Luo, X. Zhao, Y. Wei, and Z. Qian. Synthesis, characterization, degradation, and in vitro drug release behavior of thermosensitive hydrogel based on peg-pcl-peg block copolymers. Int J Pharm. 2009; 365(1-2): 89-99.

135. Gong, C., S. Shi, P. Dong, B. Kan, M. Gou, X. Wang, X. Li, F. Luo, X. Zhao, Y. Wei, and Z. Qian. Synthesis and characterization of peg-pcl-peg thermosensitive hydrogel. Int J Pharm. 2009; 365(1-2): 89-99.

136. Gao, X., B. Kan, M. Gou, J. Zhang, G. Guo, N. Huang, X. Zhao, and Z. Qian. Preparation of anti-cd40 antibody modified magnetic pcl-peg-pcl microspheres. J Biomed Nanotechnol. 2011; 7(2): 285-91.

137. Gou, M., M. Dai, Y. Gu, X. Li, Y. Wen, L. Yang, K. Wang, Y. Wei, and Z. Qian. Basic fibroblast growth factor loaded biodegradable pcl-peg-pcl copolymeric nanoparticles: Preparation, in vitro release and immunogenicity study. J Nanosci Nanotechnol. 2008; 8(5): 2357-61.

138. Gou, M., M. Dai, X. Li, L. Yang, M. Huang, Y. Wang, B. Kan, Y. Lu, Y. Wei, and Z. Qian. Preparation of mannan modified anionic pcl-peg-pcl nanoparticles at one-step for bfgf antigen delivery to improve humoral immunity. Colloids Surf B Biointerfaces. 2008; 64(1): 135-9.

139. Nguyen, T.H.A. and V.C. Nguyen. Formation of nanoparticles in aqueous solution from poly(ε-caprolactone)–poly(ethylene glycol)–poly(ε-caprolactone). Adv Nat Sci Nanosci Nanotechnol. 2010; 1: 025012.

140. Baimark, Y. Preparation of organic solvent/surfactant-free microspheres of methoxy poly (ethylene glycol)-b-poly (ε-caprolactone) by a melt dispersion method. Asian J Appl Sci. 2009; 2(49): 341-347.

141. Cuong, N.V., C.H. Chen, Y.T. Chen, and M.F. Hsieh. Preparation of nanoparticle of methoxy poly(ethylene glycol)/poly(epsilon-caprolactone)/methoxy poly(ethylene glycol) triblock copolymer for drug delivery applications. Apcmbe 2008: 7th Asian-Pacific Conference on Medical and Biological Engineering. 2008; 19: 190-193.

142. Shi, B., C. Fang, M.X. You, Y. Zhang, S. Fu, and Y.Y. Pei. Stealth mepeg-pcl micelles: Effects of the polymer composition on micelle physicochemical characteristics, in vitro drug release, in vivo pharmacokinetics in rats and biodistribution in s180 tumor bearing mice. Colloid Polym Sci. 2005; 283: 954-967.

143. Li, R., X. Li, L. Xie, D. Ding, Y. Hu, X. Qian, L. Yu, Y. Ding, X. Jiang, and B. Liu. Preparation and evaluation of peg-pcl nanoparticles for local tetradrine delivery. Int J Pharm. 2009; 379(1): 158-66.

144. Kim, S.Y., Y.M. Lee, I.G. Shin, and J.S. Kang. Indomethacin-loaded methoxy poly(ethylene glycol)/poly(ε-caprolactone) diblock copolymeric nanosphere: Pharmacokinetic characteristics of indomethacin in the normal sprague-dawley rats. Biomaterials. 2001; 22: 2049-2056.

145. Kim, J.H. and Y.H. Bae. Albumin loaded microsphere of amphiphilic poly(ethylene glycol)/ poly(alpha-ester) multiblock copolymer. Eur J Pharm Sci. 2004; 23(3): 245-51.

146. Rastogi, R., S. Anand, and V. Koul. Polymerosomes of pcl and peg demonstrate enhanced therapeutic efficacy of insulin. Curr Nanosci. 2009; 5: 409-416.

147. Gong, C.Y., S. Shi, X.Y. Peng, B. Kan, L. Yang, M.J. Huang, F. Luo, X. Zhao, Y.Q. Wei, and Z.Y. Qian. Biodegradable thermosensitive injectable peg-pcl-peg hydrogel for bfgf antigen delivery to improve humoral immunity. Growth Factors. 2009; 27(6): 377-83.

148. Fu, Y. and W.J. Kao. Drug release kinetics and transport mechanisms of non-degradable and degradable polymeric delivery systems. Expert Opin Drug Deliv. 2010; 7(4): 429-44.

149. Lao, L.L., S.S. Venkatraman, and N.A. Peppas. Modeling of drug release from biodegradable polymer blends. Eur J Pharm Biopharm. 2008; 70(3): 796-803.

150. Siepmann, J. and F. Siepmann. Mathematical modeling of drug delivery. Int J Pharm. 2008; 364(2): 328-43.

151. Arifin, D.Y., L.Y. Lee, and C.H. Wang. Mathematical modeling and simulation of drug release from microspheres: Implications to drug delivery systems. Adv Drug Deliv Rev. 2006; 58(12-13): 1274-325.

152. Dash, S., P.N. Murthy, L. Nath, and P. Chowdhury. Kinetic modeling on drug release from controlled drug delivery systems. Acta Pol Pharm. 2010; 67(3): 217-23.

153. Higuchi, T. Mechanism of sustained-action medication. Theoretical analysis of rate of release of solid drugs dispersed in solid matrices. J Pharm Sci. 1963; 52: 1145-9.

154. Zhang, Z. and G. Huang. Micro- and nano-carriermediated intra-articular drug delivery systems for the treatment of osteoarthritis. Journal of Nanotechnology. 2012; 2012: 1-11.

155. Kaur, A. and S.L. Harikumar. Controlled drug delivery approaches for rheumatoid arthritis. J Appl Pharm Sci. 2012; 02(08): 21-32.

156. Larsen, C., J. Ostergaard, S.W. Larsen, H. Jensen, S. Jacobsen, C. Lindegaard, and P.H. Andersen. Intra-articular depot formulation principles: Role in the management of postoperative pain and arthritic disorders. J Pharm Sci. 2008; 97(11): 4622-54.

157. Foong, K.S., R. Patel, A. Forbes, and R.M. Day. Anti-tumor necrosis factor-alpha-loaded microspheres as a prospective novel treatment for crohn's disease fistulae. Tissue Eng Part C Methods. 2010; 16(5): 855-64.

158. Thakkar, H., R.K. Sharma, A.K. Mishra, K. Chuttani, and R.S. Murthy. Efficacy of chitosan microspheres for controlled intra-articular delivery of celecoxib in inflamed joints. J Pharm Pharmacol. 2004; 56(9): 1091-9.

159.   Thakkar, H., R.K. Sharma, A.K. Mishra, K. Chuttani, and R.R. Murthy. Albumin microspheres as carriers for the antiarthritic drug celecoxib. AAPS PharmSciTech. 2005; 6(1): E65-73.

160.   Lin, S.Y., K.S. Chen, H.H. Teng, and M.J. Li. In vitro degradation and dissolution behaviours of microspheres prepared by three low molecular weight polyesters. J Microencapsul. 2000; 17(5): 577-86.

161.   Tuncay, M., S. Calis, H.S. Kas, M.T. Ercan, I. Peksoy, and A.A. Hincal. Diclofenac sodium incorporated plga (50:50) microspheres: Formulation considerations and in vitro/in vivo evaluation. Int J Pharm. 2000; 195(1-2): 179-88.

162.   Tuncay, M., S. Calis, H.S. Kas, M.T. Ercan, I. Peksoy, and A.A. Hincal. In vitro and in vivo evaluation of diclofenac sodium loaded albumin microspheres. J Microencapsul. 2000; 17(2): 145-55.

163.   Lu, Y., G. Zhang, D. Sun, and Y. Zhong. Preparation and evaluation of biodegradable flubiprofen gelatin micro-spheres for intra-articular administration. J Microencapsul. 2007; 24(6): 515-24.

164.   Fernandez-Carballido, A., R. Herrero-Vanrell, I.T. Molina-Martinez, and P. Pastoriza. Sterilized ibuprofen-loaded poly(d,l-lactide-co-glycolide) microspheres for intra-articular administration: Effect of gamma-irradiation and storage. J Microencapsulation. 2004; 21(6): 653-665.

165.   Liang, L.S., P.T. Salo, D.A. Hart, and H.M. Burt. Intra-articular treatment of inflammatory arthritis with microsphere formulations of methotrexate: Pharmacokinetics and efficacy determination in antigen-induced arthritic rabbits. Inflamm Res. 2009; 58(8): 445-56.

166.   Liang, L.S., J. Jackson, W. Min, V. Risovic, K.M. Wasan, and H.M. Burt. Methotrexate loaded poly(l-lactic acid) microspheres for intra-articular delivery of methotrexate to the joint. J Pharm Sci. 2004; 93(4): 943-56.

167.   Liang, L.S., W. Wong, and H.M. Burt. Pharmacokinetic study of methotrexate following intra-articular injection of methotrexate loaded poly(l-lactic acid) microspheres in rabbits. J Pharm Sci. 2005; 94(6): 1204-15.

168.   Bozdag, S., S. Calis, H.S. Kas, M.T. Ercan, I. Peksoy, and A.A. Hincal. In vitro evaluation and intra-articular administration of biodegradable microspheres containing naproxen sodium. J Microencapsul. 2001; 18(4): 443-56.

169.   Liggins, R.T., T. Cruz, W. Min, L. Liang, W.L. Hunter, and H.M. Burt. Intra-articular treatment of arthritis with microsphere formulations of paclitaxel: Biocompatibility and efficacy determinations in rabbits. Inflamm Res. 2004; 53(8): 363-72.

170.   Natarajan, V., N. Krithica, B. Madhan, and P.K. Sehgal. Formulation and evaluation of quercetin polycaprolactone microspheres for the treatment of rheumatoid arthritis. J Pharm Sci. 2011; 100(1): 195-205.

171.   Fu, S., G. Guo, C. Gong, S. Zeng, H. Liang, F. Luo, X. Zhang, X. Zhao, Y. Wei, and Z. Qian. Injectable biodegradable thermosensitive hydrogel composite for orthopedic tissue engineering. 1. Preparation and characterization of nanohydroxyapatite/poly(ethylene glycol)-poly(epsilon-caprolactone)-poly(ethylene glycol) hydrogel nanocomposites. J Phys Chem B. 2009; 113(52): 16518-25.

172.   Pourcelle, V., H. Freichels, F. Stoffelbach, R. Auzely-Velty, C. Jerome, and J. Marchand-Brynaert. Light induced functionalization of pcl-peg block copolymers for the covalent immobilization of biomolecules. Biomacromolecules. 2009; 10(4): 966-74.

173.   Carrascosa, C., L. Espejo, S. Torrado, and J.J. Torrado. Effect of gamma-sterilization process on plga microspheres loaded with insulin-like growth factor-i (igf-i). J Biomater Appl. 2003; 18(2): 95-108.

174.   Dorati, R., I. Genta, L. Montanari, F. Cilurzo, A. Buttafava, A. Faucitano, and B. Conti. The effect of gamma-irradiation on plga/peg microspheres containing ovalbumin. J Cont Rel. 2005; 107(1): 78-90.

175.   Wong, H.M., J.J. Wang, and C.H. Wang. In vitro sustained release of human immunoglobulin g from biodegradable microspheres. Industrial & Engineering Chemistry Research. 2001; 40(3): 933-948.

176.   Morita, T., Y. Sakamura, Y. Horikiri, T. Suzuki, and H. Yoshino. Protein encapsulation into biodegradable microspheres by a novel s/o/w emulsion method using poly(ethylene glycol) as a protein micronization adjuvant. Journal of Controlled Release. 2000; 69(3): 435-444.

177.   Ghassemi, A.H., M.J. van Steenbergen, H. Talsma, C.F. van Nostrum, W. Jiskoot, D.J.A. Crommelin, and W.E. Hennink. Preparation and characterization of protein loaded microspheres based on a hydroxylated aliphatic polyester, poly/lactic-co-hydroxymethyl glycolic acid. J Cont Rel. 2009; 138: 57-63.

178.   Ravi, S., K.K. Peh, Y. Darwis, B.K. Murthy, T.R. Singh, and C. Mallikarjun. Development and characterisation of polymeric microspheres for controlled release protein loaded drug delivery system. Indian J Pharm Sci. 2008; 70: 303-309.

179.   Emami, J., H. Hamishehkar, A.R. Najafabadi, K. Gilani, M. Minaiyan, H. Mahdavi, and A. Nokhodchi. A novel approach to prepare insulin-loaded poly(lactic-co-glycolic acid) microcapsules and the protein stability study. J Pharm Sci. 2009; 98: 1721-1731.

180. Jovanonic, N., A. Bouchard, G. Wofland, G.-J. Witkamp, D.J.A. Crommelin, and W. Jiskoot. Stabilization of igg by supercritical fluid drying: Optimization of formulation and process parameters. Eur J Pharm Biopharm. 2008; 68: 183-190.

181. Labarca, C. and K. Paigen. A simple, rapid, and sensitive DNA assay procedure. Anal Biochem. 1980; 102(2): 344-52.

182. Cho, K.Y., K.S. Lee, and J.K. Park. Effect of graft copolymer composition on the compatibility of biodegradable pcl/pcl-g-peg blend. Polymer-Korea. 2009; 33(3): 248-253.

183. Fickert, S., J. Fiedler, and R.E. Brenner. Identification, quantification and isolation of mesenchymal progenitor cells from osteoarthritic synovium by fluorescence automated cell sorting. Osteoarthritis and Cartilage. 2003; 11: 790-800.

184. Yang, J., L. Jia, L. Yin, J. Yu, Z. Shi, Q. Fang, and A. Cao. A novel approach to biodegradable block copolymers of epsilon-caprolactone and delta-valerolactone catalyzed by new aluminum metal complexes. Macromol Biosci. 2004; 4(12): 1092-104.

185. Gong, C.Y., P.W. Dong, S. Shi, S.Z. Fu, J.L. Yang, G. Guo, X. Zhao, Y.Q. Wei, and Z.Y. Qian. Thermosensitive peg-pcl-peg hydrogel controlled drug delivery system: Sol-gel-sol transition and in vitro drug release study. J Pharm Sci. 2009; 98(10): 3707-17.

186. Hwang, M.J., M.K. Joo, B.G. Choi, M.H. Park, I.W. Hamley, and B. Jeong. Multiple sol-gel transitions of peg-pcl-peg triblock copolymer aqueous solution. Macromol Rapid Commun. 2010; 31(23): 2064-9.

187. Ratner, B.D., A.S. Hoffman, F.J. Schoen, and J.E. Lemons. Classes of materials used in medicine. in Biomaterials science: An introduction to materials in medicine. 2004; Academic Press. p. 68.

188. Saez, V., J. Ramon, R. Aldana, D. Pérez, and E. Hardy. Microencapsulation of recombinant interferon α-2b into poly (d,l-lactide-co-glycolide) microspheres. Biotecnologia Aplicada. 2008; 25: 31-41.

189. Pistel, K.F. and T. Kissel. Effects of salt addition on the microencapsulation of proteins using w/o/w double emulsion technique. Journal of Microencapsulation. 2000; 17(4): 467-483.

190. Yeo, Y. and K. Park. Control of encapsulation efficiency and initial burst in polymeric microparticle systems. Arch Pharm Res. 2004; 27: 1-12.

191. Diab, R., M. Hamoudeh, O. Boyron, A. Elaissari, and H. Fessi. Microencapsulation of cytarabine using poly(ethylene glycol)-poly(epsilon-caprolactone) diblock copolymers as surfactant agents. Drug Dev Ind Pharm. 2010; 36(4): 456-69.

192.   Dong, Y. and S.S. Feng. Methoxy poly(ethylene glycol)-poly(lactide) (mpeg-pla) nanoparticles for controlled delivery of anticancer drugs. Biomaterials. 2004; 25(14): 2843-9.

193.   Pean, J.M., F. Boury, M.C. Venier-Julienne, P. Menei, J.E. Proust, and J.P. Benoit. Why does peg 400 co-encapsulation improve ngf stability and release from plga biodegradable microspheres? Pharm Res. 1999; 16(8): 1294-9.

194.   Wang, J., K.M. Chua, and C.H. Wang. Stabilization and encapsulation of human immunoglobulin g into biodegradable microspheres. J Colloid Interface Sci. 2004; 271(1): 92-101.

195.   Capan, Y., G. Jiang, S. Giovagnoli, K.H. Na, and P.P. DeLuca. Preparation and characterization of poly(d,l-lactide-co-glycolide) microspheres for controlled release of human growth hormone. AAPS Pharm Sci Tech. 2003; 86: 676.

196.   Li, S.M., H. Garreau, M. Vert, T. Petrova, N. Manolova, and I. Rashkov. Hydrolytic degradation of poly(oxyethylene)-poly-(epsilon-caprolactone) multiblock copolymers. J Appl Poly Sci. 1998; 68(6): 989-998.

197.   Cottam, E., D.W. Hukins, K. Lee, C. Hewitt, and M.J. Jenkins. Effect of sterilisation by gamma irradiation on the ability of polycaprolactone (pcl) to act as a scaffold material. Med Eng Phys. 2009; 31(2): 221-6.

198.   Masson, V., F. Maurin, H. Fessi, and J.P. Devissaguet. Influence of sterilization processes on poly(epsilon-caprolactone) nanospheres. Biomaterials. 1997; 18(4): 327-35.

199.   Dorati, R., C. Colonna, M. Serra, I. Genta, T. Modena, F. Pavanetto, P. Perugini, and B. Conti. Gamma-irradiation of pegd,lpla and peg-plga multiblock copolymers. I. Effect of irradiation doses. AAPS PharmSciTech. 2008; 9(2): 718-25.

200.   Decker, C. Radiation-induced oxidation of solid poly(ethylene oxide) .2. Mechanism. Journal of Polymer Science Part a-Polymer Chemistry. 1977; 15(4): 799-813.

201.   Dorati, R., C. Colonna, C. Tomasi, I. Genta, T. Modena, A. Faucitano, A. Buttafava, and B. Conti. Gamma-irradiation of pegd,lpla and peg-plga multiblock copolymers: Ii. Effect of oxygen and epr investigation. AAPS PharmSciTech. 2008; 9(4): 1110-8.

202.   Giteau, A., M.C. Venier-Julienne, A. Aubert-Pouessel, and J.P. Benoit. How to achieve sustained and complete protein release from plga-based microparticles? International Journal of Pharmaceutics. 2008; 350(1-2): 14-26.

203.   O'Donnell, P.B. and J.W. McGinity. Preparation of microspheres by the solvent evaporation technique. Adv Drug Deliv Rev. 1997; 28: 25-42.

204. Crotts, G., H. Sah, and T.G. Park. Adsorption determines in-vitro protein release rate from biodegradable microspheres: Quantitative analysis of surface area during degradation. Journal of Controlled Release. 1997; 47(1): 101-111.

205. Jiang, G., B.H. Woo, F. Kang, J. Singh, and P.P. DeLuca. Assessment of protein release kinetics, stability and protein polymer interaction of lysozyme encapsulated poly(d,l-lactide-co-glycolide) microspheres. J Control Release. 2002; 79(1-3): 137-45.

206. Paillard-Giteau, A., V.T. Tran, O. Thomas, X. Garric, J. Coudane, S. Marchal, I. Chourpa, J.P. Benoit, C.N. Montero-Menei, and M.C. Venier-Julienne. Effect of various additives and polymers on lysozyme release from plga microspheres prepared by an s/o/w emulsion technique. Eur J Pharm Biopharm. 2010; 75(2): 128-36.

207. Vonarbourg, A., C. Passirani, P. Saulnier, and J.P. Benoit. Parameters influencing the stealthiness of colloidal drug delivery systems. Biomaterials. 2006; 27(24): 4356-73.

208. Aly, M.N. Intra-articular drug delivery: A fast growing approach. Recent Pat Drug Deliv Formul. 2008; 2(3): 231-7.

209. Verma, A.K., A. Chanchal, and A. Maitra. Co-polymeric hydrophilic nanospheres for drug delivery: Release kinetics, and cellular uptake. Indian J Exp Biol. 2010; 48(10): 1043-52.

210. Ahmed, S.A., R.M. Gogal Jr, and J.E. Walsh. A new rapid and simple non-radioactive assay to monitor and determine the proliferation of lymphocytes: An alternative to [3h]thymidine incorporation assay. . J Immunol Methol. 1994; 170(211-224).

211. Fields, R.D. and M.V. Lancaster. Dual-attribute continuous monitoring of cell proliferation/cytotoxicity. Am Biotechnol Lab. 1993; 11(4): 48-50.

212. McNearney, T., B.A. Baethge, S. Cao, R. Alam, J.R. Lisse, and K.N. Westlund. Excitatory amino acids, tnf-alpha, and chemokine levels in synovial fluids of patients with active arthropathies. Clin Exp Immunol. 2004; 137(3): 621-7.

213. Hosaka, K., J. Ryu, S. Saitoh, T. Ishii, K. Kuroda, and K. Shimizu. The combined effects of anti-tnfa antibody and il-1 receptor antagonist in human rheumatoid arthritis synovial membrane. Cytokine. 2005; 32: 263-269.

214. Xu, S., H. Lu, J. Lin, Z. Chen, and D. Jiang. Regulation of tnfa and il1b in rheumatoid arthritis synovial fibroblasts by leukotriene b4. Rheumatol Int. 2010; 30: 1183-1189.

215. Inoue, H., M. Takamori, N. Nagata, T. Nishikawa, H. Oda, S. Yamamoto, and Y. Koshihara. An investigation of cell proliferation and soluble mediators induced by

interleukin 1b in human synovial fibroblasts: Comparative response in osteoarthritis and rheumatoid arthritis. Inflamm Res. 2001; 50: 65-72.

216.   Ida, H., T. Aramaki, H. Nakamura, K. Fujikawa, K. Arima, M. Tamai, M. Kamachi, K. Satoh, T. Origuchi, A. Kawakami, I. Furuichi, Y. Kawabe, and K. Eguchi. Different expression levels of tnf receptors on the rheumatoid synovial macrophages derived from surgery and a synovectomy as detected by a new flow cytometric analysis. Cytotechnology. 2009; 60(1-3): 161-4.

217.   Zhang, H.G., W.D. Blackburn, Jr., and P.P. Minghetti. Characterization of a sv40-transformed rheumatoid synovial fibroblast cell line which retains genotypic expression patterns: A model for evaluation of anti-arthritic agents. In Vitro Cell Dev Biol Anim. 1997; 33(1): 37-41.

218.   Kusunoki, N., T. Ito, N. Sakurai, T. Suguro, H. Handa, and S. Kawai. A novel celecoxib derivative potently induces apoptosis of human synovial fibroblasts. JPET. 2005; 314: 796-803.

219.   Tolboom, T.C., E. Pieterman, W.H. van der Laan, R.E. Toes, A.L. Huidekoper, R.G. Nelissen, F.C. Breedveld, and T.W. Huizinga. Invasive properties of fibroblast-like synoviocytes: Correlation with growth characteristics and expression of mmp-1, mmp-3, and mmp-10. Ann Rheum Dis. 2002; 61(11): 975-80.

220.   Qu, Z., C.H. Garcia, L.M. O'Rourke, S.R. Planck, M. Kohli, and J.T. Rosenbaum. Local proliferation of fibroblast-like synoviocytes contributes to synovial hyperplasia. Results of proliferating cell nuclear antigen/cyclin, c-myc, and nucleolar organizer region staining. Arthritis Rheum. 1994; 37(2): 212-20.

221.   Nuzzi, R., M. Gunetti, D. Rustichelli, B. Roagna, F. Fronticelli Bardelli, F. Fagioli, and I. Ferrero. Effect of in vitro exposure of corticosteroid drugs, conventionally used in amd treatment, on mesenchymal stem cells. Stem Cells Int. 2012; 2012: 946090.

222.   O'Dell, J.R. Methotrexate use in rheumatoid arthritis. Rheum Dis Clin North Am. 1997; 23(4): 779-96.

223.   Chatzigiannis, I., G. Kakavouli, G. Sakellariou, C. Vezyridis, and K. Voudouris. Intra-articular injection of infliximab in resistant inflamed joints of rheumatoid arthritis and spondyloarthropathies. Annals of the Rheumatic Diseases. 2004; 63: 418-419.

224.   Grattendick, K.J., J.M. Nakashima, L. Feng, S.N. Giri, and S.B. Margolin. Effects of three anti-tnf-alpha drugs: Etanercept, infliximab and pirfenidone on release of tnf-alpha in medium and tnf-alpha associated with the cell in vitro. Int Immunopharmacol. 2008; 8(5): 679-87.

225.   Jeong, J.G., J.M. Kim, H. Cho, W. Hahn, S.S. Yu, and S. Kim. Effects of il-1beta on gene expression in human rheumatoid synovial fibroblasts. Biochem Biophys Res Commun. 2004; 324(1): 3-7.

226.   Bondeson, J., S.D. Wainwright, S. Lauder, N. Amos, and C.E. Hughes. The role of synovial macrophages and macrophage-produced cytokines in driving aggrecanases, matrix metalloproteinases, and other destructive and inflammatory responses in osteoarthritis. Arthritis Res Ther. 2006; 8(6): R187.

APPENDIX A

ETHICS COMMITTEE REPORT

T.C.
HACETTEPE ÜNİVERSİTESİ
Tıp Fakültesi
Tıbbi Araştırmalar Yerel Etik Kurulu

0 4 Mart 2009

Sayı : B.30.2.HAC.0.01.00.01/6 692
Konu :

ARAŞTIRMA PROJESİ DEĞERLENDİRME RAPORU

Toplantı Tarihi : 26 ŞUBAT 2009 PERŞEMBE günü
Toplantı No : 2009/3
Proje No : TBK 06/20 (Değerlendirme Tarihi: 07.12.2006)
Karar No : TBK 06/20 - 41

Orta Doğu Teknik Üniversitesi Mühendislik Bilimleri Bölümü öğretim üyelerinden Yrd.Doç.Dr. Ayşen Tezcaner'in sorumlu araştırmacısı olduğu, Prof.Dr. Seza Özen, Prof.Dr. Bülent Atilla, Yrd.Doç.Dr. Dilek Keskin, Prof. Dr. Ali Usanmaz, Doç. Dr. Çetin Kocaefe ile birlikte çalışacakları TBK 06/20 kayıt numaralı ve *"Anti-TNF Kontrollü Salım Sisteminin Romatoid Artirit Tedavilerine Yönelik Etkilerinin Hücre Kültüründe İncelenmesi"* başlıklı proje önerisi kurulumuzda değerlendirilmiş olup, tıbbi etik açıdan uygun bulunmuştur..

1. Prof.Dr. E. Rüştü Onur   (Başkan)
2. Prof.Dr. Murat Yurdakök   (Üye)
3. Prof.Dr. Osman Abbasoğlu   (Üye)
4. Prof.Dr. Mithat Haliloğlu   (Üye)
5. Prof.Dr. Türkan Eldem   (Üye)
6. Prof.Dr. Pınar Fırat   (Üye)
7. Prof.Dr. Erdem Aydın   (Üye)
8. Prof.Dr. H. Asuman Özkara   (Üye)
9. Prof.Dr. Tanju Besler   (Üye)   KATILMADI
10. Prof.Dr. Haydar A. Demirel (Üye)
11. Prof.Dr. Bülent Sivri   (Üye)   KATILMADI
12. Prof. Dr. Zafer Çehreli   (Üye)
13. Doç.Dr. Bilgehan Yalçın   (Üye)
14. Doç.Dr. Ümit Yaşar   (Üye)
15. Doç.Dr.Mutlu Hayran   (Üye)

Hacettepe Üniversitesi Tıp Fakültesi Tıbbi, Cerrahi ve İlaç Araştırmaları Etik Kurulu 06100 Sıhhiye-Ankara
Telefon: (0 312) 305 10 82 Faks: (0 312) 310 05 80 E-posta: hums@hacettepe.edu.tr

125

APPENDIX B

CHARACTERIZATION OF MPEG AND PCL HOMOPOLYMERS
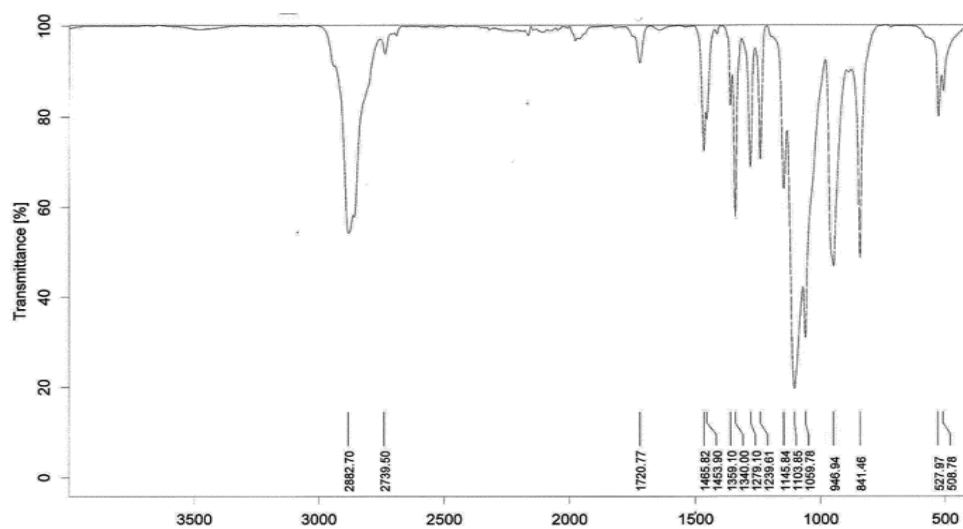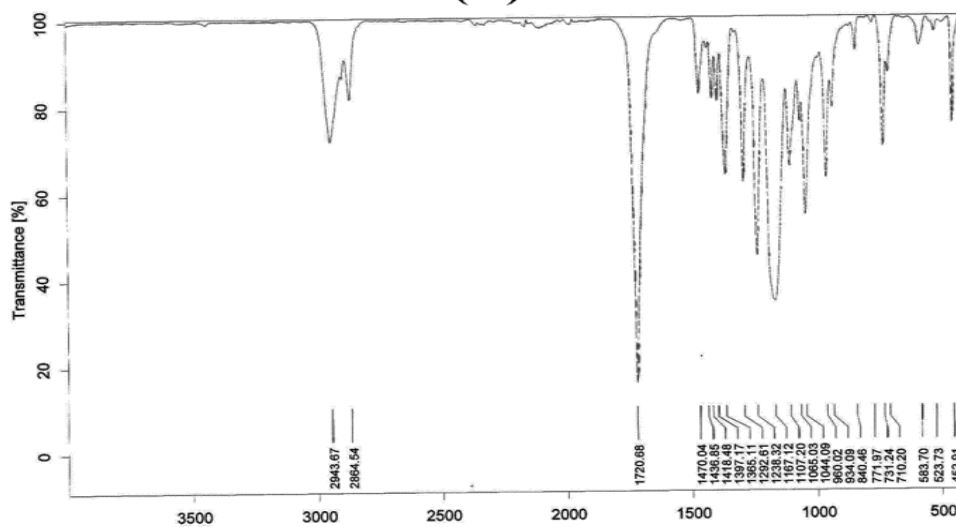
Figure B.1. FT-IR spectra of MPEG **(A)** and PCL **(B)** homopolymers

CH$_3$O-[CH$_2$CH$_2$O]$_n$-
  a   b   b

(A)

-[O-CH$_2$CH$_2$CH$_2$CH$_2$CH$_2$-CO]$_n$-
  a   b   c   d   e

(B)
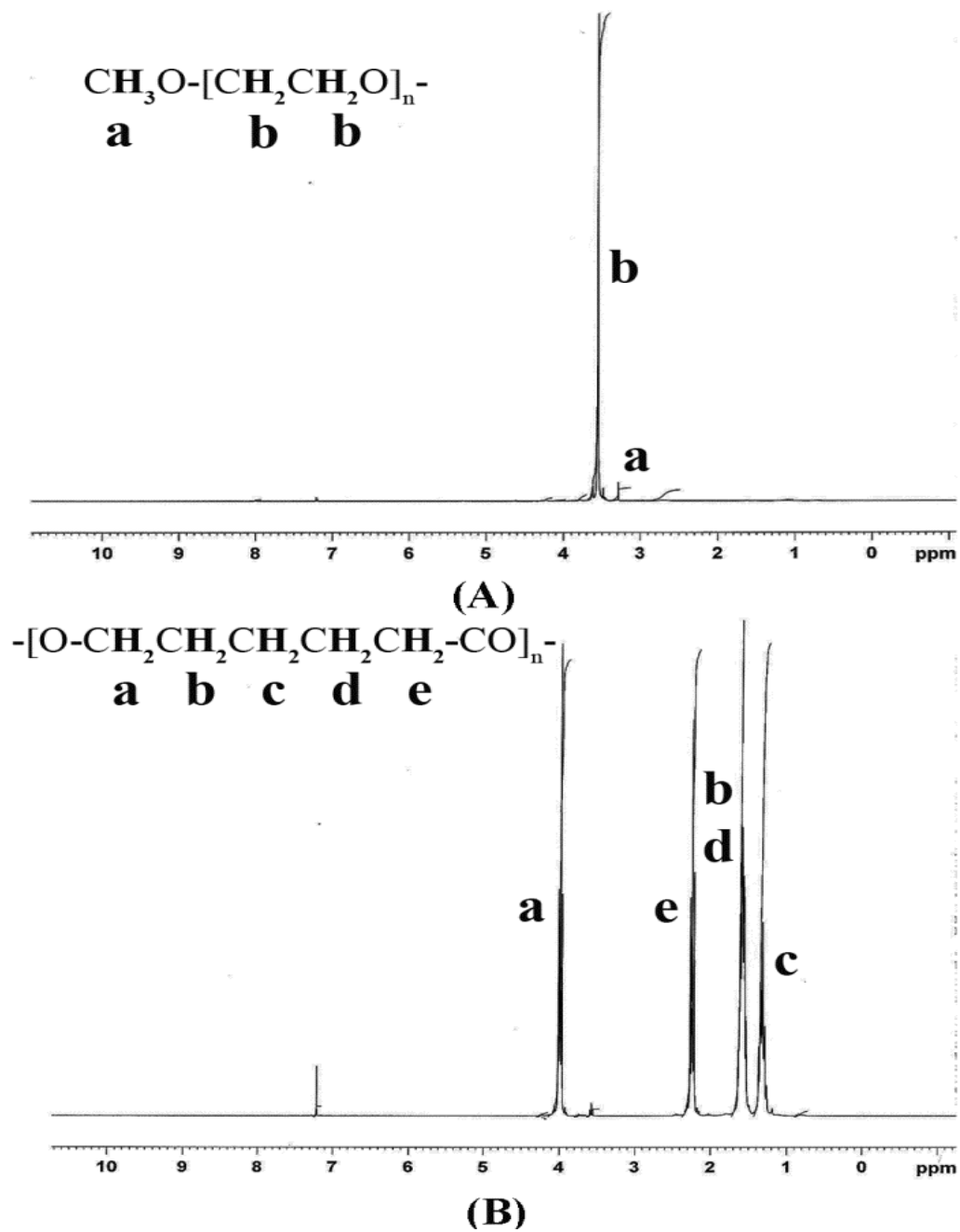
Figure B.2. ^{1}H NMR spectra of MPEG **(A)** and PCL **(B)** homopolymers

APPENDIX C

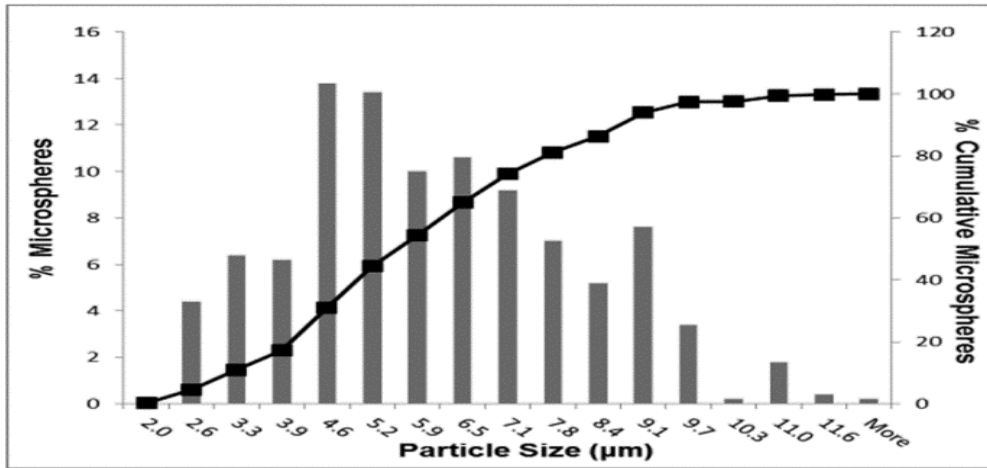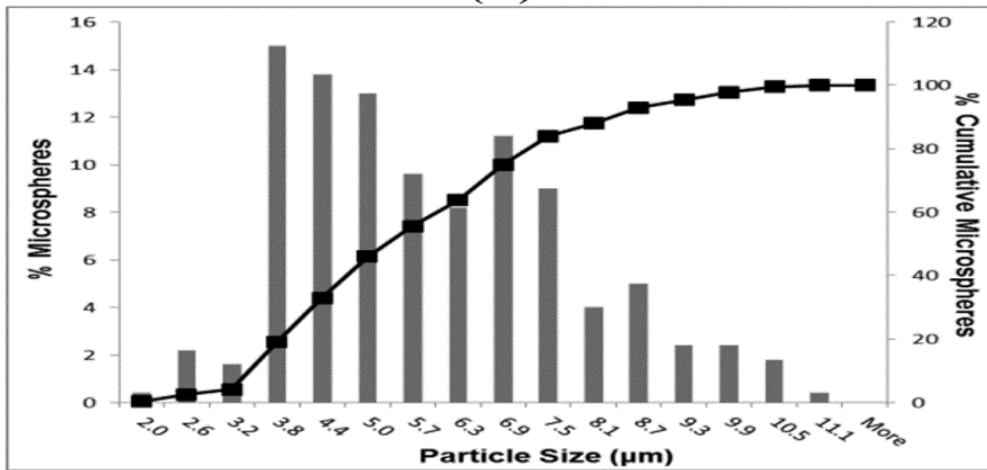## CHARACTERIZATION OF IGG LOADED PCL AND MPEG-PCL-MPEG MICROSPHERES
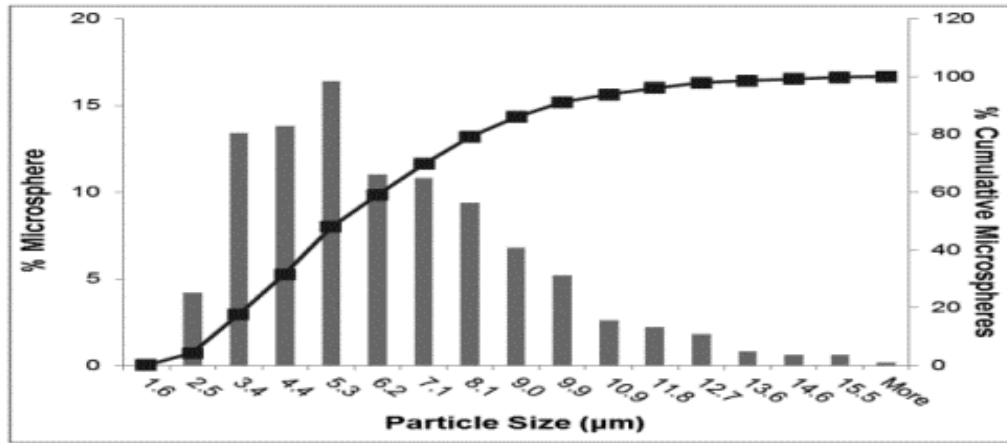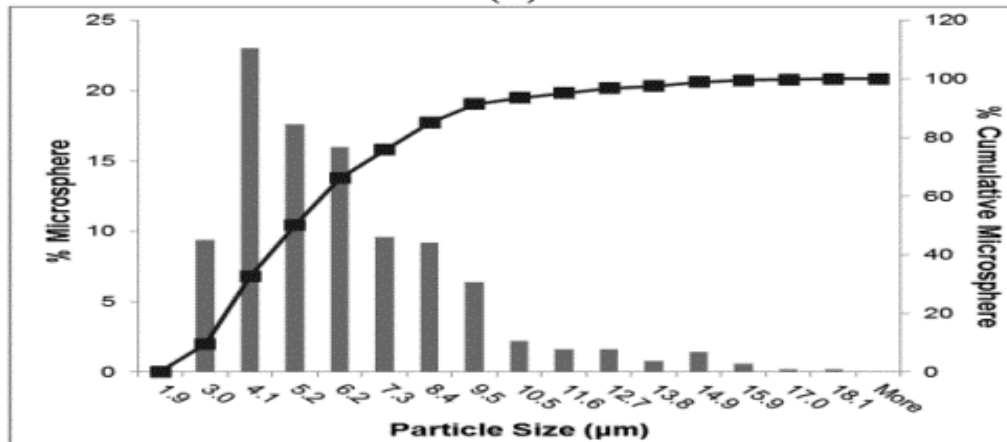
Figure C.1. Particle size distribution histograms and total cumulative percent arithmetic curves of IgG loaded (**A**) non-irradiated and (**B**) γ-irradiated PCL microspheres
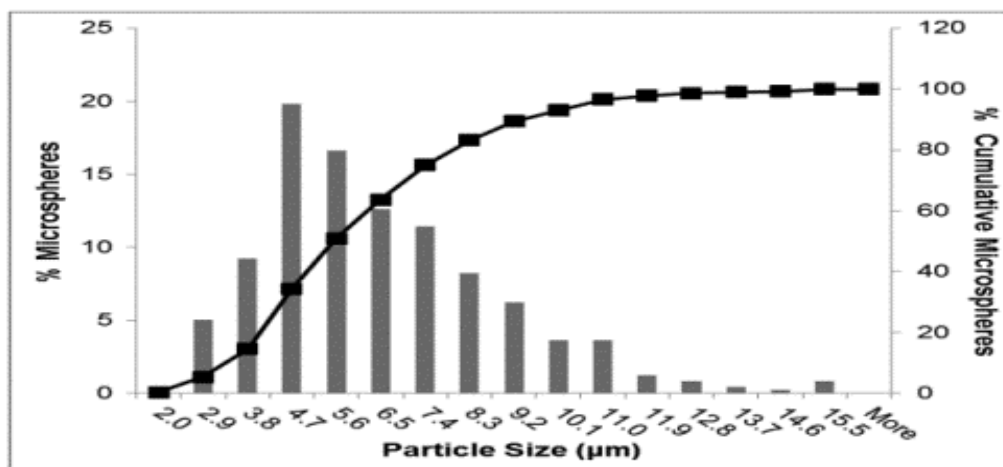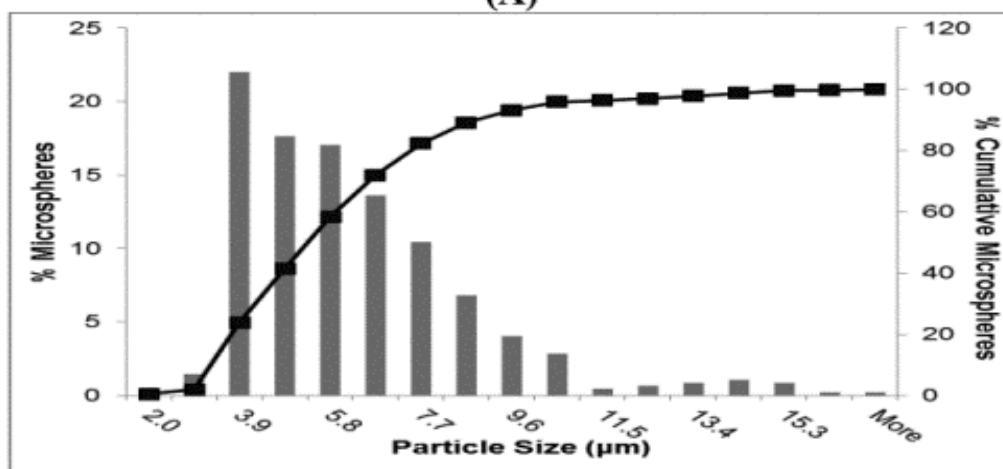
Figure C.2. Particle size distribution histograms and total cumulative percent arithmetic curves of IgG loaded **(A)** non-irradiated and **(B)** γ-irradiated MPEG-PCL-MPEG microspheres
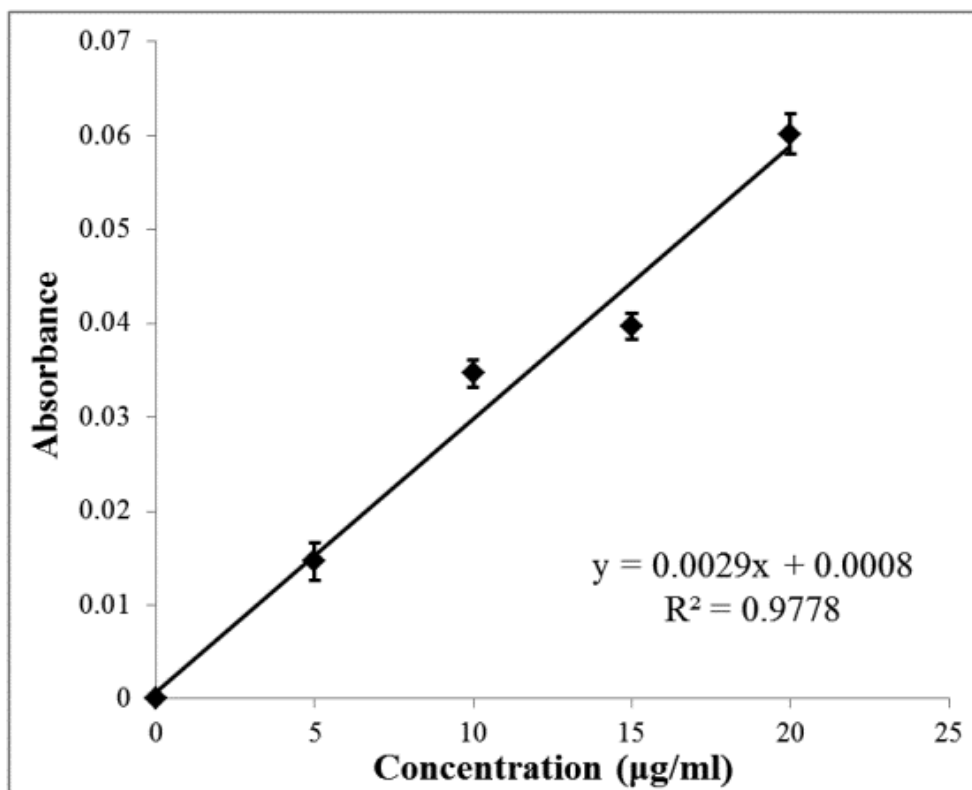
Figure C.3. Calibration curve of IgG treated with DMSO and NaOH/SDS for evaluation of protein content in microspheres
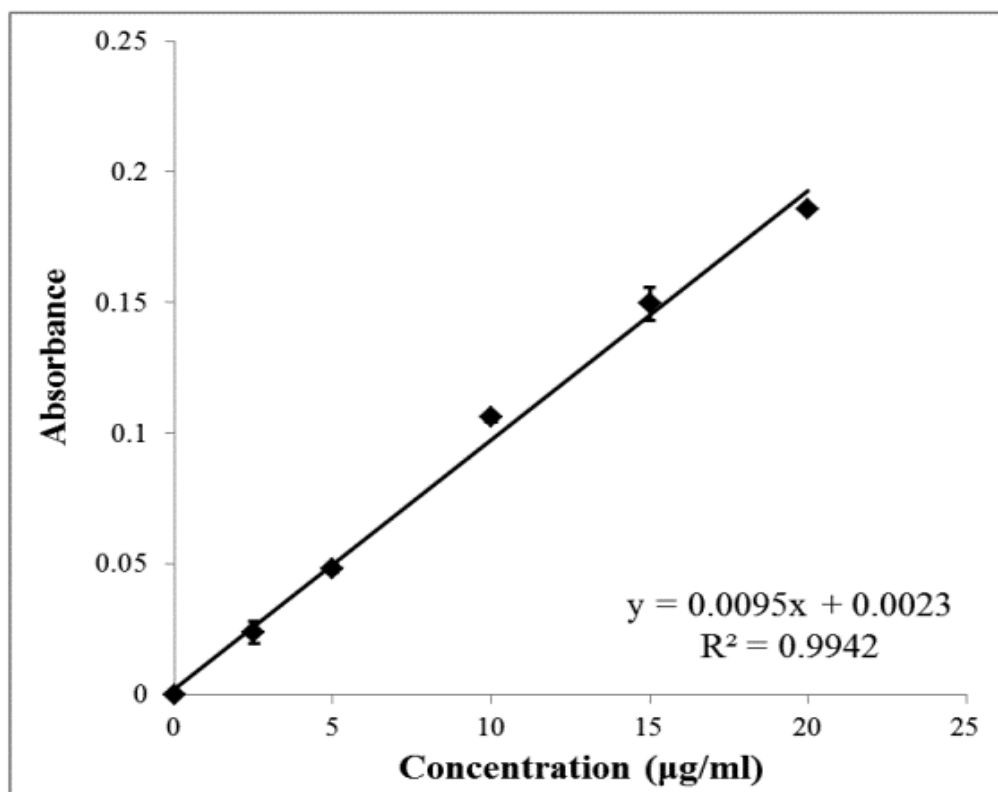
Figure C.4. Calibration curve of IgG in release medium (0.01M PBS, pH 7.4 containing 0.01% Tween 20 and 0.05% sodium azide) for µBCA assay

$$y = 0.1042x + 0.0263$$
$$R^2 = 0.9658$$
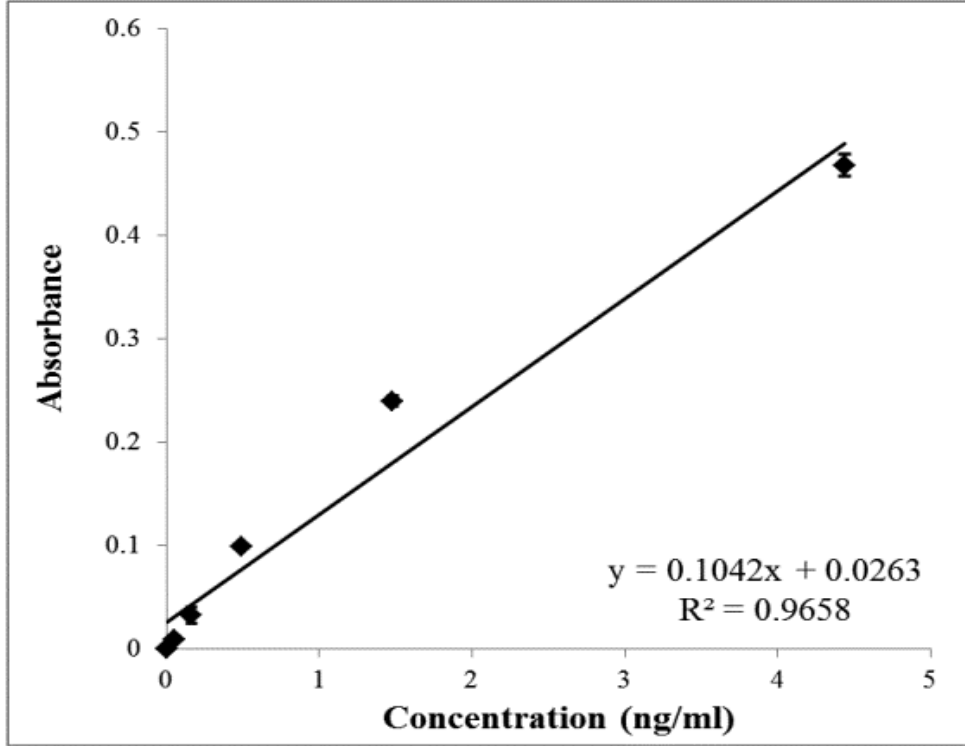
Figure C.5. Calibration curve of IgG constructed for ELISA

Table C.1. R^2 values and equations of polynomial trendlines (6th degree) obtained for the in vitro IgG release from PCL and MPEG-PCL-MPEG microspheres

|	R^2	Equation
µBCA Assay		
Non-irradiated PCL microspheres	0.9987	$y = -6\times10^{-9}\,x^6 + 2\times10^{-6}\,x^5 - 0.0002\,x^4 + 0.0108\,x^3 - 0.2876\,x^2 + 4.1829\,x + 2.3478$
γ-irradiated PCL microspheres	0.9985	$y = -6\times10^{-9}\,x^6 + 2\times10^{-6}\,x^5 - 0.0002\,x^4 + 0.01\,x^3 - 0.2596\,x^2 + 3.7962\,x + 2.3565$
Non-irradiated MEG-PCL-MPEG microspheres	0.9984	$y = -9\times10^{-9}\,x^6 + 3\times10^{-6}\,x^5 - 0.0003\,x^4 + 0.0139\,x^3 - 0.3591\,x^2 + 5.195\,x + 2.265$
γ-irradiated MEG-PCL-MPEG microspheres	0.9972	$y = -3\times10^{-9}\,x^6 + 7\times10^{-7}\,x^5 - 8\times10^{-5}\,x^4 + 0.0044\,x^3 - 0.147\,x^2 + 3.7431\,x + 3.7669$
ELISA		
Non-irradiated PCL microspheres	0.9696	$y = -6\times10^{-9}\,x^6 + 2\times10^{-6}\,x^5 - 0.0002\,x^4 + 0.0111\,x^3 - 0.2979\,x^2 + 3.622\,x + 3.0184$
γ-irradiated PCL microspheres	0.989	$y = -2\times10^{-9}\,x^6 + 7\times10^{-7}\,x^5 - 8\times10^{-5}\,x^4 + 0.0045\,x^3 - 0.124\,x^2 + 1.6368\,x + 1.449$
Non-irradiated MEG-PCL-MPEG microspheres	0.9929	$y = -4\times10^{-9}\,x^6 + 1\times10^{-6}\,x^5 - 0.0001\,x^4 + 0.0084\,x^3 - 0.2393\,x^2 + 3.5068\,x + 3.194$
γ-irradiated MEG-PCL-MPEG microspheres	0.9937	$y = -4\times10^{-9}\,x^6 + 1\times10^{-6}\,x^5 - 0.0001\,x^4 + 0.0079\,x^3 - 0.2292\,x^2 + 3.4264\,x + 2.678$
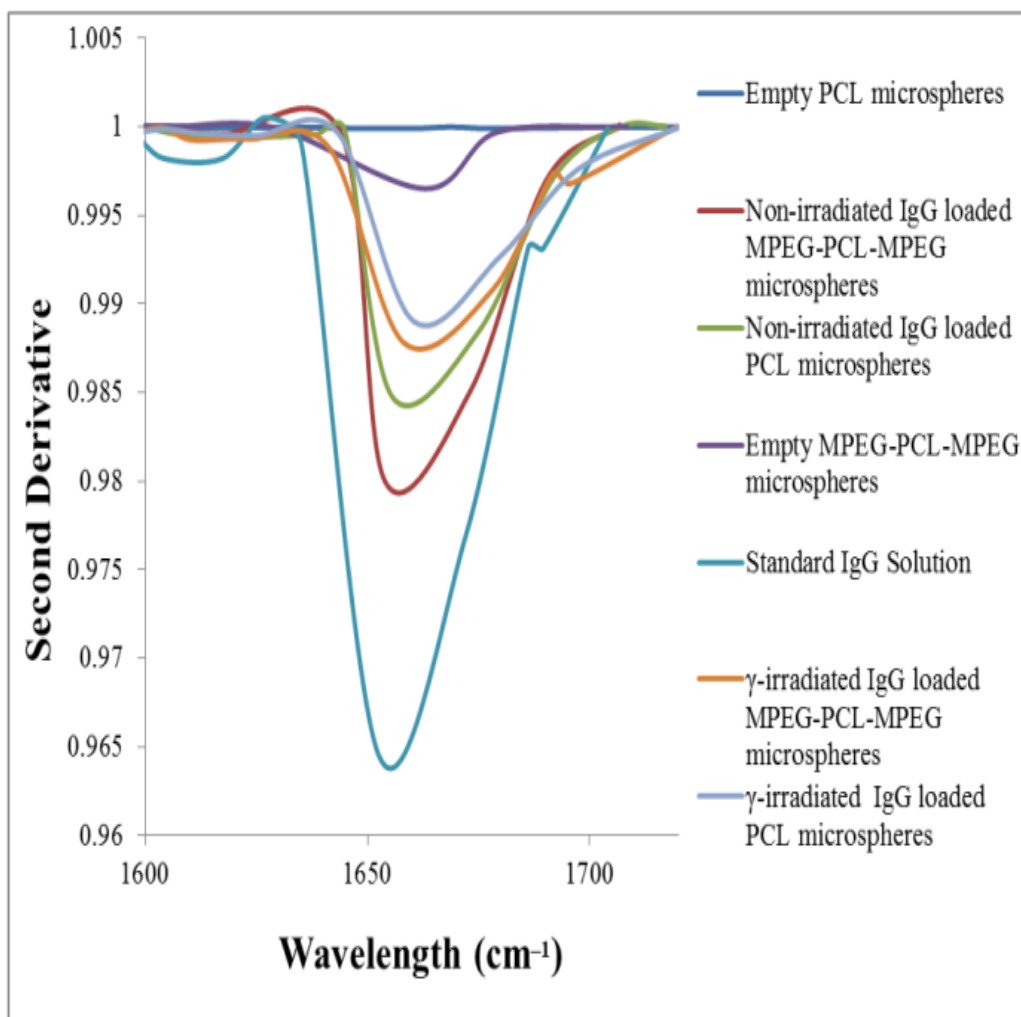
Figure C.6. Second derivatization in the amide I band region of FT-IR spectra of standard IgG solution, the supernatants from the extraction of empty microspheres and the supernatants from the extraction of IgG from γ-irradiated or non-irradiated microspheres
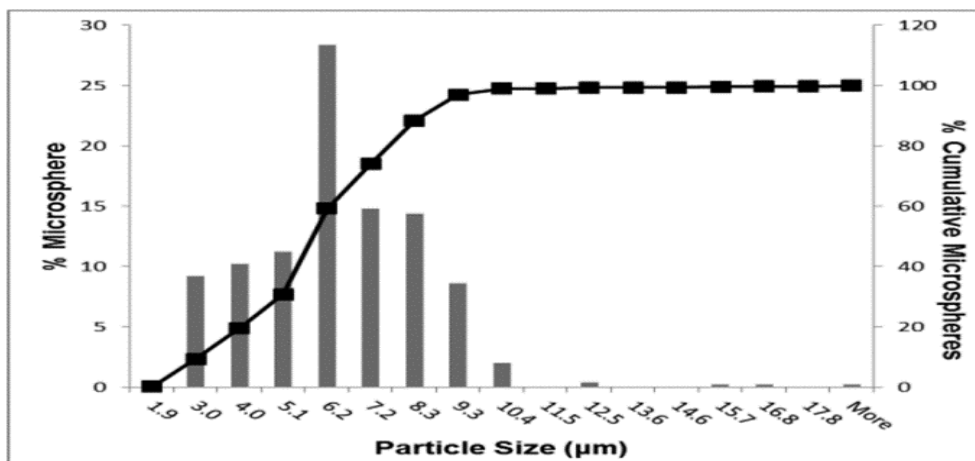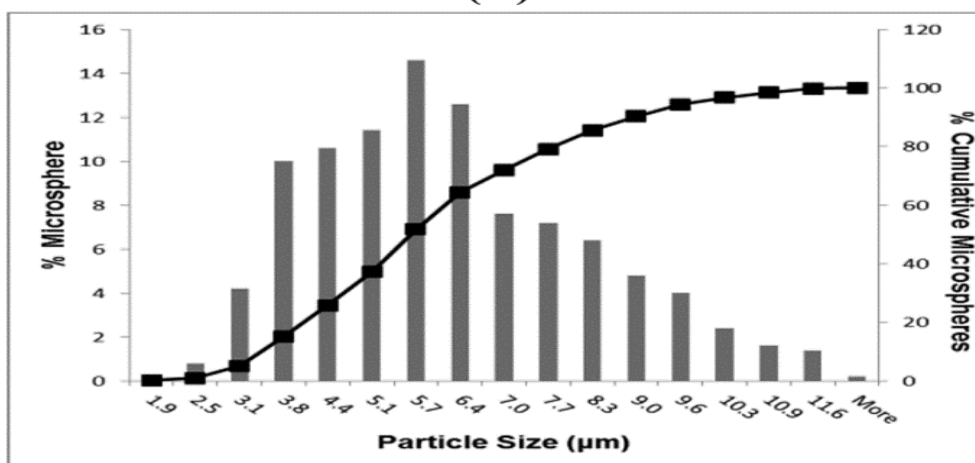
Figure C.7. Particle size distribution histograms and total cumulative percent arithmetic curves of IgG loaded **(A)** non-irradiated and **(B)** γ-irradiated PCL microspheres after the degradation study

Figure C.8. Particle size distribution histograms and total cumulative percent arithmetic curves of IgG loaded **(A)** non-irradiated and **(B)** γ-irradiated MPEG-PCL-MPEG microspheres after the degradation study
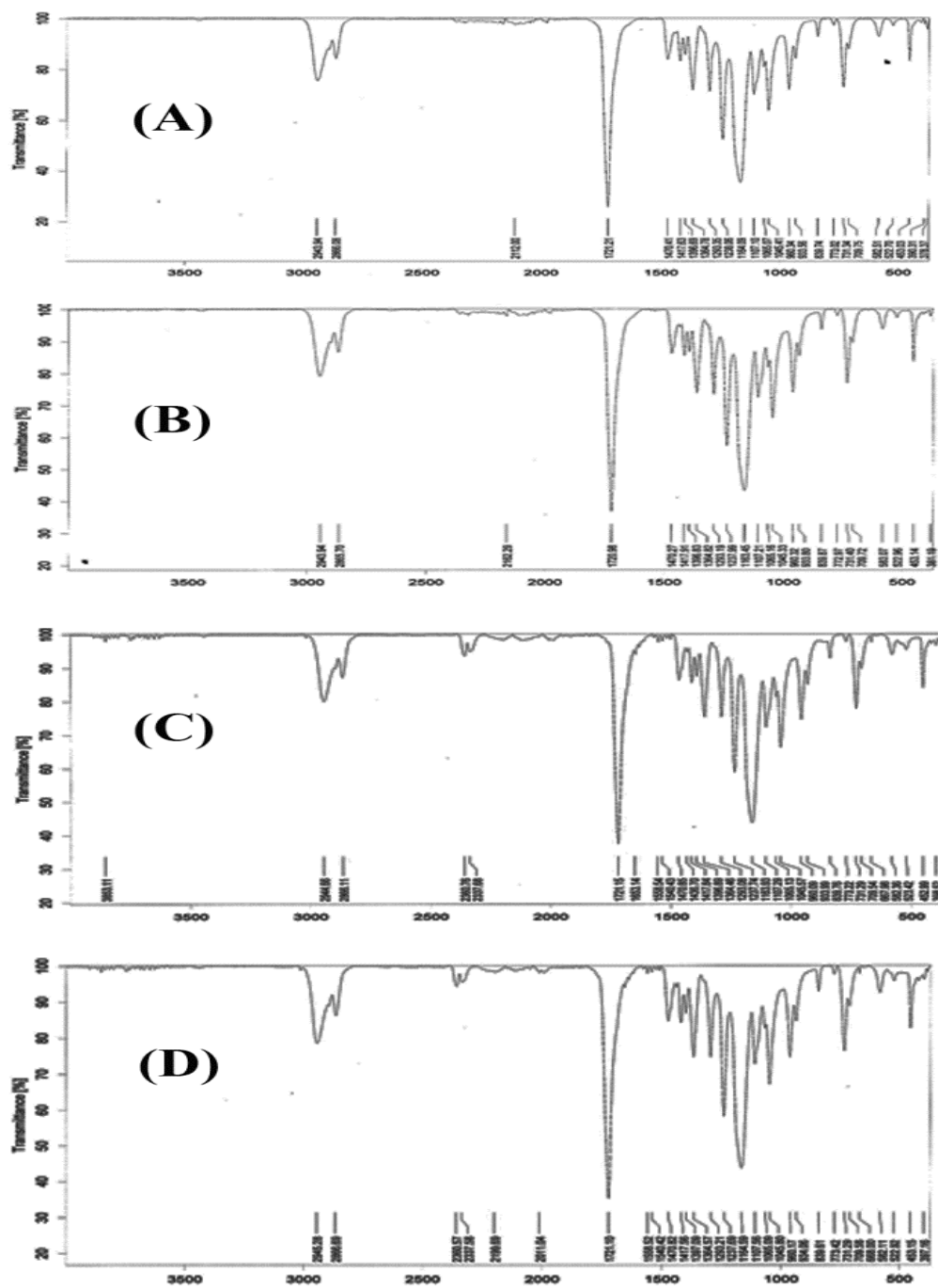
Figure C.9. FT-IR spectra of IgG loaded PCL microspheres: **(A)** non-irradiated microspheres before degradation study; **(B)** γ-irradiated microspheres before degradation study; **(C)** non-irradiated microspheres after degradation study; **(D)** γ-irradiated microspheres after degradation study
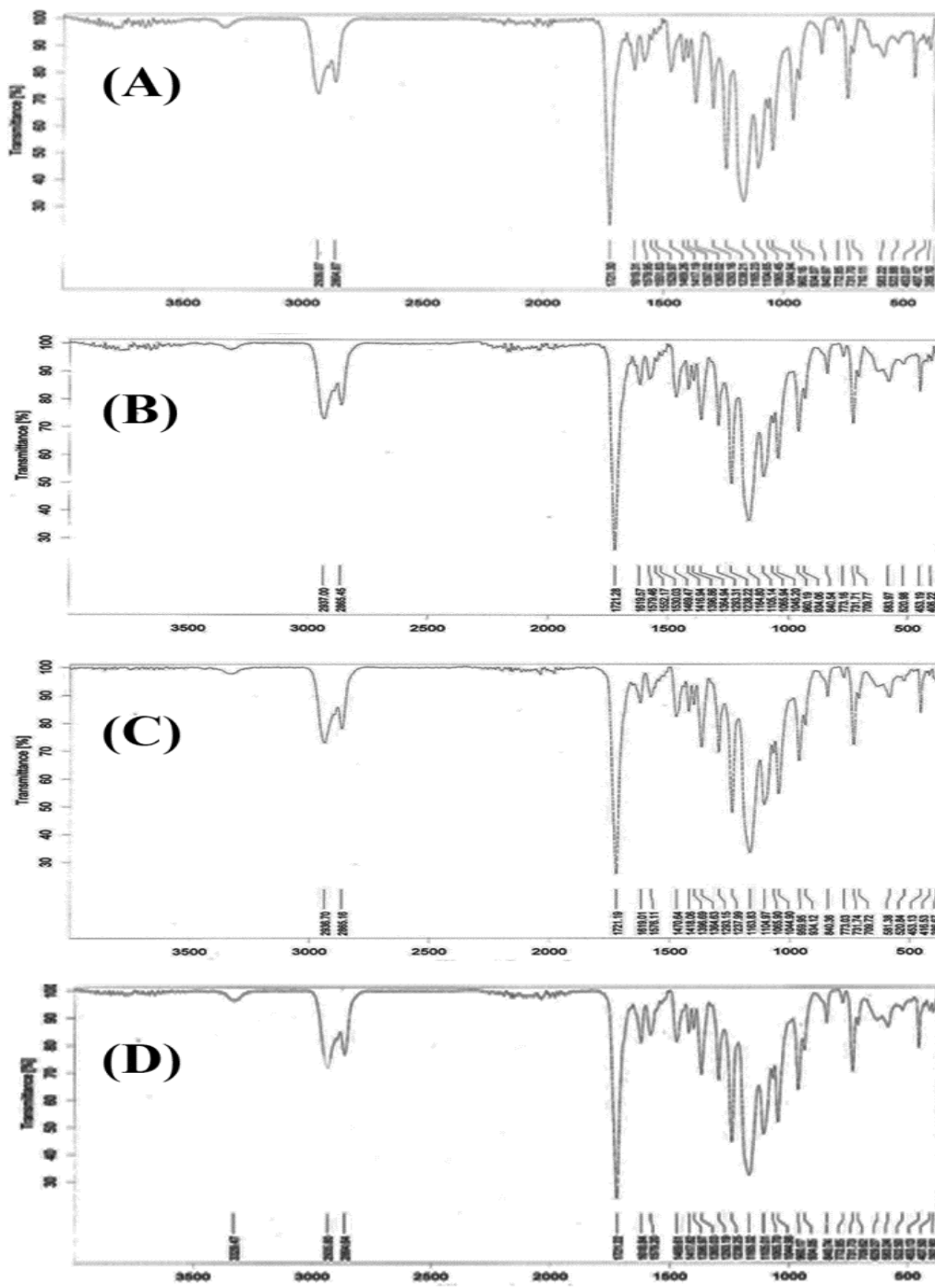
Figure C.10. FT-IR spectra of IgG loaded MPEG-PCL-MPEG microspheres: **(A)** non-irradiated microspheres before degradation study; **(B)** γ-irradiated microspheres before degradation study; **(C)** non-irradiated microspheres after degradation study; **(D)** γ-irradiated microspheres after degradation study
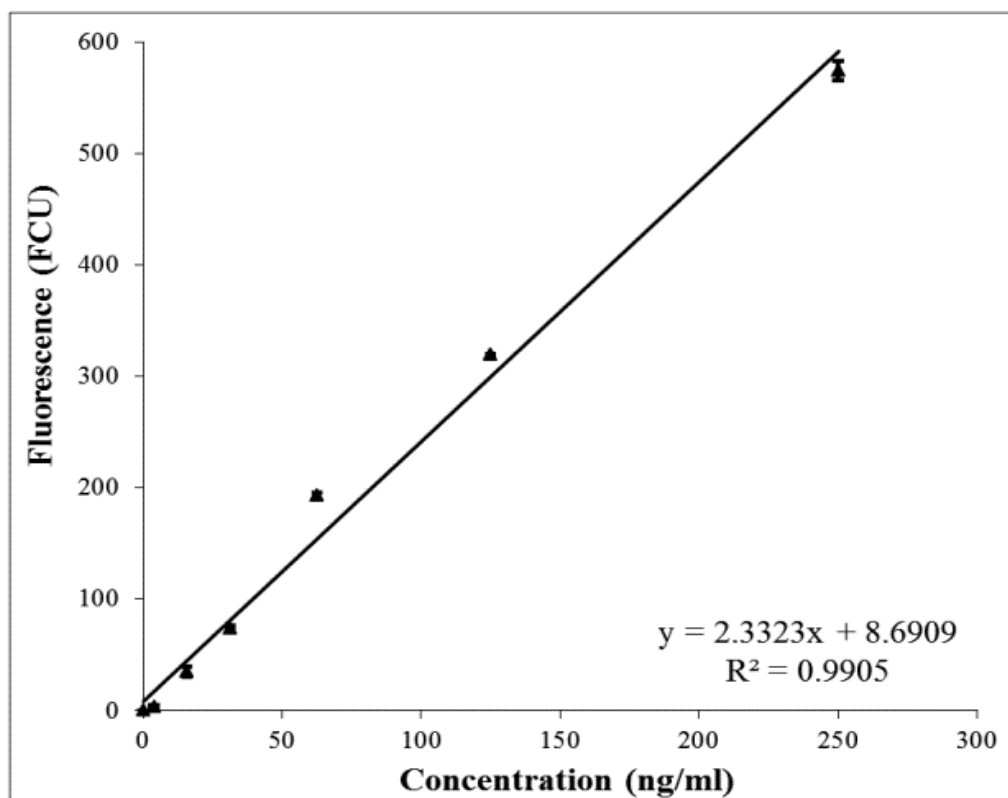
Figure C.11. Calibration curve of calf thymus DNA in TNE buffer for fluorometric quantitation of DNA

APPENDIX D

CHARACTERIZATION OF ETN LOADED PCL AND MPEG-PCL-MPEG MICROSPHERES
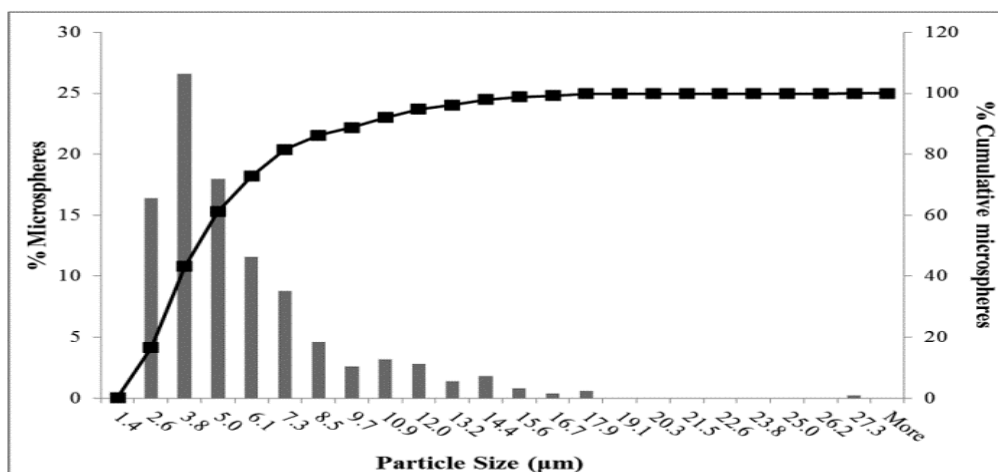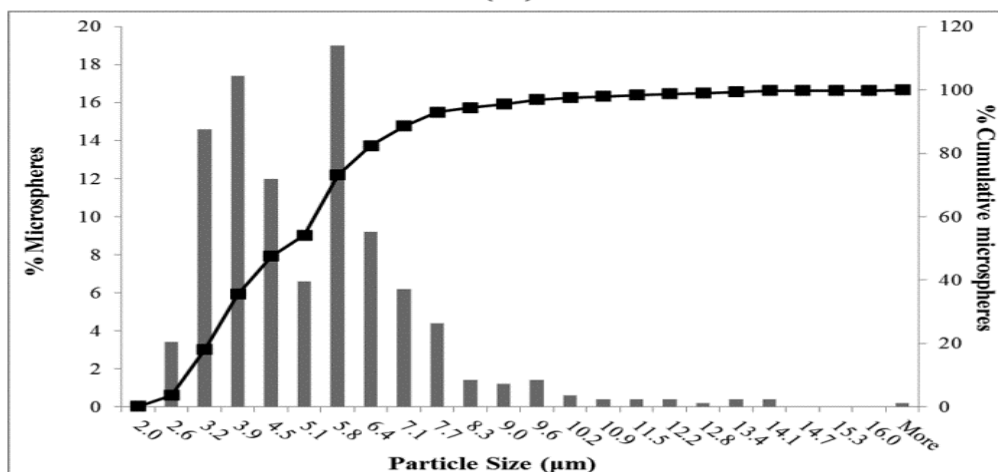
Figure D.1. Particle size distribution histograms and total cumulative percent arithmetic curves of γ-irradiated PCL **(A)** and MPEG-PCL-MPEG **(B)** microspheres loaded with ETN
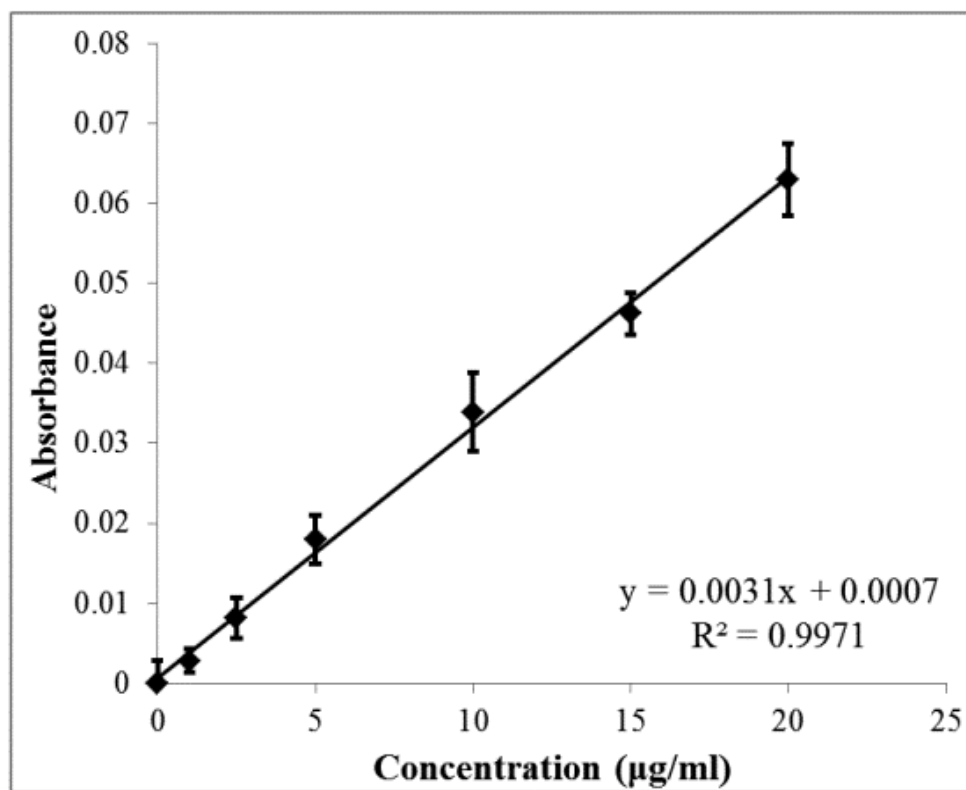
Figure D.2. Calibration curve of ETN treated with DMSO and NaOH/SDS for evaluation of protein content in microspheres
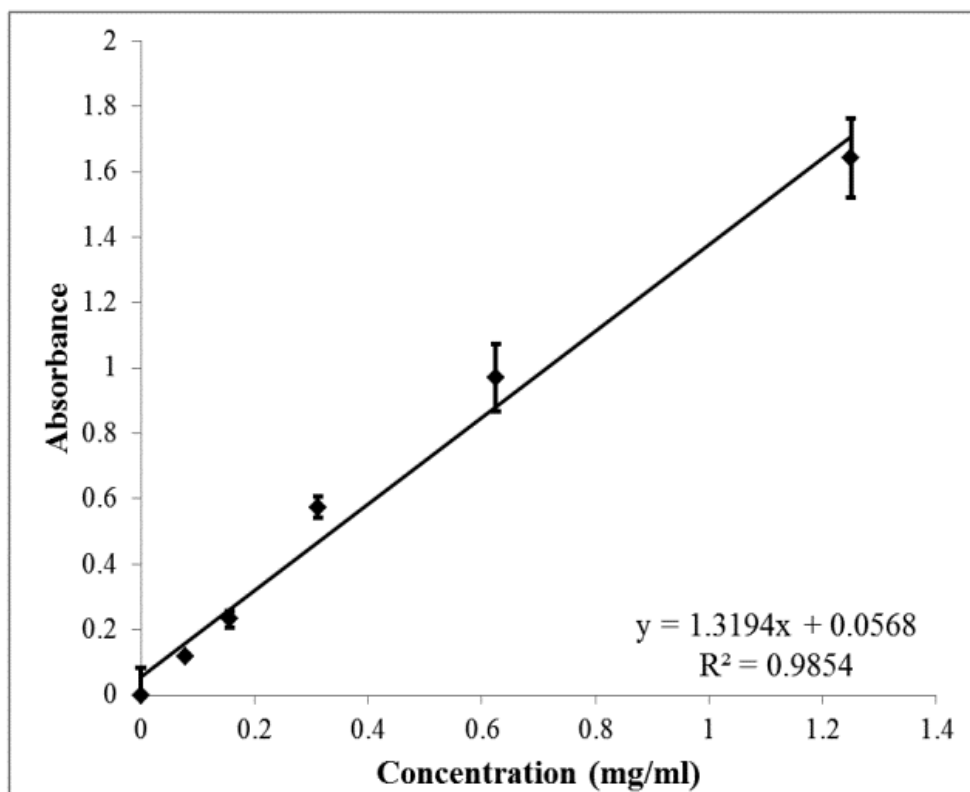
Figure D.3. Calibration curve of BSA treated with 1% SDS solution in PBS to evaluate the amount of protein adsorbed on the surface of empty PCL and MPEG-PCL-MPEG microspheres
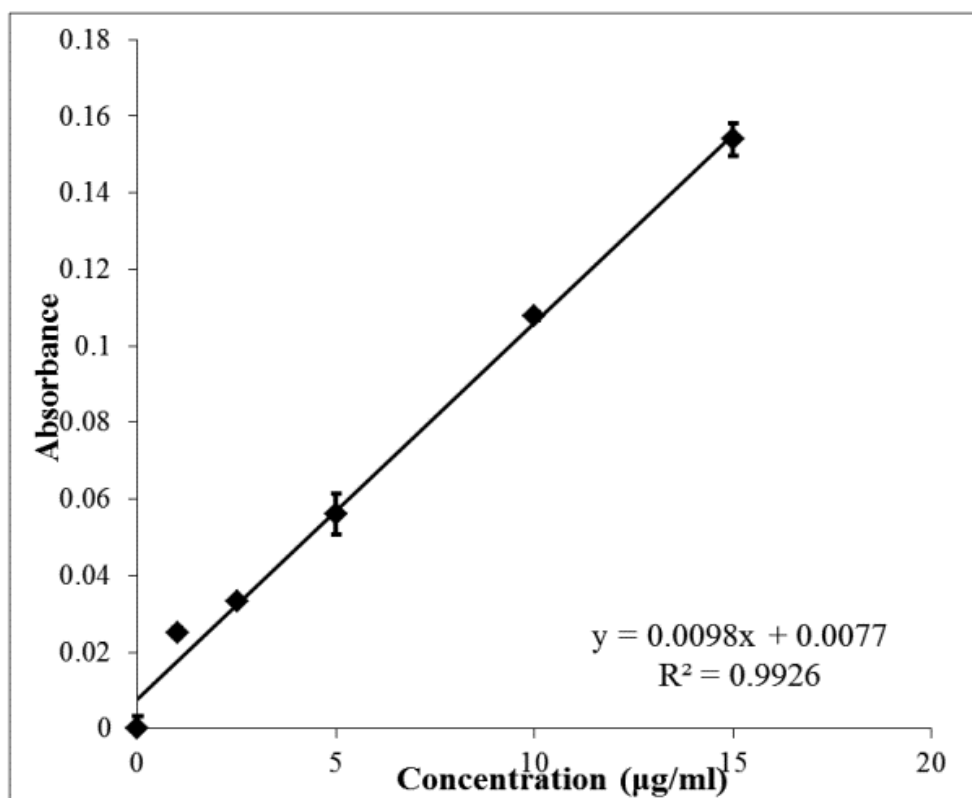
Figure D.4. Calibration curve of ETN in release medium (0.01M PBS, pH 7.4 containing 0.01% Tween 20 and 0.05% sodium azide) for μBCA assay
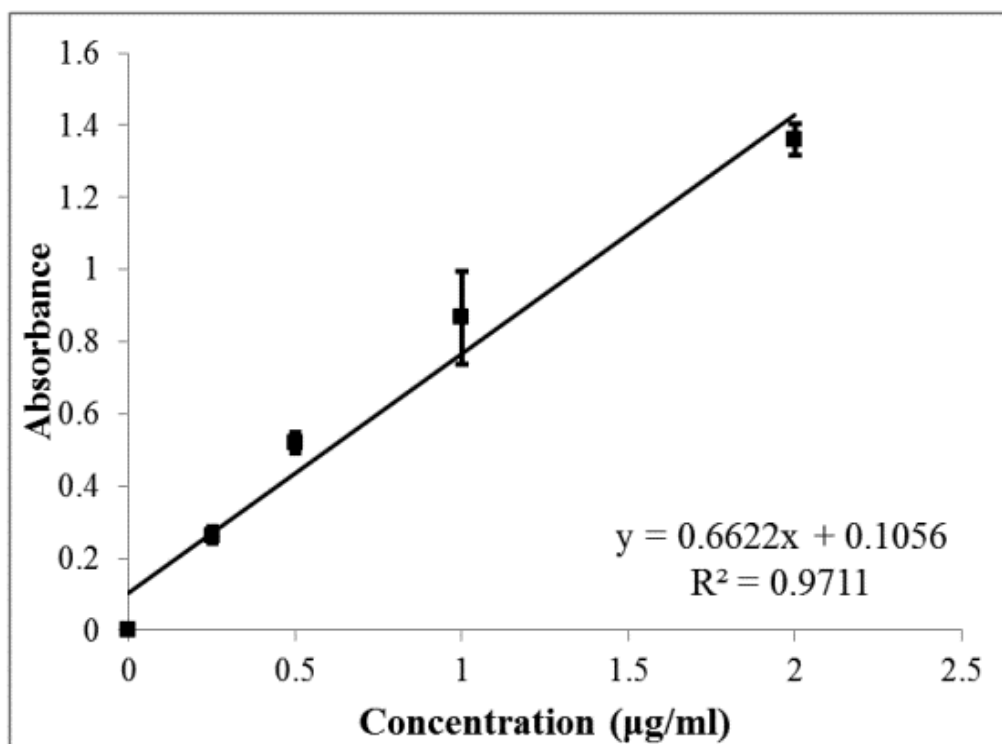
Figure D.5. Calibration curve of ETN for ELISA assay to determine the ETN released from microspheres in PBS
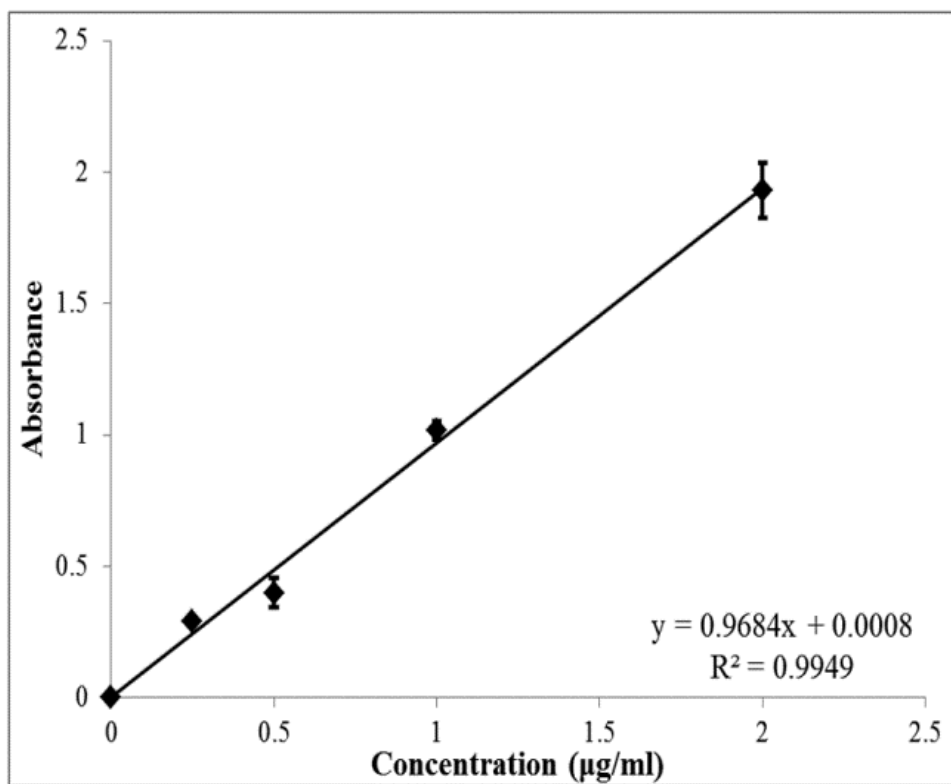
Figure D.6. Calibration curve of ETN constructed for ELISA assay to determine ETN released from microspheres in cell culture medium containing 10% FBS and in healthy and RA synovial fluids

Table D.1. R^2 values and equations of polynomial trendlines (6th degree) obtained for the in vitro ETN release from PCL and MPEG-PCL-MPEG microspheres in PBS and cell culture medium

	R^2	Equation
PBS (µBCA Assay)		
PCL	0.9961	$y = -4\times10^{-9} x^6 + 1\times10^{-6} x^5 - 0.0001 x^4 + 0.0083 x^3 - 0.2332 x^2 + 3.6174 x + 2.6798$
MPEG-PCL-MPEG	0.9914	$y = -5\times10^{-9} x^6 + 1\times10^{-6} x^5 - 0.0001 x^4 + 0.0078 x^3 - 0.2317 x^2 + 4.1083 x + 5.145$
PBS (ELISA) PCL	0.996	$y = -5\times10^{-9} x^6 + 1\times10^{-6} x^5 - 0.0002 x^4 + 0.0086 x^3 - 0.2333 x^2 + 3.5159 x + 2.6446$
MPEG-PCL-MPEG	0.994	$y = -6\times10^{-9} x^6 + 2\times10^{-6} x^5 - 0.0002 x^4 + 0.0105 x^3 - 0.284 x^2 + 4.4261 x + 4.7771$
Cell Culture Medium		
PCL	0.9986	$y = -4\times10^{-8} x^6 + 8\times10^{-6} x^5 - 0.0006 x^4 + 0.0229 x^3 - 0.4413 x^2 + 4.7548 x + 0.8089$
MPEG-PCL-MPEG	0.9942	$y = -1\times10^{-7} x^6 + 2\times10^{-5} x^5 - 0.0014 x^4 + 0.0476 x^3 - 0.8449 x^2 + 7.8442 x + 2.9786$
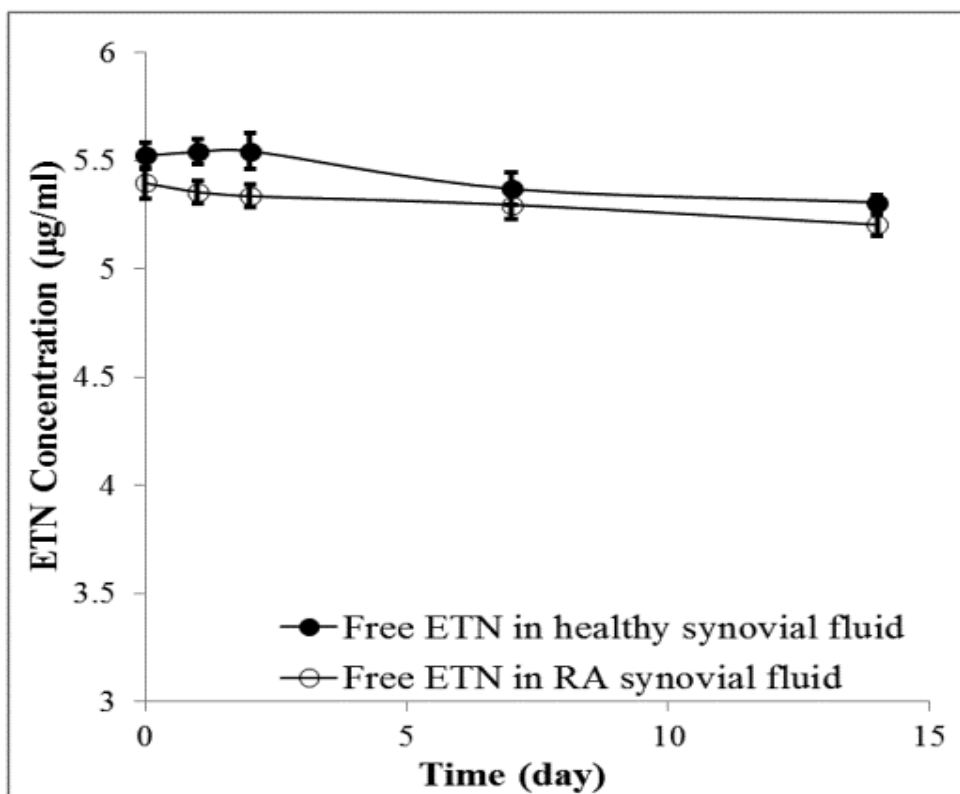
Figure D.7. Change in free ETN concentration (5 µg/ml) with time in healthy or RA synovial fluids

APPENDIX E

RESULTS OF PRELIMINARY STUDIES AND CALIBRATION CURVES FOR ELISA EXAMINATIONS
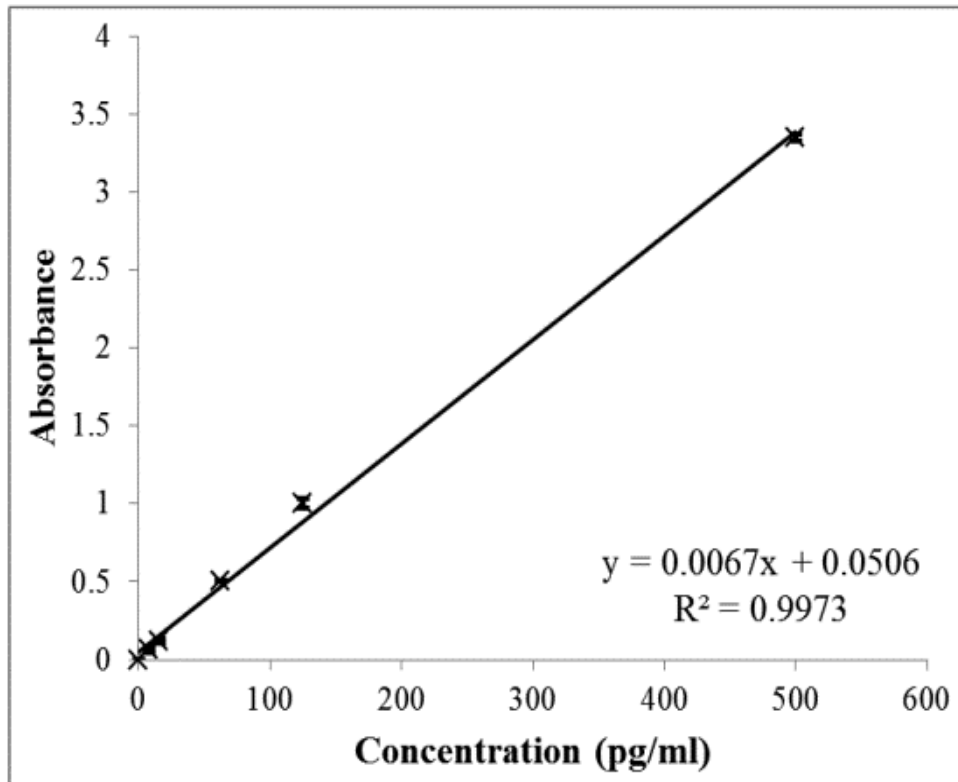
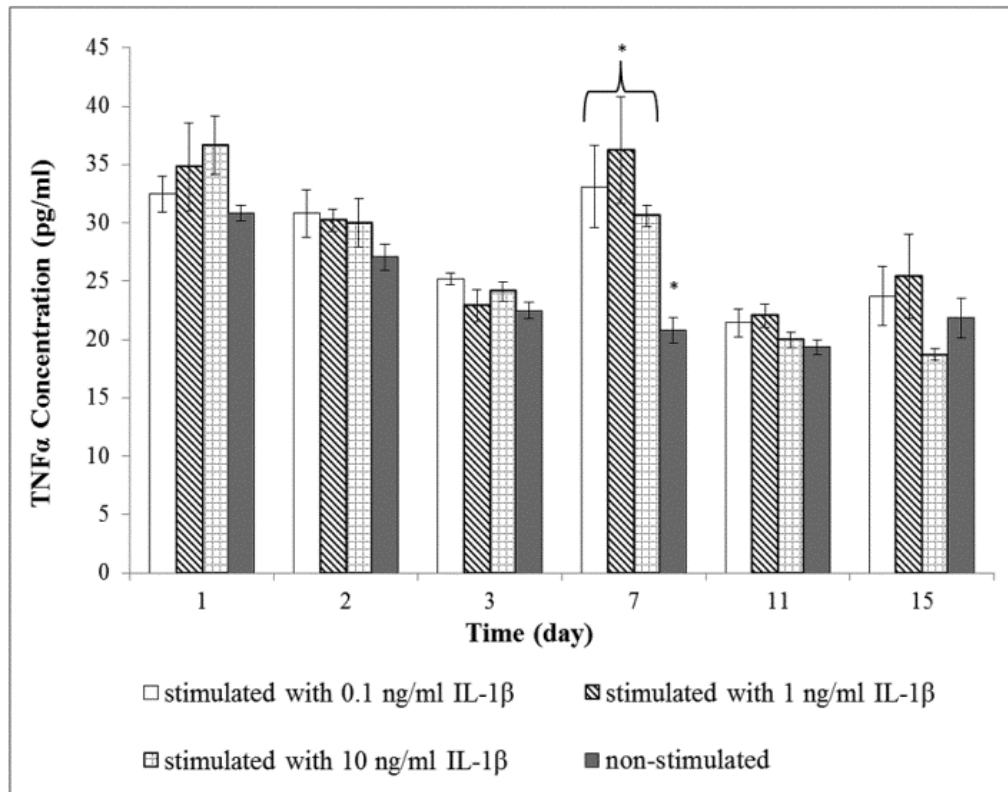**Figure E.1.** Calibration curve of TNFα constructed for ELISA

Figure E.2. TNFα levels of RA FLS before and after stimulation with various concentrations of IL-1β (Values are shown as mean ± S.E.M., n=3)
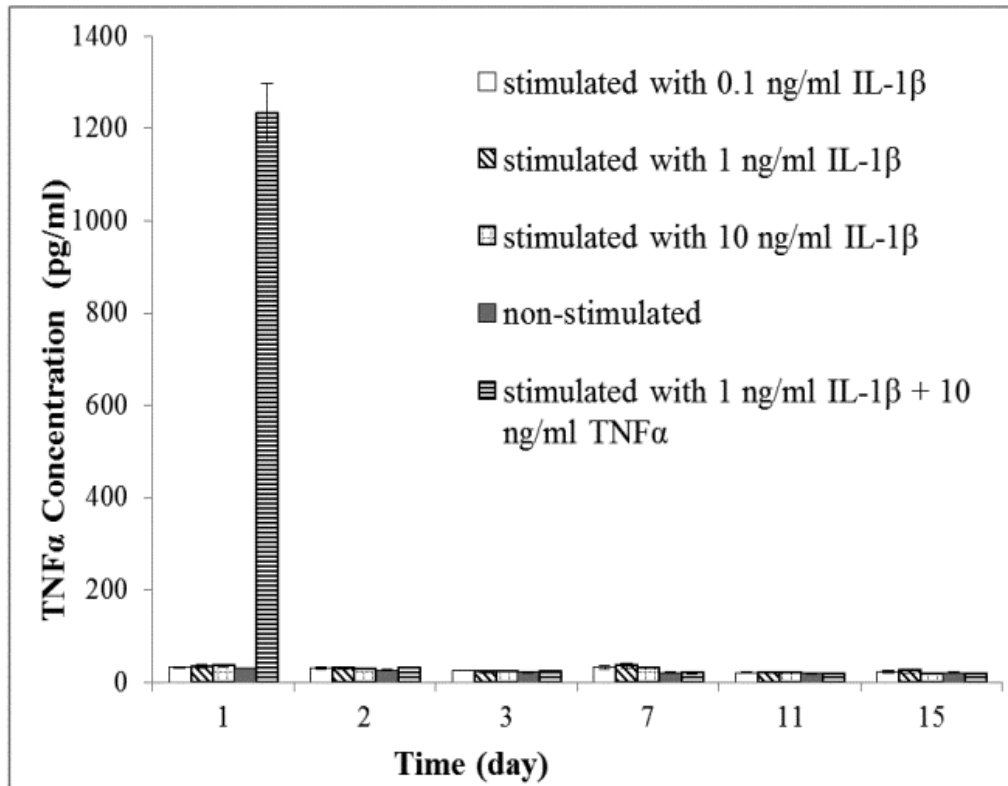
Figure E.3. TNFα levels of RA FLS before and after stimulation with various concentrations of IL-1β and with the combination of IL-1β and TNFα (Values are shown as mean ± S.E.M., n=3)
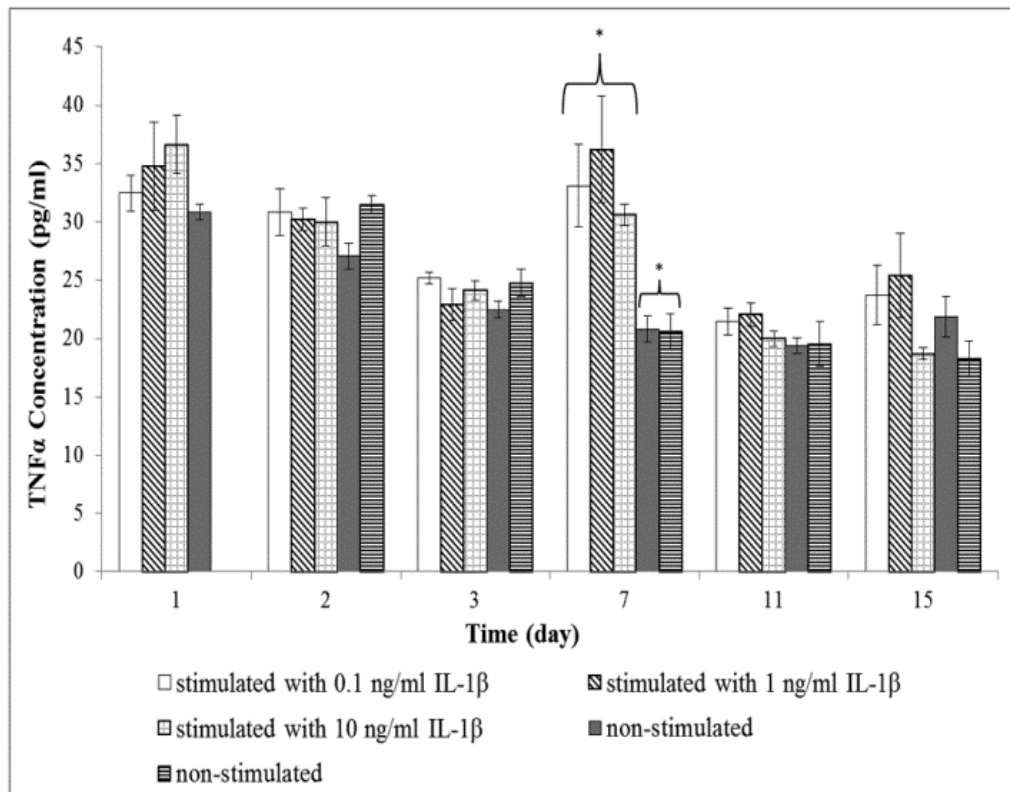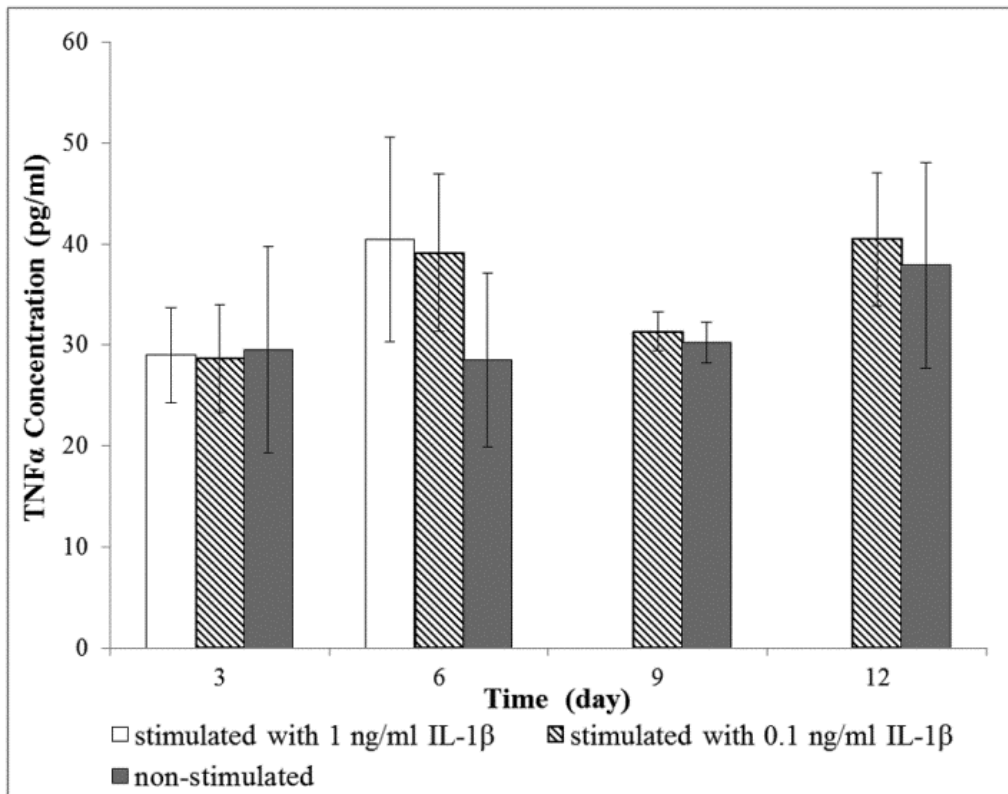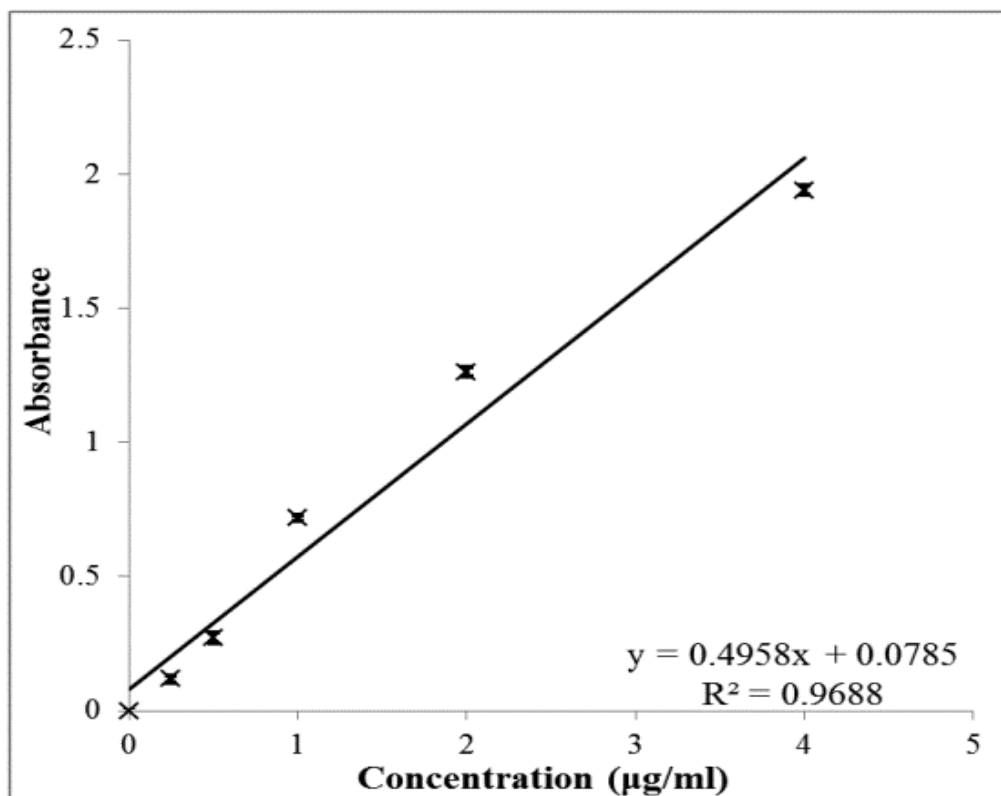
Figure E.4. TNFα levels of RA FLS before and after stimulation with various concentrations of IL-1β and with the combination of IL-1β and TNFα (Values are shown as mean ± S.E.M., n=3)

Figure E.5. TNFα levels of RA FLS before and after continuous stimulation with two different concentrations of IL-1β (Values are shown as mean ± S.E.M., n=4)

Figure E.6. Calibration curve of ETN constructed for ELISA assay to determine the changes in concentration of free ETN group (Group 3) and ETN released from microspheres in cell culture medium containing 5% FBS (Groups 4 and 5)
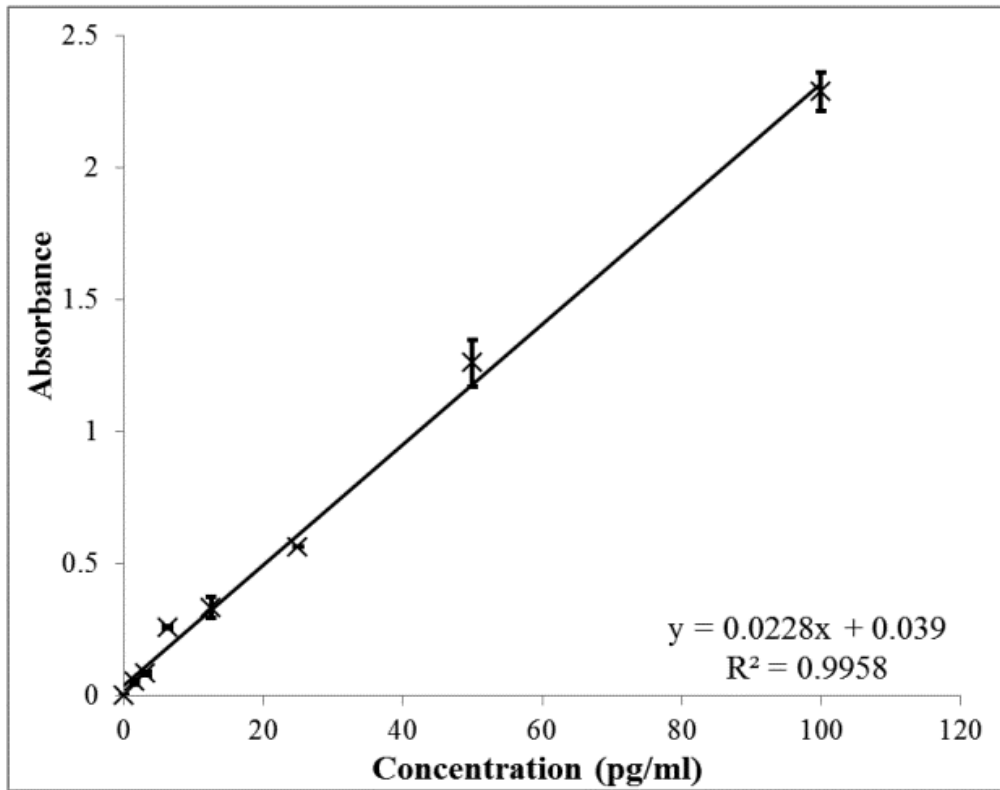
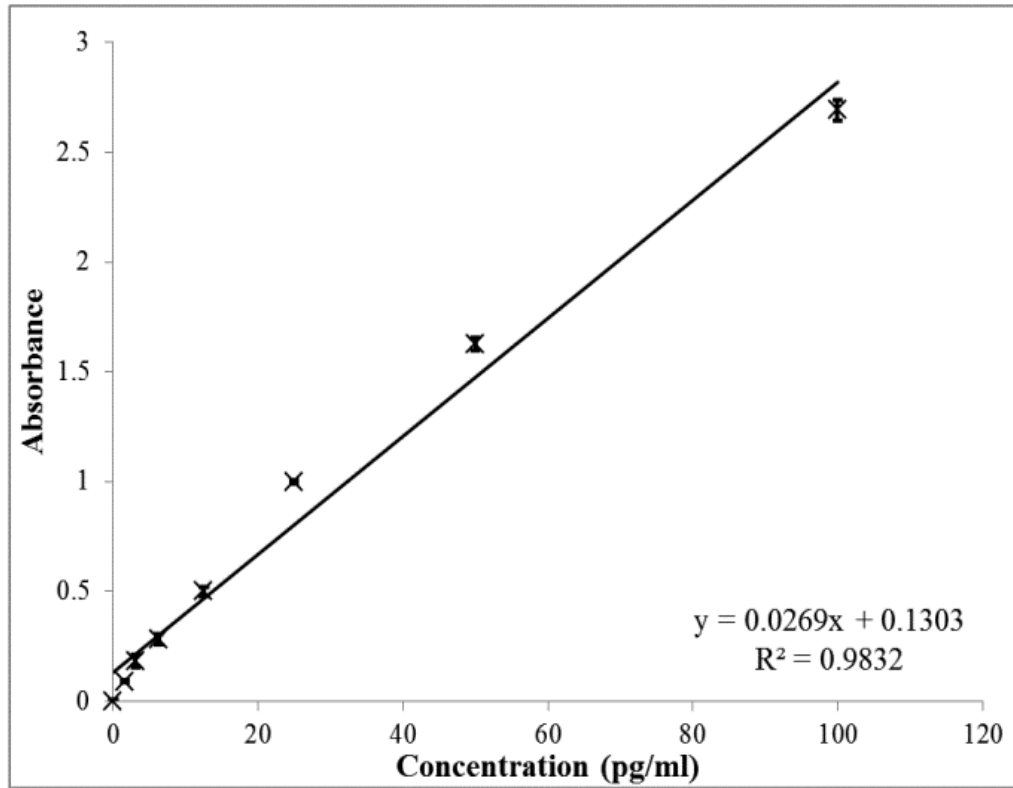**Figure E.7.** Calibration curve of IL-6 constructed for ELISA

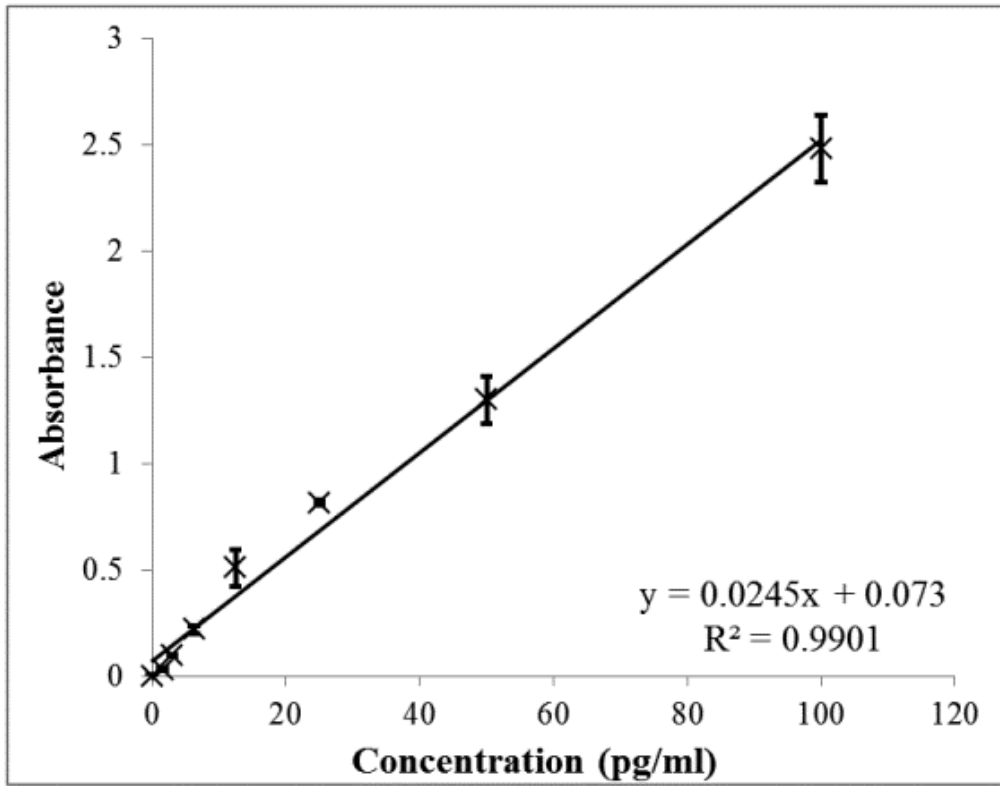**Figure E.8.** Calibration curve of IL-17 constructed for ELISA

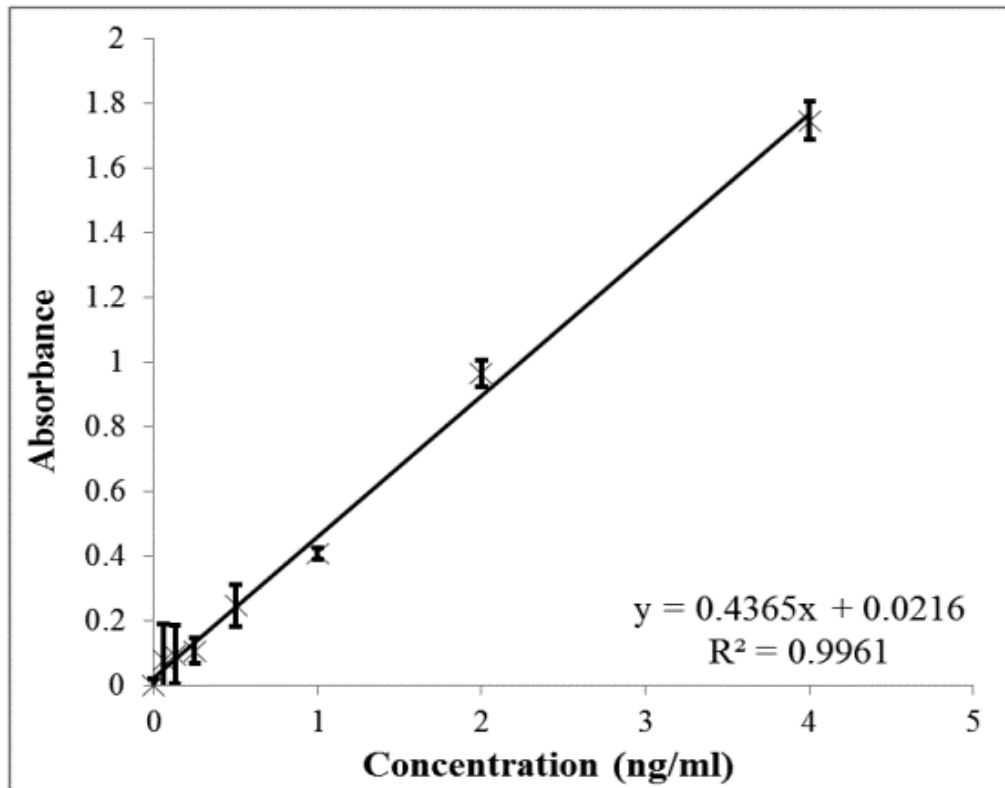**Figure E.9.** Calibration curve of IFN-γ constructed for ELISA

Figure E.10. Calibration curve of MMP-3 constructed for ELISA

The plotted data follow the relationship:

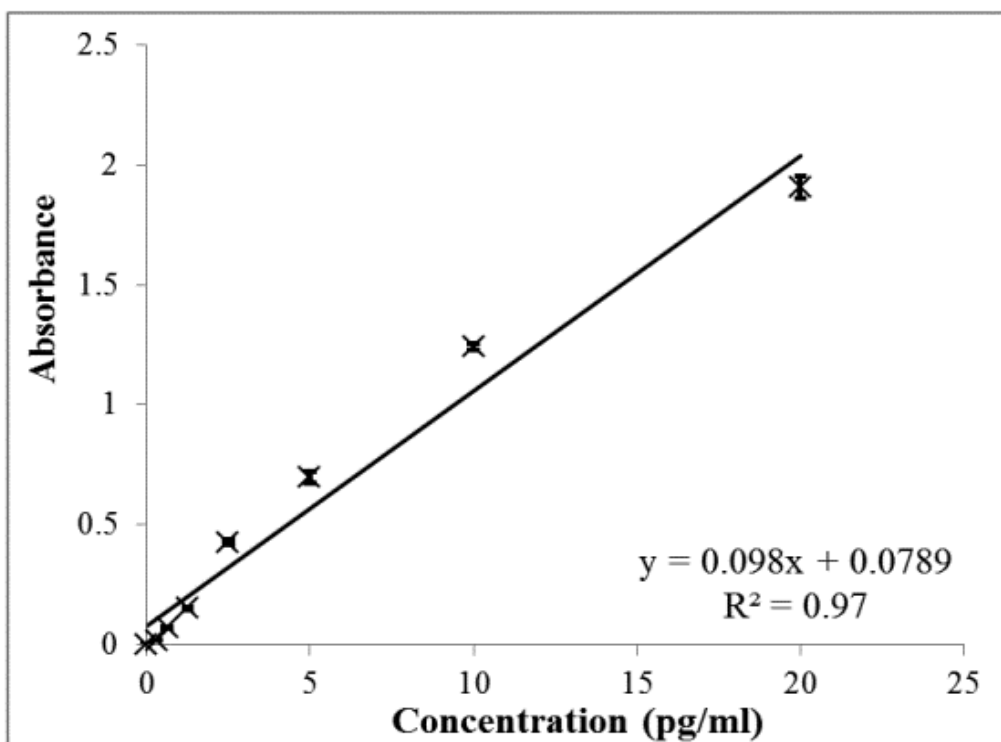$$y = 0.4365x + 0.0216$$
$$R^2 = 0.9961$$

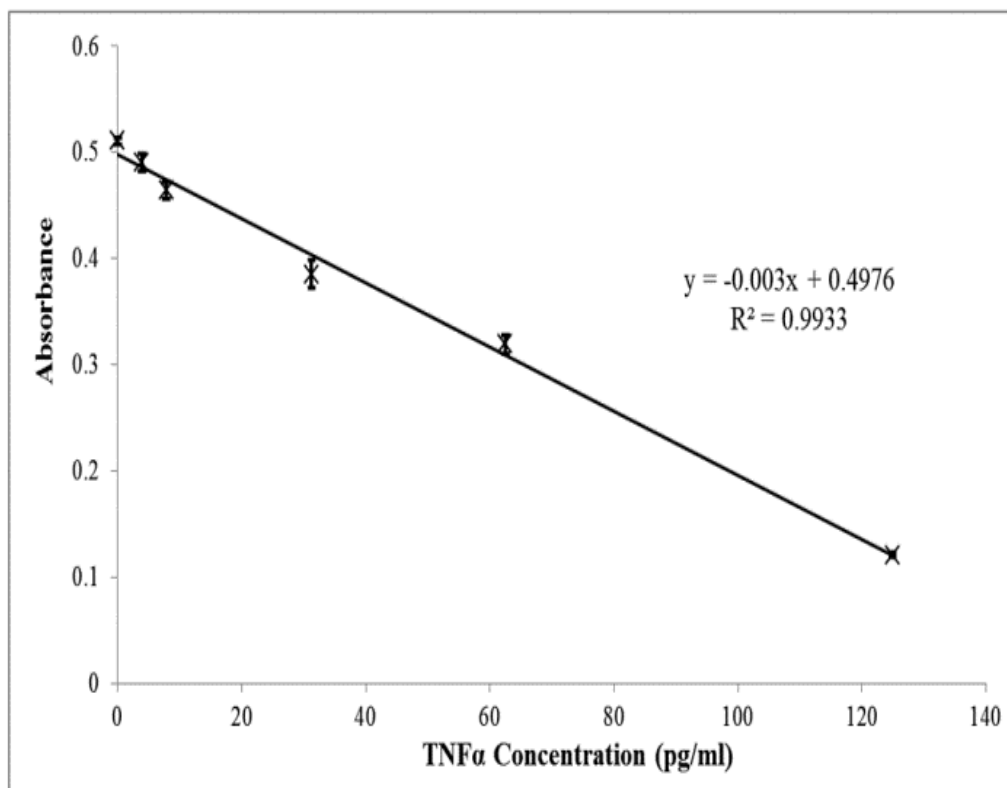**Figure E.11.** Calibration curve of MMP-13 constructed for ELISA

Figure E.12. Calibration curve for MTT assay obtained by measuring the viability of Wehi-164 incubated with predetermined amounts of human TNFα standard solutions

CURRICULUM VITAE

PERSONAL INFORMATION

Surname, Name: Erdemli, Özge
Nationality: Turkish (TC)
Date and Place of Birth: 29 January 1980, Ankara
Marital Status: Single
Phone: +90 312 438 52 98
email: ozgeerdemli@gmail.com

EDUCATION

Degree	Institution	Year of Graduation
MS	METU, Engineering Sciences	2007
BS	Hacettepe University, Chemistry	2003
High School	Çankaya Anadolu High School, Ankara	1998

WORK EXPERIENCE

Year	Place	Enrollment
2004-2005	Alp Medical	Product Manager
2005-2013	METU Department of Engineering Sciences	Research Assistant

FOREIGN LANGUAGES

Advanced English, Basic German

PUBLICATIONS

1. V. Yaprakci, Ö. Erdemli, A. Kayabolen, A. Tezcaner, F. Bozkurt, D. Keskin. In vitro/In vivo comparison of cefuroxime release from polycaprolactone (PCL)/Calcium sulfate (CaS) implants for osteomyelitis treatment. Biotechnol. Appl. Biochem. (2013) doi: 10.1002/bab.1118.
2. Ö. Erdemli, Ö. Çaptuğ, H. Bilgili, A.Tezcaner, D. Keskin. In vitro and in vivo evaluation of the effects of demineralized bone matrix or calcium sulfate addition to polycaprolactone-bioglass composites. J Mater Sci Mater Med. (2010) 21 295-308.
3. Patent application: Controlled Drug Delivery Systems for Anti-TNFα (PCT/TR2012/000148)

HOBBIES

Guitar playing, Photography, Books, Movies